NONLINEAR EVOLUTION OF WAVES AND THEIR ASSOCIATED EFFECTS IN SPACE AND LABORATORY PLASMAS

THESIS

Submitted to

DELHI TECHNOLOGICAL UNIVERSITY
in fulfilment of the requirements for the degree of

DOCTOR OF PHILOSOPHY

by

Ms. JYOTI
(2K18/Ph.D./AP/506)

Under the supervision of

Prof. Suresh C. Sharma
Supervisor
Department of Applied Physics
Delhi Technological University (DTU)

Prof. R. P. Sharma
Co-Supervisor
Department of Centre for Energy Studies (CES)
Indian Institute of Technology (IIT), Delhi

Department of Applied Physics
Delhi Technological University, Delhi-110042, India

OCTOBER 2023

Dedicated

To

Beloved Parents

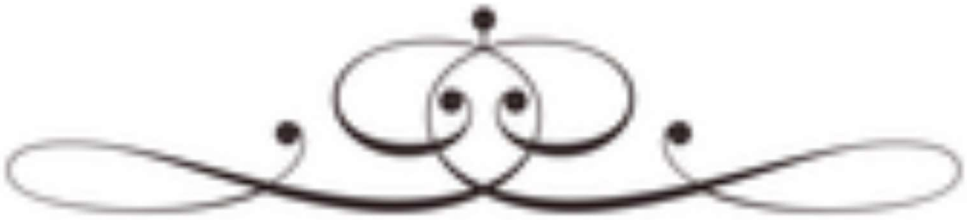

Delhi Technological University

(Govt. of National Capital Territory of Delhi)
Shahbad Daulatpur, Bawana Road, Delhi-110042

CERTIFICATE

This is to certify that the thesis entitled **"Nonlinear Evolution of Waves and their Associated Effects in Space and Laboratory Plasmas"** submitted by **Ms. Jyoti (2K18/Ph.D/AP/506)** to Delhi Technological University (DTU), Delhi, India for the degree of Doctor of Philosophy, is a bonafide record of the research work carried out by her under our supervision and guidance. The work embodied in this thesis has been carried out in the Plasma & Nano Simulation Lab, Department of Applied Physics, Delhi Technological University (DTU), Delhi, India. The work of this thesis is original and has not been submitted in parts or fully to any other Institute or University for the award of any other degree or diploma.

Prof. Suresh C. Sharma
Supervisor
Department of Applied Physics
Delhi Technological University
Delhi-110042, India

Prof. R. P. Sharma
Co-Supervisior
Centre for Energy Studies (CES)
Indian Institute of Technology, Delhi
New Delhi-110016, India

Prof. A. S. Rao
Head, Department of Applied Physics
Delhi Technological University
Delhi-110042, India

Delhi Technological University
(Govt. of National Capital Territory of Delhi)
Shahbad Daulatpur, Bawana Road,
Delhi-110042

CANDIDATE'S DECLARATION

I, **Ms. Jyoti**, hereby certify that the thesis titled ***"Nonlinear Evolution of Waves and their Associated Effects in Space and Laboratory Plasmas"*** submitted in the fulfilment of the requirements for the award of the degree of Doctor of Philosophy is an authentic record of my research work carried out under the supervision of **Prof. Suresh C. Sharma** and **Prof. R. P. Sharma.** Any material borrowed or referred to is duly acknowledged.

JYOTI
(2K18/Ph.D/AP/506)
Delhi Technological University
Shahbad Daulatpur, Bawana Road
Delhi-110042, India

ACKNOWLEDGEMENTS

This Ph.D. thesis is the result of challenging journey, and it would not have been possible to write this doctoral thesis without the support of kind people around me, to only some of whom it is possible to give particular mention here.

Foremost, I would like to give my gratitude to my supervisor, ***Prof. Suresh C. Sharma*****,** Department of Applied Physics, Delhi Technological University, Delhi, India for his supervision, valuable guidance, and genuine advice from the early stage of this research. His dedication, timely advice, meticulous scrutiny, scientific intuition and instinct have exceptionally inspired and enriched my growth as the student and research scholar. I would like to convey my deep sense of gratitude to my co-supervisor, ***Prof. R. P. Sharma***, Centre for Energy Studies, IIT Delhi, for his continued support and encouragement. I owe their special thanks for enabling me to accomplish my Ph.D thesis on time. I am privileged to have a supervisor & Co-supervisor who cared so much about my work and who provided me constant support. Their enthusiasm in research has always motivated me to take challenges for solving the advance and complex problems in my research field. The critical comments rendered by them during the discussions are appreciated.

My sincere thanks also goes to ***Prof. Prateek Sharma,*** Vice Chancellor, DTU, ***Prof. Yogesh Singh*** and ***Prof. J.P. Saini,*** Ex-Hon'ble Vice-chancellor, DTU, and other officials of DTU for their precious support and providing ample research facilities to conduct this research.

I would also thank profusely, ***Prof. Rinku Sharma,*** Dean (Academic-PG), DTU, and ***Prof. A.S. Rao,*** Head of the Department, for his originality that has triggered and nourished my maturity and benefitted me for long time. Moreover, I would also thank all other faculty and staff members of Department of Applied Physics, DTU for their help and cooperation throughout my research period.

I express my heart-felt gratitude to ***Dr. Neha Pathak, Mr. Rajesh, Ms. Garima Patel, Dr. Indraj Singh***, ***Mr. Ramesh Kumar,*** for their constant motivation and support during the course of my Ph.D. thesis. Their scientific inputs, personal helps, moral support and encouragement have always made me feel at ease and enhance the quality of my research.

I would also like to express huge and warm thanks to my other fellow lab mates in Plasma & Nano Simulation Research Laboratory; ***Dr. Umang Sharma, Dr. Monika Yadav, Ms. Anshu Dahiya, Ms. Shruti, Mr. Sagar, Mr. Harender Mor, Dr. Mansha, Ms. Ritu, Mr. Aditya, Mr. Himank Sagar and Ms. Monika Verma*** for the stimulating discussions, selfless support, and for all the fun we have had in the last four years.

I am indebted to some of my dear friends ***Ms. Priyanka Maan, Dr. Amita Gandhi, Ms. Sangeeta, Ms. Komal, Mr. Rajat Bajaj, Mr. Ankit Kumar and Ms. Richa*** for influencing me in a positive way and for their moral support and motivation, which drives me to give my best.

I would like to acknowledge all the teachers I learnt from since my childhood specially from ***Hindu College Sonipat***, I would not have been here without their guidance, blessings and support.I would also like to thank ***University Grant Commission (UGC), Government of India*** for providing me Senior research fellowship.

Last but not the least, I would like to pay high regards to my father ***Mr. Jaichand,*** my mother ***Mrs. Bhanmati,*** they have always encouraged me to explore my potential and pursue my dreams. They helped me a lot to reach this stage in my life. I would also like to thank my brothers and sisters for their everlasting encouragement, motivation and support throughout my research work. I would also like to thank my younger brothers ***Mr. Harish,*** and ***Mr. Abhishek,*** for supporting me spiritually throughout writing this thesis and my life in general. Their cooperation, understanding, and sincere encouragement were the sustaining factors in accomplishing this thesis successfully. Also, I want to thank my nephew ***Ankit, Sahaj and Satvik*** for their unconditional love, their contagious laughter and light hearted presence, which lightened my challenging PhD journey and offered a welcome feeling of joy and innocence.

I would like to special thanks to ***Mr. Ashwani Saroha*** my lifepartner for his love, constant care, and emotional support throughout my life**.**

Above all, I thank the Almighty Nirankar God for giving me the strength and patience to work through all these years so that today I can stand proudly with my head held high.

(JYOTI)

ABSTRACT

Plasma turbulence is a phenomenon that occurs in a variety of astrophysical, space plasmas and fusion energy. It is generated by several factors including shearing flows, density gradients, currents, and temperature, and is essential for particle heating and energy dissipation. A broad variety of waves (like plasma waves, lower hybrid wave, upper hybrid wave, magnetosonic wave, whistler wave, alfven wave etc) can be supported in plasma by the collective motion of charged particles. These waves are very important for the dynamics and behaviour of plasma systems. These wave modes are responsible for the various astrophysical phenomena like turbulence, magnetic reconnection, cascading heating, and acceleration of plasma particles. The objective of this proposed thesis is to investigate the amplification of beam driven whistler waves from background noise levels, resulting from the energy of the beam. This amplification is expected to reach a significant amplitude, leading to the emergence of nonlinear effects caused by the ponderomotive force. Consequently, these nonlinear effects are anticipated to induce the localization of whistler waves, ultimately leading to the development of a turbulent state. On the account of this nonlinear ponderomotive force, the whistler wave gets localized and density cavities and humps are formed. For understanding the nonlinear stage of the wave growth and the saturation, we consider the nonlinear interaction of a high-frequency whistler wave with a low-frequency wave such as ion acoustic waves (IAWs), magnetosonic waves (MSWs) are considering the ponderomotive nonlinearity due to the whistler wave. Using the two-fluid approach, nonlinear dynamical equations have been derived. Additionally, to solve the model equations, numerical simulation is used, with the pseudo-spectral technique for spatial integration and the finite difference method for temporal integration to explain the localization, turbulence, spectral break, and spectral indices in power spectrum. Also, fluctuations in whistler's electric field shows that it is turbulent in nature.

Further, for a better understanding of the physics behind whistler wave localization, a semi-analytical model has been developed. Also, this simplified model has been investigated for the whistler's convergent and divergent behaviour. Numerical outcomes of the study show the whistler turbulence in the magnetic reconnection sites created by the electron beam and show localized structures and whistler fluctuations, which are to the observations of Zhao et al. [1].

It is thought that Whistler waves, which are generated at electron scales, have a significant impact on the microphysics of magnetic reconnection in the electron diffusion area. So, additionally, the thesis also intends to study the generation of whistler coherent structures formation and later whistler turbulence generation at magnetic reconnection site due to the energetic electron beam (as observed by Magnetospheric Multiscale Mission (MMS)) along with the influence of magnetic island. Nonlinear processes, such as ponderomotive force, density change, and the existence of magnetic islands, might be considered the cause of whistler turbulence. To determine the transverse scale sizes of coherent structures, a semi-analytical model has also been devised. Transverse scale of localized structures in the presence of pre-existing magnetic islands are modified by power of whistler wave. We also analyze the contour plot of magnetic field lines, which serves as a spatial representation of the breaking and reconnection of magnetic field lines, leading to the release of trapped magnetic energy. Simulation outcomes shows the nonlinear evolution of multiple X-O points in the presence of magnetic islands shows chaotic structures at later time and may be responsible to the generation of turbulence. We have also shown the evolution of current sheet, their scale size of the order of electron skin depth. The corresponding power spectrum is also evaluated and discussed its relevance with Biskamp observations. Regarding the mechanics and energetics of the reconnection process, the separatix's characteristics are a useful source of knowledge. Along with this, we have also studied the formation of thermal tail of energetic electrons, which may be responsible for the heating and acceleration of plasma particles.

LIST OF PUBLICATIONS

International Journals

1. **Jyoti**, Suresh C. Sharma, Neha Pathak, and R. P. Sharma, "**Beam-driven whistler mode nonlinear saturation and turbulence in the magnetopause**", *Physics of Plasmas* 29, 092104 (2022) https://doi.org/10.1063/5.0098108.

2. **Jyoti,** Suresh C. Sharma, and R. P. Sharma, "**Localization and turbulence of Beam-Driven Whistler wave with Magnetosonic wave in Magnetopause**", *Physics of Plasmas* 30, 022904 (2023) https://doi.org/10.1063/5.0134920.

3. **Jyoti,** Suresh C. Sharma, and R. P. Sharma, "**Localization of beam generated whistler wave and turbulence generation in reconnection region of magnetopause**", *Physics of Plasmas* 31(2), 022902 (2024) https://doi.org/10.1063/5.0169397.

4. **Jyoti,** Suresh C. Sharma, and R. P. Sharma, "**Localization of beam generated whistler wave and turbulence generation in reconnection region of magnetopause**" *Physica Scripta* 99(3), 035610 (2024) https://doi.org/10.1088/1402-4896/ad289a.

5. **Jyoti,** Suresh C. Sharma, and R. P. Sharma, "**Coherent structures of Beam-driven whistler mode in the presence of magnetic islands in magnetopause**" *The European Physical Journal Plus 139(3), 270 (2024) https://doi.org/10.1140/epjp/s13360-024-05036-y*.

International/National peer reviewed proceedings

1. Presented a paper entitled, "**Solitary structures associated with parallel whistler field at magnetopause**", in the 48th EPS Conference on Plasma Physics-2022", at the Maastricht Exhibition & Congress Centre in Maastricht, the Netherland.

2. Poster Presented a paper entitled, "**A Schematic study of nonlinear whistler wave in magnetopause region through numerical simulation**" in the 2nd International Conference on Plasma Theory and Simulations (PTS -2022)", Department of Physics, University of Lucknow, India.

3. Poster Presented a paper entitled, "**Beam-driven whistler turbulence in solar-wind**" in the International Conference on Advances in Science and Technology in 21st century (ICAST)", Department of Science, Markanda National College, Shahabad, Markanda, Haryana.

4. Presented a poster entitled, "**Magnetic Reconnection and Particle Acceleration by Beam-Generated Whistler Wave in Space Plasmas**", in the USO-PRL Solar Physics Workshop (USPW-2023) on the "Multi-scale Phenomena on the Sun: Present Capabilities and Future Challenges" held from 3rd-5th April, 2023 by the USO-PRL, Udaipur, India.

5. Poster Presented a paper entitled, "**Nonlinear Evolution of Beam-Generated Whistler wave in the Magnetopause**" in the 3rd International Conference on Plasma Theory and Simulations (PTS -2023)", School of Physical Sciences, Jawaharlal Nehru University, New Delhi – 110067, India.

6. **Jyoti**, Suresh C. Sharma and R.P. Sharma presented a poster entitled, "**Beam-driven whistler turbulence in the presence of magnetic islands at magnetic reconnection sites**", 2nd International Conference on International Conference on Atomic, Molecular, Material, Nano and Optical Physics with Applications (ICAMNOP–2023), Department of Applied Physics, DTU 2023, India, 20th - 22nd December, 2023.

CONTENTS

LIST OF FIGURES

Fig. No. **Page No.**

LIST OF TABLES

Table No. **Page No.**

CHAPTER -1

Introduction and Literature Review

1.1 Background

Along with solid, liquid, and gas, plasma is often referred to as "the fourth state of matter". When energy is applied, a liquid will boil and turn into a gas; similarly, heating a gas will create plasma. In general, plasma holds similarities to gaseous state, however, it differs from gases in various respects. Any ionized gas is not considered to be plasma. The first need for an ionised gas to behave like plasma is that it be quasineutral. If the system's physical dimension L is significantly bigger than the Debye length λ_D, the plasma shows quasineutral behaviour. The second requirement is that the number of charged particles in the Debye sphere i.e., $n\lambda_D^3$ be significantly more than unity (where n is the plasma number density and λ_D is the Debye length). Debye length is defined as the distance over which significant charge separation may occur. Thus, we can say plasma is quasi-neutral gas of charged particles such as electrons, ions and neutral particles whose shows the collective behaviour and behaviour of these charged particles governed by the electric and magnetic field which is generated by other moving charged particles. These requirements ensure that the plasma behaves collectively, allowing it to move as a fluid rather than as a collection of distinct charge particles.

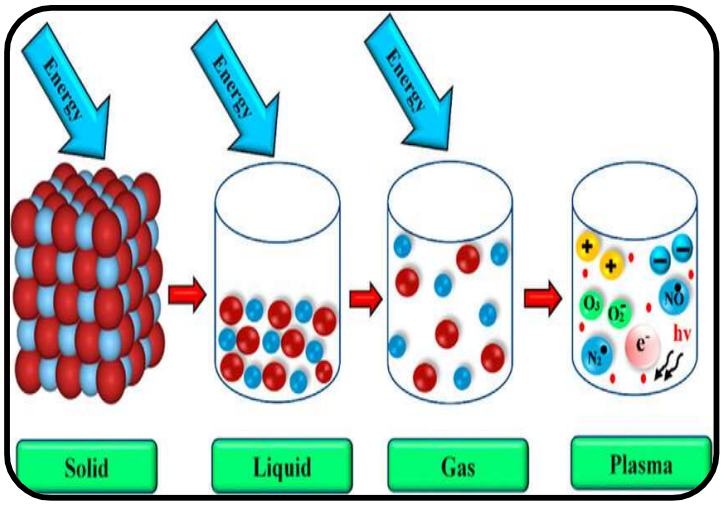

Figure 1.1 State of matter.

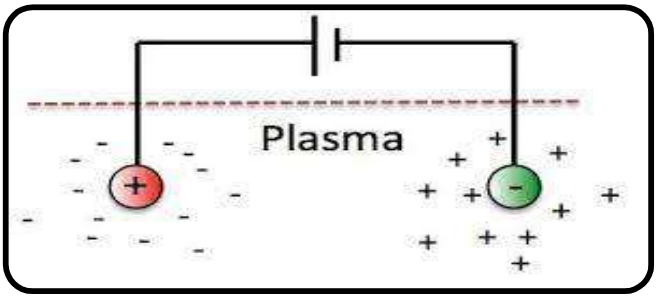

Figure 1.2 Debye shielding

1.2 Wave modes in plasmas

There are many distinct waves modes feasible owing to the collective behaviour of plasmas. The plasma is electrically conductive due to the free charges, making it vulnerable to electromagnetic fields. Plasmas, where electromagnetic and electrostatic waves of various frequencies may propagate, are abundant with wave phenomena. The behaviour and characteristics of plasmas are greatly affected by these wave modes. When describing linear wave events in homogeneous plasmas, it is typically sufficient to compute the dispersion relation, where the frequency $\omega(k)$ is correlated with the wavenumber k . These waves' phase and group velocities are described by

$$\mathrm{v}_{ph}=\frac{\omega(\mathrm{k})}{k}\hat{\mathrm{k}} \qquad \text{and} \qquad \mathrm{v}_{g}=\frac{d\omega}{dk}.$$

The phase velocity, aligned with the wave vector k, determines the direction and magnitude of the wave front or phase propagation $\phi(\mathrm{x.t})=\mathrm{k.r}-\omega(\mathrm{k})\mathrm{t}$. However, the group velocity may deviate from the phase velocity, indicating the direction of energy and information transfer within the wave.

Space is the natural laboratory to study these waves in magnetized plasmas. These wave modes display distinct dispersive properties depending on the plasma conditions. These plasma modes are of great research interest as they play an imperative role in various nonlinear phenomena in space and astrophysical plasmas. The dynamics of the system under consideration is influenced by the nature of nonlinearity employed and the dispersive properties of the medium. Here are a few plasma wave modes that are often seen like whistler waves, Langmuir wave, alfven wave, kinetic alfven wave, upper hybrid wave, lower hybrid waves, ion acoustic waves and nonlinear interaction of these wave modes[2]–[7] contributes to formation of turbulent cascade modes. Among these wave modes, it is tremendously assumed that in space and laboratory plasmas, a whistler wave plays a vital role.

Whistler waves are a particular kind of electromagnetic wave that can exist in the magnetosphere and ionosphere of the earth. Whistler waves can be generated artificially by human activities such as radio transmissions and are frequently linked to natural occurrences like lightning strikes. Also, whistler wave can be generated by electron beam, temperature instabilities, and current-driven plasma instabilities[8]–[13]. Frequency of whistler wave lies in the range of $\omega_{LH} < \omega < \omega_{ce}$, where ω_{LH} is the lower hybrid frequency and ω_{ce} is the electron cyclotron frequency. The electromagnetic waves under consideration exhibit right-hand polarization and can propagate either parallel or obliquely to the background magnetic field in the rest frame of the plasma. The dispersion relation of the whistler wave is given by [14]

$$\left[\omega_0^2(1+k^2\lambda_e^2)^2 - k^2k_z^2\lambda_i^2v_A^2\right]E_z = 0.$$

And, the dispersion relation of the whistler wave under the conditions, $k_{0x} = k_{0y} = 0, k_0 = k_{0z}$ and $k_0\lambda_e >> 1$, $\omega_{ce} > \omega_0$ is given by [15]

$$k_0^2 = \frac{\omega_0^2}{c^2}\left(1 - \frac{\omega_{pe}^2}{\omega_0(\omega_0 - \omega_{ce})}\right).$$

Alfvén waves are a specific type of plasma wave that develops in magnetized plasmas, such as those found in astrophysical environments like the magnetosphere of the Earth, the corona of the Sun, and other planetary plasmas. Named after the Swedish physicist Hannes Alfvén, who won the 1970 Nobel Prize in Physics for his significant contributions to magnetohydrodynamics (MHD)[16] and plasma physics, these waves are named after him. Alfven wave are low frequency electromagnetic wave, propagating parallel to ambient magnetic field. These are nondispersive wave, having dispersion relation $\omega = k_z v_A$.

Here $v_A\left(= B_0 \Big/ \sqrt{4\pi n_0 m_i}\right)$ is the velocity of Alfven wave. B_0 is the background magnetic field, m_i is the mass of ions, and n_0 is the unperturbed number density. However, when its perpendicular wavelength becomes similar to the ion gyroradius or the electron inertial length, they exhibit dispersive nature.

An et al.[17] have examined the stimulation of electrostatic beam mode and whistler waves in a beam-plasma system. It was found that electrostatic beam-mode waves are confined within the beam, but whistler waves have the ability to propagate outside the beam, resulting in the

dissipation of energy. Many observations have been reported for the excitations of whistler waves by the electron beam in a magnetized plasma[1], [18].

Gary et al.[9] investigated the many implications that the whistler-anisotropy instability plays in whistler turbulence using particle-in-cell simulations. They discovered that the whistler-anisotropy instability can operate as a turbulence-regulating mechanism in the kinetic range via wave-particle interactions.

Whistler-mode waves are a prominent type of plasma waves that have been extensively studied due to their major influence on the structure of the dissipation zone and the effectiveness of reconnection. Consequently, they have received substantial study interest and attention[19], [20]. In previous observations, Whistler mode waves have been detected in proximity to the X line during magnetopause crossings. Additionally, numerical modeling has been conducted to further investigate this phenomenon. As a result, a theory has emerged suggesting that these waves may serve as a mediator in the reconnection process[21]. In recent times, there has been a study conducted on the process of coalescence of several magnetic islands that were first formed in an extended current sheet. The focus of this study was mostly on the scaling of the inner structural size of the coalesced islands and the subsequent progressive heating of the plasma[22]. Cerri et al.[23] also showed that the presence of large-scale turbulent motions leads to the establishment of a scaling of -5/3 spectrum at $k\lambda_i < 1$ by the pressure strain interaction. Simultaneously, these turbulent motions contribute to the production of current sheets, which serve as sites for magnetic reconnection events. Also, they examined the contribution of electron-scale current sheets to particle energization associated with magnetic reconnection. In addition to the whistler wave modes, the magnetosonic wave (MSW) modes are also expected to be a significant contender for the purpose of particle heating and acceleration in space plasmas [24]–[27].

These waves are of significant importance in numerous nonlinear phenomena that manifest in space and astrophysical plasmas. mainly, these phenomena manifest as non-thermal distributions inside plasma. Plasma acceleration and particle heating in many systems are reliant upon their important roles. The nonlinear features of these waves are of significant interest in study, both from theoretical and experimental perspectives.

1.3 Solar and Magnetospheric plasmas

Solar wind is a stream of energetic charge particles that flows outward from the solar corona. The corona is the sun's outer atmosphere, which has a temperature of roughly 10^6 K (the sun's surface temperature is 6000 K). This solar wind stream is made up of fast, energetic protons and electrons. Because of the sun's million-degree atmosphere, gravitational forces are insufficient to hold the charged particles in place, and they pour out into space in all directions. This gravitationally unbound plasma is pushed by the pressure gradient between the corona and the inner heliosphere, which drives the solar wind. The solar magnetic field is extended into interplanetary space, where it is known as the interplanetary magnetic field (IMF). The IMF amplitude is around 5-10 nT, while the density of the solar wind plasma is approximately 10 cm^{-3}. There are three types of solar wind based on their parameters: Fast wind is normally between 450 and 700 km/h, slow wind is between 200 and 400 km/h, and intermittent solar wind is between 200 and 400 km/h. It is considered a very turbulent medium with large-scale field fluctuations.

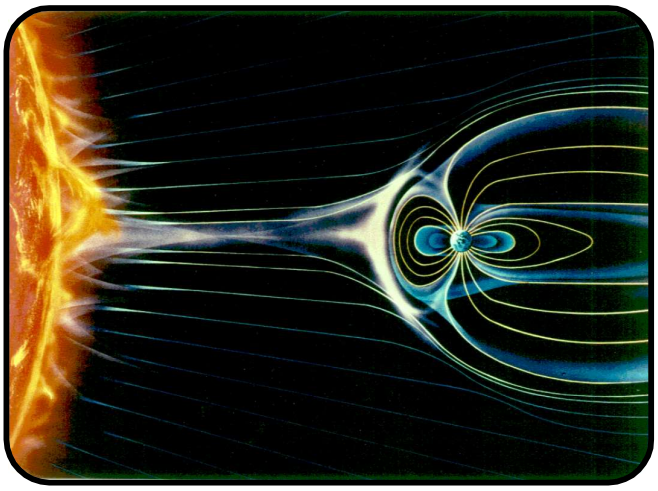

Figure 1.3 Image of solar wind

Turbulence in the solar wind is a common factor in the movement of energetic particles across the solar-terrestrial system. The most difficult difficulties in space plasmas are solar wind acceleration and heating [28]–[30].

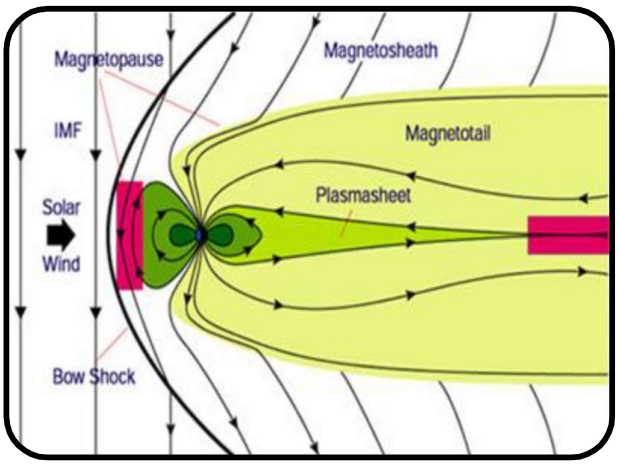

Figure 1.4 Interaction of sun earth system.

The **magnetosphere** develops by the interaction of solar wind and the Earth's magnetic field. This interaction takes place at approximately an astronomical unit (1AU) from the Sun. Around this point, the pressure caused by the Earth's

magnetic field is balanced by the pressure created by solar wind plasma. As a result, the solar wind circulates throughout the magnetosphere. The Earth's magnetosphere is a complex arrangement of particle populations that are confined inside a certain region. This confinement is facilitated by the presence of free energy, which is supplied by the solar wind. As a result of this interaction, internal convection processes are induced within the magnetosphere. Particle anisotropies and free energy for plasma waves are driven by convection of particle populations into the stronger field of Earth's dipole. Multiple couplings between the varied particle populations occur from the multiple plasma instabilities, leading to a complicated evolution of those distinct particle populations. The Earth's magnetosphere is classified into three distinct areas, each with its own particle population. The first region is the extended field "magnetotail" on the Earth's nightside. The principal particle populations observed in the magnetotail include the ion plasma sheet, the electron plasma sheet, the cusp-mantle (comprising ions and electrons), and the polar wind (comprising ions and electrons). The "outer dipole" is the second region, where the ion and electron plasma sheets, substorm-injected ions and electrons, the electron and ion radiation belts, cloak ions and electrons, and polar-wind ions and electrons all are found. The third region, referred to as the "inner dipole," is located in close proximity to the Earth. It encompasses various components, including the plasmasphere, which consists of ions and electrons, the ion plasma sheet, substorm-injected ions, as well as the electron and ion radiation belts. The plasmapause, which is the outside limit of the dense, cold plasmasphere, is the barrier between the inner and outer dipole regions.

The relevance of plasma waves on the emergence of the solar wind as well as the evolution and interactions of the Earth's magnetosphere's numerous particle populations is overwhelming. The magnetospheric and solar-wind systems are comprised of many electron and ion populations, which mostly interact through plasma waves. Energy transfer has been recognized as a critical concern in the field of space plasma physics. Previous measurements have revealed the existence of many wave modes, including the Dispersive Alfvén wave, whistler waves, ion cyclotron waves, and lower hybrid waves, as well as their role in particle heating and acceleration. Various processes for energy transmission have been hypothesized in the literature, including wave-wave interaction, wave-particle contact, vortical structures, turbulence, and magnetic reconnection.

1.4 Turbulence

Turbulence is an inherent characteristic of both space and astrophysical plasma and is defined as a combination of random fluctuations occurring across many scales. The aforementioned fluctuations can manifest as changes in velocity, density, as well as electric and magnetic fields. Turbulence theory illustrates the process by which energy is transferred from larger length scales to smaller length scales, ultimately leading to its dissipation [31]–[34]. The transfer of energy is based on the wave-particle interaction [35] and wave-wave interaction [36], [37]. Turbulence plays a significant role in the process of particle heating in space and astrophysical plasmas, including the emergence of stars, galaxies, and cosmic rays, among others. The energy cascade mechanism can be illustrated with the power density spectrum, which is characterized by frequency and wavenumber. In general, the energy spectrum can be classified into three distinct ranges. The initial range pertains to a significant scale, referred to as an injection range, which is alternatively recognized as an energy-containing scale. The second range is commonly referred to as the inertial range. At this particular scale, the turbulence has achieved a quasi-steady state, wherein the time needed for energy transfer is shorter than the time required for diffusion. The third aspect pertains to the dissipation range, when fluctuations undergo a transformation into thermal energy, leading to the heating of particles.

In 1941, Kolmogorov proposed a theoretical framework to describe the distribution of kinetic energy across various scales in the context of incompressible isotropic turbulence [38]. According to Kolmogorov's hypothesis, the energy density E(k) is contingent upon both the energy dissipation rate (per unit volume) and the wave number. Kolmogorov derived a scaling law using dimensional analysis, which suggests that in the inertial range, the distribution of energy follows a scale of $k^{-5/3}$. The study conducted by Biskamp and Welter [39] involved the examination of 2D electron magnetohydrodynamics (EMHD) turbulence by numerical simulation. The researchers observed that the power spectrum of the turbulence adhered to Kolmogorov scaling i.e., $E_k \sim k^{-5/3}$ for $k\lambda_e > 1$, and $E_k \sim k^{-7/3}$ for $k\lambda_e < 1$. In a recent study conducted by Zhao et al.[1] the phenomenon of whistler turbulence was identified at magnetic reconnection sites. The researchers hypothesize that the creation of this turbulence is attributed to powerful electron beams resulting from magnetic reconnection.

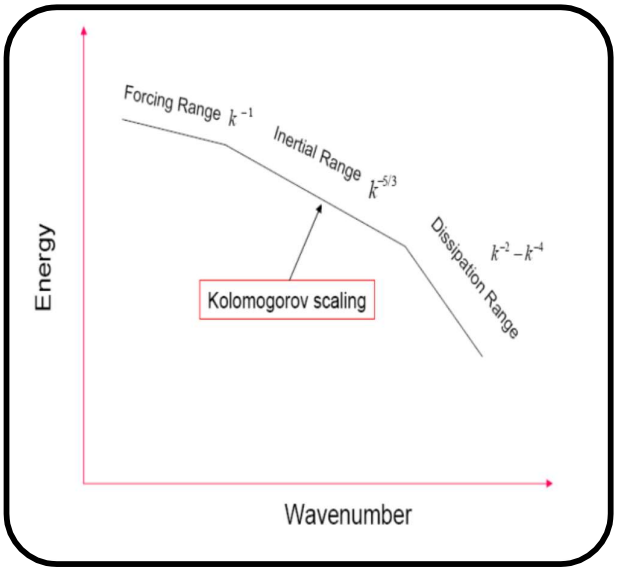

Figure 1.5 Kolmogorov scaling

Solar wind is the natural laboratory to explain the plasma turbulence [35]. The coupling mechanism between waves might be regarded as a potential contributor to the production of turbulence. The manifestation of turbulence extends beyond the solar wind, since it is also detected within the magnetosphere [40], [41] and at magnetic reconnection locations within the magnetosphere [31], [42].

1.5 Magnetic reconnection

Magnetic reconnection is a key mechanism of energy conversion that takes place in various laboratory and astrophysical plasmas. The process of reconnection involves the conversion of magnetic energy into kinetic and thermal energy by altering the structure of the magnetic field across current sheets [43]. The findings from particle simulations suggest that the majority of magnetic energy is converted into ion kinetic energy during the process of magnetic reconnection involving a solitary X line [44], [45]. Hence, the acquisition of significant kinetic energy by electrons during magnetic reconnection remains an unresolved enigma.

Magnetic reconnection within the Earth's magnetosphere is triggered by the influence of solar wind. The phenomenon in question is often attributed to its role in causing disruptions inside the magnetosphere of the Earth, namely manifesting as substorms and magnetic storms. Magnetic reconnection can potentially enable a flow of solar wind plasma and electromagnetic energy into

the magnetosphere through either low- or high-latitude magnetopause reconnection. Within the magnetotail lobes, the process of magnetic reconnection effectively transforms the stored energy into the internal and kinetic energy of the plasma. In the context of controlled nuclear fusion, this process serves as a hindrance to the magnetic confinement of the fusion fuel. Magnetic reconnection occurs in an area of a current sheet, or neutral sheet, where magnetic fields of opposite polarity approach to combine.

1.5.1 Magnetic Reconnection and Turbulence

Magnetic reconnection is a phenomenon wherein the conversion of magnetic energy into plasma kinetic energy occurs rapidly. Satellite measurements have revealed that a significant portion, ranging from 20% to 50%, of the magnetic energy that is released undergoes conversion into electron kinetic energy [46]. Furthermore, this conversion process also plays a role in facilitating the emergence of turbulence. This phenomenon is accountable for the process of plasma heating and plasma acceleration. It is therefore essential to quantify the role of turbulence in reconnection; Although, turbulence and reconnection appear to be closely related and it is known that turbulence impacts reconnection, the mechanics of their interaction is still not entirely established.

Many authors have explored how turbulence affects the rate of reconnection, specifically how the already present turbulence might change Sweet-Parker reconnection and how turbulence may form because of reconnection. Forced turbulence experiments indicate that turbulent reconnection is quicker than laminar reconnection, and the reconnection rate rises with increasing turbulence level. Additionally, magnetic reconnection itself causes turbulence, which feeds back on itself.

1.6 Spacecraft observations

Observations demonstrate that magnetic reconnection occurs in the magnetosphere at the MHD, ion, and electron scales. The Magnetospheric Multiscale (MMS) mission was started in 2015 to study magnetic reconnection processes at the terrestrial magnetopause and magnetotail. It expands the study of magnetic reconnection at the electron scale in Earth's magnetosphere boundary regions [47]. Over the past decade, there has been a significant advancement in the understanding of waves and turbulence associated with reconnection. This progress has been made possible by the utilization of high-resolution multi-point in situ data. The initial breakthroughs in this field were made by the Cluster and THEMIS missions, and more recent findings have been obtained from the Magnetospheric

Multiscale (MMS) mission [21], [48]–[51]. Recently, spacecraft such as THEMIS and Cluster data have detected whistler-mode waves around reconnection sites [21], [52], [53] and cause electron acceleration in reconnection [54]. Li. et al. [55] analyze reconnection event observed by the Magnetospheric Multiscale (MMS) mission at the earth's magnetopause. In the course of this occurrence, the spacecraft traversed the reconnection current sheet that extends between the magnetospheric and magnetosheath regions. Notably, the presence of whistler waves was detected on both the magnetospheric and magnetosheath sides. Previous observations have shown the importance of various waves in the vicinity of reconnection sites of magnetosphere like upper hybrid wave/Langmuir wave [56] , Electrostatic solitary wave [48], lower hybrid waves [57] etc.

Based on empirical data obtained from spacecraft observations and supported by numerical simulations, it has been observed that separatrix zones tend to generate rapid electron beams, a phenomenon that is frequently characterized by instability. Waves approaching the plasma frequency, such as Langmuir, beam-mode, or UH waves, are suggested for fast weak beams. Both Langmuir waves and upper hybrid waves have been reported in magnetotail reconnection from Wind and Cluster observations [56], [58].

The findings of whistler mode waves in the magnetic reconnection zone at the dayside magnetopause were reported by Zhao et al. [1] .They utilized data from the magnetospheric multiscale (MMS) mission to provide evidence for the excitation of whistler waves by electron beams in the medium energy range.

The process of reconnection facilitates the transmission of energy from the solar wind to the Earth's magnetosphere, as well as the subsequent release of energy in the magnetotail. Eastwood et al. [31] presented observations of both electric and magnetic field fluctuations within a magnetic reconnection ion diffusion area in the Earth's magnetotail using Cluster spacecraft data. Chaston et al. [59] accomplished a study on THEMIS data and revealed the presence of a turbulent spectrum in the vicinity of the magnetopause reconnection location. The spectrum, which comprises a range of wavenumbers from the ion gyro-radius to the electron inertial lengths, exhibits a scaling of $k^{-3/2}$ in the inertial range. Beyond a certain breakpoint, at smaller scales, the spectrum becomes steeper with a spectral index of k^{-3}. The flow of energy via a turbulent cascade can be characterised by the involvement of either kinetic Alfvén waves, whistler waves, or the interplay between both types of waves.

1.7 Theoretical models

The momentum expression for every particle in the vicinity of the electromagnetic field is used to describe the dynamics of the plasma. Explaining the plasma dynamics would be a very difficult procedure in practice. Consequently, many models that make use of approximations have been used to characterise the plasma state. Various models are employed to characterize the state of plasmas, depending on the specific problem at hand. These models include the single particle approach, the kinetic theory, and the fluid theory. The utilization of a single-particle methodology offers microscopic a vantage points of the plasma, wherein the movement of an individual charged particle is considered within the context of electric and magnetic fields. When dealing with many particles, the single-particle approach can be more time-consuming. More crucially, this approach cannot be applied to dynamical circumstances in which the plasma currents and charges produce self-consistent fields. For this scenario, the plasma motions can be signified numerically using kinetic theory. For some purposes, the fluid description is preferable to kinetic theory, because the kinetic theory's seven independent variables can make both analytical and numerical computations difficult.

1.7.1 Single Particle Model

To investigate low-density plasma, a single particle model is defined. The current of charged particles is minimal and has no effect on the electromagnetic fields. This method is an initial stage towards understanding plasma collective behaviour. This approach is only applicable to magnetized plasmas when the applied external field is substantially stronger than the magnetic field created by charged particle motion. The momentum equation for charge species in the presence of an external field is as follows:

$$m\frac{d\vec{v}}{dt} = q\left(\vec{E} + \frac{1}{c}v \times \vec{B}\right).$$

Here, m, v and q are the mass, velocity, and charge of charged particles respectively.

In the presence of magnetostatic field along the z-axis, the particle will gyrate in a circular motion perpendicular to the magnetic field with gyroradius (r_g) expressed as:

$r_g = \frac{v_\perp}{\omega_g}$, here $v_\perp$ is the velocity of charged particle in x-y plane, and $\omega_g (= qB/m)$ is the gyrofrequency. If velocity part parallel to the external field, the particle will undergo a helical path.

1.7.2 Single-fluid theory

When the density of plasma is high enough then the whole plasma may be considered as a single fluid theory is known as magnetohydrodynamics (MHD) which applies to the study of very low frequency phenomena in highly conducting magnetized fluids.

1.7.3 Magnetohydrodynamics (MHD) Model

Plasma is treated as a single fluid in the MHD model, with all particles moving at the same velocity. As a result, the thermal and fluid velocity of plasma particles are ignored in this case.

Finally, the electron frequency is estimated to be greater than the characteristic plasma frequency. The linear combination to describe the plasma as a fluid, like liquid mercury, with a mass density ρ, and an electrical conductivity $\frac{1}{\eta}$. These are the equations of magnetohydrodynamics (MHD).

For a quasineutral plasma with singly charged ions, we can define the mass density ρ, current density j, and mass velocity v as follows:

$$\rho = n_i M + n_e m \approx n(M+m). \tag{1.1}$$

$$v = \frac{1}{\rho}(n_i M v_i + n_e m v_e) \approx \frac{M v_i + m v_e}{M+m}. \tag{1.2}$$

$$j = e(n_i v - n_e v_e) \approx ne(v_i - v_e). \tag{1.3}$$

The equation of motion incorporates a gravitational force component to account for the non-electromagnetic force exerted on the plasma. The ion and electron plasma can be expressed in the following manner:

$$Mn\frac{\partial v_i}{\partial t} = en(E + v_i \times B) - \nabla p_i + Mng + P_{ie}. \tag{1.4}$$

$$mn\frac{\partial v_i}{\partial t} = -en(E + v_e \times B) - \nabla p_e + mng + P_{ei}. \tag{1.5}$$

Now adding above two eqs. we obtained,

$$n\frac{\partial}{\partial t}(M v_i + m v_e) = en(v_i - v_e) \times B) - \nabla p_i + n(M+m)g. \tag{1.6}$$

The electric field has cancelled out as we have collision terms P_{ei}=-P_{ie}

Further simplifying above equation one can obtain the single fluid equation describing the mass flow given below: $\rho\frac{\partial v}{\partial t} = j\times B - \nabla p_i + \rho g.$ (1.7)

The electric field does not appear explicitly because the fluid is neutral. An alternative equation can be derived by considering a distinct linear combination of two fluid equations. First, we multiply equation (1.4) by the variable m and equation (1.5) by the variable M. Then, we subtract the later equation from the former equation.

$$\mathrm{Mm}n\frac{\partial}{\partial t}(v_i - v_e) = en(M+m)E + en(mv_i + Mv_e)\times B - m\nabla p_i + M\nabla p_i - (M+m)P_{ei}. \quad (1.8)$$

Using eqs. (1.1), (1.2) and (1.3), eq. (1.8) becomes

$$\frac{\mathrm{Mm}n}{e}\frac{\partial}{\partial t}\left(\frac{j}{n}\right) = e\rho E - (M+m)ne\eta j - m\nabla p_i + M\nabla p_e + en\left(mv_i + Mv_e\right)\times B. \quad (1.9)$$

The last term of eq. (1.9) can be simplified as:

$$mv_i + Mv_e = Mv_i + mv_e + M(v_e - v_i) + m(v_i - v_e) = \frac{\rho}{n}v - (M-m)\frac{j}{ne}. \quad (1.10)$$

Dividing eq. (1.9) by $e\rho$, we have now,

$$E + v\times B - \eta j = \frac{1}{e\rho}\left[\frac{Mmn}{e}\frac{\partial}{\partial t}\left(\frac{j}{n}\right) + (M+m)j\times B + m\nabla p_i - M\nabla p_e\right]. \quad (1.11)$$

The $\frac{\partial}{\partial t}$ term can be neglected in slow motions, where inertial effects are unimportant. In the limit $m/M \to 0$, then eq. (1.11) becomes,

$$E + v\times B = \eta j + \frac{1}{ne}\left[j\times B - \nabla p_e\right]. \quad (1.12)$$

This eq. (1.12) is called as Ohm's law describes the electrical properties of the conducting fluid. The term $j\times B$ is called the Hall current term. It often happens that this last term are small enough to be neglected; then Ohm's law can be written as:

$$E + v\times B = \eta j. \quad (1.13)$$

Equation of continuity for mass ρ and charge σ are easily obtained from the sum and difference of the ion and electron equations of continuity. Thus, the set of MHD equations consists of following equations

$$\rho\frac{\partial v}{\partial t} = j\times B - \nabla p + \rho g. \qquad (1.14)$$

$$E + v\times B = \eta j. \qquad (1.15)$$

$$\frac{\partial \rho}{\partial t} + \nabla.(\rho v) = 0. \qquad (1.16)$$

$$\frac{\partial \sigma}{\partial t} + \nabla.j = 0. \qquad (1.17)$$

This equation of set together with Maxwell's equations is often used to describe the equilibrium state of the plasma. Although it can be utilized for determining plasma waves, it is significantly less precise than the two-fluid equations we have been utilizing. The simplicity of the MHD equations exceeds their drawbacks for resistivity-related problems. Astrophysicists working on cosmic electrodynamics, hydrodynamicists working on MHD energy conversion, and fusion theorists working with complex magnetic geometries have all extensively utilized the MHD equations.

1.7.4 Two-Fluid theory

When the plasma density is high, it becomes an impossible task to follow the trajectory of each particle and to predict plasma behaviour. Fortunately, when collision between plasma particles becomes very frequent each species can be treated as a fluid described by local density, velocity and temperature. Here, the identity of individual species is neglected and only the motion of fluid elements is considered. In this approach, the plasma is treated as a mixture of two or more interpenetrating fluids depending on the number of plasma species. Here, Euler equations (continuity, momentum and energy equations) are used for each fluid. The continuity and momentum equations for species are following as:

Continuity equation $\quad \frac{\partial n_j}{\partial t} + \nabla.(n_j\vec{v}_j) = 0.$

Momentum equation $\quad m_j n_j\left[\frac{\partial v_j}{\partial t} + (\vec{v}_j.\nabla)\vec{v}_j\right] = q_j n_j\left(\vec{E} + \vec{v}_j\times\vec{B}\right) - \nabla p_j.$

where n_j, q_j, v_j, p_j and m_j are the number density, charge on species, flow of velocity, pressure, and mass of j^{th} species, respectively.

1.7.5 Statistical approach

The statistical technique is commonly employed to describe the macroscopic behavior of plasma, given its composition of a significant number of interacting particles. In this context, the distribution function for the system of particles is introduced, and the relevant kinetic equations that dictate the evolution of the distribution function in the phase space are subsequently solved. An example of a kinetic equation is the Vlasov equation, which assumes negligible close collisions and describes the interaction of charged particles through self-consistent internal electromagnetic fields.

1.8 Objective of the Thesis

It is widely recognised that the formation of coherent structures results in the development of turbulence. Several turbulence studies have been conducted based on nonlinearity via coherent structure creation. Various plasma waves have been seen in the neighbourhood of the X-line at reconnection sites and pointed out as key potential in turbulence generation in magnetopause at reconnection sites. This chapter presents a proposed model wherein the amplification of beam driven whistler waves occurs from the initial noise level, resulting from the energy of the beam. The amplification process leads to the attainment of a significant amplitude, wherein nonlinear effects arising from the ponderomotive force contribute to the localization of whistler waves. Ultimately, this localization process leads to the emergence of a turbulent state. For understanding the nonlinear stage of the wave growth and the saturation, we consider the nonlinear interaction of a high-frequency with a low-frequency wave, considering the ponderomotive nonlinearity due to the high frequency wave. This nonlinear coupling of waves results in the emergence of coherent structures, which shows the generation of turbulence. For better understanding of localization concept, we also study the semianalytical model.

1.9 Organization of Thesis Work

The thesis holds seven chapters and brief chapter-wise summary of proposed thesis work is as follows:

CHAPTER 1: Introduction and literature review

This chapter presents background on plasma dynamics including different theories to describe these dynamics. A brief introduction to plasma-supporting wave modes, along with solar and magnetospheric plasmas, has been presented. Some keywords are defined, and the outcomes of spacecraft observations are also discussed. This chapter also discusses the motivation for doing the current analysis and the thesis outline.

CHAPTER 2: Beam-driven whistler mode nonlinear saturation and turbulence in the magnetopause

For understanding the nonlinear stage of the wave growth and the saturation, we consider the nonlinear interaction of a high-frequency whistler wave with a low-frequency IAW, taking into account the ponderomotive nonlinearity due to the whistler wave.

This chapter presents a proposed model wherein the amplification of beam driven whistler waves occurs from the initial noise level, resulting from the energy of the beam. The amplification process leads to the attainment of a significant amplitude, wherein nonlinear effects arising from the ponderomotive force contribute to the localization of whistler waves. Ultimately, this localization process leads to the emergence of a turbulent state. Using the Two-fluid approach, nonlinear dynamical equations have been derived. Additionally, to solve the model equations, numerical simulation is used, with the pseudo-spectrum technique for spatial integration and the finite difference method for temporal integration. Further, for a better understanding of the physics behind whistler wave localization, a semianalytical model has been developed. Also, this simplified model has been investigated for the whistler's convergent and divergent behaviour. The outcomes of the numerical simulation of the coupled system are shown here. These results show the localization of whistler waves and spectra of turbulence applicable to the magnetopause regime, which is consistent with the observations. The formation of the filamentary structure indicates the generation of turbulence.

CHAPTER 3: Localization and turbulence of Beam-Driven Whistler wave with Magnetosonic wave in Magnetopause

In this problem, non-linear interactions of high frequency whistler wave and low frequency magnetosonic wave has been considered. Since MSWs is an electromagnetic wave, we have considered perturbation in density as well as in magnetic field. Further localized structures and turbulent spectra of non-linear whistler wave has been studied. To study the convergent and divergent behaviour of non-linear whistler wave, a semianalytical method is investigated.

CHAPTER 4: Localization of beam generated whistler wave and turbulence generation in reconnection region of magnetopause.

For this problem, we develop a model based upon the two-fluid approximation to study whistler dynamics, propagating in the medium with the pre-existing chain of magnetic islands and under the influence of background density perturbation originate from ponderomotive nonlinearity of wave. Dynamics of nonlinear whistler have been solved with pseudo-spectral approach and finite difference method with modified predictor-corrector method and Runge Kutta method for the semianalytical model. Also, we observed that power of whistler wave also impacts the scale size of coherent structures and current sheet dimension.

CHAPTER 5: Coherent structures of Beam-driven whistler mode in the presence of magnetic islands in magnetopause.

The primary objectives of this study are to draw attention to significant achievements in our understanding of whistler turbulence generation at magnetic reconnection due to the intense electron beam to be observed by magnetospheric multiscale mission (MMS) (Zhao et al., 2021 [23]) along with the influence of magnetic island. A beam-driven whistler wave has been simulated in three dimensions to do this. The whistler wave in this model originates as noise owing to the energy of the beam and rises to a large amplitude, where nonlinear

processes from the ponderomotive force drive the whistler wave to localize, which ultimately results in the turbulent state. We have also studied the power spectra which is used to study the formation of thermal tail of energetic electrons.

CHAPTER 6: Nonlinear propagation of whistler-mode in the presence of magnetic islands in the magnetopause.

The motivation of this paper is to study the nonlinear interaction of 3D whistler wave with magnetosonic wave in the presence of magnetic island at magnetic reconnection sites due to the perturbation in wave's own amplitude. From numerical simulation results, we observed localization plots, contour plots, power spectra and current sheet of non-linear whistler wave. The current sheet deeds as a location for intense plasma heating, energy dissipation and particle acceleration

CHAPTER 7: Summary, Conclusion and Future Scope of the Thesis Work

This chapter summarizes the thesis work and presents its key results. This chapter also discusses the potential extension of the current work as well as other chances to succeed.

1.10 References

[1] S. Q. Zhao *et al.*, "Observations of the Beam-Driven Whistler Mode Waves in the Magnetic Reconnection Region at the Dayside Magnetopause," *J. Geophys. Res. Space Phys.*, vol. 126, no. 2, pp. 1–11, 2021, doi: 10.1029/2020JA028525.

[2] H. Huang, Y. Yu, L. Dai, and T. Wang, "Kinetic Alfvén Waves Excited in Two-Dimensional Magnetic Reconnection," *J. Geophys. Res. Space Phys.*, vol. 123, no. 8, pp. 6655–6669, 2018, doi: 10.1029/2017JA025071.

[3] D. B. Graham *et al.*, "Universality of Lower Hybrid Waves at Earth's Magnetopause," *J. Geophys. Res. Space Phys.*, vol. 124, no. 11, 2019, doi: 10.1029/2019JA027155.

[4] G. Ganguli, C. Crabtree, M. Mithaiwala, L. Rudakov, and W. Scales, "Evolution of lower hybrid turbulence in the ionosphere," *Phys. Plasmas*, vol. 22, no. 11, 2015, doi: 10.1063/1.4936281.

[5] I. H. Cairns and B. F. McMillan, "Electron acceleration by lower hybrid waves in magnetic reconnection regions," *Phys. Plasmas*, vol. 12, no. 10, 2005, doi: 10.1063/1.2080567.

[6] C. Krafft and A. S. Volokitin, "Electromagnetic radiation from upper-hybrid wave turbulence in inhomogeneous solar plasmas," *Plasma Phys. Control Fusion*, vol. 62, no. 2, 2020, doi: 10.1088/1361-6587/ab569d.

[7] M. V. Goldman, D. L. Newman, J. G. Wang, and L. Muschietti, "Langmuir turbulence in space plasmas.," *PhST.*, vol. 63, pp. 28–33, 1996, doi: 10.1088/0031-8949/1996/T63/003.

[8] S. P. Gary and I. H. Cairns, "Electron temperature anisotropy instabilities: Whistler, electrostatic and z mode," *J. Geophys. Res. Space Phys.*, vol. 104, no. A9, 1999, doi: 10.1029/1999ja900296.

[9] C. Cui, S. P. Gary, and J. Wang, "Whistler turbulence vs. whistler anisotropy instability: Particle-in-cell simulation and statistical analysis," *Frontiers in Astronomy and Space Sciences*, vol. 9, 2022, doi: 10.3389/fspas.2022.941241.

[10] L. James, L. Jassal, and V. K. Tripathi, "Whistler and electron-cyclotron instabilities in a plasma duct," *J. Plasma Phys.*, vol. 54, no. 1, pp. 119–128, 1995, doi: 10.1017/S0022377800018377.

[11] I. Talukdar, V. K. Tripathi, and V. K. Jain, "Whistler instability in a magnetospheric duct," *J. Plasma Phys.*, vol. 41, no. 2, pp. 231–238, 1989, doi: 10.1017/S0022377800013817.

[12] Y. Zhang, H. Matsumoto, and H. Kojima, "Whistler mode waves in the magnetotail," *J. Geophys. Res. Space Phys.*, vol. 104, no. A12, pp. 28633–28644, 1999, doi: 10.1029/1999ja900301.

[13] D. A. Gurnett, L. A. Frank, and R. P. Lepping, "Plasma waves in the distant magnetotail," *J. Geophys. Res.*, vol. 81, no. 34, pp. 6059–6071, 1976, doi: 10.1029/ja081i034p06059.

[14] D. Biskamp, *Nonlinear Magnetohydrodynamics*. 1993. doi: 10.1017/cbo9780511599965.

[15] F. F. Chen, *Introduction to Plasma Physics and Controlled Fusion*. 1984. doi: 10.1007/978-1-4757-5595-4.

[16] H. Alfvén, "Existence of electromagnetic-hydrodynamic waves," *Nature*, vol. 150, no. 3805. 1942. doi: 10.1038/150405d0.

[17] X. An, J. Bortnik, B. Van Compernolle, V. Decyk, and R. Thorne, "Electrostatic and whistler instabilities excited by an electron beam," *Phys. Plasmas*, vol. 24, no. 7, 2017, doi: 10.1063/1.4986511.

[18] Jyoti, S. C. Sharma, N. Pathak, and R. P. Sharma, "Beam-driven whistler mode nonlinear saturation and turbulence in the magnetopause," *Phys. Plasmas*, vol. 29, no. 9, p. 092104, Sep. 2022, doi: 10.1063/5.0098108.

[19] X. Tang *et al.*, "THEMIS observations of the magnetopause electron diffusion region: Large amplitude waves and heated electrons," *Geophys. Res. Lett.*, vol. 40, no. 12, 2013, doi: 10.1002/grl.50565.

[20] C. Cattell *et al.*, "Discovery of very large amplitude whistler-mode waves in Earth' s radiation belts," *Geophys. Res. Lett.*, vol. 35, pp. 1–7, 2008, doi: 10.1029/2007GL032009.

[21] X. H. Deng and H. Matsumoto, "Rapid magnetic reconnection in the earth's magnetosphere mediated by whistler waves," *Nature*, vol. 410, no. 6828, 2001, doi: 10.1038/35069018.

[22] T. K. M. Nakamura *et al.*, "Spatial and time scaling of coalescing multiple magnetic islands," *Phys. Plasmas*, vol. 30, no. 2, 2023, doi: 10.1063/5.0127107.

[23] S. S. Cerri and F. Califano, "Reconnection and small-scale fields in 2D-3V hybrid-kinetic driven turbulence simulations," *New J. Phys.*, vol. 19, no. 2, 2017, doi: 10.1088/1367-2630/aa5c4a.

[24] R. B. Horne, G. V. Wheeler, and H. S. C. K. Alleyne, "Proton and electron heating by radially propagating fast magnetosonic waves," *J. Geophys. Res. Space Phys.*, vol. 105, no. A12, 2000, doi: 10.1029/2000ja000018.

[25] B. Lembege, S. T. Ratliff, J. M. Dawson, and Y. Ohsawa, "Ion heating and acceleration by strong magnetosonic waves," *Phys. Rev. Lett.*, vol. 51, no. 4, 1983, doi: 10.1103/PhysRevLett.51.264.

[26] R. B. Horne, R. M. Thorne, S. A. Glauert, N. P. Meredith, D. Pokhotelov, and O. Santolík, "Electron acceleration in the Van Allen radiation belts by fast magnetosonic waves," *Geophys. Res. Lett.*, vol. 34, no. 17, 2007, doi: 10.1029/2007GL030267.

[27] H. Zhang, Z. Liu, F. Wang, B. Liu, L. Wei, and W. Duan, "The upper-limited amplitude of the nonlinear magnetosonic solitary wave in a magnetized plasma", *Astrophysics and Space Science*, doi: 10.1007/s10509-022-04121-x.

[28] J. V. Hollweg and P. A. Isenberg, "Generation of the fast solar wind: A review with emphasis on the resonant cyclotron interaction," *Journal of Geophysical Research: Space Physics*, vol. 107, no. A7. 2002. doi: 10.1029/2001JA000270.

[29] E. N. Parker, "Dynamics of the Interplanetary Gas and Magnetic Fields.," *Astrophys. J.*, vol. 128, 1958, doi: 10.1086/146579.

[30] S. R. Cranmer, "Coronal holes," *Living Reviews in Solar Physics*, vol. 6. 2009. doi: 10.12942/lrsp-2009-3.

[31] J. P. Eastwood, T. D. Phan, S. D. Bale, and A. Tjulin, "Observations of turbulence generated by magnetic reconnection," *Phys. Rev. Lett.*, vol. 102, no. 3, pp. 1–4, 2009, doi: 10.1103/PhysRevLett.102.035001.

[32] D. A. Roberts, W. Klein, M. L. Goldstein, and W. H. Matthaeus, "The nature and evolution of magnetohydronamic fluctuations in the solar wind: VOYAGER OBSERVATIONS", *Journal of Geophysical Research,* vol. 92, 1987.

[33] W. H. Matthaeus and M. L. Goldstein, "Stationarity of magnetohydrodynamic fluctuations in the solar wind," *J. Geophys. Res.*, vol. 87, no. A12, p. 10347, 1982, doi: 10.1029/ja087ia12p10347.

[34] W. H. Matthaeus, "Turbulence in space plasmas: Who needs it?," *Phys. Plasmas*, vol. 28, no. 3, 2021, doi: 10.1063/5.0041540.

[35] R. Bruno and V. Carbone, "The solar wind as a turbulence laboratory," *Living Rev. Sol Phys.*, vol. 10, 2013, doi: 10.12942/lrsp-2013-2.

[36] E. M. Tejero, C. Crabtree, D. D. Blackwell, W. E. Amatucci, G. Ganguli, and L. Rudakov, "Experimental characterization of nonlinear processes of whistler branch waves," *Phys. Plasmas*, vol. 23, no. 5, 2016, doi: 10.1063/1.4946020.

[37] B. T. Tsurutani, A. L. Brinca, E. J. Smith, R. T. Okida, R. R. Anderson, and T. E. Eastman, "A statistical study of ELF-VLF plasma waves at the magnetopause," *J. Geophys. Res.*, vol. 94, no. A2, p. 1270, 1989, doi: 10.1029/ja094ia02p01270.

[38] A. N. Kolmogorov, "The local structure of turbulence in incompressible viscous fluid for very large Reynolds numbers," *Proceedings of The Royal Society*, vol. 434, no. 1890, 1941.

[39] D. Biskamp, E. Schwarz, and J. F. Drake, "Two-dimensional electron magnetohydrodynamic turbulence," *Phys. Rev. Lett.*, vol. 76, no. 8, 1996, doi: 10.1103/PhysRevLett.76.1264.

[40] G. Zimbardo *et al.*, "Magnetic turbulence in the geospace environment," *Space Sci. Rev.*, vol. 156, no. 1–4, 2010, doi: 10.1007/s11214-010-9692-5.

[41] G. Zimbardo, "Magnetic turbulence in space plasmas: In and around the Earth's magnetosphere," *Plasma Phys. Control Fusion*, vol. 48, no. 12 B, 2006, doi: 10.1088/0741-3335/48/12B/S28.

[42] W. H. Matthaeus and S. L. Lamkin, "Turbulent magnetic reconnection," *Physics of Fluids*, vol. 29, no. 8, 1986, doi: 10.1063/1.866004.

[43] G. H. H. Suen, C. J. Owen, D. Verscharen, T. S. Horbury, P. Louarn, and R. De Marco, "Magnetic reconnection as an erosion mechanism for magnetic switchbacks," *Astron. Astrophys.*, vol. 675, 2023, doi: 10.1051/0004-6361/202345922.

[44] M. Yamada, J. Yoo, J. Jara-Almonte, H. Ji, R. M. Kulsrud, and C. E. Myers, "Conversion of magnetic energy in the magnetic reconnection layer of a laboratory plasma," *Nat. Commun.*, vol. 5, 2014, doi: 10.1038/ncomms5774.

[45] S. Wang, R. Wang, Q. Lu, J. L. Burch, and S. Wang, "Energy Dissipation via Magnetic Reconnection Within the Coherent Structures of the Magnetosheath Turbulence," *J. Geophys. Res. Space Phys.*, vol. 126, no. 4, 2021, doi: 10.1029/2020JA028860.

[46] Q. Lu, K. Huang, Y. Guan, S. Lu, and R. Wang, "Energy Dissipation in Magnetic Islands Formed during Magnetic Reconnection," *Astrophys. J.*, vol. 954, no. 2, 2023, doi: 10.3847/1538-4357/acea86.

[47] J. L. Burch and T. D. Phan, "Magnetic reconnection at the dayside magnetopause: Advances with MMS," *Geophys. Res. Lett.*, vol. 43, no. 16, 2016, doi: 10.1002/2016GL069787.

[48] H. Matsumoto, X. H. Deng, H. Kojima, and R. R. Anderson, "Observation of electrostatic solitary waves associated with reconnection on the dayside magnetopause boundary," *Geophys. Res. Lett.*, vol. 30, no. 6, 2003, doi: 10.1029/2002GL016319.

[49] D. B. Graham *et al.*, "Large-Amplitude High-Frequency Waves at Earth's Magnetopause," *J. Geophys. Res. Space Phys.*, vol. 123, no. 4, 2018, doi: 10.1002/2017JA025034.

[50] D. Cao *et al.*, "MMS observations of whistler waves in electron diffusion region," *Geophys. Res. Lett.*, vol. 44, no. 9, pp. 3954–3962, 2017, doi: 10.1002/2017GL072703.

[51] D. Cao *et al.*, "MMS observations of whistler waves in electron diffusion region", *Geophys. Res. Lett.,* doi: 10.1002/2017GL072703.

[52] X. H. Deng *et al.*, "Observations of electrostatic solitary waves associated with reconnection by Geotail and Cluster," *Advances in Space Research*, vol. 37, no. 7, 2006, doi: 10.1016/j.asr.2005.05.129.

[53] S. Y. Huang *et al.*, "Observations of Whistler Waves in the Magnetic Reconnection Diffusion Region," in *2018 2nd URSI Atlantic Radio Science Meeting, AT-RASC 2018*, 2018. doi: 10.23919/URSI-AT-RASC.2018.8471382.

[54] J. Burch and J. Drake, "Reconnecting Magnetic Fields," *Am. Sci.*, vol. 97, no. 5, 2009, doi: 10.1511/2009.80.392.

[55] Z. Li, Q. M. Lu, R. S. Wang, X. L. Gao, and H. Y. Chen, "In situ evidence of resonant interactions between energetic electrons and whistler waves in magnetopause reconnection," *Earth and Planetary Physics*, vol. 3, no. 6, 2019, doi: 10.26464/epp2019048.

[56] W. M. Farrell, M. D. Desch, K. W. Ogilvie, M. L. Kaiser, and K. Goetz, "The role of upper hybrid waves in magnetic reconnection," *Geophys. Res. Lett.*, vol. 30, no. 24, 2003, doi: 10.1029/2003GL017549.

[57] C. A. Cattell and F. S. Mozer, "Experimental determination of the dominant wave mode in the active near-Earth magnetotail," *Geophys. Res. Lett.*, vol. 13, no. 3, 1986, doi: 10.1029/GL013i003p00221.

[58] X. H. Deng *et al.*, "Geotail encounter with reconnection diffusion region in the Earth's magnetotail: Evidence of multiple X lines collisionless reconnection?," *J. Geophys. Res. Space Phys.*, vol. 109, no. A5, 2004, doi: 10.1029/2003JA010031.

[59] C. Chaston *et al.*, "Turbulent heating and cross-field transport near the magnetopause from THEMIS," *Geophys. Res. Lett.*, vol. 35, no. 17, pp. 2–6, 2008, doi: 10.1029/2008GL033601.

CHAPTER-2

Beam-driven Whistler mode Nonlinear saturation and Turbulence in the Magnetopause

2.1 Introduction

Turbulence is ubiquitous in the universe and has been commonly observed in space plasma. To study turbulence, space plasma provides the natural laboratory. Turbulence is a state in which nonlinear interactions, such as cascades to finer scales, result in a chaotic structure and dynamics in fluids and plasmas. It is considered that turbulence acts as the energy source for particle acceleration[1] and energization in space plasmas[2]. Turbulence theory explains the injection of energy at larger length scales to the smaller length scales and at last, it is dissipated[3]–[6]. The cascading of energy is based on the wave-wave interaction[7], [8] and wave-particle interaction[9]. Magnetic reconnection is a basic energy conversion mechanism in which magnetic energy is transformed into plasma kinetic and thermal energy by rearranging magnetic topology. Magnetic reconnection plays a vital role in space and the astronomical plasmas like magnetopause[10], [11], solar-wind[12], magnetosphere, solar corona, and laboratory space-plasmas[13], [14]. Magnetic reconnection and turbulence are two interconnected processes[15], [16], but their relationship has not been fully understood so far now and a lot of research is going on to understand their interconnection.

Plasma supports numerous wave modes like whistler wave, lower hybrid wave (LHW), Alfven waves, magnetosonic waves, upper hybrid wave (UHW), and ion-acoustic wave (IAW) which have implications in energetics in space and laboratory plasmas[17]–[19]. Several astronomical phenomena can be explained by these different wave modes[20], [21]. At the magnetic reconnection sites, various waves including whistler-mode have been observed along with the energetic electron beam generation by magnetic reconnection[22], [23]. Whistler waves are significant in magnetic reconnection and turbulence, according to observation and simulation research. Whistler waves can be generated by lightning, electron beam[24]–[27], and current-driven plasma instabilities [28],[29]. An et al. [30] have examined the stimulation of

electrostatic beam-mode and whistler waves in a beam-plasma system and discovered that electrostatic beam-mode waves are contained within the beam, whereas whistler waves can escape the beam, carrying energy away with them. A lot of observations have been reported for the excitations of whistler waves by the electron beam in a magnetized plasma[28], [31], [32]. Furthermore, the wave-particle interaction of the whistler wave is vital in energizing the relativistic electrons[33], [34].

Many researchers have studied the whistler turbulence generation around magnetopause[35], [36]. THEMIS, POLAR, and Cluster spacecraft have also observed the whistler wave turbulence in magnetopause [37]–[39]. Many observations have been reported in the literature regarding the whistler turbulence[40]–[42]. Biskamp *et al.*[43] studied the 2D electron magnetohydrodynamics (EMHD) turbulence by numerical simulation and reported the power spectrum follow Kolmogorov scaling i.e, $E_k \sim k^{-5/3}$ for $k\lambda_e > 1$ and $k^{-7/3}$ for $k\lambda_e < 1$. Galtier *et al.*[44] presented the weak turbulence theory and conclude that nonlinear interactions of whistler waves transfer the energy. The recent studies observed the parallel propagating whistler waves[45], [46] and oblique whistler waves in different regions of magnetosphere[47]–[49]. Recently, Zhao et al.[50] have observed the whistler turbulence at magnetic reconnection sites and it is expected that energetic electron beams by magnetic reconnection are responsible for the generation of this whistler wave turbulence. They observed the beam-driven whistler waves in the dayside magnetosphere using the data of Magnetospheric Multiscale (MMS) mission[50], [51] and observed the maximum growth rate of the wave at $k\lambda_e \sim 0.53$ in the wave frequency range $0.1\omega_{ce} - 0.5\omega_{ce}$. Here, k is the wave number, λ_e is the electron skin-depth, and ω_{ce} is electron gyrofrequency. They also observed the whistler turbulence and presented the power spectra distributions of the electric and magnetic fields. But it is not clear how the beam energy generated by magnetic reconnection is used to excite the whistler wave from noise level and then reaches a turbulent state. The motivation of the present work is to understand this process of beam-driven whistler wave from noise and reaching to the turbulent state. In the literature, some work has been reported in the context of beam-driven turbulence but the specific studies related to beam-driven whistler localization and turbulence have not been reported to the best of our knowledge. In the context of solar wind, beam-driven upper hybrid turbulence[52] has been studied. Krafft *et al.*[53] have studied the coupled dynamics of parallel propagating (propagation wave vector along static

magnetic field) whistler wave and low-frequency wave and observed the different aspects of modulational instabilities and whistler solitions. Krafft *et al.*[32] have observed the evolution

of the beam-whistler wave system but turbulence and turbulence scaling have not been studied. Goldman *et al.*[54] have studied the localization and turbulence of the Langmuir wave by using the 1-D Vlasov simulation code. In a beam-plasma system, observations of filamentary structure and strong turbulence for the electron cyclotron wave are reported[55]. Recently, Choi *et al.*[56] have observed the whistler waves using the fast Fourier transform, analyzed the electron velocity distribution function, and shows strong electrostatic fluctuations.

In this present work, we have proposed a model in which beam-driven whistler wave will grow from the noise level due to the energy of the beam and will attain a large amplitude such that nonlinear effects due to ponderomotive force will lead to the localization of whistler waves and finally this will lead to the turbulent state. For understanding the nonlinear stage of the wave growth and the saturation, we consider the nonlinear interaction of a high-frequency whistler wave with a low-frequency IAW, taking into account the ponderomotive nonlinearity due to the whistler wave. Using the Two-fluid approach, nonlinear dynamical equations have been derived. Additionally, to solve the model equations, numerical simulation is used, with the pseudo-spectrum technique for spatial integration and the finite difference method for temporal integration. Further, for a better understanding of the physics behind whistler wave localization, a semianalytical model has been developed. Also, this simplified model has been investigated for the whistler's convergent and divergent behaviour. The outcomes of the numerical simulation of the coupled system are shown here. These results show the localization of whistler waves and spectra of turbulence applicable to the magnetopause regime, which is consistent with the observations[50]. The formation of the filamentary structure indicates the generation of turbulence.

The following is the layout of the paper: -

In section II, the Basic formulation of the model is presented. In section III, model equations are solved numerically and simulation results are presented. A semianalytical method is presented in section IV. Summary and conclusion have been given in section V.

2.2 Model Equations

Taking background density variations into consideration, the suggested theoretical model explains whistler turbulence in plasma at magnetopause. Whistler turbulence caused by electron beams has been assumed to be well-developed in this study. The model accounts for

density fluctuations, plasma response at high and low frequencies, fast and slow wave dynamics, as well as other nonlinear and linear processes such as ponderomotive force effects and wave coupling.

The analysis that follows is divided into two parts. The dynamical equation for a high-frequency wave, such as a whistler wave, is first obtained. The dynamics of the low-frequency ion acoustic wave and its connection with the whistler wave are covered in the second half. The two-dimensional whistler wave system with electron beam is described by using the two-fluid model where the beam-driven whistler with positive in our computational reasons. As a result, an instability growth rate $\gamma' > 0$ is introduced phenomenologically in the dynamics of whistler.

2.2.1 Whistler dynamics in presence of beam

Two fluid models are used to obtain the dynamical equation for whistler wave (2D plane) propagating in the $x-z$ plane with wave vector $\vec{k} = k_x\hat{x} + k_z\hat{z}$, in a magnetized plasma with an ambient magnetic field along the z-axis.

The basic equations that are used to obtain the whistler dynamics are

Wave equation

$$\nabla^2\vec{E} - \nabla(\nabla.\vec{E}) = \frac{4\pi}{c^2}\frac{\partial\vec{J}}{\partial t} + \frac{1}{c^2}\frac{\partial^2\vec{E}}{\partial t^2}. \qquad (2.1)$$

Equation of motion for electrons

$$m_e\left[\frac{\partial\vec{v}_e}{\partial t} + (\vec{v}_e.\nabla\vec{v}_e)\right] = -e\vec{E} - \frac{e}{c}(\vec{v}_e \times \vec{B}_0). \qquad (2.2)$$

Equation of motion for ions

$$m_i\left[\frac{\partial\vec{v}_i}{\partial t} + (\vec{v}_i.\nabla\vec{v}_i)\right] = e\vec{E} + \frac{e}{c}(\vec{v}_i \times \vec{B}_0), \qquad (2.3)$$

where m_e, m_i denotes the mass of an electron and ion, v_e, v_i denotes the velocity of the electron and ion, e denotes the charge on the electron, and B_0 denotes the background magnetic field.

Using Eqs. (2.2) and (2.3), velocity components are obtained, and then $\vec{J} = n_i e\vec{v}_i - n_e e v_e$, we can find the components of Eq. (2.1):

x-component

$$\left(-k_z^2 + \frac{\omega_0^2}{(\omega_{ci}^2-\omega_0^2)\lambda_i^2} + \frac{\omega_0^2}{(\omega_{ce}^2-\omega_0^2)\lambda_e^2} + \frac{\omega_0^2}{c^2}\right)E_x + \left(\frac{i\omega_0\omega_{ci}}{(\omega_{ci}^2-\omega_0^2)\lambda_i^2} - \frac{i\omega_0\omega_{ce}}{(\omega_{ce}^2-\omega_0^2)\lambda_e^2}\right)E_y + k_x k_z E_z = 0. \quad (2.4)$$

y-component

$$\left(\frac{-i\omega_0\omega_{ci}}{(\omega_{ci}^2-\omega_0^2)\lambda_i^2} + \frac{i\omega_0\omega_{ce}}{(\omega_{ce}^2-\omega_0^2)\lambda_e^2}\right)E_x + \left(-k_x^2 - k_z^2 + \frac{\omega_0^2}{(\omega_{ci}^2-\omega_0^2)\lambda_i^2} + \frac{\omega_0^2}{(\omega_{ce}^2-\omega_0^2)\lambda_e^2} + \frac{\omega_0^2}{c^2}\right)E_y = 0. \quad (2.5)$$

z-component

$$(k_x k_z)E_x + \left(-k_x^2 + \frac{\omega_0^2}{c^2} - \frac{1}{\lambda_e^2}\right)E_z = 0. \quad (2.6)$$

where $\omega_{ce}\left(=\frac{eB_0}{m_e c}\right)$ is the electron gyrofrequency of wave and $\lambda_e\left(=\sqrt{\frac{c^2 m_e}{4\pi n_0 e^2}}\right)$ is the collisionless electron skin depth, n_0 is the background number density and c is the velocity of light.

Now, Combining Eqs. (2.4), (2.5), and (2.6) and applying conditions $k\lambda_i \gg 1$, we get

$$-\left(-k_z^2 - \frac{1}{\lambda_i^2} + \frac{\omega_0^2}{\lambda_e^2(\omega_{ce}^2-\omega_0^2)}\right)\left(-k^2 + \frac{\omega_0^2}{\lambda_e^2(\omega_{ce}^2-\omega_0^2)}\right)\left(k_x^2 + \frac{1}{\lambda_e^2}\right)E_x + \left(\frac{-i\omega_{ci}}{\omega_0\lambda_i^2} - \frac{i\omega_0\omega_{ce}}{\lambda_e^2(\omega_{ce}^2-\omega_0^2)}\right)\left(\frac{i\omega_{ci}}{\omega_0\lambda_i^2} + \frac{i\omega_0\omega_{ce}}{\lambda_e^2(\omega_{ce}^2-\omega_0^2)}\right)\left(k_x^2 + \frac{1}{\lambda_e^2}\right)E_x - \left(-k^2 + \frac{\omega_0^2}{\lambda_e^2(\omega_{ce}^2-\omega_0^2)}\right)k_x^2 k_z^2 E_x = 0 \quad (2.7)$$

After solving Eq. (2.7), we obtain the following equation

$$\left(\omega_0^2-\omega_{ce}^2\right)\left[\omega_0^2(1+k^2\lambda_e^2)^2-k^2k_z^2\lambda_i^2v_A^2\right]E_x=0. \tag{2.8}$$

The first component is non-resonant, while the whistler wave dispersion relation is the final term.

$$\left[\omega_0^2(1+k^2\lambda_e^2)^2-k^2k_z^2\lambda_i^2v_A^2\right]=0. \tag{2.9}$$

Further, the dynamical Equation in terms of the electric field (please see appendix-A) can be written as,

$$\begin{aligned}&-\frac{\partial^2E_x}{\partial t^2}-\lambda_e^4\frac{\partial^6E_x}{\partial x^4\partial t^2}-\lambda_e^4\frac{\partial^6E_x}{\partial z^4\partial t^2}-2\lambda_e^4\frac{\partial^6E_x}{\partial x^2\partial z^2\partial t^2}\\&\quad+2\lambda_e^2\frac{\partial^4E_x}{\partial x^2\partial t^2}+2\lambda_e^2\frac{\partial^4E_x}{\partial z^2\partial t^2}=\lambda_i^2\left(\frac{B_0^2}{4\pi n_0m_i}\right)\left(\frac{\partial^4E_x}{\partial z^2\partial x^2}+\frac{\partial^4E_x}{\partial z^4}\right),\end{aligned} \tag{2.10}$$

where $v_A\left(=\sqrt{\frac{B_0^2}{4\pi n_0m_i}}\right)$ is the speed of the Alfven waves. It is also mentioned here that beam driven growth is also considered then $\frac{d}{dt}\rightarrow\left(\frac{d}{dt}+\gamma\right)$, (for detailed explanation please see appendix-A and neglecting higher order terms).

After getting perturbation in the background number density from n_0 to n', the above equation becomes

$$\begin{aligned}&-\left(\frac{\partial^2}{\partial t^2}+2\gamma\frac{\partial}{\partial t}\right)E_x-\lambda_e^4\frac{\partial^6E_x}{\partial x^4\partial t^2}-\lambda_e^4\frac{\partial^6E_x}{\partial z^4\partial t^2}-2\lambda_e^4\frac{\partial^6E_x}{\partial x^2\partial z^2\partial t^2}\\&\quad+2\lambda_e^2\frac{\partial^4E_x}{\partial x^2\partial t^2}+2\lambda_e^2\frac{\partial^4E_x}{\partial z^2\partial t^2}=\lambda_i^2\left(\frac{B_0^2}{4\pi n'm_i}\right)\left(\frac{\partial^4E_x}{\partial z^2\partial x^2}+\frac{\partial^4E_x}{\partial z^4}\right),\end{aligned} \tag{2.11}$$

Here n' is the modified density, i.e., $n'=n_0+\delta n$, and δn is the modification in number density. Thus we can rewrite the above equation

$$\begin{aligned}&-\left(\frac{\partial^2}{\partial t^2}+2\gamma\frac{\partial}{\partial t}\right)E_x-\lambda_e^4\frac{\partial^6E_x}{\partial x^4\partial t^2}-\lambda_e^4\frac{\partial^6E_x}{\partial z^4\partial t^2}-2\lambda_e^4\frac{\partial^6E_x}{\partial x^2\partial z^2\partial t^2}\\&\quad+2\lambda_e^2\frac{\partial^4E_x}{\partial x^2\partial t^2}+2\lambda_e^2\frac{\partial^4E_x}{\partial z^2\partial t^2}=\lambda_i^2v_A^2\left(1-\frac{\delta n}{n_0}\right)\left(\frac{\partial^4E_x}{\partial z^2\partial x^2}+\frac{\partial^4E_x}{\partial z^4}\right).\end{aligned} \tag{2.12}$$

For this Eq. (2.12), the following envelope solution is assumed.

$$\tilde{E}_x=E_x(x,z,t)e^{i(k_{0x}\hat{x}+k_{0z}\hat{z}-\omega_0t)}. \tag{2.13}$$

We get the dynamical equation of a nonlinear whistler wave propagating through plasma by considering the effect of a strong whistler wave on the background density and inserting the above-mentioned solution into Eq. (2.12)

$$2i\omega_0(1+\lambda_e^4k_{0x}^4+\lambda_e^4k_{0z}^4+2\lambda_e^2k_{0x}^2+2\lambda_e^2k_{0z}^2)\frac{\partial E_x}{\partial t}+(-4\omega_0^2\lambda_e^4k_{0x}^2)\frac{\partial^2E_x}{\partial x^2}+(4\lambda_i^2v_A^2k_{0z}^2-4\omega_0^2\lambda_e^4k_{0z}^2)\frac{\partial^2E_x}{\partial z^2}+$$
$$2i(-2\omega_0^2k_{0x}^3\lambda_e^4+2\omega_0^2k_{0x}k_{0z}^2\lambda_e^4+2\omega_0^2\lambda_e^2k_{0x}+k_{0x}k_{0z}^2\lambda_i^2v_A^2)\frac{\partial E_x}{\partial x}+2i(-2\omega_0^2k_{0z}^3\lambda_e^4+2\omega_0^2k_{0z}k_{0x}^2\lambda_e^4$$
$$+2\omega_0^2\lambda_e^2k_{0z}+k_{0z}k_{0x}^2\lambda_i^2v_A^2+2k_{0z}^3\lambda_i^2v_A^2)\frac{\partial E_x}{\partial z}+(4\lambda_i^2v_A^2k_{0x}k_{0z}-8\omega_0^2k_{0z}k_{0x}\lambda_e^4)\frac{\partial^2E_x}{\partial x\partial z}+ \quad (2.14)$$
$$(9\lambda_i^2v_A^2k^2k_{0z}^2)\frac{\delta n}{n_0}E_x+2i\gamma' E_x=0\,,$$

where k_{0x}, k_{0z} are whistler wave vector components related to the background magnetic field are given below.

$k_0^2=k_{0x}^2+k_{0z}^2$ and λ_e, λ_i are the skin depth of electrons and ions.

Using the normalizing parameter,

$t_n=1/\omega_0$.

$$x_n=\frac{2i(-2\omega_0^2k_{0x}^3\lambda_e^4+2\omega_0^2k_{0x}k_{0z}^2\lambda_e^4+2\omega_0^2\lambda_e^2k_{0x}+k_{0x}k_{0z}^2\lambda_i^2v_A^2)}{2\omega_0(1+\lambda_e^4k_{0x}^4+\lambda_e^4k_{0z}^4+2\lambda_e^2k_{0x}^2+2\lambda_e^2k_{0z}^2)}.$$

$$z_n=\frac{2i(-2\omega_0^2k_{0x}^3\lambda_e^4+2\omega_0^2k_{0x}k_{0z}^2\lambda_e^4+2\omega_0^2\lambda_e^2k_{0x}+k_{0x}k_{0z}^2\lambda_i^2v_A^2+2k_{0z}^3\lambda_i^2v_A^2)}{2\omega_0(1+\lambda_e^4k_{0x}^4+\lambda_e^4k_{0z}^4+2\lambda_e^2k_{0x}^2+2\lambda_e^2k_{0z}^2)}.$$

Thus, the equation in normalized dimensionless form is given as

$$i\frac{\partial E'}{\partial t'}+c_1\frac{\partial^2E'}{\partial x'^2}+c_2\frac{\partial^2E'}{\partial z'^2}+i\frac{\partial E'}{\partial x'}+i\frac{\partial E'}{\partial z'}+c_3\frac{\partial^2E'}{\partial x'\partial z'}+c_4\left(\frac{\delta n}{n_0}\right)E'+2i\gamma' E'=0, \quad (2.15)$$

where Eq. (2.15) represents the normalized dynamical equation for the whistler wave which leads to turbulence. Here γ' is introduced to describe the beam instability driving the beam-driven whistler wave. The growth rate of the beam-driven whistler i.e., $\gamma'>0$ is incorporated phenomenologically and its value consistent with the observations reported by Zhao *et al.*[50] will be used in simulations here.

where $c_1=\dfrac{-4\omega_0^2\lambda_e^4k_{0x}^2}{2\omega_0(1+\lambda_e^4k_{0x}^4+\lambda_e^4k_{0z}^4+2\lambda_e^2k_{0x}^2+2\lambda_e^2k_{0z}^2)x_n^2}$.

$$c_2 = \frac{(4\lambda_i^2 v_A^2 k_{0z}^2 - 4\omega_0^2 \lambda_e^4 k_{0z}^2)}{2\omega_0(1+\lambda_e^4 k_{0x}^4 + \lambda_e^4 k_{0z}^4 + 2\lambda_e^2 k_{0x}^2 + 2\lambda_e^2 k_{0z}^2) z_n^2}.$$

$$c_3 = \frac{(4\lambda_i^2 v_A^2 k_{0x} k_{0z} - 8\omega^2 k_{0z} k_{0z} \lambda_e^4)}{2\omega_0(1+\lambda_e^4 k_{0x}^4 + \lambda_e^4 k_{0z}^4 + 2\lambda_e^2 k_{0x}^2 + 2\lambda_e^2 k_{0z}^2) z_n x_n}.$$

$$c_4 = \frac{9\lambda_i^2 v_A^2 k^2 k_{0z}^2}{2\omega_0(1+\lambda_e^4 k_{0x}^4 + \lambda_e^4 k_{0z}^4 + 2\lambda_e^2 k_{0x}^2 + 2\lambda_e^2 k_{0z}^2)}.$$

and $\gamma' = \frac{\gamma}{\omega_0}$ is the normalized growth rate.

$\gamma (= 0.5083\omega_{ce})$ is the growth rate of beam-driven whistler waves.

2.2.2 Ion Acoustic wave (IAW)

Consider a low-frequency ion-acoustic wave propagating parallel to the background magnetic field B_0 along the z-axis i.e., $\vec{B}_0 = B_0\hat{z}$, $\vec{k} = k_z\hat{z}$. The basic equations that are used to obtain the IAW dynamics are:

The equation of motion

$$m_j \frac{\partial \vec{v}_j}{\partial t} = q_j \vec{E} + \frac{q_j}{c}(\vec{v}_j \times \vec{B}_0) - T_j \vec{\nabla}\frac{n_j}{n_0} + \vec{F}_j, \qquad (2.16)$$

The continuity equation

$$\frac{\partial n_j}{\partial t} + \vec{\nabla}.(n_j \vec{v}_j) = 0, \qquad (2.17)$$

where v_j is the velocity of the species (j represents e for electrons and i for ions) of IAW and F_j is the ponderomotive force of the high-frequency whistler wave.

When we take the parallel component of the linearized form of Eq. (2.16) for the ions and assume, the quasi-neutrality along with the response of electrons, we get

$$\frac{\partial v_{iz}}{\partial t} = -\frac{c_s^2}{n_0}\frac{\partial n_i}{\partial z} + \left(\frac{F_{iz} + F_{ez}}{m_i}\right), \qquad (2.18)$$

where $c_s\left(=\frac{k_B(T_e+T_i)}{m_i}\right)^{1/2}$ is the speed of IAW, k_B is the Boltzmann Constant. T_e, T_i are the temperature of electron and ion, respectively. F_{ez} (F_{iz}) is the component of ponderomotive force in *z*-direction produced by whistler wave.

Differentiating Eq. (2.17) w.r.t to time again, we get

$$\frac{\partial^2 n_i}{\partial t^2}+n_0\frac{\partial^2 v_{iz}}{\partial t\partial z}=0. \tag{2.19}$$

Combining Eq. (2.18) and (2.19), we obtain the nonlinear dynamical equation of IAW

$$\frac{\partial^2 n}{\partial t^2}=-n_0\frac{\partial}{\partial z}\left[-c_s^2\frac{\partial}{\partial z}\left(\frac{n}{n_0}\right)+\frac{F_{ez}+F_{iz}}{m_i}\right]. \tag{2.20}$$

Equation (2.20) can be rewritten as

$$\left(\frac{\partial^2 n}{\partial t^2}-c_s^2\frac{\partial^2}{\partial z^2}\right)\left(\frac{n}{n_0}\right)=-\frac{\partial}{\partial z}\left[\frac{F_{ez}+F_{iz}}{m_i}\right]. \tag{2.21}$$

Now, the Ponderomotive force of the whistler wave is defined as

$$\vec{F}_j=-m_j(\vec{v}_j*.\vec{\nabla})\vec{v}_j+\frac{q_j}{c}(\vec{v}_j*\times B_w). \tag{2.22}$$

Here 'j' denote the charged species i.e., electron and ion. Thus m_j, v_j and q_j are the mass, velocity, and charge of the electron and ion, respectively. c is the speed of light and B_w is the magnetic field due to the whistler wave.

The velocity component of the whistler wave due to electron can be written as

$$v_{e1x}=\frac{-ie\omega_0}{m_e(\omega_0^2-\omega_{ce}^2)}E_x-\frac{e\omega_{ce}}{m_e(\omega_0^2-\omega_{ce}^2)}E_y. \tag{2.23}$$

$$v_{e1y}=\frac{e\omega_{ce}}{m_e(\omega_0^2-\omega_{ce}^2)}E_x-\frac{ie\omega_0}{m_e(\omega_0^2-\omega_{ce}^2)}E_y. \tag{2.24}$$

$$v_{e1z}=\frac{eE_z}{im_e\omega_0}. \tag{2.25}$$

Similarly, the velocity component of the whistler wave due to ion can be written as

$$v_{i1x} = \frac{ie\omega_0}{m_i(\omega_0^2 - \omega_{ci}^2)} E_x - \frac{e\omega_{ci}}{m_i(\omega_0^2 - \omega_{ci}^2)} E_y. \tag{2.26}$$

$$v_{i1y} = \frac{e\omega_{ci}}{m_i(\omega_0^2 - \omega_{ci}^2)} E_x + \frac{ie\omega_0}{m_i(\omega_0^2 - \omega_{ci}^2)} E_y. \tag{2.27}$$

$$v_{i1z} = \frac{-eE_z}{im_i\omega_0}. \tag{2.28}$$

Obtaining the ponderomotive force components owing to whistler wave by substituting the value of whistler wave velocity components in Eq. (2.22).

$$F_{ez} = -\left[\begin{array}{l}\left(\frac{e^2}{m_e m_i(\omega_0^2 - \omega_{ce}^2)} \frac{\partial^2}{\partial z^2}|E_x|^2\right) + \left(\frac{2e^2\omega_{ce}^2}{m_e m_i(\omega_0^2 - \omega_{ce}^2)} \frac{\partial^2}{\partial z^2}|E_x|^2\right) \\ + \left(\frac{e^2\omega_0^2\omega_{ce}^2}{m_e m_i(\omega_0^2 - \omega_{ce}^2)\alpha_1^2} \frac{\partial^2}{\partial z^2}|E_x|^2\right)\end{array}\right], \tag{2.29}$$

$$F_{iz} = \left(\frac{e^2}{m_e m_i \omega_0^2} \frac{\partial^2}{\partial z^2}|E_x|^2\right) + \left(\frac{3e^2\omega_{ci}^2}{m_e m_i \omega_0^2} \frac{\partial^2}{\partial z^2}|E_x|^2\right), \tag{2.30}$$

where $\alpha_1 = -k_z^2\lambda_e^2(\omega_0^2 - \omega_{ce}^2) - \omega_0^2$.

To obtain the dynamical equation of IAW, substitute the value of F_{ez} and F_{iz} in Eq. (2.21),

$$\left(\frac{\partial^2}{\partial t^2} - c_s^2 \frac{\partial^2}{\partial z^2}\right)\left(\frac{n}{n_0}\right) = -\frac{e^2(\alpha_1^2 + 2\alpha_1\omega_{ce}^2 + \omega_0^2\omega_{ce}^2)}{m_e m_i(\omega_0^2 - \omega_{ce}^2)\alpha_1^2} \frac{\partial^2}{\partial z^2}|E_x|^2 + \left(\frac{e^2}{m_e m_i \omega_0^2} \frac{\partial^2}{\partial z^2}|E_x|^2\right) + \left(\frac{3e^2\omega_{ci}^2}{m_e m_i \omega_0^2} \frac{\partial^2}{\partial z^2}|E_x|^2\right). \tag{2.31}$$

This is the non-linear dynamics of IAW.

We may obtain the normalized dimensionless equation of IAW by using the normalized parameter as in whistler wave dynamics,

$$\left(\frac{\partial^2}{\partial t^2} - c_5 \frac{\partial^2}{\partial z^2}\right)\left(\frac{n}{n_0}\right) = -c_6 \frac{\partial^2}{\partial z^2}|E_x|^2, \tag{2.32}$$

where $c_5 = c_s^2 \frac{t_n^2}{z_n^2}$.

and $c_6 = -\left(\frac{\omega^2(\alpha_1^2 + 2\alpha_1\omega_{ce}^2 + \omega_0^2\omega_{ce}^2) + (1+3\omega_{ci}^2)(\omega_0^2 - \omega_{ce}^2)\alpha_1^2}{m_e m_i(\omega_0^2 - \omega_{ce}^2)\alpha_1^2 t_n^2 \omega_0^2} \right) n_0 e^2 z_n^2.$

when we take the adiabatic response then Eq. (2.32) reduces to

$$\frac{n}{n_0} = \frac{c_6}{c_5}|E_x|^2. \qquad (2.33)$$

Using the normalized electric field, we obtained

$$E_n = \left[\frac{c_s^2 m_e m_i(\omega_0^2 - \omega_{ce}^2)\alpha_1^2 t_n^2 \omega_0^2}{n_0 e^2 \left\{(\alpha_1^2 + 2\alpha_1\omega_{ce}^2 + \omega_0^2\omega_{ce}^2) + (1+3\omega_{ci}^2)(\omega_0^2 - \omega_{ce}^2)\alpha_1^2\right\} z_n^2} \right]^{\frac{1}{2}},$$

Now Eq. (2.15) becomes

$$i\frac{\partial E'}{\partial t'} + c_1\frac{\partial^2 E'}{\partial x'^2} + c_2\frac{\partial^2 E'}{\partial z'^2} + i\frac{\partial E'}{\partial x'} + i\frac{\partial E'}{\partial z'} + c_3\frac{\partial^2 E'}{\partial x' \partial z'} + \frac{c_4 c_6}{c_5}|E|^2 E' + 2i\gamma' E' = 0. \qquad (2.34)$$

2.3 Numerical Simulation

To study the nonlinear dynamics of whistler, we have

(i) MNLS (Modified Nonlinear Schrödinger Equation) model by studying Eq. (2.34).

(ii) Modified Zakharov System of Equations (MZSE) by studying Eq. (2.15) and Eq. (2.32).

The pseudo-spectral approach was used to solve these normalized dimensionless equations. For the temporal evolution, a finite difference approach with a step size is also used $\Delta t = 5\times10^{-5}$ (Step size is normalized by $t_n = 6.4\times10^{-4}$ sec). Equations have been solved in the periodic domain $(10\pi\times10\pi)$ using the grid size (512×512) but in very special cases it is (4096×4096) also.

To solve these equations numerically, the imposed initial condition is:

$$E_x(x,z) = a_0(1+\beta\cos(\alpha_x x))(1+\beta\cos(\alpha_z z)). \qquad (2.35)$$

Here, $a_0 = 0.5$ is the initial amplitude of the whistler wave and $\beta = 0.1$ is the magnitude of the perturbed electric field. The perturbation in wave-number $\alpha_x = 0.2,\ \alpha_z = 0.2$.

To begin, the algorithm's accuracy was tested by translating the model equation into the nonlinear Schrödinger equation (NLS) and the plasmon number's consistency i.e., $N = \sum_k |E_k|^2$. This is conserved with an accuracy of the sixth decimal place.

The parameters used for this numerical simulation are-

$B_0 = 45nT$, $n_0 = 21cm^{-3}$, $T_e = 4.2\times10^5 K$, $\omega_{ce} = 7.9\times10^3 rad\ \sec^{-1}$, $\omega_0 = 0.2\omega_{ce}$, $\lambda_e = 1.16\times10^5 cm$, $k\lambda_e = 0.5$, $k_{0x} = 2.98\times10^{-6} cm^{-1}$, $k_{0z} = 1.72\times10^{-6} cm^{-1}$, $x_n = 0.9\lambda_e$, $z_n = 1.32\lambda_e$, $t_n = \omega_0^{-1}$.

From these parameters, we obtain $c_1 = -0.2681$, $c_2 = 1.0080$, $c_3 = 2.4398$, $c_4 = 1.1698$, $c_5 = 1.5413\times10^5$, $c_6 = 5.4\times10^5$.

2.3.1 MNLS model

For this, numerical simulation was carried out for Eq. (2.34). The outcomes of nonlinear temporal evolution are discussed here. The development of localized structures and corresponding fluctuations have been studied. The energy is initially limited within the whistler wave, but over time, nonlinear structures emerge. As time passes, intense localization occurs, resulting in a chaotic structure that is distributed in the $x-z$ plane. The ratio of magnetic fluctuation to the background magnetic field in the whistler turbulence is 0.0382. Figure 2.1 shows the electric field intensity patterns of the whistler wave. In fig. 2.1(a), whistler temporal evolution has been studied using snapshots taken at different times at grid size 512×512. With time, the intensity of the electric field grows in the initial phase due to pumped whistler wave. When the amplitude of the whistler becomes large, the ponderomotive force due to the whistler becomes appreciable and coupling with low frequency starts operative. Therefore, background density modification takes place. This leads to nonlinear dynamics of whistler waves and its localized structure formation process starts. This process continues and these structures interact with each other to form sub-localized randomly distributed structures.

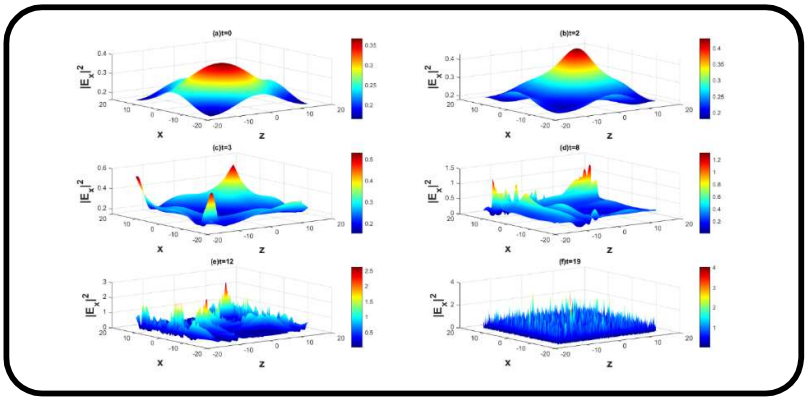

Figure 2.1 The evolution of the electric field $|E_x(x,z)|^2$ at different times in the x-z plane for modified nonlinear schrödinger equation (in normalized units).

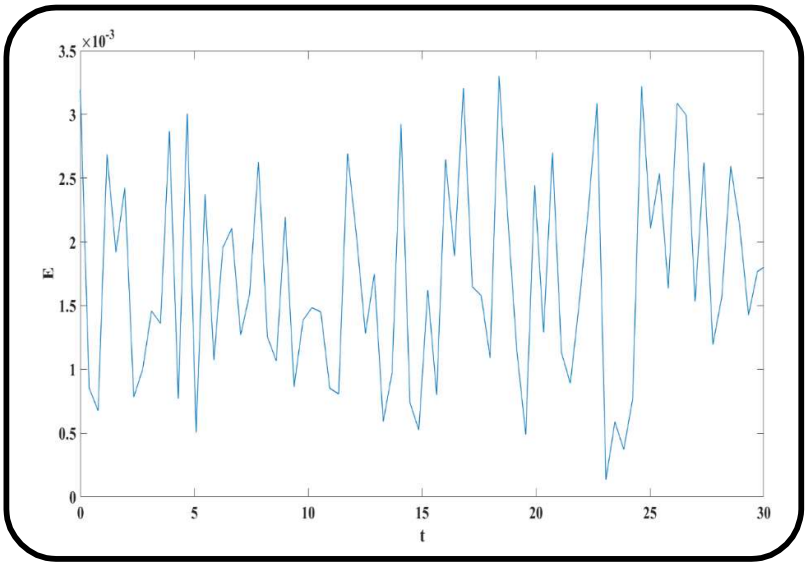

Figure 2.2 Electric Field v/s time for modified nonlinear schrödinger equation (in normalized units).

Figure 2.2 depicts the evolution of the electric field over time. Here, electric field and time are in dimensionless units $E_n = 7.9\times10^{-8}$ StatV/cm, $t_n = 6.3\times10^{-4}$ sec). It can be seen that the behaviour of the electric field is turbulent. It is observed that the peak value of whistler fluctuations is of the order of 3 (mV/m) for the present parameters. In fig. 2.3, we have presented the Fourier transform of whistler field with frequency by using the data of simulation as presented in fig. 2.2. It is obvious from fig. 2.3, that turbulence exists in the range of frequency from $0.1f_{ce}$ to $0.5f_{ce}$ and the main power is still near pump whistler frequency but several peaks also present which are having power in the turbulence stage. Therefore, our outcomes have a close relationship with those observed by Zhao *et al.*[50] as mentioned below:

1) It is to be noted that Zhao *et al.*[50] have also observed the whistler turbulence in the magnetic reconnection region generated by electron beam and reported that solitary waves exist (parallel electric field). In our case also we observed the localized structures

in Fig. 2.1 (Here we have converted all the components of electric field in terms of E_x by using their linear relationship).

2) They also observed the maximum amplitude of whistler fluctuations is of the order of 3.5 (mV/m) and in our case also, observed the maximum amplitude of whistler electric field of the order of 3 (mV/m) [see Fig. 2.1] which is quite nearly to the observations of Zhao *et al.*[50].

3) Zhao *et al.*[50] also studied the electric power spectra distribution (PSD) of whistler waves as presented in their figure 6(c). It shows the maximum power spectra distribution (PSD) nearby whistler frequency $\sim 0.2 f_{ce}$ (as observed by us in Fig. 2.3 of present paper). Moreover, it is clear from the fig. 2.3 that all the intense peaks of electric field fluctuation occur in the range $0.1 f_{ce} - 0.5 f_{ce}$ as reported by Zhao *et al*.[50]

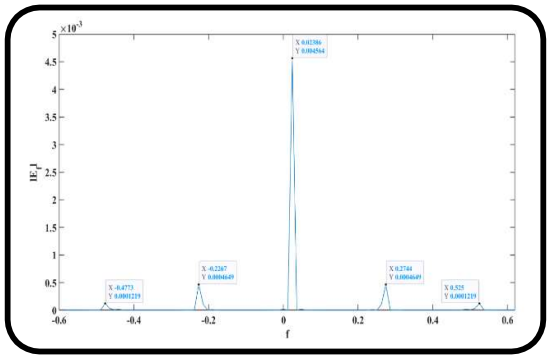

Figure 2.3 FFT plot of electric field against frequency for modified nonlinear schrödinger equation (in normalized units).

2.3.2 Modified Zakharov System of Equations (MZSE)

In this model, two coupled independent Eqs. (2.15) and (2.32) are solved. The modified density in whistler dynamics is due to density perturbation in IAW as a result of high amplitude whistler wave ponderomotive force. Whistler waves have nonlinear effects that may lead to localization. Numerical simulation was carried out for this coupled normalized dimensionless equation. The electric field intensity patterns owing to the whistler wave are depicted in Fig. 2.4. We have taken different times to illustrate the localized structure formation.

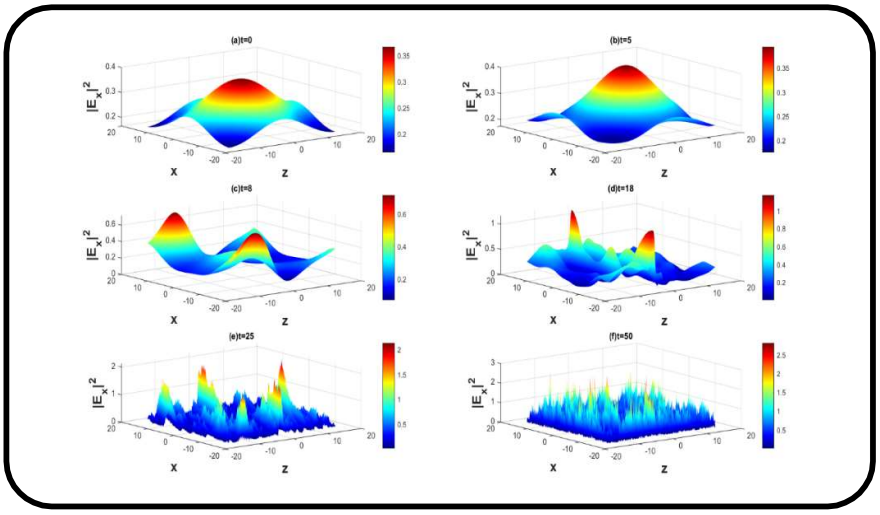

Figure 2.4 The evolution of the electric field $|E_x(x,z)|^2$ ***at different times in the x-z plane for modified Zakharov equation (in normalized units).***

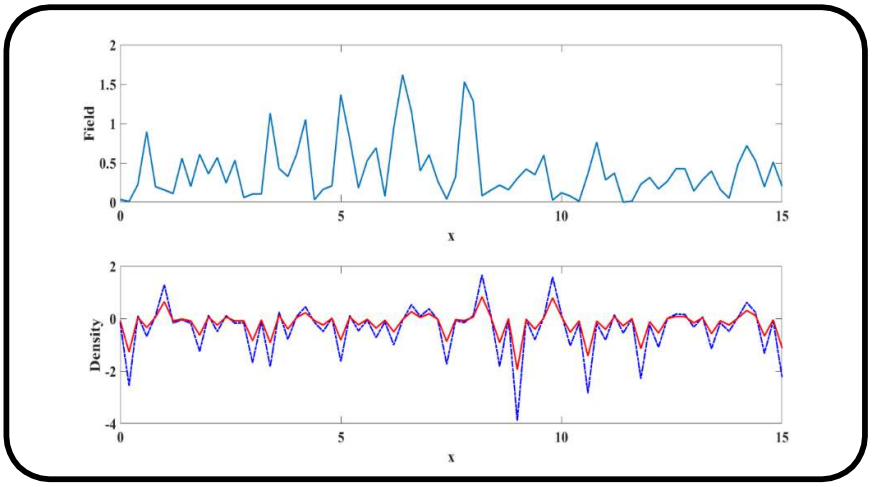

Figure 2.5 Electric field fluctuations and density fluctuations for modified Zakharov equation at T=50.

Fig. 2.5 depicts the electric field amplitude variation and density fluctuations for the modified Zakharov equations. As a result of ponderomotive force, electric field is trapped in the region of density cavity. The top panel of the Fig. 2.5 shows the electric fluctuations for the modified Zakharov equations and the bottom panel is for density fluctuations (density cavitation and humps) for MZSE and MNLS (red dotted line for MNLS and solid blue line for MZSE). From this Fig. 2.5, we see that MZSE has a slightly different value of density than MNLS as expected. It is to be mentioned that density fluctuations for MNLS have been plotted by using eq. (2.33). Turbulence can be studied by cascading of energy and cavitation process using ZSE as done by Doolen *et al.*[57]. They predict the formation of localization Langmuir states (cavitons) that are trapped in density depletions (cavities) by Zakharov system of equations (ZSE). Nicholson *et al.*[58] studied the turbulence by NLS and ZSE, in which electric field evolves via modulational instability and finally saturates into a set of solitons. Sharma *et al.*[59] also

studied the Langmuir turbulence in ionosphere by cascading of energy and cavitation process by Zakharov-Boussinesq system of equations (ZBSE) and Zakharov system of equations (ZSE). In our present model also, turbulence is generated by cavitation and renucleation process by using MNLS constituted by high-frequency whistler wave and low-frequency ion acoustic wave. Although we have shown that turbulence by localization plots (see Fig. 2.1), FFT of electric field versus time (Fig. 2.3), in addition to these we have plotted a wavenumber spectrum on grid size (512×512) for modified nonlinear Schrodinger equation and modified Zakharov equations averaged between T= 49-60 and at T=40-50, respectively as shown in Fig. 2.6 and fig 2.7.

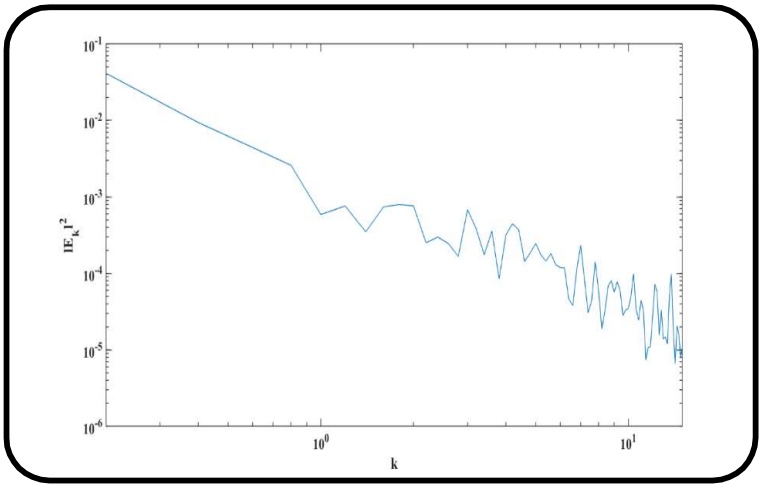

Figure 2.6 Power spectra of Electric field intensity of whistler wave $|E_k|^2$ against normalized wave vector k for modified nonlinear schrödinger equation (in normalized units).

In the present study, constant growth rate of beam-driven mode has been considered and, the quasi-steady state has not been achieved at this time and will not be achieved for further time also.

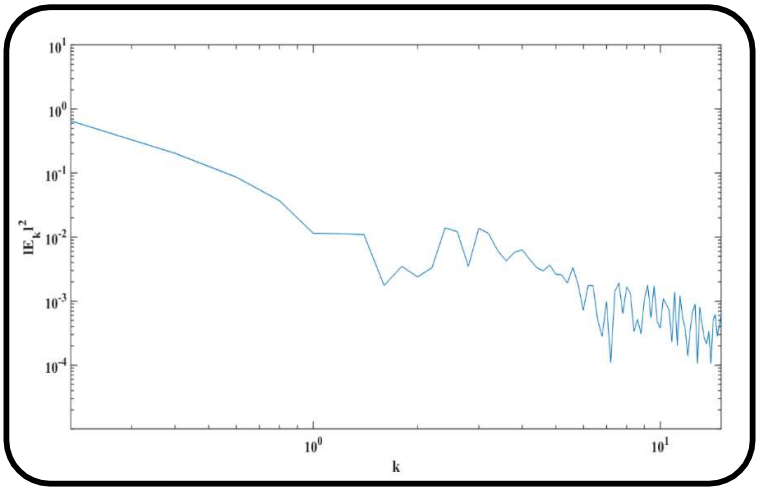

Figure 2.7 Power spectra of Electric field intensity of whistler wave $|E_k|^2$ against normalized wave vector k for modified Zakharov equation (in normalized units).

Therefore, the question of discussing power spectra doesn't arise but we are planning to overcome this shortcoming of the model in future by considering the growth rate whistler-intensity dependent (instead of taking growth rate constant). However, to visualize the turbulent spectra, when amplitude of the whistler wave is large enough, we switch off the growth rate of beam-driven

mode. Then, remodelling Eq. (2.34) into one-dimensional model, we obtain the following equation-

$$i\frac{\partial E'}{\partial t'}+c_2\frac{\partial^2 E'}{\partial z'^2}+i\frac{\partial E'}{\partial z'}+\frac{c_6c_4}{c_5}|E|^2E'=0. \qquad (2.36)$$

The Eq. (2.36) is simulated for grid size (512×512) to (4096×4096). Fig 2.7 & fig 2.8 depicts the power spectrum. The actual power spectrum in the present study is shown by a solid curve and we just give the scaling reference line with red (for -5/3 scaling) (as reported in literature). In this figure, we also get steeper spectra which can't be compared to Biskamp *et al.*[43] scaling because we are not considering the dissipation range, as viscosity and damping are not included. It will be more regressive in future work where dissipation range is taken into account in whistler propagation. By using the general dimensional argument of Kolmogorov-Obokhov[60],

$$[\varepsilon]=\left[\frac{u^2}{t}\right]=\frac{l^2}{t^3}$$

$$[E^{(1D)}]=\left[\frac{u^2}{k}\right]=\frac{l^3}{t^2}$$

where ε is the energy dissipation rate and E is the total energy. When we equate these two terms, we can obtain the correct scaling of $E^{(1D)}\propto k^{-5/3}$.

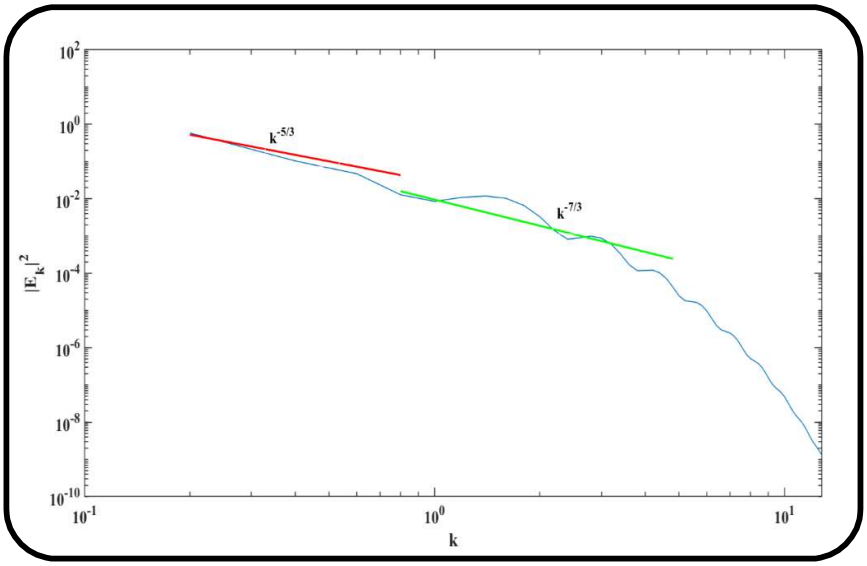

Figure 2.8 Power spectra of Electric field intensity of whistler wave $|E_k|^2$ against normalized wave vector k for modified nonlinear schrödinger equation in quasi-steady state (in

normalized units) on 512×512 **grid size.**

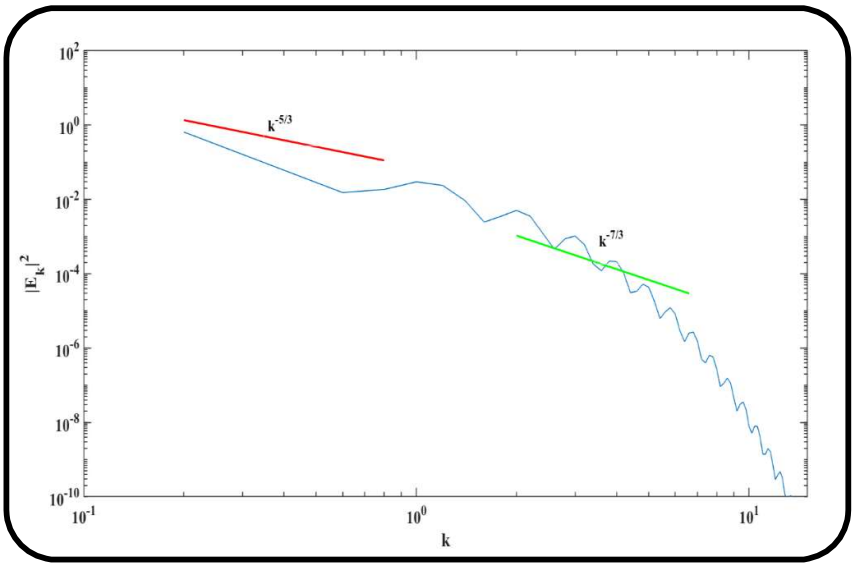

Figure 2.9 Power spectra of Electric field intensity of whistler wave $|E_k|^2$ ***against normalized wave vector*** k ***for modified nonlinear schrödinger equation in quasi-steady state (in normalized units) on*** 4096×4096 ***grid size.***

Fig. 2.10 shows the localization of whistler wave with high amplitude depicting the presence of turbulence.

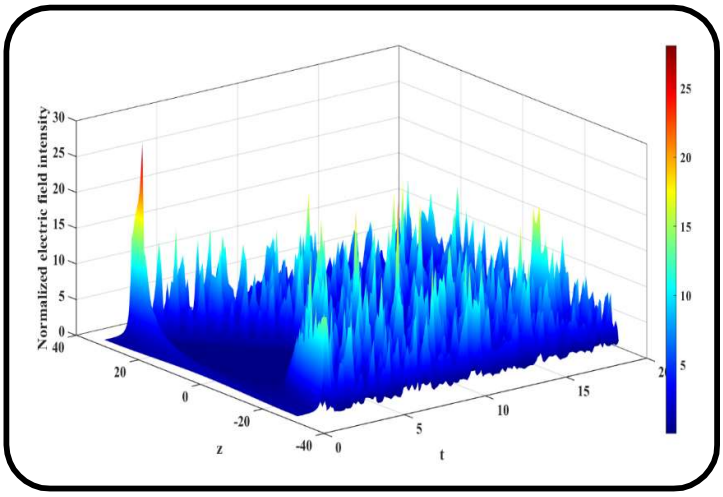

Figure 2.10 The evolution of the electric field $|E_x(t,z)|^2$ **at different times in the t-z plane for modified nonlinear schrödinger equation in quasi-steady state (in normalized units).**

2.4 Semianalytical Model

For a better understanding of the physics behind this localization of field, we have developed a simplified model i.e., the semianalytical model. Using this model, we have also calculated the characteristic transverse scale size of the localized structure.

For this steady-state model, we have to consider that whistler and IAW are propagating in the x-z plane. For this circumstance, we obtained from Eq. (2.11) the following form:

$$P\frac{\partial E_x}{\partial z}+Q\frac{\partial^2 E_x}{\partial x^2}+\left(\frac{\delta n}{n_0}\right)E_x+E_x\exp(k_i z)=0, \tag{2.37}$$

where P and Q are constants defined as:

$$P=2ik_{0z}\frac{\left(-2\omega_0^2k_{0z}^2\lambda_e^4+2\omega_0^2k_{0x}^2\lambda_e^4+2\omega_0^2\lambda_e^2+k_{0x}^2\lambda_i^2v_A^2+2k_{0z}^2\lambda_i^2v_A^2\right)}{\left(9\lambda_i^2v_A^2k_{0z}^2k^2\right)}.$$

and $\quad Q=-\dfrac{4\omega_0^2\lambda_e^4k_{0x}^2}{9\lambda_i^2v_A^2k_{0z}^2k^2}.$

This Eq. (2.37) is the usual equation obtained for the self-focusing of the beam.

we assume the variation in this model, $\tilde{E}_x$ in terms of eikonal function $'s'$ as follows:

$$\tilde{E}_x=E_0(x,z)e^{ik_{0z}s(x,z)}. \tag{2.38}$$

We get the following expression by substituting the solution of Eq. (2.38) into Eq. (2.37) and then separating the real and imaginary parts, we obtain

$$-iP\frac{\partial S}{\partial z}E_0+Q\frac{\partial^2 E_0}{\partial x^2}+Qk_{0z}^2\left(\frac{\partial S}{\partial x}\right)^2E_0+\left[\exp(\alpha'|E_x|^2)-1\right]E_0=0. \tag{39}$$

And $$\frac{iP}{k_{0z}}\frac{\partial E_0}{\partial z}+2Qk_{0z}\frac{\partial S}{\partial x}\frac{\partial E_0}{\partial x}+Qk_{0z}\frac{\partial^2 S}{\partial x^2}E_0+E_0\exp(k_i z)=0. \tag{40}$$

Furthermore, assuming that Eqs. (2.39) and (2.40) are solved in the form of a Gaussian beam profile, the following can be written as:

$$E_0^2=\frac{E_{00}^2}{f_1}\exp\left(\frac{-x^2}{r_0^2f_1^2}+k_i z\right). \tag{2.41}$$

$$S=\beta_1(z)\frac{x^2}{2}+\phi(z). \tag{2.42}$$

Substituting Eq. (2.41) and Eq. (2.42) in Eq. (2.40), we obtain

$$\beta_1=\frac{a}{f_1}\frac{df_1}{dz}. \tag{2.43}$$

Here, r_0 is the transverse scale size of the whistler wave in the *x*-direction, β_1 is the slowly varying function of *z*, and f_1 is the beam width parameter of the wave.

$$a = -\frac{(2\omega_0^2 k_{0z}^2 \lambda_e^4 + 2\omega_0^2 k_{0x}^2 \lambda_e^4 + 2\omega_0^2 \lambda_e^2 + k_{0x}^2 \lambda_i^2 v_A^2 + 2k_{0z}^2 \lambda_i^2 v_A^2)}{4\omega_0^2 \lambda_e^4 k_{0x}^2}.$$

For obtaining the beam width parameter, substitute the Eqs. (2.41), (2.42) in Eq. (2.39), then equating the coefficients of x^2 and then we obtain the following dimensionless form of equation as:

$$\frac{d^2 f_1}{d\xi^2} = 4\left(\frac{a_2}{a_1}\right)^2 \frac{R_d}{r_0^2}\left[\frac{2}{f_1^3} - \frac{1}{a_2}\frac{\alpha E_{00}^2}{f_1^2}\exp\left(\frac{\alpha E_{00}^2}{f_1} + k_i z\right)\right], \qquad (2.44)$$

where $R_d\left(=k_{0z} r_0^2\right)$ is the diffraction length and $\xi\left(=\frac{z}{R_d}\right)$, is the distance of propagation.

$$a_1 = \frac{2}{k_{0z}}\left(\frac{-2\omega_0^2 k_{0z}^2 \lambda_e^4 + 2\omega_0^2 k_{0x}^2 \lambda_e^4 + 2\omega_0^2 \lambda_e^2 + k_{0x}^2 \lambda_i^2 v_A^2 + 2k_{0z}^2 \lambda_i^2 v_A^2}{9\lambda_i^2 v_A^2 k^2}\right).$$

and $a_2 = \frac{4\omega_0^2 \lambda_e^4 k_x^2}{9\lambda_i^2 v_A^2 k^2 k_{0z}^2}$.

Eq. (2.44) describes the variation of beam width parameter(f_1) with the distance of propagation (ξ) and it is solved by using the Runge-Kutta method with the following boundary condition: $f_1|_{z=0} = 1$ and $\left.\frac{df_1}{d\xi}\right|_{z=0} = 0$. It has two terms on the right-hand side with opposite signs. The first one is for the diverging term and the second one is for the nonlinear term. This equation signifies that there is competition between these two terms because both are of opposite signs. First-term is the diffracting term that gives the divergence and the second term is the non-linear term that arises due to the ponderomotive force acting on electrons. Fig. 2.11 depicts the electric field intensity distribution of a whistler wave in the x-z plane. Here, $r_{01} = 3.41\times10^7 cm\ (200\lambda_e)$. The electric field is very low $\approx 10^{-3}$ StatV/cm due to which power is also decreasing so diffraction term dominates till $f >> 1$, as *z* propagates intensity increases of term $\exp(k_i z)$ and again f decreases less than one and intensity increases as a result focusing increases.

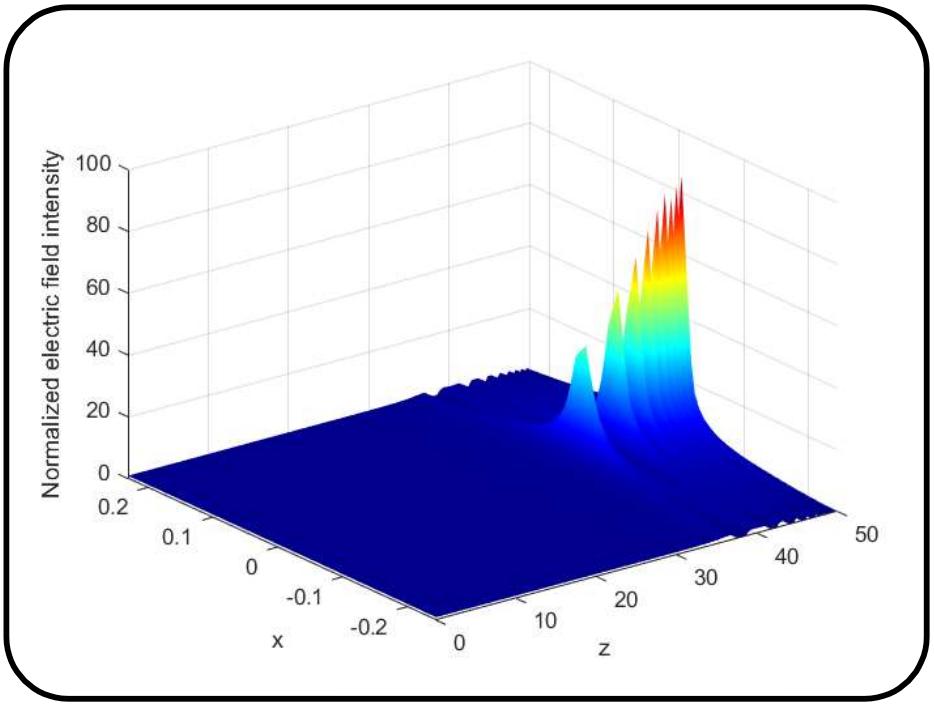

Figure 2.11 The intensity distribution of the electric field of a whistler wave in the x-z plane (in normalized units).

2.5 Summary and Conclusion

To understand the generation of whistler turbulence in the magnetic reconnection site[50], we have developed a nonlinear model based on (magnetic reconnection generated) electron beam generated whistler wave and low-frequency IAW. By using the beam-driven positive growth rate for whistler as reported by Zhao et al.[50], we have first presented the initial phase of instability development where the beam transfers energy to the whistler wave which is having almost a noise level initial amplitude and slowly grows to large amplitude. When the amplitude of the whistler becomes large, the ponderomotive force due to the whistler becomes appreciable and coupling with low frequency starts operative. Therefore, background density modification takes place. This leads to nonlinear dynamics of the whistler wave and its localized structure formation process starts. This process continues and these structures interact with each other to the formation of sub-localized randomly distributed structures. Thus, whistler turbulence is developed. In the present study, a constant growth rate of beam-driven mode has been considered. The quasi-steady state has not been achieved at this time and will not be achieved for further time also. To study a fully turbulent state, the system must go into quasi-steady state. For this, the growth rate of beam-driven mode is considered to be zero (growth rate is switched off). Then remodelling the Eq. (2.34) into one-dimensional model and taking one more run for Eq. (2.36) with grid size (512×512) to (4096×4096). The outcomes of this numerical simulation indicate the presence of turbulence. We have presented the whistler electric power spectra

having intertidal range scaling followed by steeper scaling. This impacts the heating and acceleration of plasma particles in the magnetopause by changing the formation of localized structures and turbulent spectrum. In future, we are planning to do work by varying the growth rate of the beam-driven mode. To understand the underlying physics behind localizations, we have also developed a semianalytical model and estimated the transverse scale size of these structures. This is of the order of few-electron skin-depth ($0.9\lambda_e$). It is to be mentioned here that this simplified semianalytical model is useful only in predicting the localized whistler structure and not the turbulent features which are only predicted by numerically solving nonlinear dynamical equations of whistler and IAW. Overall, because of nonlinear interactions, the power-law frequency fluctuation of the electric field spectrum gives the strong impression that this noise represents a fully evolved turbulence process, with electric field energy cascading to higher and higher frequencies. We may conclude from the preceding analysis that the interaction between the whistler wave and the IAW contributes to the energy cascade at lower scales via the production of localized structures, as mentioned above and demonstrated in our current investigation.

In the present model, we have not included the magnetic reconnection effects by including magnetic islands and current sheet formation on whistler turbulence. This work we are planning to do in future. In conclusion, our findings will contribute to a better quantitative understanding of beam-driven whistler-mode waves in the context of turbulence.

References

[1] Vetoulis, G., and J. F. Drake. "Whistler turbulence at the magnetopause: 1. Reduced equations and linear theory." *Journal of Geophysical Research: Space Physics* 104, no. A4 (1999): 6919-6928.

[2] G. M. Mason, M. I. Desai, R. A. Mewaldt, and C. M. S. Cohen, “Particle acceleration in the heliosphere,” *AIP Conf. Proc.*, vol. 1516, no. May, pp. 117–120, 2013, doi: 10.1063/1.4792550.

[3] W. H. Matthaeus and M. L. Goldstein, “Stationarity of magnetohydrodynamic fluctuations in the solar wind,” *J. Geophys. Res.*, vol. 87, no. A12, p. 10347, 1982, doi: 10.1029/ja087ia12p10347.

[4] W. H. Matthaeus, “Turbulence in space plasmas: Who needs it?,” *Phys. Plasmas.*, vol. 28, no. 3, 2021, doi: 10.1063/5.0041540.

[5] Roberts, D. A., Klein, L. W., Goldstein, M. L., & Matthaeus, W. H. (1987). The nature and evolution of magnetohydrodynamic fluctuations in the solar wind: Voyager

observations. *Journal of Geophysical Research: Space Physics*, *92*(A10), 11021-11040. https://doi.org/10.1029/JA092iA10p11021.

[6] J. P. Eastwood, T. D. Phan, S. D. Bale, and A. Tjulin, "Observations of turbulence generated by magnetic reconnection," *Phys. Rev. Lett.*, vol. 102, no. 3, pp. 1–4, 2009, doi: 10.1103/PhysRevLett.102.035001.

[7] E. M. Tejero, C. Crabtree, D. D. Blackwell, W. E. Amatucci, G. Ganguli, and L. Rudakov, "Experimental characterization of nonlinear processes of whistler branch waves," *Phys. Plasmas*, vol. 23, no. 5, 2016, doi: 10.1063/1.4946020.

[8] B. T. Tsurutani, A. L. Brinca, E. J. Smith, R. T. Okida, R. R. Anderson, and T. E. Eastman, "A statistical study of ELF-VLF plasma waves at the magnetopause," *J. Geophys. Res.*, vol. 94, no. A2, p. 1270, 1989, doi: 10.1029/ja094ia02p01270.

[9] R. Bruno and V. Carbone, "The solar wind as a turbulence laboratory," *Living Rev. Sol. Phys.*, vol. 10, 2013, doi: 10.12942/lrsp-2013-2.

[10] G. Paschmann, M. Øieroset, and T. Phan, "In-situ observations of reconnection in space," *Space Science Reviews*, vol. 178, no. 2–4. 2013. doi: 10.1007/s11214-012-9957-2.

[11] B. U. Ö. Sonnerup *et al.*, "Evidence for magnetic field reconnection at the Earth's magnetopause," *J. Geophys. Res.*, vol. 86, no. A12, 1981, doi: 10.1029/ja086ia12p10049.

[12] J. T. Gosling and A. Szabo, "Bifurcated current sheets produced by magnetic reconnection in the solar wind," *J. Geophys. Res. Space Phys.*, vol. 113, no. 10, 2008, doi: 10.1029/2008JA013473.

[13] M. Yamada, "Progress in understanding magnetic reconnection in laboratory and space astrophysical plasmas," *Physics of Plasmas*, 2007. doi: 10.1063/1.2740595.

[14] M. R. Brown, C. D. Cothran, and J. Fung, "Two fluid effects on three-dimensional reconnection in the Swarthmore Spheromak Experiment with comparisons to space data," *Physics of Plasmas*, 2006. doi: 10.1063/1.2180729.

[15] H. Karimabadi and A. Lazarian, "Magnetic reconnection in the presence of externally driven and self-generated turbulence," *Phys. Plasmas*, vol. 20, no. 11, pp. 1–17, 2013, doi: 10.1063/1.4828395.

[16] H. Karimabadi *et al.*, "The link between shocks, turbulence, and magnetic reconnection in collisionless plasmas," *Phys. Plasmas*, vol. 21, no. 6, 2014, doi: 10.1063/1.4882875.

[17] X. Wang, A. Bhattacharjee, and Z. W. Ma, "Collisionless reconnection: Effects of Hall current and electron pressure gradient," *J. Geophys. Res. Space Phys.*, vol. 105, no. A12, 2000, doi: 10.1029/1999ja000357.

[18] H. Huang, Y. Yu, L. Dai, and T. Wang, "Kinetic Alfvén Waves Excited in Two-Dimensional Magnetic Reconnection," *J. Geophys. Res. Space Phys.*, vol. 123, no. 8, 2018, doi: 10.1029/2017JA025071.

[19] Z. Vörös, E. Yordanova, D. B. Graham, Y. v. Khotyaintsev, and Y. Narita, "MMS Observations of Whistler and Lower Hybrid Drift Waves Associated with Magnetic Reconnection in the Turbulent Magnetosheath," *J. Geophys. Res. Space Phys.*, vol. 124, no. 11, 2019, doi: 10.1029/2019JA027028.

[20] J. S. Zhao, D. J. Wu, and J. Y. Lu, "On nonlinear decay of kinetic Alfvén waves and application to some processes in space plasmas," *J. Geophys. Res. Space Phys.*, vol. 115, no. 12, pp. 1–10, 2010, doi: 10.1029/2010JA015630.

[21] S. Rauf and J. A. Tataronis, "Nonlinear Plasma Waves with Steady-State D.C. Current," *J. Plasma Phys.*, vol. 52, no. 3, pp. 373–390, 1994, doi: 10.1017/S0022377800027203.

[22] D. Cao *et al.*, "MMS observations of whistler waves in electron diffusion region," *Geophys. Res. Lett.*, vol. 44, no. 9, pp. 3954–3962, 2017, doi: 10.1002/2017GL072703.

[23] M. Zhou *et al.*, "Observation of high-frequency electrostatic waves in the vicinity of the reconnection ion diffusion region by the spacecraft of the Magnetospheric Multiscale (MMS) mission," *Geophys. Res. Lett.*, vol. 43, no. 10, pp. 4808–4815, 2016, doi: 10.1002/2016GL069010.

[24] R. Gupta, V. Prakash, S. C. Sharma, and Vijayshri, "Interaction of an electron beam with whistler waves in magnetoplasmas," *Laser and Particle Beams*, vol. 33, no. 3, pp. 455–461, 2015, doi: 10.1017/S0263034615000506.

[25] L. James, L. Jassal, and V. K. Tripathi, "Whistler and electron-cyclotron instabilities in a plasma duct," *J. Plasma Phys.*, vol. 54, no. 1, pp. 119–128, 1995, doi: 10.1017/S0022377800018377.

[26] I. Talukdar, V. K. Tripathi, and V. K. Jain, "Whistler instability in a magnetospheric duct," *J. Plasma. Phys.*, vol. 41, no. 2, pp. 231–238, 1989, doi: 10.1017/S0022377800013817.

[27] C. Krafft *et al.*, "Whistler wave emission by a modulated electron beam," *Phys. Rev. Lett.*, vol. 72, no. 5, pp. 649–652, 1994, doi: 10.1103/PhysRevLett.72.649.

[28] D. A. Gurnett, L. A. Frank, and R. P. Lepping, "Plasma waves in the distant magnetotail," *J. Geophys. Res.*, vol. 81, no. 34, pp. 6059–6071, 1976, doi: 10.1029/ja081i034p06059.

[29] Y. Zhang, H. Matsumoto, and H. Kojima, "Whistler mode waves in the magnetotail," *J. Geophys. Res. Space Phys.*, vol. 104, no. A12, pp. 28633–28644, 1999, doi: 10.1029/1999ja900301.

[30] X. An, J. Bortnik, B. Van Compernolle, V. Decyk, and R. Thorne, "Electrostatic and whistler instabilities excited by an electron beam," *Phys. Plasmas*, vol. 24, no. 7, 2017, doi: 10.1063/1.4986511.

[31] A. V. Krafft, G. Matthieussent, and A. Volokitin, "Whistler waves produced by a modulated electron beam: Electromagnetic fields in the linear approach," *Phys. Plasmas*, vol. 4297, 1995, doi: 10.1063/1.870984.

[32] C. Krafft and A. Volokitin, "Nonlinear interaction of whistler waves with a modulated thin electron beam," *Phys. Plasmas*, vol. 5, no. 12, pp. 4243–4252, 1998, doi: 10.1063/1.873160.

[33] D. Summers, R. Tang, Y. Omura, and D. H. Lee, "Parameter spaces for linear and nonlinear whistler-mode waves," *Phys. Plasmas*, vol. 20, no. 7, 2013, doi: 10.1063/1.4816022.

[34] E. Camporeale and G. Zimbardo, "Wave-particle interactions with parallel whistler waves: Nonlinear and time-dependent effects revealed by particle-in-cell simulations," *Phys. Plasmas*, vol. 22, no. 9, 2015, doi: 10.1063/1.4929853.

[35] D. A. Gurnett *et al.*, "Plasma Wave Turbulence At The Magnetopause: Observations From ISEE 1 AND 2.," *J. Geophys. Res.*, vol. 84, no. A12, 1979, doi: 10.1029/JA084iA12p07043.

[36] Rezeau, L., Morane, A., Perraut, S., Roux, A., & Schmidt, R. Characterization of Alfvenic fluctuations in the magnetopause boundary layer. *Journal of Geophysical Research: Space Physics*, *94*(A1), 101-110. 1989. https://doi.org/10.1029/JA094iA01p00101.

[37] A. Vaivads, M. André, S. C. Buchert, J. E. Wahlund, A. N. Fazakerley, and N. Cornilleau-Wehrlin, "Cluster observations of lower hybrid turbulence within thin layers at the magnetopause," *Geophys. Res. Lett.*, vol. 31, no. 3, 2004, doi: 10.1029/2003GL018142.

[38] V. Angelopoulos, "The THEMIS mission," *Space Sci. Rev.*, vol. 141, no. 1–4, 2008, doi: 10.1007/s11214-008-9336-1.

[39] W. Li *et al.*, "Global distribution of whistler-mode chorus waves observed on the THEMIS spacecraft," *Geophys. Res. Lett.*, vol. 36, no. 9, 2009, doi: 10.1029/2009GL037595.

[40] O. Chang, S. P. Gary, and J. Wang, "Whistler turbulence at variable electron beta: Three-dimensional particle-in-cell simulations," *J. Geophys. Res. Space Phys.*, vol. 118, no. 6, 2013, doi: 10.1002/jgra.50365.

[41] V. A. Svidzinski, H. Li, H. A. Rose, B. J. Albright, and K. J. Bowers, "Particle in cell simulations of fast magnetosonic wave turbulence in the ion cyclotron frequency range," *Phys. Plasmas*, vol. 16, no. 12, 2009, doi: 10.1063/1.3274559.

[42] S. Saito, S. P. Gary, H. Li, and Y. Narita, "Whistler turbulence: Particle-in-cell simulations," *Phys. Plasmas*, vol. 15, no. 10, 2008, doi: 10.1063/1.2997339.

[43] D. Biskamp, E. Schwarz, and J. F. Drake, "Two-dimensional electron magnetohydrodynamic turbulence," *Phys. Rev. Lett.*, vol. 76, no. 8, 1996, doi: 10.1103/PhysRevLett.76.1264.

[44] S. Galtier and A. Bhattacharjee, "Anisotropic weak whistler wave turbulence in electron magnetohydrodynamics," *Phys. Plasmas*, vol. 10, no. 8, 2003, doi: 10.1063/1.1584433.

[45] C. M. Cully, J. W. Bonnell, and R. E. Ergun, "THEMIS observations of long-lived regions of large-amplitude whistler waves in the inner magnetosphere," *Geophys. Res. Lett.*, vol. 35, no. April, pp. 1–5, 2008, doi: 10.1029/2008GL033643.

[46] Santolík, O., Gurnett, D. A., Pickett, J. S., Parrot, M., & Cornilleau-Wehrlin, N. "A microscopic and nanoscopic view of storm-time chorus on 31 March 2001". *Geophysical research letters*, *31*(2). 2004 doi: 10.1029/2003GL018757.

[47] C. Cattell *et al.*, "Discovery of very large amplitude whistler-mode waves in Earth' s radiation belts," *Geophysical research letters,* vol. 35, pp. 1–7, 2008, doi: 10.1029/2007GL032009.

[48] Crabtree, C., Rudakov, L., Ganguli, G., Mithaiwala, M., Galinsky, V., & Shevchenko, V., "Weak turbulence in the magnetosphere : Formation of whistler wave cavity by nonlinear scattering," vol. 032903, 2012, . https://doi.org/10.1063/1.3692092.

[49] R. P. Sharma, P. Nandal, N. Yadav, and R. Uma, "Nonlinear effects associated with oblique whistler waves in space plasmas," *Phys. Plasmas*, vol. 23, no. 10, 2016, doi: 10.1063/1.4966242.

[50] S. Q. Zhao *et al.*, "Observations of the Beam-Driven Whistler Mode Waves in the Magnetic Reconnection Region at the Dayside Magnetopause," *J. Geophys. Res. Space Phys.*, vol. 126, no. 2, pp. 1–11, 2021, doi: 10.1029/2020JA028525.

[51] F. D. Wilder *et al.*, "The nonlinear behavior of whistler waves at the reconnecting dayside magnetopause as observed by the Magnetospheric Multiscale mission: A case study," *J. Geophys. Res. Space Phys.*, vol. 122, no. 5, pp. 5487–5501, 2017, doi: 10.1002/2017JA024062.

[52] C. Krafft and A. S. Volokitin, "Electromagnetic radiation from upper-hybrid wave turbulence in inhomogeneous solar plasmas," *Plasma Phys. Control Fusion*, vol. 62, no. 2, 2020, doi: 10.1088/1361-6587/ab569d.

[53] C. Krafft and A. S. Volokitin, "Whistler envelope solitons. I. Dynamics in inhomogeneous plasmas," *Phys. Plasmas*, vol. 25, no. 10, 2018, doi: 10.1063/1.5041055.

[54] M. V. Goldman, D. L. Newman, J. G. Wang, and L. Muschietti, "Langmuir turbulence in space plasmas.," *PhST.*, vol. 63, pp. 28–33, 1996, doi: 10.1088/0031-8949/1996/T63/003.

[55] P. J. Christiansen, V. K. Jain, and L. Stenflo, "Filamentary collapse in electron-beam plasmas," *Phys. Rev. Lett.*, vol. 46, no. 20, pp. 1333–1337, 1981, doi: 10.1103/PhysRevLett.46.1333.

[56] S. Choi, N. Bessho, S. Wang, L.-J. Chen, and M. Hesse, "Whistler waves generated by nongyrotropic and gyrotropic electron beams during asymmetric guide field

reconnection," *Phys. Plasmas*, vol. 29, no. 1, p. 012903, Jan. 2022, doi: 10.1063/5.0059884.

[57] G. D. Doolen, D. F. Dubois, and H. A. Rose, "Nucleation of cavitons in strong langmuir turbulence," *Phys. Rev. Lett.*, vol. 54, no. 8, 1985, doi: 10.1103/PhysRevLett.54.804.

[58] M.-M. Shen and D. R. Nicholson, "Numerical comparison of strong Langmuir turbulence models," *Physics of Fluids*, vol. 30, no. 4, 1987, doi: 10.1063/1.866307.

[59] R. P. Sharma, P. Stubbe, and A. D. Verga, "Numerical simulation of a Zakharov-Boussinesq system of equations to study Langmuir turbulence in the ionosphere," *J. Geophys. Res. Space Phys.*, vol. 101, no. A5, 1996, doi: 10.1029/96ja00043.

[60] S. Nazarenko, *Lecture Notes in Physics Vol 825: Wave Turbulence*, vol. 825. 2011.

CHAPTER-3

Localization and turbulence of Beam-Driven Whistler wave with Magnetosonic wave in Magnetopause

3.1 Introduction

In space plasma physics, heating and acceleration of plasma particles have been an active research era. Numerous suggestions have been put up to explain the heating and acceleration of plasma particles in space plasmas, but the underlying processes are still not fully understood. It is considered that plasma turbulence is a leading contender for particle and energy transmission[1], [2]. Turbulence is crucial in space plasmas because it cascades energy from larger to smaller scales, ultimately leading to dissipation and particle heating[3]–[7]. In laboratory, space, and astrophysical plasmas, magnetic reconnection is thought to emerge in a variety of applications. Magnetic reconnection is a fundamental plasma process of energy conversion mechanism, which involves changing the magnetic topology to convert magnetic energy into plasma kinetic and thermal energy. There is significant evidence that in magnetized plasmas, magnetic reconnection and turbulence are likely connected[8]–[11].

The earth's magnetosheath is the highly turbulent and heated region bounded by the bow shock and the magnetopause. Thus, it provides better conditions to investigate plasma turbulence, transport, and dissipation, which are the major unresolved issue in the modern space era. Several wave modes exist in the space plasmas[12]–[17] and non-linear interaction of these wave modes contribute to the formation of turbulent cascade modes. Among these wave modes, it is tremendously assumed that in space and laboratory plasmas whistler wave[18] plays a vital role. Whistler waves are observed in the magnetotail, radiation belts, and dayside magnetopause, among other areas of the space plasma[19]–[22]. Along with whistler wave modes, the magnetosonic wave (MSW) modes are also anticipated to be a prominent candidate for heating and accelerating the particles in space plasmas[23]–[26]. Recently, the generation of low-frequency MSWs through wave-wave interactions has been reported in earth magnetosheath[27]. For more analysis, the 2D PIC simulation studied the magnetosonic turbulence and observed the cascading of energy which might contribute to the localized steepening of magnetic fluctuation of MSWs mode[28].

Recently, Zhao et al.[29] observed the beam-driven whistler wave in the magnetopause region. They observed the solitary structures of whistler exist at f_{ce} (where f_{ce} is the electron

gyrofrequency). Krafft et al.[30] have studied the beam-driven Langmuir turbulence involving density fluctuations. Reeves et al.[31] have experimented with beam-plasma interactions to study and characterize fundamental wave-particle interactions by generating whistler waves using a modulated electron beam. Narita et al.[32] observed whistler turbulence on electron scale in the solar-wind region along with the magnetic power spectrum. Broadband spectrum of whistler mode, magnetic field fluctuations have been observed in the vicinity of magnetopause[33]. Karpman et al.[34] studied the nonlinear theory of localized whistler wave structures by non-linear Schrödinger system of equations (NLS) which leads to the formation of density enhancements that trap whistler waves. Das et al.[35] demonstrated the turbulent spectrum of whistler wave via nonlinear coupling of whistler waves with magnetosonic perturbations, thereby leading to the formation of nonlinear coherent structures. This broadband spectrum at magnetopause may result from a cascade of spectral power from low to high frequencies as the result of gradient-driven instabilities.

Biskamp et al.[36] studied the electron magnetohydrodynamic (EMHD) turbulence and studied the various wave modes and also observed turbulent structures and the energy spectrum E_k, follows the Kolmogorov-type scaling, $E_k \sim k^{-5/3}$ for $k\lambda_e > 1$ and $E_k \sim k^{-7/3}$ for $k\lambda_e < 1$ by high-resolution numerical simulations. After that, Das and Diamond[37] examined the EMHD turbulence and linear properties of whistler waves through numerical simulation.

It is evident from the literature that the energy cascade arises from turbulence and also weak turbulence theory is mediated by the non-linear interactions of whistler waves[38]. Langmuir turbulence is studied by nonlinear Schrödinger equation (NLS) and Zakharov equations (ZSE), numerically solved for an initial condition through modulational instability and finally saturates into solitons structure[39]. Doolen et al.[40] used Zakharov system of equations (ZSE), and Sharma et al.[41] used Zakharov-Boussinesq's equations to study the Langmuir turbulence using cascading of energy and cavitation process.

Although, Non-linear whistler wave along with solitons, radiation, self-focussing, and modulational instability has been studied in past by Karpman[34]. Later on, a few scientists also worked on wave turbulence. Although, a lot of studies have been done on whistler waves as discussed above but to the best of our knowledge specific research on beam-driven whistler turbulence has not been revealed. Recently, Jyoti et al.[42] studied beam-driven whistler turbulence on account of nonlinear density perturbations by ion-acoustic waves (IAWs). They studied the nonlinear structures and turbulence by cavitation process by modified Zakharov

system of equations. But in the magnetopause reconnection region along with Whistler waves, magnetosonic waves (MSWs) are frequently observed and these MSWs have magnetic perturbations along with density perturbations. Therefore, Jyoti et al.[42] work is not applicable in these realistic situations because magnetic perturbations may provide significant contributions to nonlinear structure formation and turbulence generation in the presence of beam.

Motivated from the previous studies, in the present work we have provided a model to explain how energetic electron beams (generated by the magnetic reconnection process) leads to whistler turbulence in the magnetic reconnection region of the magnetopause, as seen by the Magnetospheric Multiscale Mission (MMS)[29]. The intense electron beam source has been used in place of the magnetic reconnection mechanism in this instance.

Here, we have proposed a model in which the beam-driven whistler waves are studied. From the energy of the beam, the amplitude of beam-driven modes grows from the noise level to the higher values such that ponderomotive force will create the nonlinear effects in the whistler waves which leads to the localization and turbulence of whistler waves.

For this purpose, we have proposed that the number density of pump whistler wave becomes disturbed in the presence of the MSWs, and the components of ponderomotive force of whistler are taken into account in the MSWs dynamics (Since MSWs is an electromagnetic wave, we have considered perturbation in density as well as in magnetic field i.e., $n = n_0 + \delta n,\ B = B_0 + \delta B$). Then, the governing equations of the whistler wave and the MSWs are framed in the form of coupled nonlinear equations. For these nonlinear equations, numerical simulation is carried out using the finite difference with modified version of predictor-corrector method for temporal integration and the pseudo-spectral method for spatial integration. The outcomes of the numerical simulation show the localization and turbulent state of whistler wave. The objective of our current work is to examine the localized structure and turbulent spectra in the magnetopause region.

The paper is organized as follows: Section 2 presents the model equations, which present the derivation part of the dynamical equation of the whistler wave and the magnetosonic wave. Section 3 presents the numerical simulation. Section 4 presents the semianalytical method. Section 5 concludes the results, conclusion, and future recommendations of the current work

3.2 Model equations

The proposed theoretical model describes whistler turbulence in plasma near the magnetopause by taking background density fluctuations into account. In this work, Whistler turbulence induced by electron beams was believed to be well-developed. We have taken into account low and high-frequency plasma responses, density fluctuations, slow and fast wave dynamics including other linear and non-linear processes like wave coupling and ponderomotive force.

The analysis consists of two parts. Initially, the dynamical equation of high-frequency whistler waves is solved. Later, the dynamical equations of MSWs and the relationship between low-frequency MSWs and high-frequency whistler waves are discussed. 2D whistler wave system using an electron beam is characterized by a two-fluid model, considering positive growth rate of beam-driven whistler in our computation. Hence, phenomenologically, an instability growth rate $\gamma' > 0$ is into whistler dynamics.

3.2.1 2D Whistler dynamics

The whistler wave dynamical equation is obtained using a two-fluid model. The whistler wave is propagating in a magnetized plasma with the magnetic field along the z-axis and wave vector, $\vec{k} = k_{0x}\hat{x} + k_{0z}\hat{z}$. Here, $B\ (= B_0 + \delta B)$ is the magnetic field, B_0 the background magnetic field, and δB the perturbation in the magnetic field.

The governing dynamical equation of whistler wave can be written as (please see the appendix-A for a detailed derivation of whistler's dispersion relation)

$$\begin{aligned}&\frac{-\partial^2 E_y}{\partial t^2} - \lambda_e^4 \frac{\partial^6 E_y}{\partial x^4 \partial t^2} - \lambda_e^4 \frac{\partial^6 E_y}{\partial z^4 \partial t^2} - 2\lambda_e^4 \frac{\partial^6 E_y}{\partial x^2 \partial z^2 \partial t^2} \\ &+2\lambda_e^2 \frac{\partial^4 E_y}{\partial x^2 \partial t^2} + 2\lambda_e^2 \frac{\partial^4 E_y}{\partial z^2 \partial t^2} = \lambda_e^4 \omega_{ce}^2 \left(\frac{\partial^4 E_y}{\partial z^2 \partial x^2} + \frac{\partial^4 E_y}{\partial z^4} \right) + \lambda_e^4 \omega_{ce}^2 \left(\frac{\partial^4 E_y}{\partial z^2 \partial x^2} + \frac{\partial^4 E_y}{\partial z^4} \right) \frac{\delta B}{B_0}\end{aligned} \tag{3.1}$$

where $\lambda_e \left(= \sqrt{\frac{c^2 m_e}{4\pi n_0 e^2}} \right)$ is the electron skin depth, and $\omega_{ce} \left(= \frac{eB_0}{m_e c} \right)$ is the electron gyrofrequency.

As beam-driven growth is also considered, $\frac{d}{dt} \to \left(\frac{d}{dt} + \gamma \right)$,

$$\begin{aligned}&-\left(\frac{\partial^2}{\partial t^2} + 2\gamma \frac{\partial}{\partial t} \right) E_y - \lambda_e^4 \frac{\partial^6 E_y}{\partial x^4 \partial t^2} - \lambda_e^4 \frac{\partial^6 E_y}{\partial z^4 \partial t^2} - 2\lambda_e^4 \frac{\partial^6 E_y}{\partial x^2 \partial z^2 \partial t^2} \\ &+2\lambda_e^2 \frac{\partial^4 E_y}{\partial x^2 \partial t^2} + 2\lambda_e^2 \frac{\partial^4 E_y}{\partial z^2 \partial t^2} = \lambda_e^4 \omega_{ce}^2 \left(\frac{\partial^4 E_y}{\partial z^2 \partial x^2} + \frac{\partial^4 E_y}{\partial z^4} \right) + \lambda_e^4 \omega_{ce}^2 \left(\frac{\partial^4 E_y}{\partial z^2 \partial x^2} + \frac{\partial^4 E_y}{\partial z^4} \right) \frac{\delta B}{B_0}.\end{aligned} \tag{3.2}$$

For this Eq. (3.2), the following envelope solution is assumed.

$$\tilde{E}_y = E_y(x,z,t)e^{i(k_{0x}\hat{x}+k_{0z}\hat{z}-\omega_0 t)}. \tag{3.3}$$

Since, the nonlinear whistler wave dynamical equation is achieved by considering the effect of a strong whistler wave, substituting Eq. (3.3) in Eq. (3.2) -

$$\begin{aligned}
&2i\omega_0(1+\lambda_e^4k_{0x}^4+\lambda_e^4k_{0z}^4+2\lambda_e^2k_{0x}^2+2\lambda_e^2k_{0z}^2)\frac{\partial E_y}{\partial t}+(-4\omega_0^2\lambda_e^4k_{0x}^2)\frac{\partial^2 E_y}{\partial x^2}\\
&+(4\lambda_i^2v_A^2k_{0z}^2-4\omega_0^2\lambda_e^4k_{0z}^2)\frac{\partial^2 E_y}{\partial z^2}+(4\lambda_i^2v_A^2k_{0x}k_{0z}-8\omega_0^2k_{0z}k_{0x}\lambda_e^4)\frac{\partial^2 E_y}{\partial x\partial z}\\
&+2i(-2\omega_0^2k_{0x}^3\lambda_e^4+2\omega_0^2k_{0x}k_{0z}^2\lambda_e^4+2\omega_0^2\lambda_e^2k_{0x}+k_{0x}k_{0z}^2\lambda_i^2v_A^2)\frac{\partial E_y}{\partial x}+\\
&2i(-2\omega_0^2k_{0z}^3\lambda_e^4+2\omega_0^2k_{0z}k_{0x}^2\lambda_e^4+2\omega_0^2\lambda_e^2k_{0z}+k_{0z}k_{0x}^2\lambda_i^2v_A^2+2k_{0z}^3\lambda_i^2v_A^2)\frac{\partial E_y}{\partial z}\\
&+(9\lambda_i^2v_A^2k^2k_{0z}^2)\frac{\delta n}{n_0}E_y+(-9k_{0z}^4\omega_{ce}^2\lambda_e^4-4k_{0x}^2k_{0z}^2\lambda_e^4\omega_{ce}^2)\frac{\delta B}{B_0}=0,
\end{aligned} \tag{3.4}$$

where, k_{0x}, k_{0z} are wave vector components related to the background whistler magnetic field Using the normalizing parameter,

$$t_n = 1/\omega_0.$$

$$z_n = \frac{2i(-2\omega_0^2k_{0x}^3\lambda_e^4+2\omega_0^2k_{0x}k_{0z}^2\lambda_e^4+2\omega_0^2\lambda_e^2k_{0x}+k_{0x}k_{0z}^2\lambda_i^2v_A^2+2k_{0z}^3\lambda_i^2v_A^2)}{2\omega_0(1+\lambda_e^4k_{0x}^4+\lambda_e^4k_{0z}^4+2\lambda_e^2k_{0x}^2+2\lambda_e^2k_{0z}^2)}.$$

Thus, the normalized dimensionless form of Eq. (3.4) is as

$$\begin{aligned}
&i\frac{\partial E'}{\partial t'}+c_1\frac{\partial^2 E'}{\partial x'^2}+c_2\frac{\partial^2 E'}{\partial z'^2}+i\frac{\partial E'}{\partial x'}+i\frac{\partial E'}{\partial z'}+c_3\frac{\partial^2 E'}{\partial x'\partial z'}+\\
&c_4\left(\frac{\delta n}{n_0}\right)E'+c_5\left(\frac{\delta B}{B_0}\right)E'+2i\gamma' E'=0,
\end{aligned} \tag{3.5}$$

where Eq. (3.5) depicts the normalized dynamical equation for the beam-driven whistler wave which leads the turbulence. To describe the beam instability, we have incorporated phenomenologically γ' represents normalized growth rate and in our simulations $\gamma = 0.5083\omega_{ce}$ which is consistent with the observations of Zhao et al.

where $c_1 = \dfrac{-4\omega_0^2\lambda_e^4k_{0x}^2}{2\omega_0(1+\lambda_e^4k_{0x}^4+\lambda_e^4k_{0z}^4+2\lambda_e^2k_{0x}^2+2\lambda_e^2k_{0z}^2)x_n^2}.$

$$c_2 = \frac{(4\lambda_i^2v_A^2k_{0z}^2-4\omega_0^2\lambda_e^4k_{0z}^2)}{2\omega_0(1+\lambda_e^4k_{0x}^4+\lambda_e^4k_{0z}^4+2\lambda_e^2k_{0x}^2+2\lambda_e^2k_{0z}^2)z_n^2}.$$

$$c_3 = \frac{(4\lambda_i^2 v_A^2 k_{0x} k_{0z} - 8\omega^2 k_{0z} k_{0z} \lambda_e^4)}{2\omega_0 (1 + \lambda_e^4 k_{0x}^4 + \lambda_e^4 k_{0z}^4 + 2\lambda_e^2 k_{0x}^2 + 2\lambda_e^2 k_{0z}^2) z_n x_n}.$$

$$c_4 = \frac{9\lambda_i^2 v_A^2 k^2 k_{0z}^2}{2\omega_0 (1 + \lambda_e^4 k_{0x}^4 + \lambda_e^4 k_{0z}^4 + 2\lambda_e^2 k_{0x}^2 + 2\lambda_e^2 k_{0z}^2)}.$$

$$c_5 = (-9k_{0z}^4 \omega_{ce}^2 \lambda_e^4 - 4k_{0x}^2 k_{0z}^2 \lambda_e^4 \omega_{ce}^2)$$

and $\gamma' = \frac{\gamma}{\omega_0}$ where $\gamma (= 0.5083\omega_{ce})$ is the normalized growth rate, where $\gamma (= 0.5083\omega_{ce})$ is the beam-driven whistler wave growth rate.

3.2.2 Magnetosonic waves (MSWs)

Consider a magnetosonic wave propagating in the x-direction, i.e., $\vec{k} = k_{0x}\hat{x}$ along with the background magnetic field in the z-direction, i.e., $\vec{B} = B_0\hat{z}$. The electric field is polarised in y-direction i.e., $\vec{E} = E_y\hat{y}$. The dynamical equation for the magnetosonic wave is obtained from the basic equations that are given below:

Equation of motion

$$m_j \left[\frac{\partial \vec{v}_j}{\partial t} + (\vec{v}_j . \nabla \vec{v}_j) \right] = q_j \vec{E} + \frac{q_j}{c} (\vec{v}_j \times \vec{B}) + F_j. \quad (3.6)$$

Equation of continuity

$$\frac{\partial n_j}{\partial t} + \vec{\nabla} . (n_j \vec{v}_j) = 0 \quad (3.7)$$

Faraday's law

$$\nabla \times \vec{E} = -\frac{1}{c} \frac{\partial \vec{B}}{\partial t} \quad (3.8)$$

Ampere's -Maxwell's equation

$$\nabla \times \vec{B} = \frac{4\pi}{c} \vec{J} + \frac{1}{c} \frac{\partial \vec{E}}{\partial t}, \quad (3.9)$$

where j denotes the particle species ($j = i$ for ion and e for the electron) and m_j, v_j, q_j, T_j denotes the mass, velocity, charge, and temperature of the species respectively. n_0 is the background density. F_j is the ponderomotive force due to the whistler wave given below:

$$\vec{F}_j = -m_j(\vec{v}_j *.\vec{\nabla})\vec{v}_j + \frac{q_j}{c}(\vec{v}_j *\times\vec{B}). \tag{3.10}$$

Using the velocity components of electron and ion (please see the appendix-1 for velocity components) in Eq. (3.10), and then using Eq. (3.7) with approximation $\omega << \omega_{ci}$, then we obtained the following form of equation:

$$\left(\frac{\partial^2}{\partial t^2} - c_6\frac{\partial^2}{\partial x^2}\right)\frac{n}{n_0} = -\frac{\partial}{\partial x}\left(\frac{F_{ey}+F_{iy}}{m_i}\right), \tag{3.11}$$

Further, on putting the values of ponderomotive components in Eq. (3.11), we obtain the following equation:

$$\left(\frac{\partial^2}{\partial t^2} - c_6\frac{\partial^2}{\partial x^2}\right)\frac{n}{n_0} = -c_7\frac{\partial^2}{\partial x^2}\left|E_y^2\right|, \tag{3.12}$$

where c_6, c_7 are the constant, whose value is given below:

$$c_6 = c^2\left(\frac{c_s^2+v_A^2}{c^2+v_A^2}\right)$$

and $c_7 = \left[\frac{e^2}{m_e m_i\omega_{ce}^2} - \frac{e^2\omega_0}{m_e m_i\omega_{ce}\alpha_1}\left\{\left(1+\frac{\omega_{ce}^2}{\alpha_1}\right)+\frac{\omega_0^3}{\alpha_1\omega_{ce}}\right\} + \frac{e^2}{m_i^2\omega_{ci}^2} - \frac{e^2\omega_0}{m_e m_i\omega_{ce}\alpha_1}\left\{\left(1+\frac{\omega_{ci}^2}{\alpha_1}\right)+\frac{\omega_0^3}{\alpha_1\omega_{ci}}\right\}\right]$

$c_s\left(=\frac{v_{the}^2+v_{thi}^2}{m_i}\right)^{\frac{1}{2}}$ is the speed of the sound wave. And, $\alpha_1 = -k^2\lambda_e^2(\omega_0^2-\omega_{ce}^2)-\omega_0^2$.

Now, using the same normalizing parameter as we have used in the dynamics of whistler wave i.e., x_n, z_n and t_n. After taking the adiabatic response of Eq. (3.12), we obtain

$$E_n = \left[-\frac{1}{n_0}\left(\frac{c_6 x_n^2}{c_7 t_n^2}\right)\right]^{\frac{1}{2}}$$

we obtain the following normalization equation,

$$n' = \frac{c_7}{c_6}\left|E_y\right|^2 \tag{3.13}$$

using this Eq. (3.13) in Eq. (3.5), we obtain

$$i\frac{\partial E'}{\partial t'} + c_1\frac{\partial^2 E'}{\partial x'^2} + c_2\frac{\partial^2 E'}{\partial z'^2} + i\frac{\partial E'}{\partial x'} + i\frac{\partial E'}{\partial z'} + c_3\frac{\partial^2 E'}{\partial x'\partial z'} + \frac{c_7 c_4}{c_6}\left|E_y^2\right|E' + c_5 nE' + 2i\gamma' E' = 0, \tag{3.14}$$

3.3 Numerical Simulation

Using the 2D pseudo-spectral approach, numerical simulation has been performed. We implemented a pseudo-spectral method for space integration (in x-direction) having periodic length $L_x = 2\pi / \alpha_x$, and a finite difference method with modified version of Gazdaz[43] predictor-corrector method (in z-direction) for time evolution. For solving the system of dimensionless equations, authors have studied the algorithm of nonlinear Schrödinger (NLS) equation into following two steps-

(i) The testing of invariants plasmon number $N = \sum_k |E_k|^2$ with grid points and time steps is given below (NLS)

Table 1. Testing of invariants with Grid points 64

Time steps (dt)	10^{-5}	10^{-6}	10^{-7}	10^{-8}
N	9.99999997	9.999999996	1.00000000007	1.00000000007

Table 2. Testing of invariants with time steps $dt = 5\times10^{-5}$ (This step size $dt = 5\times10^{-5}$ is also used for the finite difference method to monitor the invariants of NLS equation to desired accuracy)

Grid points	64	128	256	512
N	9.9999991	9.999997	9.9999994	9.9999998

(ii) modified for present case and applied to magnetopause parameters below:-

For numerical simulation, equations have been solved in the periodic domain $(10\pi\times10\pi)$ with the grid size (512×512). The initial conditions used for the numerical simulations is given in Eq. (3.15) and their parameters are listed in Table 3.

$$E_y(x,z) = E_0(1+\beta\cos(\alpha_x x))(1+\beta\cos(\alpha_z z)), \qquad (3.15)$$

Table 3. Parameters used for initial conditions in numerical simulations.

Parameters	Initial amplitude E_0	Perturbed electric field β	Perturbation in wavenumbers	
			α_x	α_z

			(Normalized by x_n^{-1})	(Normalized by z_n^{-1})
Values	0.5	0.1	0.2	0.2

We have presented the results of the numerical simulation of dimensionless equations (3.5), (3.12), and (3.14) applicable to the magnetopause region. For application purposes, the typical parameters for numerical simulations are given in Table 4.

Table 4 Various parameters used for numerical simulations.

Parameters	Values
Background magnetic field, B_0	$4.5\times10^{-5}\,G$
Background density, n_0	$n_0 = 21 cm^{-3}$
Normalized magnetic field B_n, and electric field E_n	$B_n = 1.60\times10^{-6}\,G$ and $E_n = 6.8\times10^{-7}$ StatV/cm
x_n, z_n and t_n	$x_n = 1.05\times10^5\,cm, z_n = 1.54\times10^5\,cm, t_n = 6.31\times10^{-4}\,s.$
Constants	$c_1 = -0.2681,\ c_2 = 1.0080,\ c_3 = 2.4398$, $c_4 = 1.1698,$ $c_n = 0.1775$, $c_6 = 1.5413\times10^5$, $c_7 = 5.4\times10^5$.

For solving the set of dimensionless Eqs. (3.5), (3.12), and (3.14), we have developed two models:

a) Modified Nonlinear Schrödinger Equation (MNLS model)
b) Modified Zakharov System of Equations (MZSE model)

After checking the accuracy of the algorithm, it has been modified for the set of dimensionless equations, which is used to study the nonlinear coupling of whistler and magnetosonic waves.

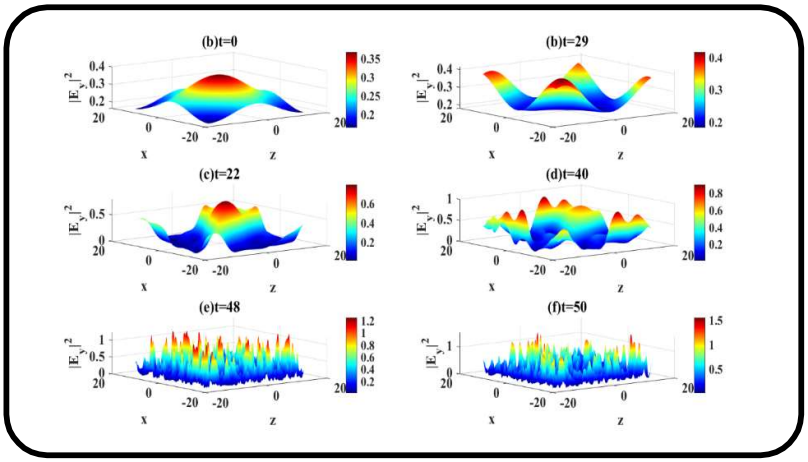

Figure 3.1 The normalized spatial evolution of whistler's electric field in 3D in magnetopause by MNLS model at (a) t=0, (b) t=29, (c) t=22, (d) t=40, (e) t=48, (f) t=50.

First, we present the results of the numerical simulation of MNLS model. For MNLS model, the numerical simulation of equation (3.14) was carried out. Fig. 3.1 depicts the spatial evolution of electric field intensity of whistler in x-z plane. The figure shows that at an initial time, the electron beam imparts energy to the system and localized structures are formed with increasing amplitude. But, at later stage when whistler amplitude reaches its peak value then system transit to the turbulent regime and we get chaotic structures. These localized structures are the results of the ponderomotive force nonlinearity-driven density modification.

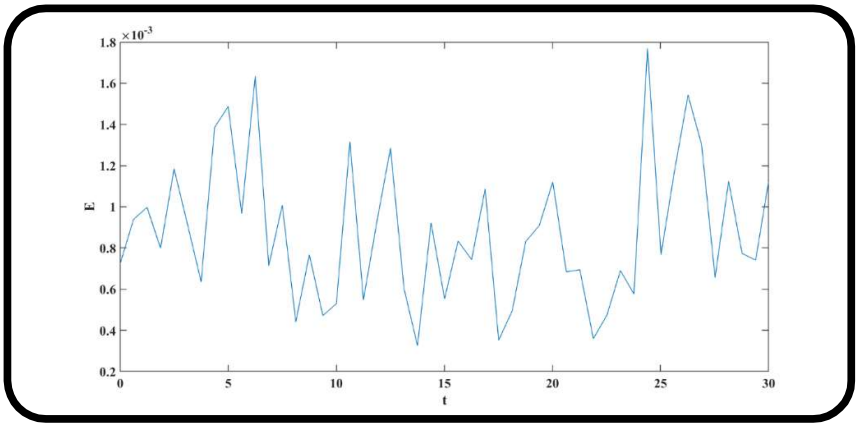

Figure 3.2 Evolution of electric field fluctuations with time by MNLS model.

Fig. 3.2 depicts the fluctuations of electric field with time. it shows the turbulent whistler and for the present computation, whistler fluctuations peak value is around 1.8mV/m for the present parameters. We have also checked that most of the power is near the pump frequency of whistler in the frequency band $0.1f_{ce} - 0.5f_{ce}$ as observed by Zhao et al.[29].

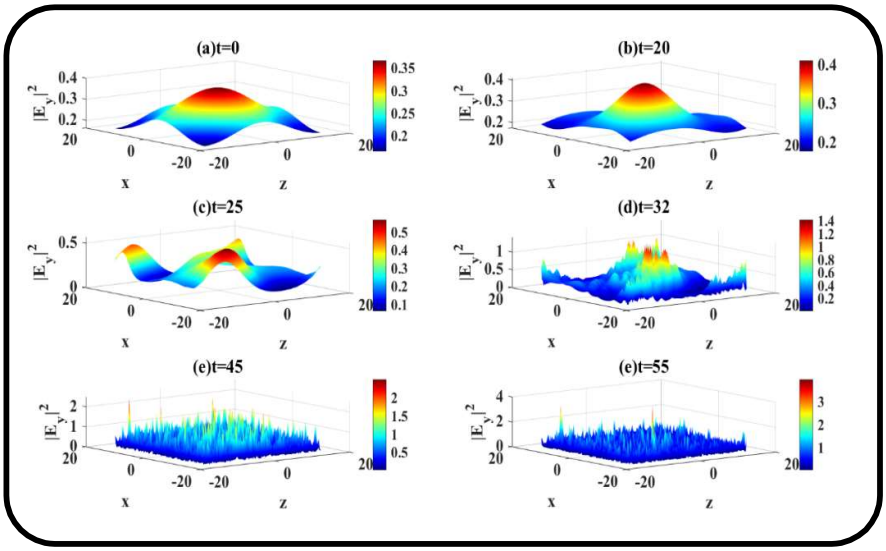

Figure 3.3 The normalized spatial evolution of whistler's electric field in 3D in magnetopause by MZSE model at (a) t=0, (b) t=20, (c) t=25, (d) t=32, (e) t=45, (f) t=55.

Fig. 3.3 depicts the spatial evolution of electric field intensity of whistler wave for MZSE model. Initially, electron beam imparts energy to the system and at later stage when whistler attains peak value of its amplitude then system transit to the turbulent regime, and corresponding localized structures are formed. Fig. 3.4 depicts the 3D spatial evolution of the density profile at normalized time t=50. It shows the density cavities and humps in the real space associated with the MSW induced by ponderomotive nonlinearity of whistler waves. The low-frequency MSWs perturbation couples nonlinearly with the pump whistler wave as a result of ponderomotive force. The whistler wave contributes energy to the perturbation as a result of this nonlinear interaction. Due to the low-frequency MSW's disturbance of the background density, the whistler's phase velocity is altered. Whistler waves get focussed and defocused as a result of phase velocity variation, which localises the wave field.

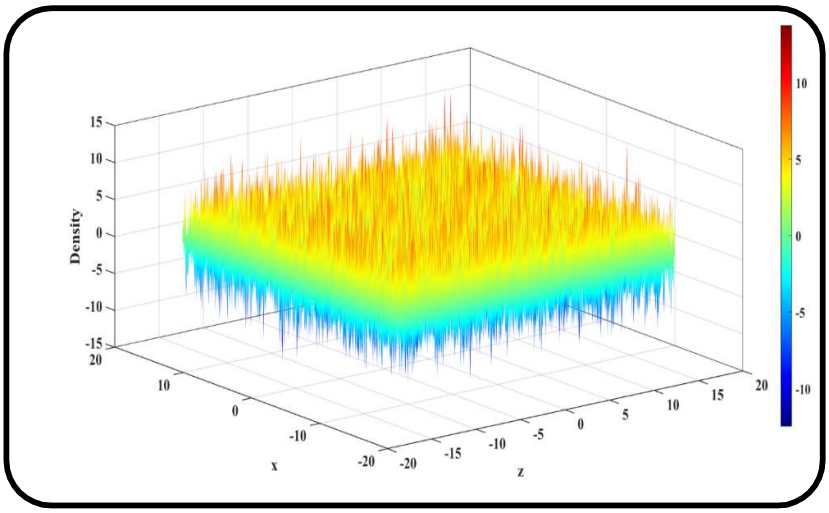

Figure 3.4 3D spatial plot of density cavitation at t=40, with accumulation and depletion regions as acquired by numerical simulation.

Consequently, whistler breaks down into filamentary structures. This localization process reveals energy exchange between pump whistler and magnetosonic waves. Fig. 3.5 illustrates the density fluctuations and amplitude variation of electric field for the MZSE. As a consequence of ponderomotive force, electric field gets trapped in the density cavity region. The modified Zakharov equation's electric fluctuations are shown in the top panel of Fig. 3.5, and density fluctuations (density cavitation and humps) for MZSE and MNLS are shown in the bottom panel (red and blue dotted lines correspond to MNLS and MZSE, respectively). This graphic demonstrates that MZSE and MNLS have slightly different density values, as would be expected. It should be noted that Eq. (3.12) was used to plot density fluctuations for MNLS.

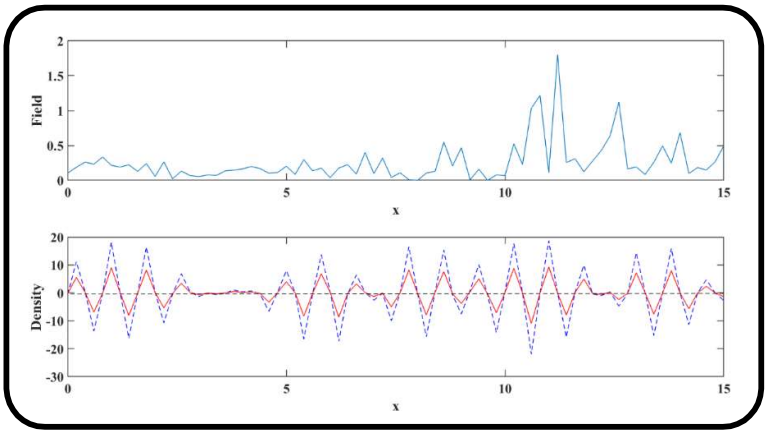

Figure 3.5 2D spatial plot of density cavitation and electric field fluctuations for MZSE at t=40.

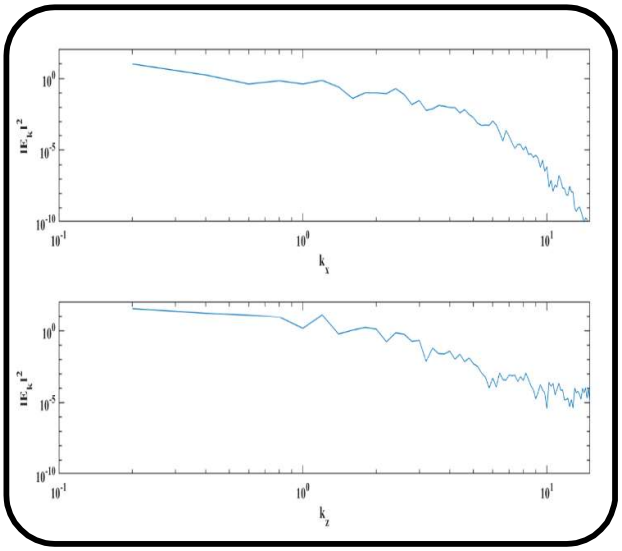

Figure 3.6 ***Evolution of electric field fluctuations power spectra at t=59 by MNLS model.***

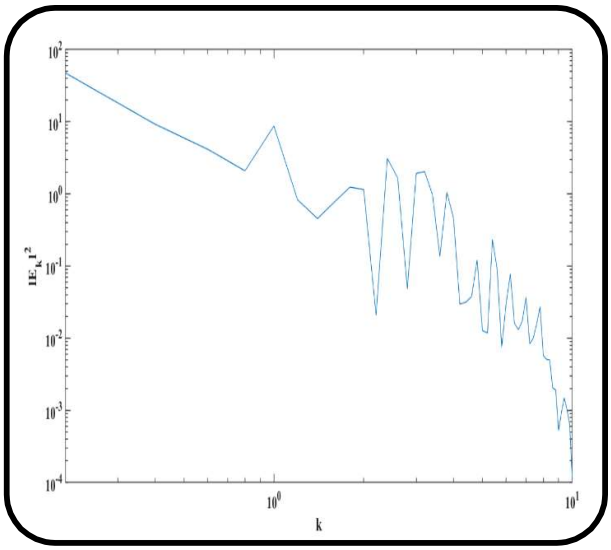

Figure 3.7 ***Evolution of electric field fluctuations power spectra at t=53 by MZSE model.***

Fig. 3.6 and 3.7 depict the wavenumber spectrum on (512×512) grid size for MNLS and MZSE model for time ensembled average T=50-60 and at T=53 respectively. In the current analysis, the constant growth rate of beam-driven mode $(\gamma=0.5083\omega_{ce})$ has been taken into account, and the quasi-steady state has not yet been achieved and won't be for some time. Therefore, it is unnecessary to explain the power spectra but we are planning to do our next problem by overcoming this shortcoming by considering the intensity-dependent growth rate. But after the whistler wave's amplitude is large enough to be seen, the beam-driven mode's growth rate is switched-off. Then remodeling Eq. (3.14) from 2D to 1D in the form of the following equation-

$$i\frac{\partial E'}{\partial t'}+c_2\frac{\partial^2 E'}{\partial z'^2}+i\frac{\partial E'}{\partial z'}+\frac{c_7c_4}{c_6}\left|E_y^2\right|E'+c_5nE'=0, \qquad (3.316)$$

Then we simulated Eq. (3.16) for grid size (4096×4096). The power spectra (Fig. 3.8 of whistler waves have been studied to investigate the energy cascading from larger to lower scales due to the localization process. The ensemble average for several electric field power spectra at the dynamic time range is implemented graphically for the quasi-steady state. The plot of ensembled averaged $|E_k|^2$ against k has been considered in this study, which is indicative of the power possessed by spatial modes between normalized time t=65-80, consisting of 15 spectra [Fig. 3.8]. Fig. 3.9 depicts the localized structure of whistler waves with high amplitude.

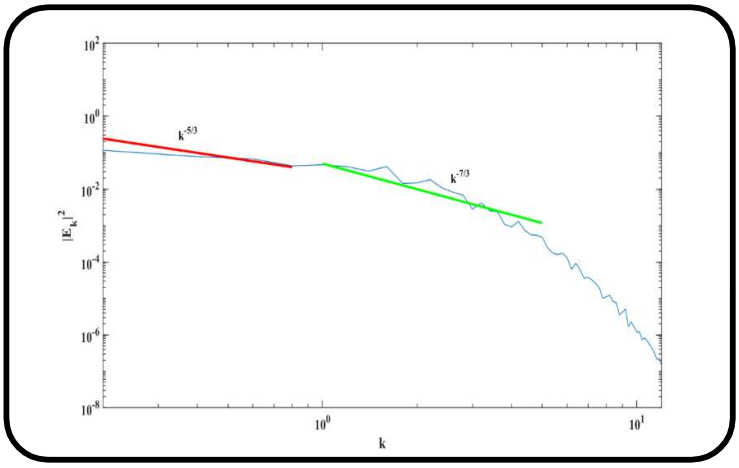

Figure 3.8 Power spectra of Electric field intensity of whistler wave $|E_k|^2$ ***against normalized wave vector k for modified nonlinear Schrödinger equation in quasi-steady state (in normalized units) on*** 4096×4096 ***grid size.***

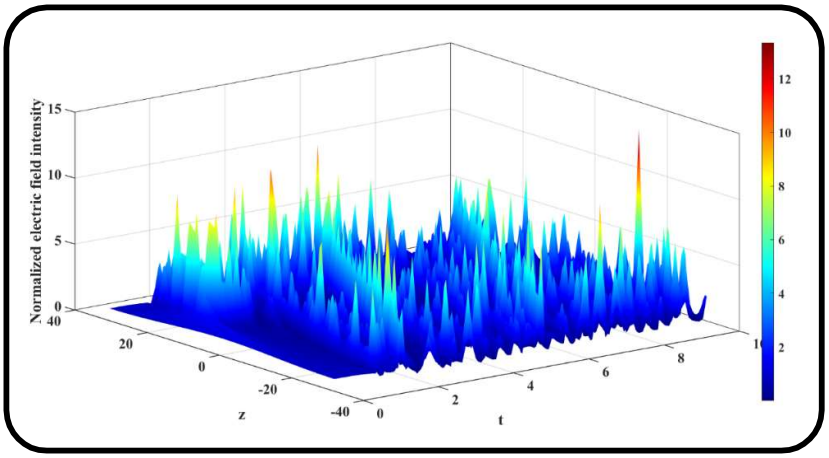

Figure 3.9 The evolution of the electric field $|E_y(t,z)|^2$ ***at different times in the t-z plane for modified nonlinear Schrödinger equation in quasi-steady state (in normalized units).***

3.4 Semianalytical Model

We have created a semianalytical model, to help us better grasp the physics underlying this localization of field. Also, we have determined the characteristic transverse scale size of the localized structure using this model.

For this steady-state model, whistler and MSWs propagation in the x-z plane must be considered. In this case, we deduced the following form from Eq. (3.5)-

$$a_1\frac{\partial E_y}{\partial z}+a_2\frac{\partial^2 E_y}{\partial x^2}+a_3\left(\frac{\delta n}{n_0}\right)E_y+a_4\left(\frac{\delta B}{B_0}\right)E_y+E_y\exp\left(k_i z\right)=0, \tag{3.17}$$

where a_1, a_2, a_3, and a_4 are constants defined as:

$$a_1 = 2ik_{0z}\frac{\left(-2\omega_0^2k_{0z}^2\lambda_e^4+2\omega_0^2k_{0x}^2\lambda_e^4+2\omega_0^2\lambda_e^2+k_{0x}^2\lambda_i^2v_A^2+2k_{0z}^2\lambda_i^2v_A^2\right)}{\left(9\lambda_i^2v_A^2k_{0z}^2k^2\right)}.$$

$$a_2 = -\frac{4\omega_0^2\lambda_e^4k_{0x}^2}{9\lambda_i^2v_A^2k_{0z}^2k^2}. \qquad a_3 = -\frac{(9k_{0z}^4\omega_{ce}^2\lambda_e^4+4k_{0x}^2k_{0z}^2\lambda_e^4\omega_{ce}^2)}{9\lambda_i^2v_A^2k_{0z}^2k^2}.$$

And, $$a_4 = 1+\frac{-4k_{0z}^4\omega_{ce}^2\lambda_e^4-2k_{0x}k_{0z}^2\lambda_e^4\omega_{ce}^2-2k_{0z}k_{0z}^2\lambda_e^4\omega_{ce}^2-4k_{0z}k_{0x}\omega_{ce}^2\lambda_e^4-k_{0z}^4\lambda_e^4\omega_{ce}^2}{9\lambda_i^2v_A^2k_0^2k_{0z}^2}.$$

Self-focusing of the beam is described by Eq. (3.17).

By taking the variation in electric field $\tilde{E}_y$ in terms of function eikonal 's' as follows

$$\tilde{E}_y = E_0(x,z)e^{ik_{0z}s(x,z)}. \tag{3.18}$$

Now, Using Eq. (3.18) into Eq. (3.17) and equating the real and imaginary parts, we obtain

$$-ia_1\frac{\partial S}{\partial z}E_0+a_2\frac{\partial^2E_0}{\partial x^2}+a_2k_{0z}^2\left(\frac{\partial S}{\partial x}\right)^2E_0+\left[\exp(\alpha'|E_x|^2)-1\right]E_0=0. \tag{3.19}$$

And $$\frac{ia_1}{k_{0z}}\frac{\partial E_0}{\partial z}+2a_2k_{0z}\frac{\partial S}{\partial x}\frac{\partial E_0}{\partial x}+a_2k_{0z}\frac{\partial^2S}{\partial x^2}E_0+E_0\exp(k_iz)=0. \tag{3.20}$$

Additionally, assuming the solution of Eqs. (3.19) and (3.20) are of Gaussian beam profile, we have

$$E_0^2 = \frac{E_{00}^2}{f_1}\exp\left(\frac{-x^2}{r_0^2f_1^2}+k_iz\right). \tag{3.21}$$

$$S = \beta_1(z)\frac{x^2}{2}+\phi(z). \tag{3.22}$$

Substituting Eqs. (3.21) and (3.22) in Eq. (3.20), we obtain

$$\beta_1 = \frac{a}{f_1}\frac{df_1}{dz}. \tag{3.23}$$

$$a = -\frac{(2\omega_0^2k_{0z}^2\lambda_e^4+2\omega_0^2k_{0x}^2\lambda_e^4+2\omega_0^2\lambda_e^2+k_{0x}^2\lambda_i^2v_A^2+2k_{0z}^2\lambda_i^2v_A^2)}{4\omega_0^2\lambda_e^4k_{0x}^2}.$$

Here, β_1 is the slowly increasing function of z, r_0 is the characteristic transverse scale size of the whistler wave along with x-direction, and f_1 is the beam width parameter of the wave.

Substituting Eqs. (3.21), (3.22) in Eq. (3.19) and equating coefficients of x^2, we obtain the dimensionless form beam width parameter-

$$\frac{d^2 f_1}{d\xi^2} = 4\left(\frac{a_2}{a_1}\right)^2 \frac{R_d}{r_0^2}\left[\frac{2}{r_0^2 f_1^3} - \frac{1}{a_2}\frac{\alpha E_{00}^2}{f_1^2}\exp\left(\frac{\alpha E_{00}^2}{f_1} + k_i z\right)\right], \tag{3.24}$$

Where $R_d\left(=k_{0z}r_0^2\right)$ is the diffraction length and $\xi\left(=\frac{z}{R_d}\right)$, is the distance of propagation.

$$a_1 = \frac{2}{k_{0z}}\left(\frac{-2\omega_0^2 k_{0z}^2\lambda_e^4 + 2\omega_0^2 k_{0x}^2\lambda_e^4 + 2\omega_0^2\lambda_e^2 + k_{0x}^2\lambda_i^2 v_A^2 + 2k_{0z}^2\lambda_i^2 v_A^2}{9\lambda_i^2 v_A^2 k^2}\right).$$

and $a_2 = \frac{4\omega_0^2\lambda_e^4 k_x^2}{9\lambda_i^2 v_A^2 k^2 k_{0z}^2}$.

Eq. (3.24) depicts the variation of f_1 (beam-width parameter) and ξ (distance of propagation). Using the Runge-Kutta method with the boundary conditions: $f_1|_{z=0} = 1$ and $\left.\frac{df_1}{d\xi}\right|_{z=0} = 0$, Eq. (3.24) is solved. On the right side, there are two words with opposing signs. First, there is one for the diverging term, and then there is one for the nonlinear term. The fact that both components in this equation have opposing signs indicates that they compete. The first term, which causes the divergence, is a diffracting term. The second term, which results from the ponderomotive force acting on the electrons, is non-linear. Fig. 3.10 depicts the electric field intensity distribution of a whistler wave in the x-z plane. Here, $r_{01} = 3.41\times10^7 cm\ (200\lambda_e)$. The electric field is very low $\approx 10^{-3}$ StatV/cm due to which power is also decreasing so diffraction term dominates till $f >> 1$, as z propagates intensity increases of term $\exp(k_i z)$ and again f decreases less than one and intensity increases as a result focusing increases.

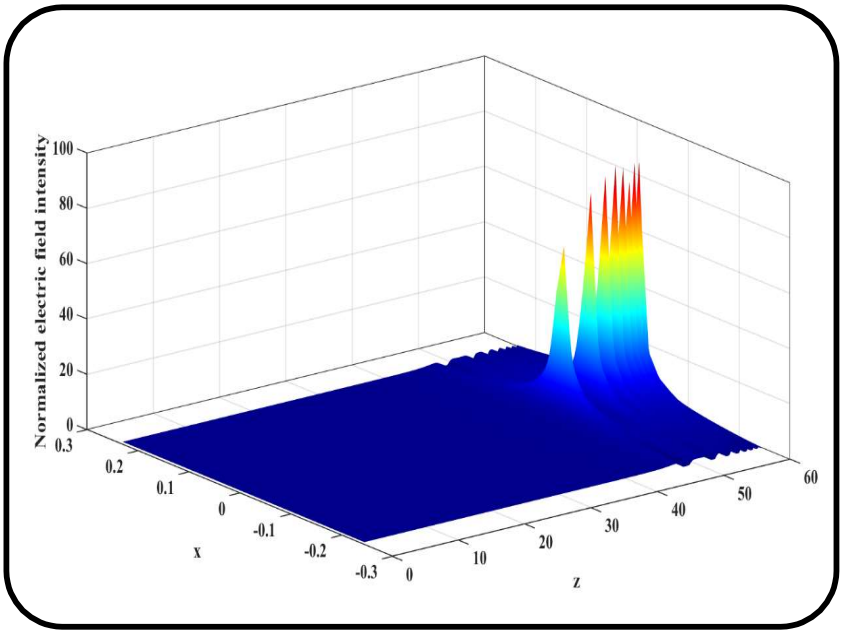

Figure 3.10 The normalized electric field intensity variation of pump wave in x-z plane obtained by the semi-analytical model after incorporating the density harmonics from simulation results.

3.5 Summary and Discussion

In the current analysis, we have studied the MNLS and MZSE model involving the nonlinear interactions of high-frequency whistler wave and low-frequency MSWs, where the coupling among these waves is due to ponderomotive nonlinear force. However, in this scenario, the energetic electron beam source has replaced the magnetic reconnection mechanism. As a result, the dynamics of beam-driven whistler-mode have been set up with the reckoning that it will mount up from the noise level due to beam energy to large amplitude such that nonlinear effects due to nonlinear ponderomotive force will lead to the localization of whistler wave, and ultimately, to the turbulent state. On the account of this nonlinear ponderomotive force, whistler wave gets localized and density cavities and humps are formed. Our attention will be drawn to three key aspects of plasma turbulence: its existence, scaling rules, the contribution of small-scale coherent structure to plasma heating, and the effect of density fluctuations on the rate at which turbulent energy cascades. In our current analysis, the cavitation and renucleation process generates turbulence by using the MNLS model established by low-frequency MSW and high-frequency whistler. Numerical simulation has been done to study all these aspects. Also, quasi-steady state has not been achieved due to the constant growth rate of beam, so to study the quasi-steady state of the system, we remodel the simulation Equation (Eq. (3.14)) into t-z domain for grid size (4096×4096). The consequences of this numerical simulation manifest the presence of turbulence. We have also examined the power spectra of whistler wave (Fig. 3.8) in 1D for grid size (4096×4096). For $k\lambda_e<1$, the power spectrum

follows scaling $\sim k^{-5/3}$, and for $k\lambda_e > 1$, it follows scaling $\sim k^{-7/3}$, known as Kolmogorov's scaling as reported in the literature which may result in the particle acceleration and heating of particles. We have also devised a semianalytical model and determined the transverse scale size of these structures to help us comprehend the physics that underlies localizations. Consequently, owing to nonlinear interactions, the power-law fluctuation of the electric field spectrum gives a huge impact that this noise is a well-grown turbulence process, with electric field energy cascading to higher frequencies. The depth of this is in the range of few-electron skin ($0.19\lambda_e$). The outcomes of the study show the whistler turbulence in the magnetic reconnection sites created by the electron beam and show localized structures and whistler fluctuations which are to the observations of Zhao et al.[29].

The effects of magnetic islands and current sheet generation on whistler turbulence due to magnetic reconnection have not been accounted for in the existing model. We want to carry out this task in the future. In conclusion, our research will help to improve the quantitative knowledge of whistler-mode waves generated by beams of light in turbulent environments.

References

[1] G. Vetoulis and J. F. Drake, "H - / d sxPt •. P .•," vol. 104, pp. 6919–6928, 1999.

[2] G. M. Mason, M. I. Desai, R. A. Mewaldt, and C. M. S. Cohen, "Particle acceleration in the heliosphere," *AIP Conf Proc*, vol. 1516, no. May, pp. 117–120, 2013, doi: 10.1063/1.4792550.

[3] A. A. Schekochihin *et al.*, "Astrophysical gyrokinetics: Kinetic and fluid turbulent cascades in magnetized weakly collisional plasmas," *Astrophysical Journal, Supplement Series*, vol. 182, no. 1, 2009, doi: 10.1088/0067-0049/182/1/310.

[4] W. H. Matthaeus and M. L. Goldstein, "Stationarity of magnetohydrodynamic fluctuations in the solar wind," *J Geophys Res*, vol. 87, no. A12, p. 10347, 1982, doi: 10.1029/ja087ia12p10347.

[5] J. P. Eastwood, T. D. Phan, S. D. Bale, and A. Tjulin, "Observations of turbulence generated by magnetic reconnection," *Phys Rev Lett*, vol. 102, no. 3, pp. 1–4, 2009, doi: 10.1103/PhysRevLett.102.035001.

[6] D. A. Roberts, W. Klein, M. L. Goldstein, and W. H. Matthaeus, "ILaboratory for Extraterrestrial," *October*, vol. 92, 1987.

[7] R. B. Horne, R. M. Thorne, S. A. Glauert, J. M. Albert, N. P. Meredith, and R. R. Anderson, "Timescale for radiation belt electron acceleration by whistler mode chorus

waves," *J Geophys Res Space Phys*, vol. 110, no. A3, 2005, doi: 10.1029/2004JA010811.

[8] S. Servidio *et al.*, "Magnetic reconnection as an element of turbulence," *Nonlinear Process Geophys*, vol. 18, no. 5, pp. 675–695, 2011, doi: 10.5194/npg-18-675-2011.

[9] W. H. Matthaeus and S. L. Lamkin, "Rapid magnetic reconnection caused by finite amplitude fluctuations," *Physics of Fluids*, vol. 28, no. 1, 1985, doi: 10.1063/1.865147.

[10] G. Kowal, D. A. Falceta-Gonçalves, A. Lazarian, and E. T. Vishniac, "Statistics of Reconnection-driven Turbulence," *Astrophys J*, vol. 838, no. 2, 2017, doi: 10.3847/1538-4357/aa6001.

[11] H. Karimabadi, V. Roytershteyn, W. Daughton, and Y.-H. Liu, "Recent Evolution in the Theory of Magnetic Reconnection and Its Connection with Turbulence," 2013. doi: 10.1007/978-1-4899-7413-6_9.

[12] S. Saito, S. P. Gary, H. Li, and Y. Narita, "Whistler turbulence: Particle-in-cell simulations," *Phys Plasmas*, vol. 15, no. 10, 2008, doi: 10.1063/1.2997339.

[13] S. P. Gary, S. Saito, and H. Li, "Cascade of whistler turbulence: Particle-in-cell simulations," *Geophys Res Lett*, vol. 35, no. 2, 2008, doi: 10.1029/2007GL032327.

[14] O. Chang, S. P. Gary, and J. Wang, "Whistler turbulence at variable electron beta: Three-dimensional particle-in-cell simulations," *J Geophys Res Space Phys*, vol. 118, no. 6, 2013, doi: 10.1002/jgra.50365.

[15] D. Shaikh, "Inhomogeneous whistler turbulence in space plasmas," *Mon Not R Astron Soc*, vol. 405, no. 4, pp. 2521–2528, 2010, doi: 10.1111/j.1365-2966.2010.16625.x.

[16] G. Ganguli, C. Crabtree, M. Mithaiwala, L. Rudakov, and W. Scales, "Evolution of lower hybrid turbulence in the ionosphere," *Phys Plasmas*, vol. 22, no. 11, 2015, doi: 10.1063/1.4936281.

[17] V. A. Svidzinski, H. Li, H. A. Rose, B. J. Albright, and K. J. Bowers, "Particle in cell simulations of fast magnetosonic wave turbulence in the ion cyclotron frequency range," *Phys Plasmas*, vol. 16, no. 12, 2009, doi: 10.1063/1.3274559.

[18] R. L. Stenzel, "Whistler waves in space and laboratory plasmas," *J Geophys Res Space Phys*, vol. 104, no. A7, 1999, doi: 10.1029/1998ja900120.

[19] Y. Zhang, H. Matsumoto, and H. Kojima, "Lion roars in the magnetosheath: The Geotail observations," *J Geophys Res Space Phys*, vol. 103, no. A3, 1998, doi: 10.1029/97ja02519.

[20] W. Masood, S. J. Schwartz, M. Maksimovic, and A. N. Fazakerley, "Electron velocity distribution and lion roars in the magnetosheath," *Ann Geophys*, vol. 24, no. 6, 2006, doi: 10.5194/angeo-24-1725-2006.

[21] L. Y. Li *et al.*, "Roles of whistler mode waves and magnetosonic waves in changing the outer radiation belt and the slot region," *J Geophys Res Space Phys*, vol. 122, no. 5, 2017, doi: 10.1002/2016JA023634.

[22] S. Y. Huang *et al.*, "Occurrence rate of whistler waves in the magnetotail reconnection region," *J Geophys Res Space Phys*, vol. 122, no. 7, 2017, doi: 10.1002/2016JA023670.

[23] R. B. Horne, G. v. Wheeler, and H. S. C. K. Alleyne, "Proton and electron heating by radially propagating fast magnetosonic waves," *J Geophys Res Space Phys*, vol. 105, no. A12, 2000, doi: 10.1029/2000ja000018.

[24] R. B. Horne, R. M. Thorne, S. A. Glauert, N. P. Meredith, D. Pokhotelov, and O. Santolík, "Electron acceleration in the Van Allen radiation belts by fast magnetosonic waves," *Geophys Res Lett*, vol. 34, no. 17, 2007, doi: 10.1029/2007GL030267.

[25] B. Lembege, S. T. Ratliff, J. M. Dawson, and Y. Ohsawa, "Ion heating and acceleration by strong magnetosonic waves," *Phys Rev Lett*, vol. 51, no. 4, 1983, doi: 10.1103/PhysRevLett.51.264.

[26] H. Zhang, Z. Liu, F. Wang, B. Liu, L. Wei, and W. Duan, "The upper-limited amplitude of the nonlinear magnetosonic solitary wave in a magnetized plasma", doi: 10.1007/s10509-022-04121-x.

[27] X. Gao, J. Sun, Q. Lu, L. Chen, and S. Wang, "Generation of Lower Harmonic Magnetosonic Waves Through Nonlinear Wave-Wave Interactions," *Geophys Res Lett*, vol. 45, no. 16, 2018, doi: 10.1029/2018GL079090.

[28] S. Saito, Y. Nariyuki, and T. Umeda, "Magnetosonic/whistler mode turbulence influences on ion dynamics," *Phys Plasmas*, vol. 25, no. 12, 2018, doi: 10.1063/1.5053760.

[29] S. Q. Zhao *et al.*, "Observations of the Beam-Driven Whistler Mode Waves in the Magnetic Reconnection Region at the Dayside Magnetopause," *J Geophys Res Space Phys*, vol. 126, no. 2, pp. 1–11, 2021, doi: 10.1029/2020JA028525.

[30] C. Krafft and A. S. Volokitin, "Electromagnetic radiation from upper-hybrid wave turbulence in inhomogeneous solar plasmas," *Plasma Phys Control Fusion*, vol. 62, no. 2, 2020, doi: 10.1088/1361-6587/ab569d.

[31] G. D. Reeves *et al.*, "The Beam Plasma Interactions Experiment: An Active Experiment Using Pulsed Electron Beams," *Frontiers in Astronomy and Space Sciences*, vol. 7, 2020, doi: 10.3389/fspas.2020.00023.

[32] Y. Narita *et al.*, "ON ELECTRON-SCALE WHISTLER TURBULENCE IN THE SOLAR WIND," *Astrophys J*, vol. 827, no. 1, 2016, doi: 10.3847/2041-8205/827/1/l8.

[33] D. A. Gurnett *et al.*, "PLASMA WAVE TURBULENCE AT THE MAGNETOPAUSE: OBSERVATIONS FROM ISEE 1 AND 2.," *J Geophys Res*, vol. 84, no. A12, 1979, doi: 10.1029/JA084iA12p07043.

[34] V. I. Karpman, "Whistler Solitons, Their Radiation and the Self-Focusing of Whistler Wave Beams," in *Nonlinear MHD Waves and Turbulence*, 2007. doi: 10.1007/3-540-47038-7_2.

[35] A. Das, R. Singh, P. Kaw, and S. Champeaux, "Nonlinear coupling of whistler wave turbulence with magnetosonic perturbations," *Phys Plasmas*, vol. 9, no. 6, 2002, doi: 10.1063/1.1480829.

[36] D. Biskamp, E. Schwarz, and J. F. Drake, "Two-dimensional electron magnetohydrodynamic turbulence," *Phys Rev Lett*, vol. 76, no. 8, 1996, doi: 10.1103/PhysRevLett.76.1264.

[37] A. Das and P. H. Diamond, "Theory of two-dimensional mean field electron magnetohydrodynamics," *Phys Plasmas*, vol. 7, no. 1, 2000, doi: 10.1063/1.873792.

[38] S. Galtier and A. Bhattacharjee, "Anisotropic weak whistler wave turbulence in electron magnetohydrodynamics," *Phys Plasmas*, vol. 10, no. 8, 2003, doi: 10.1063/1.1584433.

[39] M.-M. Shen and D. R. Nicholson, "Numerical comparison of strong Langmuir turbulence models," *Physics of Fluids*, vol. 30, no. 4, 1987, doi: 10.1063/1.866307.

[40] G. D. Doolen, D. F. Dubois, and H. A. Rose, "Nucleation of cavitons in strong langmuir turbulence," *Phys Rev Lett*, vol. 54, no. 8, 1985, doi: 10.1103/PhysRevLett.54.804.

[41] R. P. Sharma, P. Stubbe, and A. D. Verga, "Numerical simulation of a Zakharov-Boussinesq system of equations to study Langmuir turbulence in the ionosphere," *J Geophys Res Space Phys*, vol. 101, no. A5, 1996, doi: 10.1029/96ja00043.

[42] Jyoti, S. C. Sharma, N. Pathak, and R. P. Sharma, "Beam-driven whistler mode nonlinear saturation and turbulence in the magnetopause," *Phys Plasmas*, vol. 29, no. 9, p. 092104, Sep. 2022, doi: 10.1063/5.0098108.

CHAPTER-4

Localization of Beam Generated whistler wave and turbulence generation in reconnection region of magnetopause

4.1 Introduction

One of the most important plasma phenomena is known as magnetic reconnection, which includes a swift topological switch in the magnetic field and an effective conversion of magnetic energy to the kinetic energy. In laboratory, space, and astrophysical plasmas, magnetic field lines alter their topology and transform magnetic energy into plasma particles by acceleration and heating. Magnetic reconnection may be seen in the generation of solar flares, coronal mass ejections, and the interface of solar winds with the Earth's magnetosphere, and it is considered to originate during the formation of stars[1]–[8]. The astonishing potential of astrophysical plasmas to establish magnetic structure ultimately leads to the accumulation of magnetic energy inside stressed areas, including current sheets. During the process of magnetic reconnection, which results in a reconfiguration of the magnetic field as well as high-speed flows, thermal heating, and nonthermal particle acceleration, this stored energy is frequently released explosively[9]–[15]. Also, a review article on the theory of magnetic reconnection has been reported earlier[16]. Recently, the coalescence process of numerous magnetic islands originally created in an extended current sheet has been studied, with a particular emphasis on the scaling of the size of the inner structure of the coalesced islands and the accompanying progressive plasma heating process[17]. The reconnection can be examined in situ through space applications and laboratory studies[18]. However, only in situ space observations can offer precise data on the fields and particle distribution functions.

In space plasma, turbulence is prevalent and is recognized to play a significant role as it cascades energy from large to smaller scales, ultimately leading to dissipation and particles heating. There is mounting evidence that in magnetized plasmas, magnetic reconnection and turbulence are closely related[19]–[22]. The Earth's magnetosheath, magnetopause, and magnetotail are all potential sites for magnetic reconnection[23], [24]. Many authors have explored how turbulence affects the rate of reconnection, specifically how turbulence already present might change Sweet-Parker reconnection and how turbulence may form because of reconnection[19]. Forced turbulence experiments indicate that turbulent reconnection is quicker than laminar reconnection, and the reconnection rate rises with increasing turbulence level [25].

Additionally, magnetic reconnection itself causes turbulence, which feeds back on itself. Many previous studies investigated the turbulence described as the nonlinear evolution of field and large-scale islands produced at reconnection zones producing the multiple X-O point[26]. Eastwood et al.[27] reported the spacecraft observations of turbulence generated by the magnetic reconnection and fluctuations in electric, magnetic field followed by power law of scaling -5/3 and -8/3. Dynamic alignment models[28]–[30] of turbulence tend to anticipate perpendicular spectral indices close to -3/2, whereas the original 'GS95' model[31], which does not include dynamic alignment, predicts a spectral index of -5/3. Surprisingly, it has yet to be determined quantitatively which of these two types of models is true. The new perspective on reconnection relevant in space and astrophysical contexts, where plasma is generally in a fully turbulent regime is numerically analysed by simulations of two-dimensional magnetohydrodynamic turbulence reveals the presence of a large number of X-type neutral points where magnetic reconnection occurs[32]. Numerical and analytical studies suggest that when magnetic reconnection events occur within the turbulent plasma, they can disrupt these idealized scaling laws[30], [33]. Franci et al.[34] provide numerical evidence that magnetic reconnection can act as a driver for the onset of the sub-ion turbulent cascade. But Adhikari et al.[35] gives a new direction on relation of reconnection and turbulence, they examine the properties of energy transfer in reconnection and turbulence and found that the energy transfer in both simulations is found to be structurally very similar, with most of the energy transfer occurring through incompressive channels. This provides evidence that reconnection dynamics involves energy transfer analogous to standard turbulence. Recently Adhikari et al.[36] extend the turbulence diagnostics to the case of guide field reconnection and determine how the degree of magnetic shear modifies the turbulence-like properties of reconnection. Although turbulence and reconnection appear to be closely related and it is known that turbulence impacts reconnection, the mechanics of their interaction is still not entirely established.

Different wave modes are detected in earth's reconnection region, like whistler wave[37]–[43], electron cyclotron waves[38], [44], kinetic Alfvén waves[45], [46], upper hybrid waves[47], [48], lower hybrid waves[49], [50], and electrostatic solitary waves[51]–[53]. Several waves, including whistler-mode, have been seen at the magnetic reconnection regions generated due to the energetic electron beam[41], [54]–[56]. Recently, whistler-mode has been reported at Mars[57] and their generation mechanism in magnetic reconnection is based on in situ measurements from Mars Atmosphere and Volatile Evolution Mission (MAVEN). Cerri et al. also observed that large-scale turbulent motions establish a scaling of -5/3 spectrum at $k\lambda_i < 1$ and, at the same time, feed the

formation of current sheets where magnetic reconnection occurs[58]. They also investigated the role of fast magnetic reconnection in the development of a quasi-steady turbulent state by means of 2D-3V high-resolution Vlasov–Maxwell simulations. In past, Stenflo et al.[59] reported the nonlinear coupling of electron whistler mode and magnetosonic waves but without considering the concept of magnetic island and found the relevance to the non-thermal fluctuations in magnetic field which lead to the plasma heating.

The present work related to whistler wave generation and it's development into localized coherent structures in the presence of magnetic islands is motivated by Zhao et al.[55] work in which the coherent structures of whistler wave at magnetic reconnection locations has been reported due to intense electron beams. Using findings from the Magnetospheric Multiscale (MMS) mission, they studied the whistler waves generated by intense electron beam in the dayside magnetosphere and observed the maximum growth rate of the wave at $k\lambda_e \sim 0.53$ within the frequency band of $0.1\omega_{ce} - 0.5\omega_{ce}$. Here, λ_e is the electron skin-depth, k is the wave number, and ω_{ce} is electron gyrofrequency. Although, at initial stage these structures are coherent, but it is expected that at later stage it might be turbulent. To the best of our knowledge, no particular research concerning beam-driven whistler localization and turbulence has been documented in the previously reported work, despite a few works having been described in the framework of beam-driven turbulence[60], [61] but without taking the influence of magnetic islands.

The main goals of this study are to illustrate significant developments in understanding the generation of whistler wave due to the intense electron beam at magnetic reconnection as observed by magnetospheric multiscale mission (MMS)[55], and under the influence of magnetic island. In order to achieve this, a three-dimensional model of a beam-driven whistler wave has been developed. In this model, the whistler wave initiates out owing to the beam's energy and grows to a huge amplitude, where nonlinear effects from the ponderomotive force cause the whistler wave to localize, which ultimately causes the turbulent state. To grasp the nonlinear phase of wave development and saturation, we take into account the nonlinear interaction of a low-frequency ion acoustic wave (IAW) and a high-frequency whistler wave, as well as the ponderomotive nonlinearity caused by the whistler wave. Along with this, we are also analyzing the dynamics of nonlinear whistler wave in the presence of magnetic islands. Then, the governing equations for the IAWs and the whistler wave are then formulated as coupled nonlinear equations and numerically solved with the pseudo-spectral method for spatial integration and a modified version of predictor-corrector method for temporal integration.

The content of this paper is organised as- In section 2, dynamics of 3D whistler wave generated by intense electron beam is derived. Dynamics of ion acoustic wave is discussed in section 3. Numerical simulation methods and results obtained from simulation are discussed in section 4. In order to understand the basic physics behind the localization we have also studied the semianalytical model in section 5. Summary and conclusion of our current research work is given in section 6.

4.2 Dynamics of Model

4.2.1 Beam-driven whistler wave dynamics

The dynamical equation for a 3D whistler wave with an ambient magnetic field along the z-axis in a magnetized plasma propagating in the x, y, and z planes with a wave vector $\vec{k} = k_x\hat{x} + k_y\hat{y} + k_z\hat{z}$, is derived utilizing two fluid models. The governing dynamical equation of 3D whistler wave in terms of electric field can be written as (the detailed derivation has been given as Appendix-A)

$$\begin{aligned}&\frac{\partial^2 E_z}{\partial t^2}+\frac{\partial^6 E_z}{\partial t^2\partial x^4}\lambda_e^4+\frac{\partial^6 E_z}{\partial t^2\partial y^4}\lambda_e^4+\frac{\partial^6 E_z}{\partial t^2\partial z^4}\lambda_e^4+2\lambda_e^4\frac{\partial^4 E_z}{\partial t^2\partial z^2}\left(\frac{\partial^2}{\partial x^2}+\frac{\partial^2}{\partial y^2}\right)-2\lambda_e^2\left(\frac{\partial^2}{\partial x^2}+\frac{\partial^2}{\partial y^2}+\frac{\partial^2}{\partial z^2}\right)\frac{\partial E_z}{\partial t^2}\\&+\lambda_i^2 v_A^2\left(\frac{\partial^2}{\partial x^2}+\frac{\partial^2}{\partial y^2}\right)\frac{\partial^2 E_z}{\partial z^2}+\lambda_i^2 v_A^2\frac{\partial^4 E_z}{\partial z^4}+\frac{\lambda_i^2 v_A^2 B_{0y}^2}{B_{0z}^2}\left(\frac{\partial^2}{\partial x^2}+\frac{\partial^2}{\partial y^2}\right)\frac{\partial^2 E_z}{\partial y^2}+\frac{\lambda_i^2 v_A^2 B_{0y}^2}{B_{0z}^2}\frac{\partial^4 E_z}{\partial y^2\partial z^2}+\\&\frac{2\lambda_i^2 v_A^2 B_{0y}}{B_{0z}}\left(\frac{\partial^2}{\partial x^2}+\frac{\partial^2}{\partial y^2}\right)\frac{\partial^2 E_z}{\partial y\partial z}+\frac{2\lambda_i^2 v_A^2 B_{0y}}{B_{0z}}\frac{\partial^4 E_z}{\partial y\partial z^3}=0.\end{aligned}\tag{4.1}$$

where $\omega_{ce}\left(=\frac{eB_0}{m_e c}\right)$ is the electron gyrofrequency of wave, $v_A\left(=\sqrt{\frac{B_0^2}{4\pi n_0 m_i}}\right)$ is Alfven waves's speed, n_0 denotes the background number density, c denotes the velocity of light, and $\lambda_i\left(=\sqrt{\frac{c^2 m_e}{4\pi n_0 e^2}}\right)$ is the collisionless ion skin depth, $\lambda_e\left(=\sqrt{\frac{c^2 m_e}{4\pi n_0 e^2}}\right)$ is the collisionless electron skin depth. Additionally, it is reported that beam-driven growth rate is taken into account then, the aforementioned equation becomes $\frac{d}{dt}\to\left(\frac{d}{dt}+\gamma\right)$ (please see appendix),

$$\begin{aligned}&\left(\frac{\partial^2}{\partial t^2}+2\gamma\frac{\partial}{\partial t}\right)E_z+\frac{\partial^6 E_z}{\partial t^2\partial x^4}\lambda_e^4+\frac{\partial^6 E_z}{\partial t^2\partial y^4}\lambda_e^4+\frac{\partial^6 E_z}{\partial t^2\partial z^6}\lambda_e^4+2\lambda_e^4\frac{\partial^4 E_z}{\partial t^2\partial z^2}\left(\frac{\partial^2}{\partial x^2}+\frac{\partial^2}{\partial y^2}\right)-\\&2\lambda_e^2\left(\frac{\partial^2}{\partial x^2}+\frac{\partial^2}{\partial y^2}+\frac{\partial^2}{\partial z^2}\right)\frac{\partial^2 E_z}{\partial t^2}+\lambda_i^2 v_A^2\left(\frac{\partial^2}{\partial x^2}+\frac{\partial^2}{\partial y^2}\right)\frac{\partial^2 E_z}{\partial z^2}+\lambda_i^2 v_A^2\frac{\partial^4 E_z}{\partial z^4}+\\&\frac{\lambda_i^2 v_A^2 B_{0y}^2}{B_{0z}^2}\left(\frac{\partial^2}{\partial x^2}+\frac{\partial^2}{\partial y^2}\right)\frac{\partial^2 E_z}{\partial y^2}+\frac{\lambda_i^2 v_A^2 B_{0y}^2}{B_{0z}^2}\frac{\partial^4 E_z}{\partial y^2\partial z^2}+\frac{2\lambda_i^2 v_A^2 B_{0y}}{B_{0z}}\left(\frac{\partial^2}{\partial x^2}+\frac{\partial^2}{\partial y^2}\right)\frac{\partial^2 E_z}{\partial y\partial z}\\&+\frac{2\lambda_i^2 v_A^2 B_{0y}}{B_{0z}}\frac{\partial^4 E_z}{\partial y\partial z^3}=0.\end{aligned}\tag{4.2}$$

For this Eq. (4.2), the following envelope solution is assumed.

$$\tilde{E}_z = E_z(x,y,z,t)e^{i(k_{0x}\hat{x}+k_{0y}\hat{y}+k_{0z}\hat{z}-\omega_0 t)}. \tag{4.3}$$

By taking into account the impact of a whistler wave on the background density and relieving the aforementioned solution into Eq. (4.2), we can obtain the dynamical equation of a nonlinear whistler wave propagating through plasma

$$\begin{aligned}
&2i\omega_0(1+\lambda_e^4k_0^4+2\lambda_e^2k_0^2+2\lambda_e^4k_{0x}^2k_{0z}^2+2\lambda_e^4k_{0y}^2k_{0z}^2)\frac{\partial E_z}{\partial t}+(4\omega_0^2\lambda_e^4k_{0x}^2)\frac{\partial^2 E_z}{\partial x^2}+\\
&(4\omega_0^2\lambda_e^4k_{0y}^2)\frac{\partial^2 E_z}{\partial y^2}+(4\omega_0^2\lambda_e^4k_{0z}^2-4\lambda_i^2v_A^2k_{0z}^2)\frac{\partial^2 E_z}{\partial z^2}+\\
&2ik_{0x}(2\omega_0^2k_{0x}^2\lambda_e^4+2\omega_0^2k_{0z}^2\lambda_e^4+2\omega_0^2\lambda_e^2+k_{0z}^2\lambda_i^2v_A^2)\frac{\partial E_z}{\partial x}+\\
&2ik_{0y}(2\omega_0^2k_{0y}^2\lambda_e^4+2\omega_0^2k_{0z}^2\lambda_e^4+2\omega_0^2\lambda_e^2-k_{0z}^2\lambda_i^2v_A^2)\frac{\partial E_z}{\partial y}+\\
&2ik_{0z}(2\omega_0^2k_{0z}^2\lambda_e^4+2\omega_0^2k_{0x}^2\lambda_e^4+2\omega_0^2k_{0y}^2\lambda_e^4+2\omega_0^2\lambda_e^2-k_{0y}^2\lambda_i^2v_A^2-2k_{0z}^2\lambda_i^2v_A^2)\frac{\partial E_z}{\partial z}+\\
&(4\lambda_i^2v_A^2k_{0x}k_{0z}-8\omega_0^2\lambda_e^4k_{0z}k_{0x})\frac{\partial^2 E_z}{\partial x\partial z}+(4\lambda_i^2v_A^2-8\omega_0^2\lambda_e^4)k_{0y}k_{0z}\frac{\partial^2 E_z}{\partial y\partial z}+\\
&\frac{\lambda_i^2v_A^2B_{0y}^2}{B_{0z}^2}k^2k_{0y}^2E_z+\frac{2\lambda_i^2v_A^2B_{0y}}{B_{0z}}k^2k_{0y}k_{0z}E_z-(\lambda_i^2v_A^2k^2k_{0z}^2)\frac{\delta n}{n_0}E_z+2i\gamma' E_z=0,
\end{aligned} \tag{4.4}$$

where k_{0x}, k_{0y} and k_{0z} are wave vector components of whistler related to the background magnetic field are given as, $k_0^2=k_{0x}^2+k_{0y}^2+k_{0z}^2$. Here n' denotes the modified density, i.e., $n'=n_0+\delta n$, and $\frac{\delta n}{n_0}$ denotes the pertubation in plasma density due to non-linear whistler wave. we have used the relation of the magnetic field and vector potential $\left(\frac{B_{0y}}{B_{0z}}=\frac{\delta A_z}{A_0}\right)$. ($\delta A_z$, is the vector potential associated with magnetic field.)

Eq. (4.4) in normalized dimensionless form is given as

$$\begin{aligned}
&ic_1\frac{\partial E_z}{\partial t}+c_2\frac{\partial^2 E_z}{\partial x^2}+c_3\frac{\partial^2 E_z}{\partial y^2}+c_4\frac{\partial^2 E_z}{\partial z^2}+ic_5\frac{\partial E_z}{\partial x}+ic_6\frac{\partial E_z}{\partial y}+ic_7\frac{\partial E_z}{\partial z}+\\
&c_8\frac{\partial^2 E_z}{\partial x\partial z}+c_9\frac{\partial^2 E_z}{\partial y\partial z}+c_{10}\left(\frac{\delta A_z}{A_0}\right)^2E_z+c_{11}\left(\frac{\delta A_z}{A_0}\right)E_z-\frac{\delta n}{n_0}E_z+2i\gamma' E_z=0,
\end{aligned} \tag{4.5}$$

where Eq. (4.5) represents the whistler wave's normalized dynamical equation, which causes turbulence. The normalizing parameter are-

$t_n=1/\omega_0$.

$$x_n = \frac{k_{0x}(2\omega_0^2 k_{0x}^2 \lambda_e^4 + 2\omega_0^2 k_{0z}^2 \lambda_e^4 + 2\omega_0^2 \lambda_e^2 + k_{0z}^2 \lambda_i^2 v_A^2)}{\omega_0(1+\lambda_e^4 k_0^4 + 2\lambda_e^2 k_0^2 + 2\lambda_e^4 k_{0x}^2 k_{0z}^2 + 2\lambda_e^4 k_{0y}^2 k_{0z}^2)}.$$

$$z_n = \frac{2i(-2\omega_0^2 k_{0x}^3 \lambda_e^4 + 2\omega_0^2 k_{0x} k_{0z}^2 \lambda_e^4 + 2\omega_0^2 \lambda_e^2 k_{0x} + k_{0x} k_{0z}^2 \lambda_i^2 v_A^2 + 2k_{0z}^3 \lambda_i^2 v_A^2)}{2\omega_0(1+\lambda_e^4 k_{0x}^4 + \lambda_e^4 k_{0z}^4 + 2\lambda_e^2 k_{0x}^2 + 2\lambda_e^2 k_{0z}^2)}.$$

In this section, the beam instability that generates the whistler wave will be described. The growth rate of whistler wave generated by an energetic electron beam, i.e., is included phenomenologically and its value corresponding with the data published by (Zhao et al., 2021[55]) will be utilized in simulations here. The field perturbation due to magnetic islands field is incorporated in our model [62], $\frac{\delta A_z}{A_0} = \left(-\frac{x^2}{2} + b_0 \cos(ky)\right)$. So, using the profile of field perturbation Eq. (4.5) modifies as-

$$ic_1 \frac{\partial E_z}{\partial t} + c_2 \frac{\partial^2 E_z}{\partial x^2} + c_3 \frac{\partial^2 E_z}{\partial y^2} + c_4 \frac{\partial^2 E_z}{\partial z^2} + ic_5 \frac{\partial E_z}{\partial x} + ic_6 \frac{\partial E_z}{\partial y} + ic_7 \frac{\partial E_z}{\partial z} +$$
$$c_8 \frac{\partial^2 E_z}{\partial x \partial z} + c_9 \frac{\partial^2 E_z}{\partial y \partial z} + c_{10}\left(-\frac{x^2}{2} + b_0 \cos(ky)\right)^2 E_z + \qquad (4.6)$$
$$c_{11}\left(-\frac{x^2}{2} + b_0 \cos(ky)\right) E_z - \frac{\delta n}{n_0} E_z + 2i\gamma' E_z = 0 \,,$$

where $c_1 = \frac{2\omega_0(1+\lambda_e^4 k_0^4 + 2\lambda_e^2 k_0^2 + 2\lambda_e^4 k_{0x}^2 k_{0z}^2 + 2\lambda_e^4 k_{0y}^2 k_{0z}^2)}{(\lambda_i^2 v_A^2 k^2 k_{0z}^2)}$.

$$c_2 = \frac{2k_{0x}(2\omega_0^2 \lambda_e^4 k_{0x}^2 + 2\omega_0^2 \lambda_e^4 k_{0z}^2 + 2\omega_0^2 \lambda_e^2 - \lambda_i^2 k_{0z}^2 v_A^2)}{(\lambda_i^2 v_A^2 k^2 k_{0z}^2)}. \qquad c_3 = \frac{2k_{0y}(2\omega_0^2 \lambda_e^4 k_{0y}^2 + 2\omega_0^2 \lambda_e^4 k_{0z}^2 + 2\omega_0^2 \lambda_e^2 - \lambda_i^2 k_{0z}^2 v_A^2)}{(\lambda_i^2 v_A^2 k^2 k_{0z}^2)}.$$

$$c_4 = \frac{2k_{0z}(2\omega_0^2 \lambda_e^2 k_{0z}^2 + 2\omega_0^2 \lambda_e^2 k_{0x}^2 + 2\omega_0^2 \lambda_e^2 k_{0y}^2 + 2\omega_0^2 \lambda_e^2 - \lambda_i^2 v_A^2 k_{0y}^2 - 2\lambda_i^2 v_A^2 k_{0z}^2)}{\lambda_i^2 v_A^2 k^2 k_{0z}^2}.$$

$$c_5 = \frac{4\omega_0^2 k_{0x}^2 \lambda_e^4}{\lambda_i^2 v_A^2 k_0^2 k_{0z}^2}, \qquad c_6 = \frac{4\omega_0^2 k_{0y}^2 \lambda_e^4}{\lambda_i^2 v_A^2 k_0^2 k_{0z}^2}, \qquad c_7 = \frac{\left(4\omega_0^2 k_{0z}^2 \lambda_e^4 - 4\lambda_i^2 v_A^2 k_{0z}^2\right)}{\lambda_i^2 v_A^2 k_0^2 k_{0z}^2}. \quad b_0 = 0.5,$$

$$c_8 = \frac{\left(8\omega_0^2 \lambda_e^4 - 4\lambda_i^2 v_A^2\right) k_{0z} k_{0x}}{\lambda_i^2 v_A^2 k_0^2 k_{0z}^2}, \quad c_9 = \frac{\left(8\omega_0^2 \lambda_e^4 - 4\lambda_i^2 v_A^2\right) k_{0z} k_{0y}}{\lambda_i^2 v_A^2 k_0^2 k_{0z}^2}, \quad c_{10} = \frac{k_{0y}^2}{k_{0z}^2} \text{ and } c_{11} = \frac{2k_{0y}}{k_{0z}}.$$

and $\gamma' = \frac{\gamma}{\omega_0}$ is the normalized growth rate. $\gamma\left(=0.5083\omega_{ce}\right)$ is the growth rate of beam-driven whistler waves.

4.2.2 Ion Acoustic wave (IAW) dynamics

Consider a low-frequency ion-acoustic wave propagating parallel to the background magnetic field B_0 along the z-axis i.e., $\vec{B}_0 = B_0\hat{z}$, $\vec{k} = k_z\hat{z}$. To establish the IAW dynamics, the following key equations are used:

The equation of motion

$$m_j \frac{\partial \vec{v}_j}{\partial t} = q_j \vec{E} + \frac{q_j}{c}(\vec{v}_j \times \vec{B}_0) - T_j \vec{\nabla}\frac{n_j}{n_0} + \vec{F}_j. \tag{4.7}$$

The continuity equation

$$\frac{\partial n_j}{\partial t} + \vec{\nabla}.(n_j \vec{v}_j) = 0. \tag{4.8}$$

where F_j denotes the ponderomotive force of the high-frequency whistler wave and v_j denotes the velocity of the species (j stands for an electron's velocity 'e' and 'i' for an ion's velocity) of IAW.

When we assume the quasi-neutrality along with the response of the electrons and use the parallel element of the linearized version of Eq. (4.7) for the ions, we obtain

$$\frac{\partial v_{iz}}{\partial t} = -\frac{c_s^2}{n_0}\frac{\partial n_i}{\partial z} + \left(\frac{F_{iz} + F_{ez}}{m_i}\right), \tag{4.9}$$

where $c_s\left(=\frac{k_B(T_e + T_i)}{m_i}\right)^{1/2}$ denotes the IAW's, k_B denotes the Boltzmann Constant. T_i, T_e are the temperature of ion and electron, respectively. F_{ez} (F_{iz}) denotes the constituent of ponderomotive force in z-direction formed by whistler wave.

Differentiating Eq. (4.8) w.r.t to time again, we get

$$\frac{\partial^2 n_i}{\partial t^2} + n_0 \frac{\partial^2 v_{iz}}{\partial t \partial z} = 0. \tag{4.10}$$

Combining Eq. (4.9) and (4.10), we obtain the nonlinear dynamical equation of IAW

$$\frac{\partial^2 n}{\partial t^2} = -n_0 \frac{\partial}{\partial z}\left[-c_s^2 \frac{\partial}{\partial z}\left(\frac{n}{n_0}\right) + \frac{F_{ez} + F_{iz}}{m_i}\right]. \tag{4.11}$$

Equation (4.11) can be redrafted as

$$\left(\frac{\partial^2 n}{\partial t^2} - c_s^2 \frac{\partial^2}{\partial z^2}\right)\left(\frac{n}{n_0}\right) = -\frac{\partial}{\partial z}\left[\frac{F_{ez} + F_{iz}}{m_i}\right]. \tag{4.12}$$

Now, the Whistler Wave's Ponderomotive Force is stated as

$$\vec{F}_j = -m_j(\vec{v}_j *.\vec{\nabla})\vec{v}_j + \frac{q_j}{c}(\vec{v}_j * \times B_w). \tag{4.13}$$

Here, the charged species (ions and electrons) are indicated by $'j'$. Thus q_j, v_j and m_j denotes the charge, velocity, and mass of ion and electrons, respectively. Magnetic field due to the whistler wave is denoted by B_w and c denotes the speed of light.

The whistler wave's velocity component owing to electrons may be expressed as

$$v_{e1x} = \frac{-ie\omega_0}{m_e(\omega_0^2 - \omega_{ce}^2)}E_x - \frac{e\omega_{ce}}{m_e(\omega_0^2 - \omega_{ce}^2)}E_y. \tag{4.14}$$

$$v_{e1y} = \frac{e\omega_{ce}}{m_e(\omega_0^2 - \omega_{ce}^2)}E_x - \frac{ie\omega_0}{m_e(\omega_0^2 - \omega_{ce}^2)}E_y. \tag{4.15}$$

$$v_{e1z} = \frac{eE_z}{im_e\omega_0}. \tag{4.16}$$

In a similar manner, the velocity element of the whistler wave generated by an ion may be expressed as

$$v_{i1x} = \frac{ie\omega_0}{m_i(\omega_0^2 - \omega_{ci}^2)}E_x - \frac{e\omega_{ci}}{m_i(\omega_0^2 - \omega_{ci}^2)}E_y. \tag{4.17}$$

$$v_{i1y} = \frac{e\omega_{ci}}{m_i(\omega_0^2 - \omega_{ci}^2)}E_x + \frac{ie\omega_0}{m_i(\omega_0^2 - \omega_{ci}^2)}E_y. \tag{4.18}$$

$$v_{i1z} = \frac{-eE_z}{im_i\omega_0}. \tag{4.19}$$

Relieving the value of the whistler wave velocity components in Eq. (4.13) to obtain the ponderomotive force components[63] related to whistler waves.

$$F_{ez} = \frac{e^2}{2m_ec^2}\frac{\partial|E_z|^2}{\partial z} \quad \text{and} \quad F_{iz} = \frac{e^2}{2m_ic^2}\frac{\partial|E_z|^2}{\partial z}.$$

By substituting the value of F_{iz} and F_{ez} in Eq. (4.12), one may derive the dynamical equation of IAW,

$$\left(\frac{\partial^2}{\partial t^2} - c_s^2\frac{\partial^2}{\partial z^2}\right)\left(\frac{n}{n_0}\right) = -\frac{\partial}{\partial z}\left[\frac{1}{m_i}\left(\frac{e^2}{2m_ec^2} + \frac{e^2}{2m_ic^2}\right)\right]\frac{\partial^2}{\partial z^2}|E_z|^2. \tag{4.20}$$

The above Eq. (4.20) represents the non-linear dynamics of IAW. By applying the normalized parameter just like in dynamics of whistler wave, one may establish the normalized dimensionless equation of IAW.

$$\left(\frac{\partial^2}{\partial t^2}-c_{12}\frac{\partial^2}{\partial z^2}\right)\left(\frac{n}{n_0}\right)=-c_{13}\frac{\partial^2}{\partial z^2}|E_z|^2, \tag{4.21}$$

where $c_{12}=c_s^2\frac{t_n^2}{z_n^2}$.

and $c_{13}=-\left[\frac{1}{m_i}\left(\frac{e^2}{2m_ec^2}+\frac{e^2}{2m_ic^2}\right)\right]\frac{t_n^2}{z_n^2}$.

Eq. (4.21) simplifies to when we assume the adiabatic response.

$$\frac{n}{n_0}=\frac{c_{13}}{c_{12}}|A_z|^2. \tag{4.22}$$

Using the normalized electric field, we obtained $E_n=\left[\frac{2m_em_i^2c^2c_s^2}{n_0e^2(m_e+m_i)}\right]^{\frac{1}{2}}$,

Now Eq. (4.6) becomes

$$ic_1\frac{\partial E_z}{\partial t}+c_2\frac{\partial^2E_z}{\partial x^2}+c_3\frac{\partial^2E_z}{\partial y^2}+c_4\frac{\partial^2E_z}{\partial z^2}+ic_5\frac{\partial E_z}{\partial x}+ic_6\frac{\partial E_z}{\partial y}+ic_7\frac{\partial E_z}{\partial z}+c_8\frac{\partial^2E_z}{\partial x\partial z}+c_9\frac{\partial^2E_z}{\partial y\partial z}+$$
$$c_{10}\left(-\frac{x^2}{2}+b_0\cos(ky)\right)^2E_z+c_{11}\left(-\frac{x^2}{2}+b_0\cos(ky)\right)E_z-\frac{c_{13}}{c_{12}}|A_z|^2E_z+2i\gamma' E_z=0, \tag{4.23}$$

The values of numerical constants are given in below-

$n_0=21cm^{-3}$, $B_0=45nT$, $T_e=42eV$, $T_I=235eV$, $\omega_{pe}=2.5\times10^5\,rad/\sec$, $\omega_{ce}=7.9\times10^3\,rad/\sec$,

$\omega_{ci}=4.31\,rad/\sec$, $v_A=2.14\times10^7\,cm/\sec$, $c_s=1.6\times10^7\,cm/\sec$, $\lambda_i=4.9\times10^6\,cm$, $\lambda_e=1.16\times10^5\,cm$,

$E_n=1.5\times10^3\,G$ cm, $x_n=y_n=1.02\times10^6\,cm$, $z_n=1.5\times10^6\,cm$, $t_n=0.015\sec$, $b_0=0.5$,

$c_1=0.0155$, $c_2=c_3=1.02\times10^6$, $c_4=1.5\times10^6$, $c_5=c_6=2.5\times10^{10}$, $c_7=-2.0\times10^{11}$, $c_8=c_9=-7.2\times10^{11}$,

$c_{10}=12.41$, $c_{11}=7.04$, $c_{12}=1.6\times10^5$, $c_{13}=3.9\times10^3$.

4.3 Numerical Simulation and Result Discussion

To solve the dynamics of nonlinear whistler wave numerical simulation has been performed. Firstly, the accuracy of code has been checked by studying the algorithm of nonlinear Schrödinger (NLS) equation and consistency of plasmon number, $N=\sum_k|E_k|^2$ upto sixth decimal number in to two steps-

(i) The testing of invariants plasmon number $N = \sum_k |E_k|^2$ with time steps and grid points is given below (NLS)

Table 1. Testing of invariants with time steps with Grid points 2048 (This step size is also used for the finite difference method to monitor the invariants of NLS equation to desired accuracy)

Time steps (dt)	**Plasmon number, N**
$\mathbf{10^{-5}}$	9.99999997
$\mathbf{10^{-6}}$	9.999999996
$\mathbf{10^{-7}}$	1.00000000007
$\mathbf{10^{-8}}$	1.00000000007

Table 2. Testing of invariants with Grid points

Grid points	**256**	**512**	**1024**	**2048**
N	9.9999991	9.999997	9.9999994	9.9999998

(ii) Modified for present case and applied to magnetopause parameters below:-

Then, pseudo-spectral method and finite difference method with the step size of $dt = 5\times10^{-5}$ have been used in the periodic domain of $(10\pi\times10\pi\times10\pi)$ with the grid size of $(128\times128\times128)$. The initial condition imposed for numerical simulation consists of sequential X-O points represents the magnetic reconnection[64] is: -

$$E_z(x,y) = \cos(2x+2.3)+\cos(y+4.1) \tag{4.24}$$

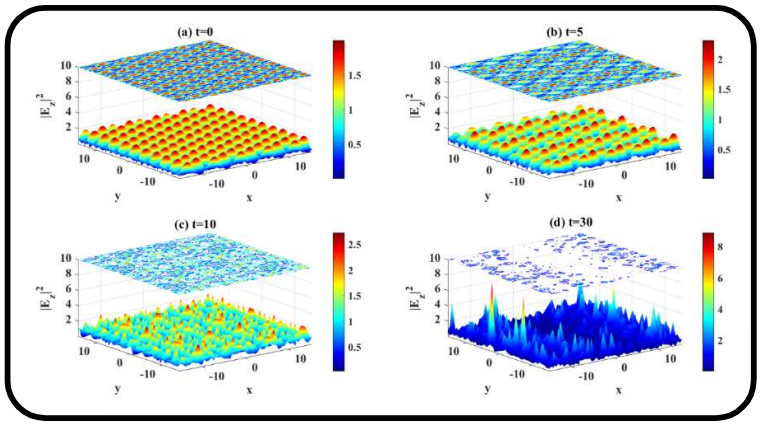

Figure 4.1 The projection plot of nonlinear whistler wave in the presence of magnetic islands and perturbation in the background density for different times (a) t=0, (b) t=3, (c) t=8, and (d) t=10, for modified nonlinear Schrodinger equation (in normalized units).

Furthermore, we hypothesize that a 3D whistler wave originates within an already-existing reconnection point. Field perturbation owing to the whistler wave as well as density modification caused by ponderomotive force nonlinearity are both responsible for the spatial fluctuation of the whistler wave field. At initial level, structures formed are coherent but with increase of the time evolution this will give rise to generation of whistler turbulence as shown in figure 4.1.

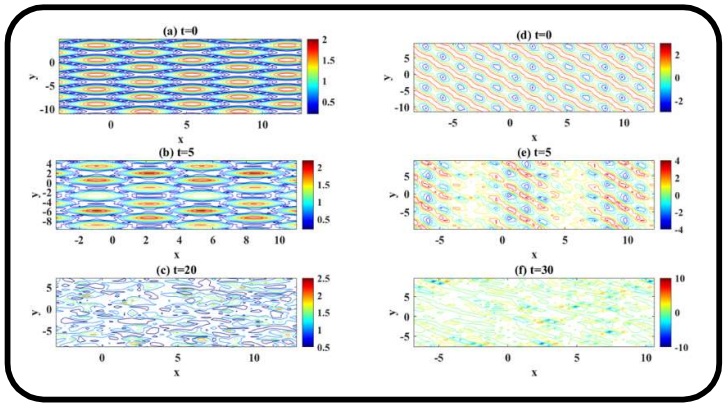

Figure 4.2 Contour plot (left panel), and current sheet (right panel) of nonlinear whistler in the presence of magnetic islands and perturbation in the background density for different times.

Plotting the contour plot of electric field lines can be utilized to reveal the existence of magnetic islands created by reconnection. We then examine the the spatial evolution of current sheet of whistler wave with t in the presence of reconnection induced magnetic islands as well as background density fluctuations. Figure 4.2 illustrates the contour plot (in left panel of figure 4.2), and current density (right panel of figure 4.2) of nonlinear whistler wave in the presence of magnetic islands and perturbation in the background density in x-y plane at different times. The figure clearly illustrates that for the very initial stage, the current is having a smooth or symmetric distribution, as time progresses, we observe that the appropriate X-O structures get deformed, and we eventually reach a wholly chaotic pattern. As a result, these chaotic structures may be responsible for the creation of whistler turbulence.

Figure 4.3 (a) Ensemble averaged power spectra of Normalized field intensity of nonlinear whistler wave $|E_k|^2$ against normalized wave vector k for modified nonlinear Schro¨dinger equation (in normalized units) in the presence of magnetic island effects. (b) Ensemble averaged power spectra of Normalized field intensity of nonlinear whistler wave $|E_k|^2$ against normalized wave vector k for modified nonlinear Schro¨dinger equation (in normalized units) in the absence of magnetic island effects.

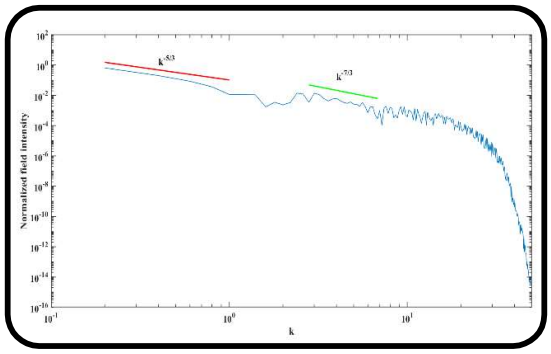

The quasi-steady state has not yet been reached and won't be for some time since the constant growth rate of the beam-driven mode was taken into account in the present investigation. As a result, addressing power spectra is not relevant, but we would like to improve the present model in future by taking into account the growth rate whistler intensity-dependent (instead of taking constant growth rate). When the whistler wave's amplitude is sufficient, we turn off the growth rate of the beam-driven mode so as to examine the turbulent spectra. So, to examine the ensemble averaged power spectrum for quasi-steady state, we write Eq. (4.23) as given below-

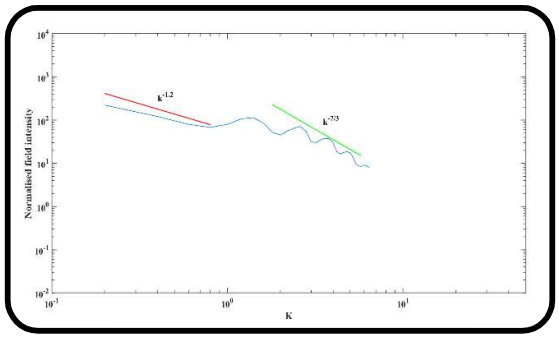

$$ic_7\frac{\partial E_z}{\partial z}+c_2\frac{\partial^2 E_z}{\partial x^2}+c_3\frac{\partial^2 E_z}{\partial y^2}+ic_5\frac{\partial E_z}{\partial x}+ic_6\frac{\partial E_z}{\partial y}+ c_8\frac{\partial^2 E_z}{\partial x\partial z}+c_9\frac{\partial^2 E_z}{\partial y\partial z}-\frac{c_{13}}{c_{12}}\left|A_z\right|^2 E_z=0\,, \tag{4.25}$$

Simulating Eq. (4.25) for grid size (512×512) and periodic domain is $(10\pi\times10\pi)$ by imposing the initial condition of Biskamp and welter (1989)[64] and then we investigated the ensemble averaged spectra in the presence of magnetic islands (anisotropic current sheet formation also) as shown in figure 4.3a. It shows the variation of $|E_k|^2$ with k at z=43-50 i.e., there are 7 spectra. We just give the scaling of reference lines (red and green scaling lines for -1.2 and -7/3 scaling) and actual power spectra is given by solid curve line. Due to the presence of magnetic islands it slightly different from Kolmogorov scaling of -5/3. But in the absence of magnetic islands, power spectrum follows the Kolmogorov scaling in the inertial range that has scaling of -5/3 and after that spectrum is steeper, shown in figure 4.3b as we have done in our earlier work[61]. It is to be mentioned here that scaling is different from -5/3 when magnetic islands are present. This is on account of current thinking fact[33], [65] that in the presence of magnetic island, MHD turbulence is fundamentally different from that envisioned in the Kolmogorov-like theory. This happens since the anisotropic, current-sheet become the sites of magnetic reconnection (magnetic islands) before the formal Kolmogorov dissipation scale is reached. As a consequence of the wave's dispersive features, this power spectrum's steepening at smaller scales signifies energy transfer from larger to smaller length scales. This specific spectral index will promote the emergence of thermal tails of energetic particles which causes the acceleration of the particles. The repetitive interaction between charged particles and localized structures can lead to energization using the Fokker-Planck equation (also called second order Fermi acceleration)[66], [67]. In this method, the repetitive interaction between charged particles and magnetic clouds generated by turbulence lead to

the acceleration of charged particles. There are Various mechanism have been used to accomplish the study of acceleration of charged particles[68]. The current study presents the localized structures of non-linear whistler wave based on the nonlinear coupling and turbulence generation. In this chaotic scenario, charged particles gain energy from localized structures by interacting repetitively, leading to particles acceleration which is similar to Fermi acceleration mechanism. To describe the repetitive interaction of charged particles with the localized structures, a quasi-linear diffusion equation is used, and it is provided by the following formula[69].

$$\frac{\partial f}{\partial t}=\frac{\partial}{\partial v}\left\{D(v)\frac{\partial f}{\partial v}\right\}.$$

Here, $D(v)$ denotes the velocity space diffusion coefficient, and $f(t,v)$ denotes the velocity distribution function. The velocity distribution function can be independent of time if the observation time is large as compared to the ponderomotive nonlinearity setting up time. In this context, the relation between spectral index η, and distribution function $f(v)$[70], [71] is given below-

$$f(v)\propto v^{2-\eta}. \tag{4.26}$$

In our current analysis $\eta\simeq 2.3$, therefore $f(v)\sim v^{-0.3}$ which leads to the formation of thermal tail of energetic electrons.

4.4 Semianalytical model

In order to understand the basic physics behind the localization of whistler wave we have investigated the semianalytical model, also by using this model we can estimate the critical size of coherent structures. Now, by modifying Eq. (4.4), we obtain following Eq.,

$$\begin{aligned}
&i\frac{2}{k_{\|}}\frac{\partial E_z}{\partial z}+\frac{(4\omega_0^2\lambda_e^4k_{\perp}^2)}{(2\omega_0^2k_{\|}^2\lambda_e^4+2\omega_0^2k_{\perp}^2\lambda_e^4+2\omega_0^2k_{\perp}^2\lambda_e^4+2\omega_0^2\lambda_e^2-k_{\perp}^2\lambda_i^2v_A^2-2k_{\|}^2\lambda_i^2v_A^2)k_{\|}^2}\frac{\partial^2E_z}{\partial x^2}+\\
&\frac{(4\omega_0^2\lambda_e^4k_{\perp}^2)}{(2\omega_0^2k_{\|}^2\lambda_e^4+2\omega_0^2k_{\perp}^2\lambda_e^4+2\omega_0^2k_{\perp}^2\lambda_e^4+2\omega_0^2\lambda_e^2-k_{\perp}^2\lambda_i^2v_A^2-2k_{\|}^2\lambda_i^2v_A^2)k_{\|}^2}\frac{\partial^2E_z}{\partial y^2}+\\
&\frac{\lambda_i^2v_A^2k^2k_{\perp}^2}{(2\omega_0^2k_{\|}^2\lambda_e^4+2\omega_0^2k_{\perp}^2\lambda_e^4+2\omega_0^2k_{\perp}^2\lambda_e^4+2\omega_0^2\lambda_e^2-k_{\perp}^2\lambda_i^2v_A^2-2k_{\|}^2\lambda_i^2v_A^2)k_{\|}^2}\left(\frac{\delta A_z}{A_0}\right)^2E_z+\\
&\frac{2\lambda_i^2v_A^2k^2k_{0y}k_{\|}}{(2\omega_0^2k_{\|}^2\lambda_e^4+2\omega_0^2k_{\perp}^2\lambda_e^4+2\omega_0^2k_{\perp}^2\lambda_e^4+2\omega_0^2\lambda_e^2-k_{\perp}^2\lambda_i^2v_A^2-2k_{\|}^2\lambda_i^2v_A^2)k_{\|}}\left(\frac{\delta A_z}{A_0}\right)E_z\\
&-\frac{(\lambda_i^2v_A^2k^2)}{(2\omega_0^2k_{\|}^2\lambda_e^4+2\omega_0^2k_{\perp}^2\lambda_e^4+2\omega_0^2k_{\perp}^2\lambda_e^4+2\omega_0^2\lambda_e^2-k_{\perp}^2\lambda_i^2v_A^2-2k_{\|}^2\lambda_i^2v_A^2)}\frac{\delta n}{n_0}E_z+E_z\exp(k_iz)=0.
\end{aligned} \tag{4.27}$$

Or we can rewrite above equation in simplified equation as-

$$i\frac{2}{k_{\|}}\frac{\partial E_z}{\partial z}+\theta_1\lambda_e^2\left(\frac{\partial^2 E_z}{\partial x^2}+\frac{\partial^2 E_z}{\partial y^2}\right)+\theta_2\left(-\frac{x^2}{2}+A_z\cos(ky)\right)^2 E_z+$$
$$\theta_3\left(-\frac{x^2}{2}+A_z\cos(ky)\right)E_z-\theta_4\frac{\delta n}{n_0}E_z+E_z\exp(k_i z)=0. \quad (4.28)$$

Where, $\theta_1=\frac{(4\omega_0^2\lambda_e^2k_\perp^2)}{(2\omega_0^2k_{\|}^2\lambda_e^4+2\omega_0^2k_\perp^2\lambda_e^4+2\omega_0^2k_\perp^2\lambda_e^4+2\omega_0^2\lambda_e^2-k_\perp^2\lambda_i^2v_A^2-2k_{\|}^2\lambda_i^2v_A^2)k_{\|}^2}$.

$\theta_2=\frac{\lambda_i^2v_A^2k^2k_\perp^2}{(2\omega_0^2k_{\|}^2\lambda_e^4+2\omega_0^2k_\perp^2\lambda_e^4+2\omega_0^2k_\perp^2\lambda_e^4+2\omega_0^2\lambda_e^2-k_\perp^2\lambda_i^2v_A^2-2k_{\|}^2\lambda_i^2v_A^2)k_{\|}^2}$.

$\theta_3=\frac{2\lambda_i^2v_A^2k^2k_\perp}{(2\omega_0^2k_{\|}^2\lambda_e^4+2\omega_0^2k_\perp^2\lambda_e^4+2\omega_0^2k_\perp^2\lambda_e^4+2\omega_0^2\lambda_e^2-k_\perp^2\lambda_i^2v_A^2-2k_{\|}^2\lambda_i^2v_A^2)k_{\|}}$.

$\theta_4=\frac{(\lambda_i^2v_A^2k^2)}{(2\omega_0^2k_{\|}^2\lambda_e^4+2\omega_0^2k_\perp^2\lambda_e^4+2\omega_0^2k_\perp^2\lambda_e^4+2\omega_0^2\lambda_e^2-k_\perp^2\lambda_i^2v_A^2-2k_{\|}^2\lambda_i^2v_A^2)}$.

Now we are assuming the envelope solution of electric field $\tilde{E}_z=E_{00}e^{ik_{0z}s(x,y,z)}$, and putting this envelope solution in Eq. (4.28) we obtained the following equation-

$$i\frac{2}{k_{0z}}\frac{\partial E_{00}}{\partial z}-2E_{00}\frac{\partial s}{\partial z}+\theta_1\lambda_e^2\left(\frac{\partial^2 E_{00}}{\partial x^2}+\frac{\partial^2 E_{00}}{\partial y^2}\right)+2ik_{\|}\theta_1\lambda_e^2\left(\frac{\partial E_{00}}{\partial x}\frac{\partial s}{\partial x}+\frac{\partial E_{00}}{\partial y}\frac{\partial s}{\partial y}\right)-$$
$$k_{\|}^2\theta_1\lambda_e^2\left(\frac{\partial s}{\partial x}+\frac{\partial s}{\partial y}\right)^2E_{00}+ik_{\|}\theta_1\lambda_e^2\left(\frac{\partial^2 s}{\partial x^2}+\frac{\partial^2 s}{\partial y^2}\right)E_{00}+\theta_2\left[\left(-\frac{x^2}{2}+b_0\cos(ky)\right)\right]^2E_{00}+ \quad (4.29)$$
$$\theta_3\left[\left(-\frac{x^2}{2}+b_0\cos(ky)\right)\right]E_{00}-\theta_4\frac{\delta n}{n_0}E_{00}+E_{00}\exp(k_i z)=0.$$

Further separating the real and imaginary part of Eq. (4.29)

$$-2\frac{\partial s}{\partial z}E_{00}+\theta_1\lambda_e^2\left(\frac{\partial^2 E_{00}}{\partial x^2}+\frac{\partial^2 E_{00}}{\partial y^2}\right)-k_{\|}^2\theta_1\lambda_e^2\left(\frac{\partial s}{\partial x}+\frac{\partial s}{\partial y}\right)^2E_{00}+$$
$$\theta_2\left[\left(-\frac{x^2}{2}+b_0\cos(ky)\right)\right]^2E_{00}+\theta_3\left[\left(-\frac{x^2}{2}+b_0\cos(ky)\right)\right]E_{00}- \quad (4.29a)$$
$$\theta_4\left[\exp(\alpha|A_z|^2-1\right]E_{00}=0.$$

$$\frac{2}{k_{\|}}\frac{\partial E_{00}}{\partial z}+2k_{\|}\theta_1\lambda_e^2\left(\frac{\partial E_{00}}{\partial x}\frac{\partial s}{\partial x}+\frac{\partial E_{00}}{\partial y}\frac{\partial s}{\partial y}\right)+k_{\|}\lambda_e^2\theta_1\left(\frac{\partial^2 s}{\partial x^2}+\frac{\partial^2 s}{\partial y^2}\right)E_{00}+E_{00}\exp(k_i z)=0. \quad (4.29b)$$

Further assuming the gaussian profile for initial distribution of wave i.e.,

$$E_{00}^2 = \frac{E_{00}^{'2}}{f_1(z)f_2(z)}\exp\left(\frac{-x^2}{r_{01}^2}-\frac{y^2}{r_{01}^2}+k_i z\right)$$
$$s = \beta_1(z)\frac{x^2}{2}+\beta_2(z)\frac{y^2}{2}+\phi(z) \qquad (4.30)$$

Using Eq. (4.30) in Eq. (29b), and collecting the terms of x^2 and y^2 we obtain following Eqs.

$$\beta_1(z) = \frac{1}{k_{\|}^2\theta_1\lambda_e^2}\frac{1}{f_1}\frac{\partial f_1}{\partial z}. \qquad (4.31)$$

$$\beta_2(z) = \frac{1}{k_{\|}^2\theta_1\lambda_e^2}\frac{1}{f_2}\frac{\partial f_2}{\partial z}.$$

Here r_{01} and r_{02} represents the current sheet size of whistler wave in x and y direction, respectively; $\beta_1(z)$ and $\beta_2(z)$ represents the slowly varying function, and f_1, f_2 represents the beam width parameter of the whistler wave. Now, for obtaining the beam-width parameters, use Eq. (4.30) in Eq. (4.29a) with paraxial approximation i.e., $x << r_{01}^2 f_{1,}\ y << r_{02}^2 f_2$ and then equating coefficients of x^2 and y^2, we obtained the following Eq.

$$\frac{\partial^2 f_1}{\partial\xi^2} = R_d^2 k_{\|}^2\left(\frac{4\theta_1^2\lambda_e^4}{r_{01}^4 f_1^4 f_2}+\frac{\theta_1\theta_3 f_1}{2}-\frac{2\theta_1\theta_4\lambda_e^2\left(\alpha E_{00}^{'2}\right)}{r_{01}^2 f_1^3 f_2}\right). \qquad (4.32)$$

$$\text{And, } \frac{\partial^2 f_2}{\partial\xi^2} = R_d^2 k_{\|}^2\left(\frac{4\theta_1^2\lambda_e^4}{r_{02}^4 f_2^4 f_1}+\frac{\theta_1\theta_3 k^2\lambda_e^2 f_2}{2}-\frac{\theta_1\theta_4\lambda_e^2\left(\alpha E_{00}^{'2}\right)}{r_{02}^2 f_2^3 f_1}\right), \qquad (4.33)$$

where $\xi = z/R_d$ and $\mathrm{R}_d = k_{0z}r_{01}^2$. Eqs. (4.32) & (4.33) are solved for the plain wavefront imposing following initial conditions- $\frac{\partial^2 f_1}{\partial\xi^2} = \frac{\partial^2 f_2}{\partial\xi^2} = 0, f_1 = f_2 = 1$ at z=0. When power of whistler wave $\left(\alpha E_{00}^{'2}\right)$ is zero, then Eqs. (4.32) and (4.33) becomes quadratic and gives the transverse scale size of localized structures of whistler wave along x-axis and y-axis i.e., $r_{01} = 7.5\lambda_e$, $r_{02} = 5.2\lambda_e$. Further, when we take finite value of power $\left(\alpha E_{00}^{'2} = 1\right)$, then the transverse scale size of localized structures of whistler wave along x-axis and y-axis i.e., $r_{01} = 0.8\lambda_e$, $r_{02} = 0.63\lambda_e$. Also, by using Ampere's law $\left(J = -\nabla^2 E_{00}^{'}\right)$, we have studied the current sheet size. One can calculate the transverse scale size of current sheet comes out $r_{01}/\sqrt{3}$ and $r_{02}/\sqrt{3}$ along x-axis and y-axis respectively. Therefore, transverse scale size of current sheet is $4.3\lambda_e$, and $3\lambda_e$ along x-axis and y-axis respectively. As a result, it shows how the

whistler power also influences the scale size of coherent structures and current sheet dimension. Recently, Leonenko et al.[72] reported the scale size of super thin electron-scale current sheet in earth's magnetotail. Also, Bruch et al.[73] reported the scale size of whistler's localized structures of the order of $(10-20)\lambda_e$ at the magnetic reconnection sites in the magnetopause.

4.5 Summary and Conclusion

Numerous waves have been observed so far in the reconnection region. The magnetic reconnection zone near the dayside magnetopause exhibits implications of beam-driven whistler mode waves, according to observed data from the MMS[55]. This article deals with the study of beam-driven whistler wave dynamics due to modified background density and with the modified background field of fully developed chain of magnetic islands. Furthermore, these equations are normalized and resolved using finite difference method and pseudospectral method. The outcomes of the numerical simulations illustrate that nonlinear whistler wave propagating in the magnetic islands gets localized and current sheets are formed having transverse scale size of the order electron inertial length. Although, Stenflo et al.[59] also investigated the nonlinear coupling of waves but in the absence of magnetic islands. Also, they have considered the linear growth rate of the system and their results are relevant to non-thermal magnetic field fluctuations which lead to plasma heating. But, in our model, we studied the nonlinear saturation of waves in the presence of magnetic islands. The outcomes of the numerical simulation are summarized here.

1) Simulation results reveal the localization of whistler wave. The resolution of the numerical model under consideration is of the order $2.15\lambda_e$, i.e., $(\{System\ length \times x_n\}/Grid\ size)$, which is appropriate enough to resolve the structures which are formed. And, in our analysis, localized structures are of the order of $3\lambda_e$. These localized structures of the magnetic field offer a lane for energy cascading from large to small scale spatial size.
2) Contour plot of electric field or sketching electric field lines can be utilized to reveal the existence of magnetic islands created by reconnection. We then examine the spatial evolution of current sheet of whistler wave with t in the presence of reconnection induced magnetic islands as well as background density fluctuations. Which illustrates that for the very initial stage, the current is having a smooth or symmetric distribution, as time progresses, we observe that the appropriate X-O structures get deformed, and we eventually reach a wholly chaotic pattern. These chaotic structures may be responsible for the creation of whistler turbulence.
3) We investigated the ensemble averaged spectra of whistler wave to observe the energy cascading from larger to lower scale due to localization process. We just give the scaling of reference lines

(red and green scaling lines for -1.2 and -7/3 scaling respectively) and actual power spectra is given by solid curve line.

Also, we observed that power of whistler wave also impacts the scale size of coherent structures and current sheet dimension. From semianalytical model, we have also calculated the transverse scale size of whistler's localized structures and the current sheet size. When the power of whistler wave is zero, then scale size of current sheet is of the order of $7.5\lambda_e$, and $5.2\lambda_e$ along x-axis and along y-axis respectively. Further, When the power of whistler wave is finite, then scale size of current sheet is of the order of $4.3\lambda_e$, and $3\lambda_e$ along x-axis and along y-axis respectively.

The outcomes demonstrate whistler turbulence at magnetic reconnection locations produced by the electron beam as well as localized structures and whistler fluctuations that correspond to observations reported by Zhao et al.[55]. This causes the heating and acceleration of plasma particles in the magnetopause. Moreover, the nonlinear implementations of coupled waves are already ongoing and could further support to the validity of the model. As a result, our study will enable us to gain a better quantitative understanding of whistler-mode waves produced by energetic electron beams in turbulent circumstances.

Acknowledgments

Jyoti wishes to acknowledge the financial assistance (Award no. 515500) provided by the University Grant Commission (UGC), Govt. of India.

Data Availability Statement

The data that support the findings of this study are available from the corresponding author upon reasonable request.

References

[1] J. Birn and E. R. Priest, *Reconnection of magnetic fields: Magnetohydrodynamics and collisionless theory and observations*. 2007. doi: 10.1017/CBO9780511536151.

[2] M. Yamada, J. Yoo, J. Jara-Almonte, H. Ji, R. M. Kulsrud, and C. E. Myers, "Conversion of magnetic energy in the magnetic reconnection layer of a laboratory plasma," *Nat. Commun.*, vol. 5, 2014, doi: 10.1038/ncomms5774.

[3] G. B. Field, " Magnetic Effects: Cosmical Magnetic Fields . Their Origin and Their Activity. E. N. Parker. Clarendon (Oxford University Press), New York, 1979. xviii, 842 pp., illus. $95.

International Series of Monographs on Physics.," *Science (1979)*, vol. 207, no. 4432, 1980, doi: 10.1126/science.207.4432.753.a.

[4] R. M. Kulsrud, "Magnetic reconnection in a magnetohydrodynamic plasma," *Phys. Plasmas*, vol. 5, no. 5 PART 1, 1998, doi: 10.1063/1.872827.

[5] T. Li, E. Priest, and R. Guo, "Three-dimensional magnetic reconnection in astrophysical plasmas," *Proceedings of the Royal Society A: Mathematical, Physical and Engineering Sciences*, vol. 477, no. 2249. 2021. doi: 10.1098/rspa.2020.0949.

[6] D. Biskamp, E. Schwarz, A. Zeiler, A. Celani, and J. F. Drake, "Electron magnetohydrodynamic turbulence," *Phys. Plasmas*, vol. 6, no. 2–3, 1999, doi: 10.1063/1.873312.

[7] W. Gonzalez and E. Parker, *Magnetic Reconnection concepts and Applications*, vol. 237, no. 4. 1994.

[8] M. Yamada, R. Kulsrud, and H. Ji, "Magnetic reconnection," *Rev. Mod. Phys.*, vol. 82, no. 1, 2010, doi: 10.1103/RevModPhys.82.603.

[9] R. E. Ergun *et al.*, "Magnetic Reconnection, Turbulence, and Particle Acceleration: Observations in the Earth's Magnetotail," *Geophys. Res. Lett.*, vol. 45, no. 8, 2018, doi: 10.1002/2018GL076993.

[10] M. Hoshino and Y. Lyubarsky, "Relativistic reconnection and particle acceleration," *Space Science Reviews*, vol. 173, no. 1–4. 2012. doi: 10.1007/s11214-012-9931-z.

[11] G. R. Werner, D. A. Uzdensky, M. C. Begelman, B. Cerutti, and K. Nalewajko, "Non-thermal particle acceleration in collisionless relativistic electron-proton reconnection," *Mon. Not. R. Astron. Soc.*, vol. 473, no. 4, 2018, doi: 10.1093/mnras/stx2530.

[12] S. Lu *et al.*, "Turbulence and Particle Acceleration in Collisionless Magnetic Reconnection: Effects of Temperature Inhomogeneity across Pre-reconnection Current Sheet," *Astrophys. J.*, vol. 878, no. 2, 2019, doi: 10.3847/1538-4357/ab1f6b.

[13] G. R. Werner and D. A. Uzdensky, "Nonthermal Particle Acceleration in 3D Relativistic Magnetic Reconnection in Pair Plasma," *Astrophys. J.*, vol. 843, no. 2, 2017, doi: 10.3847/2041-8213/aa7892.

[14] R. E. Ergun *et al.*, "Observations of Particle Acceleration in Magnetic Reconnection–driven Turbulence," *Astrophys. J.*, vol. 898, no. 2, 2020, doi: 10.3847/1538-4357/ab9ab6.

[15] D. Kagan, E. Nakar, and T. Piran, "Physics of the saturation of particle acceleration in relativistic magnetic reconnection," *Mon. Not. R. Astron. Soc.*, vol. 476, no. 3, 2018, doi: 10.1093/MNRAS/STY452.

[16] D. Biskamp, "Magnetic Reconnection in Plasmas."

[17] T. K. M. Nakamura *et al.*, "Spatial and time scaling of coalescing multiple magnetic islands," *Phys. Plasmas*, vol. 30, no. 2, 2023, doi: 10.1063/5.0127107.

[18] J. L. Burch, T. E. Moore, R. B. Torbert, and B. L. Giles, "Magnetospheric Multiscale Overview and Science Objectives," *Space Science Reviews*, vol. 199, no. 1–4. 2016. doi: 10.1007/s11214-015-0164-9.

[19] H. Karimabadi and A. Lazarian, "Magnetic reconnection in the presence of externally driven and self-generated turbulence," *Phys. Plasmas*, vol. 20, no. 11, pp. 1–17, 2013, doi: 10.1063/1.4828395.

[20] H. Karimabadi, V. Roytershteyn, W. Daughton, and Y. H. Liu, "Recent evolution in the theory of magnetic reconnection and its connection with turbulence," *Space Science Reviews*, vol. 178, no. 2–4. 2013. doi: 10.1007/s11214-013-0021-7.

[21] H. Karimabadi *et al.*, "The link between shocks, turbulence, and magnetic reconnection in collisionless plasmas," *Phys. Plasmas*, vol. 21, no. 6, 2014, doi: 10.1063/1.4882875.

[22] A. Lazarian, G. L. Eyink, and E. T. Vishniac, "Relation of astrophysical turbulence and magnetic reconnectiona," *Phys. Plasmas*, vol. 19, no. 1, 2012, doi: 10.1063/1.3672516.

[23] Z. Vörös *et al.*, "MMS Observation of Magnetic Reconnection in the Turbulent Magnetosheath," *J. Geophys. Res. Space Phys.*, vol. 122, no. 11, 2017, doi: 10.1002/2017JA024535.

[24] A. Retinò, D. Sundkvist, A. Vaivads, F. Mozer, M. André, and C. J. Owen, "In situ evidence of magnetic reconnection in turbulent plasma," *Nat. Phys.*, vol. 3, no. 4, 2007, doi: 10.1038/nphys574.

[25] G. Kowal, D. A. Falceta-Gonçalves, A. Lazarian, and E. T. Vishniac, "Statistics of Reconnection-driven Turbulence," *Astrophys. J.*, vol. 838, no. 2, 2017, doi: 10.3847/1538-4357/aa6001.

[26] W. H. Matthaeus and S. L. Lamkin, "Turbulent magnetic reconnection," *Physics of Fluids*, vol. 29, no. 8, 1986, doi: 10.1063/1.866004.

[27] J. P. Eastwood, T. D. Phan, S. D. Bale, and A. Tjulin, "Observations of turbulence generated by magnetic reconnection," *Phys. Rev. Lett.*, vol. 102, no. 3, pp. 1–4, 2009, doi: 10.1103/PhysRevLett.102.035001.

[28] A. Mallet and A. A. Schekochihin, "A statistical model of three-dimensional anisotropy and intermittency in strong Alfvénic turbulence," *Mon. Not. R. Astron. Soc.*, vol. 466, no. 4, 2017, doi: 10.1093/mnras/stw3251.

[29] S. Boldyrev, "Spectrum of magnetohydrodynamic turbulence," *Phys Rev Lett*, vol. 96, no. 11, 2006, doi: 10.1103/PhysRevLett.96.115002.

[30] A. Mallet, A. A. Schekochihin, and B. D. G. Chandran, "Disruption of sheet-like structures in Alfvénic turbulence by magnetic reconnection," *Mon Not R Astron Soc*, vol. 468, no. 4, 2017, doi: 10.1093/mnras/stx670.

[31] P. Goldreich and S. Sridhar, "Toward a Theory of Interstellar Turbulence. II. Strong Alfvenic Turbulence," *Astrophys J*, vol. 468, p. 763, 1995.

[32] S. Servidio, W. H. Matthaeus, M. A. Shay, P. A. Cassak, and P. Dmitruk, "Magnetic reconnection in two-dimensional magnetohydrodynamic turbulence," *Phys Rev Lett*, vol. 102, no. 11, 2009, doi: 10.1103/PhysRevLett.102.115003.

[33] N. F. Loureiro and S. Boldyrev, "Role of Magnetic Reconnection in Magnetohydrodynamic Turbulence," *Phys Rev Lett*, vol. 118, p. 245101, 2017.

[34] L. Franci *et al.*, "Magnetic Reconnection as a Driver for a Sub-ion-scale Cascade in Plasma Turbulence," *Astrophys J*, vol. 850, no. 1, 2017, doi: 10.3847/2041-8213/aa93fb.

[35] S. Adhikari *et al.*, "Energy transfer in reconnection and turbulence," *Phys Rev E*, vol. 104, no. 6, 2021, doi: 10.1103/PhysRevE.104.065206.

[36] S. Adhikari *et al.*, "Effect of a guide field on the turbulence like properties of magnetic reconnection," *Phys Plasmas*, vol. 30, no. 082904, pp. 1–15, 2023.

[37] X. H. Wei *et al.*, "Cluster observations of waves in the whistler frequency range associated with magnetic reconnection in the Earth's magnetotail," *J Geophys Res Space Phys*, vol. 112, no. 10, 2007, doi: 10.1029/2006JA011771.

[38] X. Yu, Q. Lu, R. Wang, X. Gao, L. Sang, and S. Wang, "Simultaneous Observation of Whistler Waves and Electron Cyclotron Harmonic Waves in the Separatrix Region of Magnetopause Reconnection," *J Geophys Res Space Phys*, vol. 126, no. 10, 2021, doi: 10.1029/2021JA029609.

[39] S. Y. Huang *et al.*, "Two types of whistler waves in the hall reconnection region," *J Geophys Res Space Phys*, vol. 121, no. 7, 2016, doi: 10.1002/2016JA022650.

[40] F. D. Wilder *et al.*, "Observations of whistler mode waves with nonlinear parallel electric fields near the dayside magnetic reconnection separatrix by the Magnetospheric Multiscale mission," *Geophys Res Lett*, vol. 43, no. 12, 2016, doi: 10.1002/2016GL069473.

[41] S. Y. Huang *et al.*, "Observations of Whistler Waves in the Magnetic Reconnection Diffusion Region," in *2018 2nd URSI Atlantic Radio Science Meeting, AT-RASC 2018*, 2018. doi: 10.23919/URSI-AT-RASC.2018.8471382.

[42] D. Cao *et al.*, "MMS observations of whistler waves in electron diffusion region," *Geophys Res Lett*, vol. 44, no. 9, pp. 3954–3962, 2017, doi: 10.1002/2017GL072703.

[43] X. H. Deng and H. Matsumoto, "Rapid magnetic reconnection in the earth's magnetosphere mediated by whistler waves," *Nature*, vol. 410, no. 6828, 2001, doi: 10.1038/35069018.

[44] H. Viberg, Y. v. Khotyaintsev, A. Vaivads, M. André, and J. S. Pickett, "Mapping HF waves in the reconnection diffusion region," *Geophys Res Lett*, vol. 40, no. 6, 2013, doi: 10.1002/grl.50227.

[45] C. C. Chaston *et al.*, "Drift-kinetic Alfvén waves observed near a reconnection X line in the Earth's magnetopause," *Phys Rev Lett*, vol. 95, no. 6, pp. 5–8, 2005, doi: 10.1103/PhysRevLett.95.065002.

[46] C. Chaston *et al.*, "Turbulent heating and cross-field transport near the magnetopause from THEMIS," *Geophys Res Lett*, vol. 35, no. 17, Sep. 2008, doi: 10.1029/2008GL033601.

[47] W. M. Farrell, M. D. Desch, K. W. Ogilvie, M. L. Kaiser, and K. Goetz, "The role of upper hybrid waves in magnetic reconnection," *Geophys Res Lett*, vol. 30, no. 24, 2003, doi: 10.1029/2003GL017549.

[48] D. B. Graham *et al.*, "Large-Amplitude High-Frequency Waves at Earth's Magnetopause," *J Geophys Res Space Phys*, vol. 123, no. 4, 2018, doi: 10.1002/2017JA025034.

[49] D. B. Graham *et al.*, "Universality of Lower Hybrid Waves at Earth's Magnetopause," *J Geophys Res Space Phys*, vol. 124, no. 11, 2019, doi: 10.1029/2019JA027155.

[50] M. Zhou *et al.*, "Observation of waves near lower hybrid frequency in the reconnection region with thin current sheet," *J Geophys Res Space Phys*, vol. 114, no. 2, 2009, doi: 10.1029/2008JA013427.

[51] X. H. Deng *et al.*, "Observations of electrostatic solitary waves associated with reconnection by Geotail and Cluster," *Advances in Space Research*, vol. 37, no. 7, 2006, doi: 10.1016/j.asr.2005.05.129.

[52] H. Matsumoto, X. H. Deng, H. Kojima, and R. R. Anderson, "Observation of electrostatic solitary waves associated with reconnection on the dayside magnetopause boundary," *Geophys Res Lett*, vol. 30, no. 6, 2003, doi: 10.1029/2002GL016319.

[53] C. M. Liu *et al.*, "Ion-Beam-Driven Intense Electrostatic Solitary Waves in Reconnection Jet," *Geophys Res Lett*, vol. 46, no. 22, 2019, doi: 10.1029/2019GL085419.

[54] C. Krafft *et al.*, "Whistler wave emission by a modulated electron beam," *Phys Rev Lett*, vol. 72, no. 5, pp. 649–652, 1994, doi: 10.1103/PhysRevLett.72.649.

[55] S. Q. Zhao *et al.*, "Observations of the Beam-Driven Whistler Mode Waves in the Magnetic Reconnection Region at the Dayside Magnetopause," *J Geophys Res Space Phys*, vol. 126, no. 2, pp. 1–11, 2021, doi: 10.1029/2020JA028525.

[56] A. Vaivads, Y. Khotyaintsev, M. André, and R. A. Treumann, "Plasma waves near reconnection sites," *Lecture Notes in Physics*, vol. 687, 2006, doi: 10.1007/3-540-33203-0_10.

[57] Wang Jing *et al.*, "In Situ Observations of Whistler-mode Waves in Magnetic Reconnection at Mars," *Astrophys J*, vol. 944, no. 1, pp. 1–9, 2023.

[58] S. S. Cerri and F. Califano, "Reconnection and small-scale fields in 2D-3V hybrid-kinetic driven turbulence simulations," *New J Phys*, vol. 19, no. 2, 2017, doi: 10.1088/1367-2630/aa5c4a.

[59] Stenflo, M. Y. Yu, and P. K. Shukla, "Electromagnetic modulations of electron whistlers on plasmas," *J Plasma Phys*, vol. 36, no. 3, 1986, doi: 10.1017/S0022377800011892.

[60] Jyoti, S. C. Sharma, N. Pathak, and R. P. Sharma, "Beam-driven whistler mode nonlinear saturation and turbulence in the magnetopause," *Phys Plasmas*, vol. 29, no. 9, p. 092104, Sep. 2022, doi: 10.1063/5.0098108.

[61] Jyoti, S. C. Sharma, and R. P. Sharma, "Localization and turbulence of beam-driven whistler wave with magnetosonic wave in magnetopause," *Phys Plasmas*, vol. 30, no. 2, Feb. 2023, doi: 10.1063/5.0134920.

[62] R. Fitzpatrick and F. L. Waelbroeck, "Two-fluid magnetic island dynamics in slab geometry. II. Islands interacting with resistive walls or resonant magnetic perturbations," *Phys Plasmas*, vol. 12, no. 2, 2005, doi: 10.1063/1.1833391.

[63] N. Pathak, N. Yadav, S. Sharma, P. Sharma, and R. P. Sharma, "Localization of whistler wave and turbulent spectra in the magnetotail region," *J Geophys Res Space Phys*, vol. 122, no. 2, pp. 1751–1762, 2017, doi: 10.1002/2016JA023640.

[64] D. Biskamp and H. Welter, "Dynamics of decaying two-dimensional magnetohydrodynamic turbulence," *Physics of Fluids B*, vol. 1, no. 10, 1989, doi: 10.1063/1.859060.

[65] S. Boldyrev and N. F. Loureiro, "Role of reconnection in inertial kinetic-Alfvén turbulence," *Phys Rev Res*, vol. 1, no. 1, 2019, doi: 10.1103/PhysRevResearch.1.012006.

[66] S. Ichimaru., "Basic Principles of Plasma Physics: a Statistical Approach. By S. Ichimaru. Benjamin Frontiers in Physics, 1973. 324 pp. $19.50 (hardcover), $12.50 (paperback).," *J Plasma Phys*, vol. 13, no. 3, 1975, doi: 10.1017/s0022377800025289.

[67] M. Colunga, J. F. Luciani, and P. Mora, "Electron acceleration in localized plasma waves," *Physics of Fluids*, vol. 29, no. 10, 1986, doi: 10.1063/1.865857.

[68] V. N. Tsytovich, "Radiative-resonant collective wave-particle interactions," *Physics Reports*, vol. 178, no. 5–6. 1989. doi: 10.1016/0370-1573(89)90084-7.

[69] R. P. Sharma, H. D. Singh, and M. Malik, "Alfvén wave filamentation and particle acceleration in solar wind and magnetosphere," *J Geophys Res Space Phys*, vol. 111, no. 12, 2006, doi: 10.1029/2006JA011759.

[70] N. H. Bian and P. K. Browning, "Particle Acceleration in a Model of a Turbulent Reconnecting Plasma: A Fractional Diffusion Approach," *Astrophys J*, vol. 687, no. 2, 2008, doi: 10.1086/593145.

[71] W. Rozmus, R. P. Sharma, J. C. Samson, and W. Tighe, "Nonlinear evolution of stimulated Raman scattering in homogeneous plasmas," *Physics of Fluids*, vol. 30, no. 7, 1987, doi: 10.1063/1.866152.

[72] M. V. Leonenko, E. E. Grigorenko, and L. M. Zelenyi, "Spatial Scales of Super Thin Current Sheets with MMS Observations in the Earth's Magnetotail," *Geomagnetism and Aeronomy*, vol. 61, no. 5, 2021, doi: 10.1134/S0016793221050091.

[73] J. L. Burch *et al.*, "Localized Oscillatory Energy Conversion in Magnetopause Reconnection," *Geophys Res Lett*, vol. 45, no. 3, 2018, doi: 10.1002/2017GL076809.

CHAPTER-5

Coherent Structures of Beam-Driven Whistler mode in the presence of Magnetic Islands in the Magnetopause

5.1 Introduction

Turbulence and magnetic reconnection are essential plasma processes that have a complicated and intricate relationship in which reconnection jets can be a driver for turbulence, and turbulence may produce small-scale reconnection events as a fundamental element of the nonlinear dynamics and disrupt existing magnetic reconnection events [1–5]. Both phenomena are present throughout the Universe in a variety of plasmas, including astrophysical (such as galaxy clusters [6], accretion discs [7], and interstellar medium [8,9]), heliospheric (such as the solar corona [10], planetary magnetospheres [11–13] and solar wind [14,15]), and laboratory plasmas [16,17].

In many astrophysical environments, magnetic reconnection is an energy conversion process that results in energetic phenomena like geomagnetic storms and aurora, solar flares and coronal mass ejections, x-ray flares in magnetars, and magnetic interactions between neutron stars and their accretion discs. A more extensive understanding of reconnection is a crucial goal for plasma physics on Earth and in space, yet most situations are too remote, too hot, or too tiny to allow for comprehensive in situ observations [18]. Numerous spacecraft missions have studied the Earth's magnetosphere; some of these missions made multipoint measurements in and near areas with collisionless magnetic reconnection [19–24]. Turbulence is common and is understood to play a crucial role in space plasma as it cascades energy from large to small scales, ultimately resulting in dissipation and particle heating. The evidence for the intimate relationship between magnetic reconnection and turbulence in magnetized plasmas is growing [4,5,25]. It has been observed that magnetic spectrum scaling exhibits Kolmogorov scaling of -5/3 in reconnection as well as in turbulence which provides evidence that reconnection dynamics involves energy transfer analogous to standard turbulence [26]. Several review articles discuss the way how turbulence can become the host of reconnecting current sheet and how reconnecting current sheet can drive turbulence [27–30].

It is known that several wave modes are connected to reconnection at the dayside magnetopause such as upper hybrid wave [31], lower hybrid wave, magnetosonic wave [32] kinetic Alfven wave [33], electrostatic solitary wave [34,35], whistler mode waves [36–41]. Whistler-mode waves are among

them, and due to their prominence as the mostly seen and significant plasma waves that may influence the dissipation region's structure and the effectiveness of reconnection, they are the subject of the most research and attention [42,43]. Whistler mode waves have been seen in the past close to the X line during magnetopause crossings and have also been numerically modelled, which has given rise to the hypothesis that the waves may act as a mediator in the reconnection process [37].

The features of reconnection that develop in a turbulent environment in both three dimensions and two dimensions have been extensively studied in recent literature [44,45]. These studies frequently concentrate on reconnection rates, dimensionality, and spectra, as well as on additional topics such as violations of flux freezing in turbulence with reconnection-related consequences. Also, it is reported that strong turbulence is generated by nonlinear coupling of large amplitude unstable plasma modes, by the explosive reorganization of large-scale magnetic fields [46]. In this article, main emphasis is on the formation of coherent structures and how the turbulence is excited in astrophysical and laboratory plasmas. More recent studies reported the small-scale turbulence-driven magnetic reconnection in Earth's magnetosheath and revealed a novel type of reconnection, known as electron-only reconnection can occur [47]. Recently, some observational evidence reported that correlation length of the turbulence can impact the nature of turbulence-driven reconnection, thus influencing the small-scale nonlinear dynamics and dissipation of turbulent fluctuations [48]. Some researchers investigated the semi-collisional regime of the plasmoid instability analytically and numerically, which is an extension of a Sweet-Parker sheet of the semi-collisional tearing mode [49].

Whistler coherent structures have been reported at magnetic reconnection sites with the expectation that an intense electron beam is responsible for the generation of coherent structures [50]. Also, they reported the generation of whistler waves by a strong electron beam (generated by reconnection process) in the dayside magnetosphere reconnection region and analyzed data from the Magnetospheric Multiscale Mission (MMS); the highest growth rate of the wave was found to be at $k\lambda_e \sim 0.53$ within the frequency range of $0.1\omega_{ce} - 0.5\omega_{ce}$. Further, it might be expected that at later on stage, these structures results in the whistler turbulence. However, it is worth pointing out again that whistler-mode waves in the reconnection region are mostly reported and studied in the vicinity of the Earth. As far as we are aware, there is not too much reporting of beam-driven whistler-mode waves in the reconnection region at the magnetopause.

The primary objectives of this study are to understand the formation of the whistler coherent structure and current sheet formation at magnetic reconnection site due to the intense electron beam (as observed by magnetospheric multiscale mission (MMS)) along with the influence of magnetic island.

A beam-driven whistler wave has been simulated in three dimensions to do this. The whistler wave in this model originates from noise owing to the energy of the beam and rises to a large amplitude, where nonlinear processes from the ponderomotive force drive the whistler wave to localize, which ultimately results in the turbulent state. To better understand the nonlinear stage of wave development and saturation, we take into account the nonlinear interaction of a high-frequency whistler wave with a low-frequency MSWs, accounting for the ponderomotive nonlinearity fetched by the whistler wave. The evolution of whistler localized structures and current sheets is illustrated by the results of numerical simulations based on theoretical modelling. Nonlinear processes, such as ponderomotive force, density change, and the existence of magnetic islands, might be considered the cause of whistler coherent structures. To determine the scale size of coherent structures and current sheets, we have studied the semianalytical model also.

The layout of the article is as follows: - the model equations of whistler wave and magnetosonic waves are derived in section 2. In section 3, we discussed the numerical methods, techniques, and conditions which we have used for the numerical simulation work and the results of numerical simulation. A semianalytical model is discussed in section 4 for understanding the concept of localization. Finally, section 5 explains the summary and conclusion of this article.

5.2 Analytical model

5.2.1 Whistler dynamics in the presence of beam

The dynamical equation for a 3D whistler wave with an ambient magnetic field along the z-axis in a magnetized plasma propagating in the x, y, and z axis with a wave vector $\vec{k} = k_x\hat{x} + k_y\hat{y} + k_z\hat{z}$, is derived utilizing two-fluid models. The governing dynamical equation of 3D whistler wave in terms of vector potential can be written as (the detailed derivation has been given as Appendix-A)

$$\begin{aligned}
&\frac{\partial^2 A_z}{\partial t^2} + \frac{\partial^6 A_z}{\partial t^2 \partial x^2}\lambda_e^4 + \frac{\partial^6 A_z}{\partial t^2 \partial y^2}\lambda_e^4 + \frac{\partial^6 A_z}{\partial t^2 \partial z^2}\lambda_e^4 + 2\lambda_e^4 \frac{\partial^4 A_z}{\partial t^2 \partial z^2}\left(\frac{\partial^2}{\partial x^2} + \frac{\partial}{\partial y^2}\right) - \\
&2\lambda_e^2\left(\frac{\partial^2}{\partial x^2} + \frac{\partial^2}{\partial y^2} + \frac{\partial^2}{\partial z^2}\right)\frac{\partial^2 A_z}{\partial t^2} + \lambda_i^2 v_A^2\left(\frac{\partial^2}{\partial x^2} + \frac{\partial^2}{\partial y^2}\right)\frac{\partial^2 A_z}{\partial z^2} + \\
&\lambda_i^2 v_A^2 \frac{\partial^4 A_z}{\partial z^4} + \frac{\lambda_i^2 v_A^2 B_{0y}^2}{B_{0z}^2}\left(\frac{\partial^2}{\partial x^2} + \frac{\partial^2}{\partial y^2}\right)\frac{\partial^2 A_z}{\partial y^2} + \frac{\lambda_i^2 v_A^2 B_{0y}^2}{B_{0z}^2}\frac{\partial^4 A_z}{\partial y^2 \partial z^2} + \\
&\frac{2\lambda_i^2 v_A^2 B_{0y}}{B_{0z}}\left(\frac{\partial^2}{\partial x^2} + \frac{\partial^2}{\partial y^2}\right)\frac{\partial^2 A_z}{\partial y \partial z} + \frac{2\lambda_i^2 v_A^2 B_{0y}}{B_{0z}}\frac{\partial^4 A_z}{\partial y \partial z^3} = 0,
\end{aligned} \tag{5.1}$$

where $\omega_{ce}\left(=\frac{eB_0}{m_e c}\right)$ is the electron gyrofrequency of wave, $v_A\left(=\sqrt{\frac{B_0^2}{4\pi n_0 m_i}}\right)$ is Alfven wave's speed, n_0 denotes the background number density, c denotes the velocity of light, and $\lambda_i\left(=\sqrt{\frac{c^2 m_i}{4\pi n_0 e^2}}\right)$ is the collisionless ion skin depth, $\lambda_e\left(=\sqrt{\frac{c^2 m_e}{4\pi n_0 e^2}}\right)$ is the collisionless electron skin depth. Additionally, it is reported that beam-driven growth rate is taken into account then, the aforementioned equation becomes $\frac{d}{dt}\rightarrow\left(\frac{d}{dt}+\gamma\right)$ (please see appendix),

$$\begin{aligned}
&\left(\frac{\partial^2}{\partial t^2}+2\gamma\frac{\partial}{\partial t}\right)A_z+\frac{\partial^6 A_z}{\partial t^2\partial x^2}\lambda_e^4+\frac{\partial^6 A_z}{\partial t^2\partial y^2}\lambda_e^4+\frac{\partial^6 A_z}{\partial t^2\partial z^2}\lambda_e^4+2\lambda_e^4\frac{\partial^4 A_z}{\partial t^2\partial z^2}\left(\frac{\partial^2}{\partial x^2}+\frac{\partial^2}{\partial y^2}\right)-\\
&2\lambda_e^2\left(\frac{\partial^2}{\partial x^2}+\frac{\partial^2}{\partial y^2}+\frac{\partial^2}{\partial z^2}\right)\frac{\partial^2 A_z}{\partial t^2}+\lambda_i^2 v_A^2\left(\frac{\partial^2}{\partial x^2}+\frac{\partial^2}{\partial y^2}\right)\frac{\partial^2 A_z}{\partial z^2}+\lambda_i^2 v_A^2\frac{\partial^4 A_z}{\partial z^4}+\\
&\frac{\lambda_i^2 v_A^2 B_{0y}^2}{B_{0z}^2}\left(\frac{\partial^2}{\partial x^2}+\frac{\partial^2}{\partial y^2}\right)\frac{\partial^2 A_z}{\partial y^2}+\frac{\lambda_i^2 v_A^2 B_{0y}^2}{B_{0z}^2}\frac{\partial^4 A_z}{\partial y^2\partial z^2}+\\
&\frac{2\lambda_i^2 v_A^2 B_{0y}}{B_{0z}}\left(\frac{\partial^2}{\partial x^2}+\frac{\partial^2}{\partial y^2}\right)\frac{\partial^2 A_z}{\partial y\partial z}+\frac{2\lambda_i^2 v_A^2 B_{0y}}{B_{0z}}\frac{\partial^4 A_z}{\partial y\partial z^3}=0.
\end{aligned}\tag{5.2}$$

For this Eq. (5. 2), the following envelope solution is assumed.

$$\tilde{A}_z=A_z(x,y,z,t)e^{i(k_{0x}\hat{x}+k_{0y}\hat{y}+k_{0z}\hat{z}-\omega_0 t)}.\tag{5.3}$$

By considering the impact of a whistler wave on the background density and relieving the aforementioned solution into Eq. (5.2), we can obtain the dynamical equation of a nonlinear whistler wave propagating through plasma.

$$\begin{aligned}
&2i\omega_0(1+\lambda_e^4k_0^4+2\lambda_e^2k_0^2+2\lambda_e^4k_{0x}^2k_{0z}^2+2\lambda_e^4k_{0y}^2k_{0z}^2)\frac{\partial A_z}{\partial t}+(4\omega_0^2\lambda_e^4k_{0x}^2)\frac{\partial^2 A_z}{\partial x^2}+\\
&(4\omega_0^2\lambda_e^4k_{0y}^2)\frac{\partial^2 A_z}{\partial y^2}+(4\omega_0^2\lambda_e^4k_{0z}-4\lambda_i^2v_A^2k_{0z}^2)\frac{\partial^2 A_z}{\partial z^2}+\\
&2ik_{0x}(2\omega_0^2k_{0x}^2\lambda_e^4+2\omega_0^2k_{0z}^2\lambda_e^4+2\omega_0^2\lambda_e^2+k_{0z}^2\lambda_i^2v_A^2)\frac{\partial A_z}{\partial x}+\\
&2ik_{0y}(2\omega_0^2k_{0y}^2\lambda_e^4+2\omega_0^2k_{0z}^2\lambda_e^4+2\omega_0^2\lambda_e^2-k_{0z}^2\lambda_i^2v_A^2)\frac{\partial A_z}{\partial y}+\\
&2ik_{0z}(2\omega_0^2k_{0z}^2\lambda_e^4+2\omega_0^2k_{0x}^2\lambda_e^4+2\omega_0^2k_{0y}^2\lambda_e^4+2\omega_0^2\lambda_e^2-k_{0y}^2\lambda_i^2v_A^2-2k_{0z}^2\lambda_i^2v_A^2)\frac{\partial A_z}{\partial z}+\\
&(4\lambda_i^2v_A^2k_{0x}k_{0z}-8\omega_0^2\lambda_e^4k_{0z}k_{0x})\frac{\partial^2 A_z}{\partial x\partial z}+(4\lambda_i^2v_A^2-8\omega_0^2\lambda_e^4)k_{0y}k_{0z}\frac{\partial^2 A_z}{\partial y\partial z}+\\
&\frac{\lambda_i^2v_A^2B_{0y}^2}{B_{0z}^2}k^2k_{0y}^2A_z+\frac{2\lambda_i^2v_A^2B_{0y}}{B_{0z}}k^2k_{0y}k_{0z}A_z-(\lambda_i^2v_A^2k^2k_{0z}^2)\frac{\delta n}{n_0}A_z+2i\gamma' A_z=0,
\end{aligned}\tag{5.4}$$

where k_{0x}, k_{0y} and k_{0z} are wave vector components of whistler related to the background magnetic field are given as, $k_0^2 = k_{0x}^2 + k_{0y}^2 + k_{0z}^2$. Here n' denotes the modified density, i.e., $n' = n_0 + \delta n$, and $\frac{\delta n}{n_0}$ denotes the perturbation in plasma density due to non-linear whistler wave. We have used the relation of the magnetic field and vector potential $\left(\frac{B_{0y}}{B_{0z}} = \frac{\delta A_z}{A_0}\right)$.

(δA_z , is the vector potential associated with the magnetic field)

Eq. (5.4) in normalized dimensionless form is given as

$$ic_1\frac{\partial A_z}{\partial t} + c_2\frac{\partial^2 A_z}{\partial x^2} + c_3\frac{\partial^2 A_z}{\partial y^2} + c_4\frac{\partial^2 A_z}{\partial z^2} + ic_5\frac{\partial A_z}{\partial x} + ic_6\frac{\partial A_z}{\partial y} + ic_7\frac{\partial A_z}{\partial z} +$$

$$c_8\frac{\partial^2 A_z}{\partial x \partial z} + c_9\frac{\partial^2 A_z}{\partial y \partial z} + c_{10}\left(\frac{\delta A_z}{A_0}\right)^2 A_z + c_{11}\left(\frac{\delta A_z}{A_0}\right)A_z - \frac{\delta n}{n_0}A_z + 2i\gamma' A_z = 0, \tag{5.5}$$

where Eq. (5.5) represents the whistler wave's normalized dynamical equation. In this section, the beam instability that generates the whistler wave will be described. The growth rate of whistler wave generated by an energetic electron beam, that is included phenomenologically and its value corresponding with the data published by Zhao et al. [50]) will be used in simulations here. To get the dynamical equation, we introduce the field perturbation due to magnetic islands profile, since the magnetic reconnection is visualized within the framework of magnetic island as mentioned by Fitzpatrick et al. [51],

$$\frac{\delta A_z}{A_0} = \left(-\frac{x^2}{2} + b_0\cos(ky)\right). \tag{5.6}$$

So, using the profile of field perturbation Eq. (5.5) modifies as-

$$ic_1\frac{\partial A_z}{\partial t} + c_2\frac{\partial^2 A_z}{\partial x^2} + c_3\frac{\partial^2 A_z}{\partial y^2} + c_4\frac{\partial^2 A_z}{\partial z^2} + ic_5\frac{\partial A_z}{\partial x} + ic_6\frac{\partial A_z}{\partial y} + ic_7\frac{\partial A_z}{\partial z} +$$

$$c_8\frac{\partial^2 A_z}{\partial x \partial z} + c_9\frac{\partial^2 A_z}{\partial y \partial z} + c_{10}\left(-\frac{x^2}{2} + b_0\cos(ky)\right)^2 A_z + \tag{5.7}$$

$$c_{11}\left(-\frac{x^2}{2} + b_0\cos(ky)\right)A_z - \frac{\delta n}{n_0}A_z + 2i\gamma' A_z = 0,$$

where $c_1 = \frac{2\omega_0(1+\lambda_e^4 k_0^4 + 2\lambda_e^2 k_0^2 + 2\lambda_e^4 k_{0x}^2 k_{0z}^2 + 2\lambda_e^4 k_{0y}^2 k_{0z}^2)}{(\lambda_i^2 v_A^2 k^2 k_{0z}^2)}$.

$$c_2=\frac{2k_{0x}(2\omega_0^2\lambda_e^4k_{0x}^2+2\omega_0^2\lambda_e^4k_{0z}^2+2\omega_0^2\lambda_e^2-\lambda_i^2k_{0z}^2v_A^2)}{(\lambda_i^2v_A^2k^2k_{0z}^2)}. \qquad c_3=\frac{2k_{0y}(2\omega_0^2\lambda_e^4k_{0y}^2+2\omega_0^2\lambda_e^4k_{0z}^2+2\omega_0^2\lambda_e^2-\lambda_i^2k_{0z}^2v_A^2)}{(\lambda_i^2v_A^2k^2k_{0z}^2)}.$$

$$c_4=\frac{2k_{0z}(2\omega_0^2\lambda_e^2k_{0z}^2+2\omega_0^2\lambda_e^2k_{0x}^2+2\omega_0^2\lambda_e^2k_{0y}^2+2\omega_0^2\lambda_e^2-\lambda_i^2v_A^2k_{0y}^2-2\lambda_i^2v_A^2k_{0z}^2)}{\lambda_i^2v_A^2k^2k_{0z}^2}.$$

$$c_5=\frac{4\omega_0^2k_{0x}^2\lambda_e^4}{\lambda_i^2v_A^2k_0^2k_{0z}^2}, \qquad c_6=\frac{4\omega_0^2k_{0y}^2\lambda_e^4}{\lambda_i^2v_A^2k_0^2k_{0z}^2}, \qquad c_7=\frac{\left(4\omega_0^2k_{0z}^2\lambda_e^4-4\lambda_i^2v_A^2k_{0z}^2\right)}{\lambda_i^2v_A^2k_0^2k_{0z}^2}. \quad b_0=0.5,$$

$$c_8=\frac{\left(8\omega_0^2\lambda_e^4-4\lambda_i^2v_A^2\right)k_{0z}k_{0x}}{\lambda_i^2v_A^2k_0^2k_{0z}^2}, \qquad c_9=\frac{\left(8\omega_0^2\lambda_e^4-4\lambda_i^2v_A^2\right)k_{0z}k_{0y}}{\lambda_i^2v_A^2k_0^2k_{0z}^2}, \qquad c_{10}=\frac{k_{0y}^2}{k_{0z}^2} \text{ and } c_{11}=\frac{2k_{0y}}{k_{0z}}.$$

and $\gamma'=\frac{\gamma}{\omega_0}$ is the normalized growth rate. $\gamma\left(=0.5083\omega_{ce}\right)$ is the growth rate of beam-driven whistler waves. The normalizing parameters are-

$t_n=1/\omega_0.$

$$x_n=\frac{k_{0x}(2\omega_0^2k_{0x}^2\lambda_e^4+2\omega_0^2k_{0z}^2\lambda_e^4+2\omega_0^2\lambda_e^2+k_{0z}^2\lambda_i^2v_A^2)}{\omega_0(1+\lambda_e^4k_0^4+2\lambda_e^2k_0^2+2\lambda_e^4k_{0x}^2k_{0z}^2+2\lambda_e^4k_{0y}^2k_{0z}^2)}.$$

$$z_n=\frac{2i(-2\omega_0^2k_{0x}^3\lambda_e^4+2\omega_0^2k_{0x}k_{0z}^2\lambda_e^4+2\omega_0^2\lambda_e^2k_{0x}+k_{0x}k_{0z}^2\lambda_i^2v_A^2+2k_{0z}^3\lambda_i^2v_A^2)}{2\omega_0(1+\lambda_e^4k_{0x}^4+\lambda_e^4k_{0z}^4+2\lambda_e^2k_{0x}^2+2\lambda_e^2k_{0z}^2)}.$$

5.2.2 Magnetosonic waves dynamics (MSWs)

Consider a magnetosonic wave propagating in the x-direction, i.e., $\vec{k}=k_{0x}\hat{x}$ along with the background magnetic field in the z-direction, i.e., $\vec{B}=B_0\hat{z}$. The electric field is polarised in y-direction i.e., $\vec{E}=E_y\hat{y}$. The dynamical equation for the magnetosonic wave is obtained from the basic equations such as the equation of motion, continuity equation, Faraday's law, and Ampere's -Maxwell's equation following the procedure used by Jyoti et al. [52] as

$$\left(\frac{\partial^2}{\partial t^2}-c_{12}\frac{\partial^2}{\partial x^2}\right)\frac{n}{n_0}=-c_{13}\frac{\partial^2}{\partial x^2}|A_z|^2, \tag{5.8}$$

where c_{12}, c_{13} are the constant whose value is given below:

$$c_{12}=c^2\left(\frac{c_s^2+v_A^2}{c^2+v_A^2}\right)$$

and $c_{13}=\left[\frac{e^2}{m_em_i\omega_{ce}^2}-\frac{e^2\omega_0}{m_em_i\omega_{ce}\alpha_1}\left\{\left(1+\frac{\omega_{ce}^2}{\alpha_1}\right)+\frac{\omega_0^3}{\alpha_1\omega_{ce}}\right\}+\frac{e^2}{m_i^2\omega_{ci}^2}-\frac{e^2\omega_0}{m_em_i\omega_{ce}\alpha_1}\left\{\left(1+\frac{\omega_{ci}^2}{\alpha_1}\right)+\frac{\omega_0^3}{\alpha_1\omega_{ci}}\right\}\right]$

$c_s\left(=\frac{v_{th_e}^2+v_{th_i}^2}{m_i}\right)^{\frac{1}{2}}$ is the speed of the sound wave. And, $\alpha_1=-k^2\lambda_e^2(\omega_0^2-\omega_{ce}^2)-\omega_0^2$.

Now, using the same normalizing parameter as we have used in the dynamics of whistler wave i.e., x_n, z_n and t_n. After taking the adiabatic response of Eq. (5.8), we obtain

$$\frac{n}{n_0}=\frac{c_{13}}{c_{12}}|A_z|^2. \tag{5.9}$$

we obtain the following normalization equation,

$$A_n=\left[\frac{c_{12}}{c_{13}}n_0\right]^{\frac{1}{2}}$$

using this Eq. (5.9) in Eq. (5.7), we obtain

$$\begin{aligned}&ic_1\frac{\partial A_z}{\partial t}+c_2\frac{\partial^2 A_z}{\partial x^2}+c_3\frac{\partial^2 A_z}{\partial y^2}+c_4\frac{\partial^2 A_z}{\partial z^2}+ic_5\frac{\partial A_z}{\partial x}+ic_6\frac{\partial A_z}{\partial y}+ic_7\frac{\partial A_z}{\partial z}+c_8\frac{\partial^2 A_z}{\partial x\partial z}+c_9\frac{\partial^2 A_z}{\partial y\partial z}\\&+c_{10}\left(-\frac{x^2}{2}+b_0\cos(ky)\right)^2A_z+c_{11}\left(-\frac{x^2}{2}+b_0\cos(ky)\right)A_z-\frac{c_{13}}{c_{12}}|A_z|^2A_z+2i\gamma' A_z=0,\end{aligned} \tag{5.10}$$

This is the model equation of dynamical system of 3D nonlinear whistler in the presence of magnetic islands.

Parameters used in numerical simulations are:

$n_0=21cm^{-3}$, $B_0=45nT$, $T_e=42eV$, $T_I=235eV$, $\omega_{pe}=2.5\times10^5\,rad/\sec$, $\omega_{ce}=7.9\times10^3\,rad/\sec$,

$\omega_{ci}=4.31\,rad/\sec$, $v_A=2.14\times10^7\,cm/\sec$, $c_s=1.6\times10^7\,cm/\sec$, $\lambda_i=4.9\times10^6\,cm$, $\lambda_e=1.16\times10^5\,cm$,

$A_n=5.03\times10^8\,G$ cm, $x_n=y_n=1.02\times10^6\,cm$, $z_n=1.5\times10^6\,cm$, $t_n=0.015\sec$,

The values of numerical constants are given below-

$c_1=0.0155$, $c_2=c_3=1.02\times10^6$, $c_4=1.5\times10^6$, $c_5=c_6=2.5\times10^{10}$, $c_7=-2.0\times10^{11}$, $c_8=c_9=-7.2\times10^{11}$,

$c_{10}=12.41$, $c_{11}=7.04$, $c_{12}=1.6\times10^5$, $c_{12}=7.2\times10^{14}$, $c_{13}=3.43\times10^{14}$.

5.3 Numerical Simulation and Result Discussion

For solving the dynamics of Eq. (5.10), we have developed modified nonlinear Schrödinger model (MNLS). To solve Eq. (5.10) numerically, we have used the 3D pseudospectral method. For space integration having periodic length $L_x=\frac{2\pi}{\alpha_x}$ and $L_y=\frac{2\pi}{\alpha_y}$, pseudospectral approach and finite difference approach for time evolution utilizing a modified version of the predictor-corrector method has been

used [53]. For doing numerical simulation, periodic domain $(10\pi\times10\pi\times10\pi)$ and grid size $(128\times128\times128)$ of the system are used. The model equation has been transformed into the nonlinear Schrodinger (NLS) equation to evaluate its accuracy, by testing the consistency of the plasmon number up to order of 10^{-6} and then we modify this code according to our problem and run this code for two cases.

Case 1. The initial condition for numerical simulation consists of sequential X-O points as below and used by [54] : -

$$A_z(x,y)=\cos(2x+2.3)+\cos(y+4.1) \tag{5.11}$$

Figure 5.1 shows the spatial evolution of normalized vector potential over time in the x-y plane and at a fixed z. Furthermore, we assume that a 3D whistler wave originates from reconnection region that already exists. The spatial fluctuation of the whistler wave field is generated by density modification caused by ponderomotive force nonlinearity as well as field disruption due to the whistler wave. Initially, the structures generated are coherent, but as time progresses, it is expected that this will result in the development of whistler turbulence, as seen in Figure 5.1.

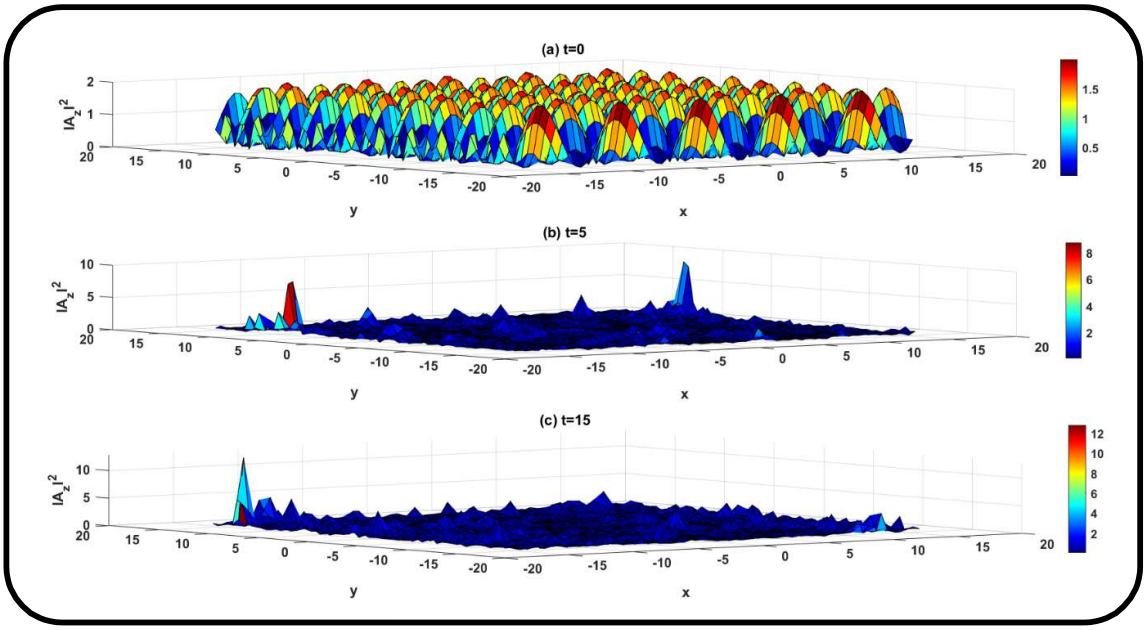

Figure 5.1 The spatial evolution of vector potential in x-y plane (a) t=0, (b) t=5, and (c) t=15, for modified nonlinear Schrödinger equation (in normalized units).

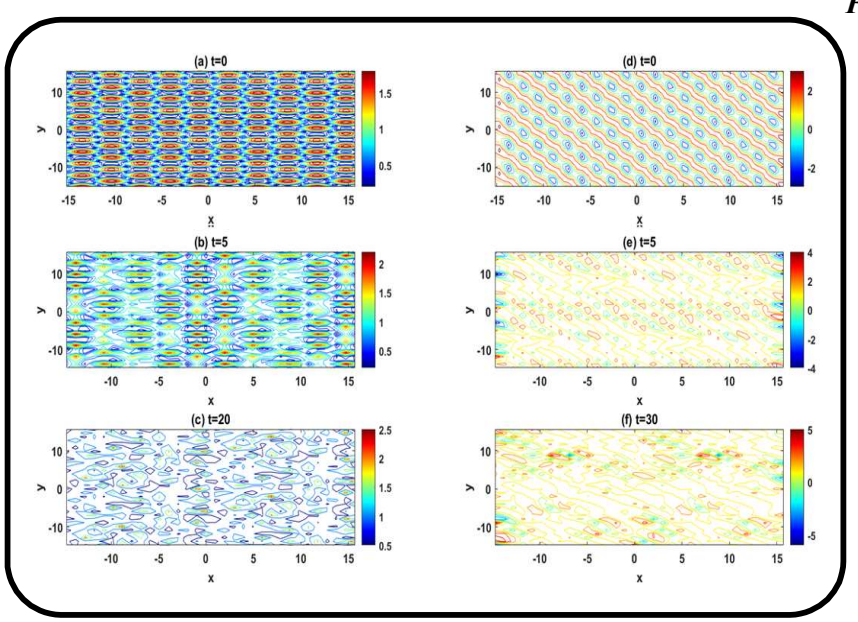

Figure 5.2 Evolution of contour plot of vector potential (Left panel), and current sheet formation (Right panel) in the x-y plane at different times.

To locate magnetic islands produced by reconnection, one might plot the contour plot of vector potential or draw magnetic field lines. The rise of magnetic flux, which is associated with the current density function by Ampere's law, is then calculating by looking at the spatial development of the current density function. The contour plot of the vector potential (Left panel) in the x-y plane at various time is shown in Figure 5.2, along with the current density (Right panel). As time goes on, we see that the relevant X-O structures starts modifying, and finally, a completely chaotic pattern is obtained.

Case 2. The initial condition for numerical simulation consists of a single O-point represents the magnetic reconnection [51] is: -

$$\frac{\delta A_z}{A_0} = \left(-\frac{x^2}{2} + b_0 \cos(ky) \right).$$

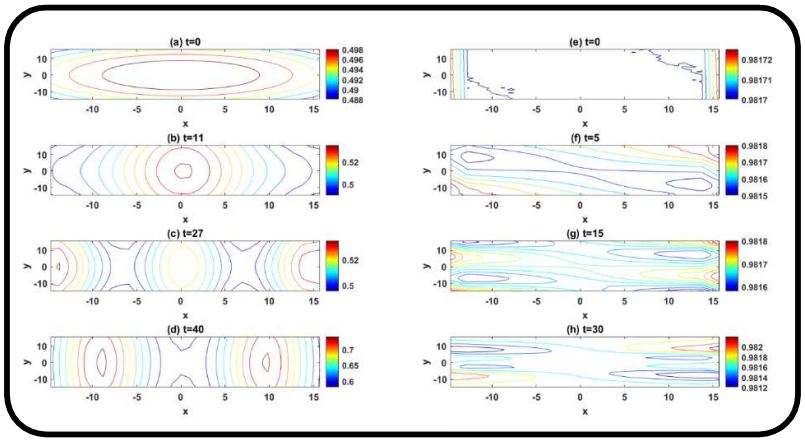

Figure 5.1 Evolution of contour plot of vector potential (left panel), and current sheet formation (right panel) in the x-y plane at different times.

Figure 5.3 depicts the contour plot of vector potential (left panel) and current sheet (right panel) formation at different times. In left panel, initially magnetic field lines forms a single O-structures. As time passage, this single O-point emerges into

multiple O-points associated with X-points in this way X-O structures are formed with increasing amplitude. Formation of separatix between X and O points is clearly visible in this figure. In right panel, we have shown the temporal evolution of current sheets. By using the relation of $j = \nabla^2 A_z$, current density can be obtained. Bhat et al. [49] have observed the contour plot of vector potential as presented in figure 4 of their paper at different times. At intial stage, the system is just before the plasmoid formation but after that plasmoids (small islands) are formed, and due to the highly symmetric configuration of magnetic field, the plasmoid is stuck in the middle of current sheet (reconnection sites). Later on stage, these plasmoid well into the nonlinear stage. In our analysis also, it might be expected that as the time evolves plasmoids are formed.

Quasi-steady state of system

As the constant growth rate of the beam-driven mode was taken into account due to which quasi-steady state has not yet been attained and won't be for furthermore time. So, to see the turbulent power spectra we switch off the growth rate term and then remodel our system Eq. (5.10) into the following form

$$ic_7\frac{\partial A_z}{\partial z}+c_2\frac{\partial^2 A_z}{\partial x^2}+c_3\frac{\partial^2 A_z}{\partial y^2}+ic_5\frac{\partial A_z}{\partial x}+ic_6\frac{\partial A_z}{\partial y}$$
$$+c_8\frac{\partial^2 A_z}{\partial x\partial z}+c_9\frac{\partial^2 A_z}{\partial y\partial z}-\frac{c_{13}}{c_{12}}\left|A_z\right|^2 A_z=0. \qquad (5.12)$$

Then solving Eq. (5.12) numerically with the pseudospectral method for space integration (along x-direction and y-direction) and finite difference method for time evolution (along z-direction). After that simulating this Eq. (5.12) for higher grid size (512×512). Power spectra obtained from numerical simulation is shown in figure 5.4. The obtained power spectra show an approximate scaling of $k^{-5/3}$ [consistent with Biskamp et al. [55]] in inertial range and $k^{-7/3}$ at the shorter wavelength, we get steeper spectra. This power spectra illustrate the signature of turbulence. The charged particles can be accelerated by this energy.

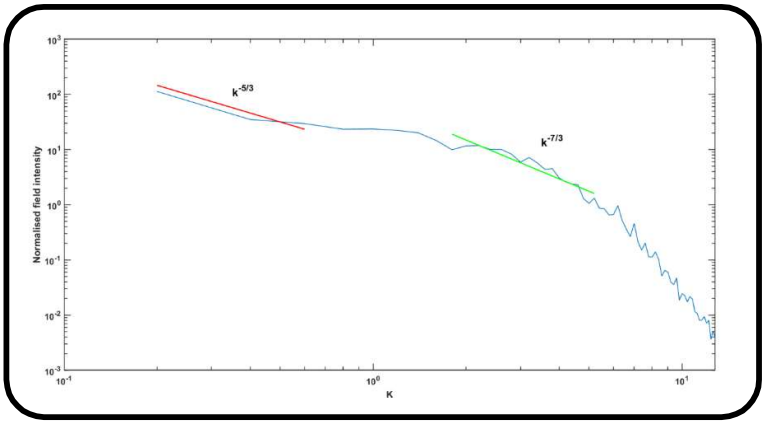

Figure 5.2 Power spectra of Normalized field intensity of whistler wave against normalized wave vector k for Modified Nonlinear Schrödinger equation (in normalized units).

Numerous kinds of processes, such as Fermi acceleration, resonant wave-particle acceleration, and acceleration through radiative-resonant interactions, have been proposed in the literature to examine the acceleration of charged particles in plasmas. In this work, we investigate the production of the thermal tail of energetic electrons, which may be the cause of the electron acceleration and heating, from the power-law scaling of turbulence generation. The interaction between localized structures and plasma particles may be understood with the aid of the Fokker-Plank equation. Particle energization can result from these kinds of random and frequent interactions. Second-order Fermi acceleration [56,57] is the mechanism behind this.

To investigate the interactions between strongly localized fields (structures) and plasma particles, one can utilize the quasi-linear diffusion equation. The expression for quasi- linear diffusion equation is given below [56,58]

$$\frac{\partial f}{\partial t} = \frac{\partial}{\partial v}\left\{ D(v)\frac{\partial f}{\partial v} \right\}. \tag{5.13}$$

Here, $f(t,v)$ denotes the velocity distribution function and $D(v)$ denotes the velocity space diffusion coefficient. When the observation time is longer than the characteristic time of setting up of ponderomotive nonlinearity, the distribution function $f(v,t)$ can be assumed as time independent. In this context, the relation between spectral index η, and distribution function $f(v)$ [59] is given below-

$$f(v) \propto v^{2-\eta}. \tag{5.14}$$

In our current analysis $\eta \simeq 2.3$, therefore $f(v) \sim v^{-0.3}$ it leads to the formation of thermal tail of energetic electrons. Therefore, this enhances the thermal tail segment of the distribution function and paves the way for thermal heating of the particles.

5.4 Semianalytical model

In order to understand the basic physics behind the localization of whistler wave we have investigated the semianalytical model, also by using this model we can estimate the critical size of coherent structures and current sheet scale size. For simplification, we have considered a steady-state model. Now, by modifying Eq. (5.4), we obtain the following Eq.,

$$i\frac{2}{k_{\|}}\frac{\partial A_z}{\partial z}+\frac{(4\omega_0^2\lambda_e^4k_{\perp}^2)}{(2\omega_0^2k_{\|}^2\lambda_e^4+2\omega_0^2k_{\perp}^2\lambda_e^4+2\omega_0^2k_{\perp}^2\lambda_e^4+2\omega_0^2\lambda_e^2-k_{\perp}^2\lambda_i^2v_A^2-2k_{\|}^2\lambda_i^2v_A^2)k_{\|}^2}\frac{\partial^2A_z}{\partial x^2}+$$
$$\frac{(4\omega_0^2\lambda_e^4k_{\perp}^2)}{(2\omega_0^2k_{\|}^2\lambda_e^4+2\omega_0^2k_{\perp}^2\lambda_e^4+2\omega_0^2k_{\perp}^2\lambda_e^4+2\omega_0^2\lambda_e^2-k_{\perp}^2\lambda_i^2v_A^2-2k_{\|}^2\lambda_i^2v_A^2)k_{\|}^2}\frac{\partial^2A_z}{\partial y^2}+$$
$$\frac{\lambda_i^2v_A^2k^2k_{\perp}^2}{(2\omega_0^2k_{\|}^2\lambda_e^4+2\omega_0^2k_{\perp}^2\lambda_e^4+2\omega_0^2k_{\perp}^2\lambda_e^4+2\omega_0^2\lambda_e^2-k_{\perp}^2\lambda_i^2v_A^2-2k_{\|}^2\lambda_i^2v_A^2)k_{\|}^2}\left(\frac{\delta A_z}{A_0}\right)^2A_z+ \qquad (5.15)$$
$$\frac{2\lambda_i^2v_A^2k^2k_{0y}k_{\|}}{(2\omega_0^2k_{\|}^2\lambda_e^4+2\omega_0^2k_{\perp}^2\lambda_e^4+2\omega_0^2k_{\perp}^2\lambda_e^4+2\omega_0^2\lambda_e^2-k_{\perp}^2\lambda_i^2v_A^2-2k_{\|}^2\lambda_i^2v_A^2)k_{\|}}\left(\frac{\delta A_z}{A_0}\right)A_z$$
$$-\frac{(\lambda_i^2v_A^2k^2)}{(2\omega_0^2k_{\|}^2\lambda_e^4+2\omega_0^2k_{\perp}^2\lambda_e^4+2\omega_0^2k_{\perp}^2\lambda_e^4+2\omega_0^2\lambda_e^2-k_{\perp}^2\lambda_i^2v_A^2-2k_{\|}^2\lambda_i^2v_A^2)}\frac{\delta n}{n_0}A_z+A_z\exp(k_iz)=0.$$

Or we can rewrite the above equation in simplified equation as-

$$i\frac{2}{k_{\|}}\frac{\partial A_z}{\partial z}+\theta_1\lambda_e^2\left(\frac{\partial^2A_z}{\partial x^2}+\frac{\partial^2A_z}{\partial y^2}\right)+\theta_2\left(-\frac{x^2}{2}+b_0\cos(ky)\right)^2A_z+$$
$$\theta_3\left(-\frac{x^2}{2}+b_0\cos(ky)\right)A_z-\theta_4\frac{\delta n}{n_0}A_z+A_z\exp(k_iz)=0, \qquad (5.16)$$

where, $\theta_1=\frac{(4\omega_0^2\lambda_e^2k_{\perp}^2)}{(2\omega_0^2k_{\|}^2\lambda_e^4+2\omega_0^2k_{\perp}^2\lambda_e^4+2\omega_0^2k_{\perp}^2\lambda_e^4+2\omega_0^2\lambda_e^2-k_{\perp}^2\lambda_i^2v_A^2-2k_{\|}^2\lambda_i^2v_A^2)k_{\|}^2}.$

$$\theta_2=\frac{\lambda_i^2v_A^2k^2k_{\perp}^2}{(2\omega_0^2k_{\|}^2\lambda_e^4+2\omega_0^2k_{\perp}^2\lambda_e^4+2\omega_0^2k_{\perp}^2\lambda_e^4+2\omega_0^2\lambda_e^2-k_{\perp}^2\lambda_i^2v_A^2-2k_{\|}^2\lambda_i^2v_A^2)k_{\|}^2}.$$

$$\theta_3=\frac{2\lambda_i^2v_A^2k^2k_{\perp}}{(2\omega_0^2k_{\|}^2\lambda_e^4+2\omega_0^2k_{\perp}^2\lambda_e^4+2\omega_0^2k_{\perp}^2\lambda_e^4+2\omega_0^2\lambda_e^2-k_{\perp}^2\lambda_i^2v_A^2-2k_{\|}^2\lambda_i^2v_A^2)k_{\|}}.$$

$$\theta_4=\frac{(\lambda_i^2v_A^2k^2)}{(2\omega_0^2k_{\|}^2\lambda_e^4+2\omega_0^2k_{\perp}^2\lambda_e^4+2\omega_0^2k_{\perp}^2\lambda_e^4+2\omega_0^2\lambda_e^2-k_{\perp}^2\lambda_i^2v_A^2-2k_{\|}^2\lambda_i^2v_A^2)}.$$

Now we are assuming the envelope solution of vector potential $\tilde{A}_z=A_{00}e^{ik_{0z}s(x,y,z)}$, and putting this envelope solution in Eq. (5.16) we obtained the following equation-

$$i\frac{2}{k_{0z}}\frac{\partial A_{00}}{\partial z}-2A_{00}\frac{\partial s}{\partial z}+\theta_1\lambda_e^2\left(\frac{\partial^2 A_{00}}{\partial x^2}+\frac{\partial^2 A_{00}}{\partial y^2}\right)+2ik_{\|}\theta_1\lambda_e^2\left(\frac{\partial A_{00}}{\partial x}\frac{\partial s}{\partial x}+\frac{\partial A_{00}}{\partial y}\frac{\partial s}{\partial y}\right)-$$
$$k_{\|}^2\theta_1\lambda_e^2\left(\frac{\partial s}{\partial x}+\frac{\partial s}{\partial y}\right)^2 A_{00}+ik_{\|}\theta_1\lambda_e^2\left(\frac{\partial^2 s}{\partial x^2}+\frac{\partial^2 s}{\partial y^2}\right)A_{00}+\theta_2\left[\left(-\frac{x^2}{2}+b_0\cos(ky)\right)\right]^2 A_{00}+ \quad (5.17)$$
$$\theta_3\left[\left(-\frac{x^2}{2}+b_0\cos(ky)\right)\right]A_{00}-\theta_4\frac{\delta n}{n_0}A_{00}+A_z\exp(k_i z)=0.$$

Further separating the real and imaginary parts of Eq. (5.17)

$$-2\frac{\partial s}{\partial z}A_{00}+\theta_1\lambda_e^2\left(\frac{\partial^2 A_{00}}{\partial x^2}+\frac{\partial^2 A_{00}}{\partial y^2}\right)-k_{\|}^2\theta_1\lambda_e^2\left(\frac{\partial s}{\partial x}+\frac{\partial s}{\partial y}\right)^2 A_{00}+$$
$$\theta_2\left[\left(-\frac{x^2}{2}+b_0\cos(ky)\right)\right]^2 A_{00}+\theta_3\left[\left(-\frac{x^2}{2}+b_0\cos(ky)\right)\right]A_{00}- \quad (5.18)$$
$$\theta_4\left[\exp(\alpha|A_z|^2-1\right]A_{00}+A_{00}\exp(k_i z)=0.$$

$$\frac{2}{k_{\|}}\frac{\partial A_{00}}{\partial z}+2k_{\|}\theta_1\lambda_e^2\left(\frac{\partial A_{00}}{\partial x}\frac{\partial s}{\partial x}+\frac{\partial A_{00}}{\partial y}\frac{\partial s}{\partial y}\right)+k_{\|}\lambda_e^2\theta_1\left(\frac{\partial^2 s}{\partial x^2}+\frac{\partial^2 s}{\partial y^2}\right)A_{00}=0. \quad (5.19)$$

Further assuming the Gaussian profile for initial distribution of wave i.e.,

$$A_{00}^2=\frac{A_{00}^{'2}}{f_1(z)f_2(z)}\exp\left(\frac{-x^2}{r_{01}^2}-\frac{y^2}{r_{01}^2}+k_i z\right)$$
$$s=\beta_1(z)\frac{x^2}{2}+\beta_2(z)\frac{y^2}{2}+\phi(z) \quad (5.20)$$

Using Eq. (5.20) in Eq. (5.19), and collecting the terms x^2 and y^2, we obtain the following Eqs.

$$\beta_1(z)=\frac{1}{k_{\|}^2\theta_1\lambda_e^2}\frac{1}{f_1}\frac{\partial f_1}{\partial z}. \quad (5.21)$$

$$\beta_2(z)=\frac{1}{k_{\|}^2\theta_1\lambda_e^2}\frac{1}{f_2}\frac{\partial f_2}{\partial z}.$$

Here r_{01} and r_{02} represents the current sheet size of whistler wave in x and y direction, respectively; $\beta_1(z)$ and $\beta_2(z)$ represents the slowly varying function, and f_1, f_2 represents the beam width parameter of the whistler wave. Now, for obtaining the beam-width parameters, use Eq. (5.20) in Eq. (5.18) with paraxial approximation i.e., $x<<r_{01}^2 f_1$, $y<<r_{02}^2 f_2$ and then equating coefficients of x^2 and y^2, we obtained the following Eq.

$$\frac{\partial^2 f_1}{\partial \xi^2} = R_d^2 k_{\|}^2 \left(\frac{4\theta_1^2 \lambda_e^4}{r_{01}^4 f_1^4 f_2} + \frac{\theta_1 \theta_3 f_1}{2} - \frac{2\theta_1 \theta_4 \lambda_e^2 \left(\alpha A_{00}^{'2}\right)}{r_{01}^2 f_1^3 f_2} \right). \tag{5.22}$$

And, $$\frac{\partial^2 f_2}{\partial \xi^2} = R_d^2 k_{\|}^2 \left(\frac{4\theta_1^2 \lambda_e^4}{r_{02}^4 f_2^4 f_1} + \frac{\theta_1 \theta_3 k^2 \lambda_e^2 f_2}{2} - \frac{\theta_1 \theta_4 \lambda_e^2 \left(\alpha A_{00}^{'2}\right)}{r_{02}^2 f_2^3 f_1} \right), \tag{5.23}$$

where $\xi = z / R_d$ and $\mathrm{R}_d = k_{0z} r_{01}^2$. Eqs. (5.22) & (5.23) are solved for the plain wavefront imposing following initial conditions- $\frac{\partial^2 f_1}{\partial \xi^2} = \frac{\partial^2 f_2}{\partial \xi^2} = 0, f_1 = f_2 = 1$ at z=0. When the power of whistler wave $\left(\alpha A_{00}^{'2}\right)$ is zero, then the transverse scale size of localized structures along the x-axis and y-axis are obtained as $r_{01} = 7.5\lambda_e$, $r_{02} = 5.2\lambda_e$, respectively. Further, when we take the finite value of power $\left(\alpha A_{00}^{'2} = 1\right)$, then the transverse scale size of localized structures along the x-axis and y-axis are obtained as, $r_{01} = 0.8\lambda_e$, $r_{02} = 0.63\lambda_e$, respectively. Also, by using Ampere's law $\left(J = -\nabla^2 A_{00}^{'}\right)$, we have studied the current sheet size. One can calculate the transverse scale size of the current sheet comes out to be of the order of $r_{01}/\sqrt{3}$ and $r_{02}/\sqrt{3}$ along the x-axis and y-axis, respectively. Therefore, when power is finite then transverse scale size of current sheet is $0.46\lambda_e$, and $0.346\lambda_e$ along the x-axis and y-axis, respectively. When power is zero then transverse scale size of current sheet is $4.33\lambda_e$, and $3\lambda_e$ along the x-axis and y-axis, respectively. As a result, it shows how the whistler power also influences the scale size of coherent structures and current sheet dimension. Recently, the scale size of super thin electron-scale current sheet in the Earth's magnetotail has been reported [60]. Also, Bruch et al. [61] reported the scale size of whistler's localized structures of the order of $(10-20)\lambda_e$ at the magnetic reconnection sites in the magnetopause.

5.5 Summary and Conclusion

This paper investigates the coherent structures, and current sheet of beam-driven whistler wave in Magnetopause in the presence of magnetic islands. The dynamics of the beam-driven whistler-mode has been established under the presumption that it would rise from the noise level caused by the beam energy to a large amplitude, where nonlinear effects caused by nonlinear ponderomotive force would lead to the localization of the whistler wave and, ultimately, the turbulent state. The nonlinear interaction between high-frequency whistler wave and low-frequency magnetosonic wave have been taken into consideration. The dynamical equation for the system is developed using the two-fluid model. The pseudo-spectral approach is utilized for

spatial integration and the finite difference method is used for temporal integration in order to solve the model problem. The results of the numerical simulations show that nonlinear whistler waves propagating in magnetic islands get localized, and current sheets with transverse scale sizes on the order of electron inertial length are evolved. We have also studied the power spectra which is utilized to study the formation of thermal tail of energetic electrons. The outcomes of the numerical simulation are concluded below.

1) The findings of the simulation show that the whistler wave localizes from noise level to significant amplitude. Chaotic and localized structures in Figure 5.1 are an indication of coherent structures. These magnetic field localizations provide a pathway for energy to cascade from large to small-scale spatial sizes.
2) To identify magnetic islands produced by reconnection, contour plots of vector potential or sketches of magnetic field lines might be used. Single O-point emerges into multiple O-points associated with X-points in this way X-O structures are formed with increasing amplitude. Emergence of new field associated with these X-O structures is seen. In order to comprehend the expansion of magnetic flux, which is associated with current density function by Ampere's law, it is also necessary to look at the spatial development of current density function. The necessary X-O structures begin to deform over time, and eventually, a chaotic pattern is reached. We observed that in our simulation, current sheets likewise grow into turbulent state.
3) Separatix plays a crucial part in magnetic reconnection by drawing a line dividing areas of magnetic field lines with varied connectivity. It serves as a location for the breaking and reconnection of magnetic field lines, which causes the release of magnetic energy that has been trapped. Regarding the mechanics and energetics of the reconnection process, the separatix's characteristics are a useful source of knowledge.
4) The observed spectral power indices show a scaling nearly -5/3 in inertial range [agrees with Biskamp et al. [55] observations] and at smaller scales, we observe steeper spectra of the scaling of nearly -7/3. This power spectra illustrate the signature of turbulence. The charged particles can be accelerated by this energy.
5) Energy transfer is facilitated by the formation of turbulence through interactions with whistler-localized structures with plasma particles. We hypothesize that the particle acceleration and plasma heating at the magnetopause might be caused by these interactions enhancing the thermal tail of energetic electrons.

6) We concluded that whistler wave power exerts an effect on the scale size of coherent structures as well as the dimension of the current sheet. We have also determined the current sheet size and the transverse scale size of whistler's localized structures using the semianalytical model. When the power of whistler wave is finite, then scale size of current sheet is of the order of $4.3\lambda_e$ and $3\lambda_e$ along x-axis and along y-axis, respectively. Furthermore, when the power of whistler wave is zero, then scale size of current sheet is of the order of $7.5\lambda_e$ and $5.2\lambda_e$ along the x-axis and along y-axis, respectively. It means that transverse scale of localized structures in the presence of pre-existing magnetic islands is modified by the power of whistler wave. The physics behind this association may be further explored in further studies.

Although, spectra in quasi steady state are nearly of the order of -5/3 in inertial range [which is in agreement of Biskamp et al. [55]] and then at shorter wavelength we obtain steeper spectra of the scaling factor nearly of the order of -7/3 but development of turbulent state is the unique point of this study in which we studied the current sheet formation & this current sheet emerges into turbulent state. A detailed analysis of all different possibilities that are encountered in the beam-driven turbulence generation, Plasmoid formation, and heating and acceleration of plasma particles is beyond the scope of this paper and will be left to future work.

References

[1] Ergun R E, Pathak N, Usanova M E, Qi Y, Vo T, Burch J L, Schwartz S J, Torbert R B, Ahmadi N, Wilder F D, Chasipis A, Newman D L, Stawarz J E, Hesse M, Turner D L and Gershman D 2022 Observation of Magnetic Reconnection in a Region of Strong Turbulence *Astrophys J Lett* **935**

[2] Carbone V, Veltri P and Mangeney A 1990 Coherent structure formation and magnetic field line reconnection in magnetohydrodynamic turbulence *Physics of Fluids A* **2**

[3] Ergun R E, Ahmadi N, Kromyda L, Schwartz S J, Chasapis A, Hoilijoki S, Wilder F D, Stawarz J E, Goodrich K A, Turner D L, Cohen I J, Bingham S T, Holmes J C, Nakamura R, Pucci F, Torbert R B, Burch J L, Lindqvist P-A, Strangeway R J, Le Contel O and Giles B L 2020 Observations of Particle Acceleration in Magnetic Reconnection–driven Turbulence *Astrophys J* **898**

[4] Karimabadi H and Lazarian A 2013 Magnetic reconnection in the presence of externally driven and self-generated turbulence *Phys Plasmas* **20** 1–17

[5] Lazarian A, Eyink G L and Vishniac E T 2012 Relation of astrophysical turbulence and magnetic reconnectiona *Phys Plasmas* **19**

[6] Ruszkowski M and Oh S P 2011 Galaxy motions, turbulence and conduction in clusters of galaxies *Mon. Not. R. Astron. Soc.* **414**

[7] Santos-Lima R, De Gouveia Dal Pino E M and Lazarian A 2012 The role of turbulent magnetic reconnection in the formation of rotationally supported protostellar disks *Astrophysical Journal* **747,** 21.

[8] Ferrière K 2020 Plasma turbulence in the interstellar medium *Plasma Phys. Control Fusion* **62,** 0140014.

[9] Falceta-Gonçalves D, Kowal G, Falgarone E and Chian A C L 2014 Turbulence in the interstellar medium *Nonlinear Process Geophys.* **21,** 587-604.

[10] Cranmer S R, Asgari-Targhi M, Miralles M P, Raymond J C, Strachan L, Tian H and Woolsey L N 2015 The role of turbulence in coronal heating and solar wind expansion *Philosophical Transactions of the Royal Society A: Mathematical, Physical and Engineering Sciences* **373,** 20140148.

[11] Kaminker V, Delamere P A, Ng C S, Dennis T, Otto A and Ma X 2017 Local time dependence of turbulent magnetic fields in Saturn's magnetodisc *J. Geophys. Res. Space Phys.* **122,** 3972-3984.

[12] Saur J, Politano H, Pouquet A and Matthaeus W H 2002 Evidence for weak MHD turbulence in the middle magnetosphere of Jupiter *Astron. Astrophys.* **386(2),** 699-708.

[13] Wang Jing, Yu Jiang, Ren Aojun, Chen Zuzheng, Xu Xiaojun, Cui Jun and Cao Jinbin 2023 In Situ Observations of Whistler-mode Waves in Magnetic Reconnection at Mars *Astrophys. J.* **944** 1–9

[14] Chen C H K, Bale S D, Bonnell J W, Borovikov D, Bowen T A, Burgess D, Case A W, Chandran B D G, de Wit T D, Goetz K, Harvey P R, Kasper J C, Klein K G, Korreck K E, Larson D, Livi R, MacDowall R J, Malaspina D M, Mallet A, McManus M D, Moncuquet M, Pulupa M, Stevens M L and Whittlesey P 2020 The Evolution and Role of Solar Wind Turbulence in the Inner Heliosphere The Astrophysical Journal Supplement Series, 246(2), 53.

[15] Marsch E 2018 Solar wind and kinetic heliophysics *Annales Geophysicae* **36,** 1607-1630.

[16] White T G, Oliver M T, Mabey P, Kühn-Kauffeldt M, Bott A F A, Döhl L N K, Bell A R, Bingham R, Clarke R, Foster J, Giacinti G, Graham P, Heathcote R, Koenig M, Kuramitsu Y, Lamb D Q, Meinecke J, Michel T, Miniati F, Notley M, Reville B, Ryu D, Sarkar S, Sakawa Y, Selwood M P, Squire J, Scott R H H, Tzeferacos P, Woolsey N, Schekochihin A A and Gregori G 2019 Supersonic plasma turbulence in the laboratory *Nature Communications* **10(1),** 1758.

[17] Brown M R and Schaffner D A 2014 Laboratory sources of turbulent plasma: A unique MHD plasma wind tunnel *Plasma Sources Science and Technology* **23(6),** 063001.

[18] Burch J and Drake J 2009 Reconnecting Magnetic Fields: The huge amounts of energy released from the relinking of magnetic fields in outer space are both mysterious and potentially destructive *American Scientist* **97,** 392-399.

[19] Nagai T, Shinohara I, Fujimoto M, Matsuoka A, Saito Y and Mukai T 2011 Construction of magnetic reconnection in the near-Earth magnetotail with Geotail *J. Geophys. Res. Space Phys.* **116, A4**

[20] Vaivads A, Khotyaintsev Y, André M, Retinò A, Buchert S C, Rogers B N, Décréau P, Paschmann G and Phan T D 2004 Structure of the magnetic reconnection diffusion region from four-spacecraft observations *Phys. Rev. Lett.* **93,** 105001.

[21] Goldstein M L, Escoubet P, Hwang K J, Wendel D E, Viñas A F, Fung S F, Perri S, Servidio S, Pickett J S, Parks G K, Sahraoui F, Gurgiolo C, Matthaeus W and Weygand J M 2015 Multipoint observations of plasma phenomena made in space by Cluster *J Plasma Phys.* **81,** 325810301.

[22] Mozer F S, Bale S D and Phan T D 2002 Evidence of Diffusion Regions at a Subsolar Magnetopause Crossing *Phys. Rev. Lett.* **89,** 015002.

[23] Øieroset M, Phan T D, Fujimoto M, Lin R P and Lepping R P 2001 In situ detection of collisionless reconnection in the Earth's magnetotail *Nature* **412,** 414-417.

[24] Paschmann G, Sonnerup B U Ö, Papamastorakis I, Sckopke N, Haerendel G, Bame S J, Asbridge J R, Gosling J T, Russell C T and Elphic R C 1979 Plasma acceleration at the Earth's magnetopause: Evidence for reconnection *Nature* **282,** 243-246.

[25] Karimabadi H, Roytershteyn V, Daughton W and Liu Y-H 2013 Recent Evolution in the Theory of Magnetic Reconnection and Its Connection with Turbulence *Microphysics of Cosmic Plasmas*, 231-247.

[26] Adhikari S, Parashar T N, Shay M A, Matthaeus W H, Pyakurel P S, Fordin S, Stawarz J E and Eastwood J P 2021 Energy transfer in reconnection and turbulence *Phys. Rev. E* **104,** 065206.

[27] Cargill P J, Vlahos L, Baumann G, Drake J F and Nordlund Å 2012 Current fragmentation and particle acceleration in solar flares *Space Sci. Rev.* **173,** 223-245.

[28] Lazarian A, Vlahos L, Kowal G, Yan H, Beresnyak A and De Gouveia Dal Pino E M 2012 Turbulence, magnetic reconnection in turbulent fluids and energetic particle acceleration *Space Sci. Rev.* **173,** 557-622.

[29] Karimabadi H, Roytershteyn V, Vu H X, Omelchenko Y A, Scudder J, Daughton W, Dimmock A, Nykyri K, Wan M, Sibeck D, Tatineni M, Majumdar A, Loring B and Geveci B 2014 The link between shocks, turbulence, and magnetic reconnection in collisionless plasmas *Phys. Plasmas* **21(6).**

[30] Matthaeus W H 2021 Turbulence in space plasmas: Who needs it? *Phys. Plasmas* **28(3).**

[31] Graham D B, Vaivads A, Khotyaintsev Y V., André M, Le Contel O, Malaspina D M, Lindqvist P A, Wilder F D, Ergun R E, Gershman D J, Giles B L, Magnes W, Russell C T, Burch J L and Torbert R B 2018 Large-Amplitude High-Frequency Waves at Earth's Magnetopause *J. Geophys. Res. Space Phys.* **123,** 2630-2657.

[32] Cao J B, Wei X H, Duan A Y, Fu H S, Zhang T L, Reme H and Dandouras I 2013 Slow magnetosonic waves detected in reconnection diffusion region in the Earth's magnetotail *J. Geophys. Res. Space Phys.* **118,** 1659-66.

[33] Chaston C, Bonnell J, McFadden J P, Carlson C W, Cully C, Le Contel O, Roux A, Auster H U, Glassmeier K H, Angelopoulos V and Russell C T 2008 Turbulent heating and cross-field transport near the magnetopause from THEMIS *Geophys. Res. Lett.* **35** 2–6

[34] Liu C M, Vaivads A, Graham D B, Khotyaintsev Y V., Fu H S, Johlander A, André M and Giles B L 2019 Ion-Beam-Driven Intense Electrostatic Solitary Waves in Reconnection Jet *Geophys. Res. Lett.* **46,** 12702-12710.

[35] Matsumoto H, Deng X H, Kojima H and Anderson R R 2003 Observation of electrostatic solitary waves associated with reconnection on the dayside magnetopause boundary *Geophys. Res. Lett.* **30(6).**

[36] Wei X H, Cao J B, Zhou G C, Santolík O, Rème H, Dandouras I, Cornilleau-Wehrlin N, Lucek E, Carr C M and Fazakerley A 2007 Cluster observations of waves in the whistler frequency range associated with magnetic reconnection in the Earth's magnetotail *J. Geophys. Res. Space Phys.* **112,** A10.

[37] Deng X H and Matsumoto H 2001 Rapid magnetic reconnection in the earth's magnetosphere mediated by whistler waves *Nature* **410,** 557-560.

[38] Wilder F D, Ergun R E, Goodrich K A, Goldman M V., Newman D L, Malaspina D M, Jaynes A N, Schwartz S J, Trattner K J, Burch J L, Argall M R, Torbert R B, Lindqvist P A, Marklund G, Le Contel O, Mirioni L, Khotyaintsev Y V., Strangeway R J, Russell C T, Pollock C J, Giles B L, Plaschke F, Magnes W, Eriksson S, Stawarz J E, Sturner A P and Holmes J C 2016 Observations of whistler mode waves with nonlinear parallel electric fields near the dayside magnetic reconnection separatrix by the Magnetospheric Multiscale mission *Geophys. Res. Lett.* **43,** 5909-5917.

[39] Cao D, Fu H S, Cao J B, Wang T Y, Graham D B, Chen Z Z, Peng F Z, Huang S Y, Khotyaintsev Y V., André M, Russell C T, Giles B L, Lindqvist P A, Torbert R B, Ergun R E, Le Contel O and Burch J L 2017 MMS observations of whistler waves in electron diffusion region *Geophys. Res. Lett.* **44** 3954–62.

[40] Yu X, Lu Q, Wang R, Gao X, Sang L and Wang S 2021 Simultaneous Observation of Whistler Waves and Electron Cyclotron Harmonic Waves in the Separatrix Region of Magnetopause Reconnection *J. Geophys. Res. Space Phys.* **126(10),** e2021JA029609.

[41] Huang S Y, Yuan Z G, Fu H S, Vaivads A, Sahraoui F, Khotyaintsev Y V., Retino A, Zhou M, Graham D, Fujimoto K, Deng X H, Ni B B, Pang Y, Fu S and Wang D D 2018 Observations of Whistler Waves in the Magnetic Reconnection Diffusion Region *2018 2nd URSI Atlantic Radio Science Meeting, AT-RASC 2018, IEEE, 1-4.*

[42] Tang X, Cattell C, Dombeck J, Dai L, Wilson L B, Breneman A and Hupach A 2013 THEMIS observations of the magnetopause electron diffusion region: Large amplitude waves and heated electrons *Geophys. Res. Lett.* **40,** 2884-2890.

[43] Cattell C, Wygant J R, Goetz K, Kersten K, Kellogg P J, Rosenvinge T Von, Bale S D, Roth I, Temerin M, Hudson M K, Mewaldt R A, Wiedenbeck M, Maksimovic M, Ergun R, Acuna M and Russell C T 2008 Discovery of very large amplitude whistler-mode waves in Earth' s radiation belts Geophysical Research Letters **35** 1–7

[44] Zhou M, Loureiro N F and Uzdensky D A 2020 Multi-scale dynamics of magnetic flux tubes and inverse magnetic energy transfer *J. Plasma Phys* **86,** 4.

[45] Lazarian A, Eyink G L, Jafari A, Kowal G, Li H, Xu S and Vishniac E T 2020 3D turbulent reconnection: Theory, tests, and astrophysical implications *Phys. Plasmas* **27,** 1.

[46] Vlahos L and Isliker H 2023 Formation and Evolution of Coherent Structures in 3D Strongly Turbulent Magnetized Plasmas *Phys. Plasmas* **30,** 4.

[47] Phan T D, Eastwood J P, Shay M A, Drake J F, Sonnerup B U Ö, Fujimoto M, Cassak P A, Øieroset M, Burch J L, Torbert R B, Rager A C, Dorelli J C, Gershman D J, Pollock C, Pyakurel P S, Haggerty C C, Khotyaintsev Y, Lavraud B, Saito Y, Oka M, Ergun R E, Retino A, Le Contel O, Argall M R, Giles B L, Moore T E, Wilder F D, Strangeway R J, Russell C T, Lindqvist P A and Magnes W 2019 Publisher Correction: Electron magnetic reconnection without ion coupling in Earth's turbulent magnetosheath (Nature, (2018), 7704, (202-206).

[48] Stawarz J E, Eastwood J P, Phan T D, Gingell I L, Pyakurel P S, Shay M A, Robertson S L, Russell C T and Le Contel O 2022 Turbulence-driven magnetic reconnection and the magnetic correlation length: Observations from Magnetospheric Multiscale in Earth's magnetosheath *Phys. Plasmas* **29,** 1.

[49] Bhat P and Loureiro N F 2018 Plasmoid instability in the semi-collisional regime *J. Plasma Phys.* **84,** 6.

[50] Zhao S Q, Xiao C J, Liu T Z, Chen H, Zhang H, Shi M J, Teng S, Zhang H S, Wang X G, Pu Z Y and Liu M Z 2021 Observations of the Beam-Driven Whistler Mode Waves in the Magnetic Reconnection Region at the Dayside Magnetopause *J. Geophys. Res. Space Phys.* **126,** 1–11.

[51] Fitzpatrick R and Waelbroeck F L 2005 Two-fluid magnetic island dynamics in slab geometry. II. Islands interacting with resistive walls or resonant magnetic perturbations *Phys. Plasmas* **12,** 0406133.

[52] Jyoti, Sharma S C and Sharma R P 2023 Localization and turbulence of beam-driven whistler wave with magnetosonic wave in magnetopause *Phys Plasmas* **30,** 2.

[53] Gazdag J 1976 Time-differencing schemes and transform methods *J. Comput. Phys.* **20** 196–207

[54] Biskamp D and Welter H 1989 Dynamics of decaying two-dimensional magnetohydrodynamic turbulence *Physics of Fluids B* **1,** 1964-1979.

[55] Biskamp D, Schwarz E and Drake J F 1996 Two-dimensional electron magnetohydrodynamic turbulence *Phys. Rev. Lett.* **76,** 1264.

[56] S. Ichimaru. 1975 Basic Principles of Plasma Physics: a Statistical Approach. By S. Ichimaru. Benjamin Frontiers in Physics, 1973. 324 pp. $19.50 (hardcover), $12.50 (paperback). *J. Plasma Phys* **13,** 571-572.

[57] Colunga M, Luciani J F and Mora P 1986 Electron acceleration in localized plasma waves *Physics of Fluids* **29,** 3407-14.

[58] Fuchs V, Krapchev V, Ram A and Bers A 1985 Diffusion of electrons by coherent wavepackets *Physica D* **14,** 141-160.

[59] Bian N H and Browning P K 2008 Particle Acceleration in a Model of a Turbulent Reconnecting Plasma: A Fractional Diffusion Approach *Astrophysics J.* **687,** L111.

[60] Leonenko M v., Grigorenko E E and Zelenyi L M 2021 Spatial Scales of Super Thin Current Sheets with MMS Observations in the Earth's Magnetotail *Geomagnetism and Aeronomy* **61,** 688-695.

[61] Burch J L, Ergun R E, Cassak P A, Webster J M, Torbert R B, Giles B L, Dorelli J C, Rager A C, Hwang K J, Phan T D, Genestreti K J, Allen R C, Chen L J, Wang S, Gershman D, le Contel O,

Russell C T, Strangeway R J, Wilder F D, Graham D B, Hesse M, Drake J F, Swisdak M, Price L M, Shay M A, Lindqvist P A, Pollock C J, Denton R E and Newman D L 2018 Localized Oscillatory Energy Conversion in Magnetopause Reconnection, *Geophys. Res. Lett.* **45,** 1237-1245.

CHAPTER-6

Non-linear propagation of Whistler-mode in the presence of Magnetic Islands in the Magnetopause

6.1 Introduction

Magnetopause is a perfect in-situ laboratory for examining non-linear and turbulent processes in a magnetized plasma fluid due to its wide range of spatial and temporal length scales coupled to a mixture of waves, fluctuations, structures, and non-linear turbulent interactions. Various spacecraft observations found that reconnection occurs associated with the turbulence in the Earth's magnetosheath [1]–[3]. Because of the magnetopause's important role in magnetic reconnection and the resulting transfer of plasma and energy into the magnetosphere it has been the focus of many studies [4]–[6], and missions like Magnetospheric Multiscale Mission (MMS), Cluster, and THEMIS, which have delved deeper into the current sheet structure and its formation. It has been proposed that wave-particle interactions in high energy circumstances, which cause the dissipation, are caused by plasma turbulence. Numerous phenomena and processes, including particle energization, magnetic field dynamics, and the transfer of mass and energy across the boundary, are significantly affected by the existence of plasma turbulence in the magnetopause. Recent discoveries of thin (electron scale) layers [7], [8] at the magnetopause have gained new insights into magnetopause physics and have increased the hope of using the multi-satellite mission Cluster to solve the mystery of reconnection [9], [10].

Magnetic reconnection is a ubiquitous phenomenon happening in space, and laboratory plasmas and studied in various space regions like solar wind [11], magnetosphere [12]–[17] etc. The creation of solar flares, coronal mass ejections, and the interaction of solar winds with the Earth's magnetosphere are all examples of magnetic reconnection [18]–[21] and it is thought to have originated during the star-forming process. The astonishing potential of astrophysical plasmas to establish magnetic structure leads to the accumulation of magnetic energy inside stressed areas, including current sheets. This stored energy is frequently released explosively during the magnetic reconnection process, which causes a reconfiguration of the magnetic field as well as high-speed flows, thermal heating, and nonthermal particle acceleration [22]–[24].

It is extensively understood that turbulence, which frequently occurs in space plasma, plays a vital role in the dissipation and heating of the particles as it cascades energy from large to small scales. There is growing evidence that magnetic reconnection and turbulence are strongly connected in magnetized plasmas [25]–[28]. Numerous investigators have studied how turbulence influences the flow of reconnection, especially how existing turbulence may impact Sweet-Parker reconnection and how turbulence may develop because of reconnection [29]. Using numerical simulations and theoretical considerations, electron-only magnetic reconnection has been investigated [30]–[33]. Numerous studies cover several aspects concerning how turbulence can host reconnecting current sheets and how reconnecting current sheets can trigger turbulence [26], [34], [35]. The emergence of irregular variations in the magnetic field is an additional aspect of turbulence in magnetized plasmas that is ubiquitous [36], [37]. For many years, researchers have examined the turbulence spectrum of magnetic field fluctuations at enormous inertial magnetohydrodynamic scales. Whistler cascade, which moves energy from large magnetohydrodynamic scales to smaller ones, is governed by the Kolmogorov power law [38], [39]. Also, it is observed that magnetic spectrum scaling exhibits Kolmogorov scaling of -5/3 in reconnection as well as in turbulence which provides evidence that reconnection dynamics involves energy transfer analogous to standard turbulence [40].

One of the main aims of this study is to investigate the role of electron-scale current sheets in particle energization and to analyze the scope of which particle energy conversion may be related to magnetic reconnection. To achieve this, we examine the whistler at magnetic reconnection sites caused by an energetic electron beam (as observed by Magnetospheric Multiscale Mission (MMS)) in the presence of magnetic islands and nonlinearity associated with waves. For this, we develop a model of beam-driven whistler wave originating from the noise caused by the energy of beam and rising to a large amplitude, where nonlinear effects from ponderomotive force drive the nonlinear whistler wave. In this model, the nonlinear dynamics of 3D whistler wave with magnetosonic wave have been solved in the presence of nonlinearity as well as the ponderomotive force and we introduce the constant growth rate of beam driven whistler wave. The results of numerical simulations carried out using theoretical modeling provide a glimpse of the evolution of magnetic field lines in the form of contour plots and current sheets formation. Also, we have studied the power spectrum for the quasi-steady state.

The article is set up as follows: - In section 2, the model equations for whistler and magnetosonic waves are developed. The numerical methodologies, approaches, and circumstances that we employed for the numerical simulation work, as well as the outcomes of the numerical simulation,

were covered in section 3 of the article. In section 4, we discussed a semianalytical model to analyze the scale size of current sheets. Section 5 covers the article's summary and conclusion in detail.

6.2 Analytical model

6.2.1 Whistler dynamics in the presence of beam

The dynamical equation for a 3D whistler wave with an ambient magnetic field along the z-axis in a magnetized plasma propagating in the x, y, and z-axis with a wave vector $\vec{k} = k_x\hat{x} + k_y\hat{y} + k_z\hat{z}$, is derived utilizing two-fluid models. The governing dynamical equation of 3D whistler wave in terms of vector potential can be written as (the detailed derivation has been given as Appendix-A)

$$\begin{aligned}&\frac{\partial^2 A_z}{\partial t^2} + \frac{\partial^6 A_z}{\partial t^2 \partial x^2}\lambda_e^4 + \frac{\partial^6 A_z}{\partial t^2 \partial y^2}\lambda_e^4 + \frac{\partial^6 A_z}{\partial t^2 \partial z^2}\lambda_e^4 + 2\lambda_e^4 \frac{\partial^4 A_z}{\partial t^2 \partial z^2}\left(\frac{\partial^2}{\partial x^2} + \frac{\partial}{\partial y^2}\right) - \\ &2\lambda_e^2\left(\frac{\partial^2}{\partial x^2} + \frac{\partial^2}{\partial y^2} + \frac{\partial^2}{\partial z^2}\right)\frac{\partial^2 A_z}{\partial t^2} + \lambda_i^2 v_A^2\left(\frac{\partial^2}{\partial x^2} + \frac{\partial^2}{\partial y^2}\right)\frac{\partial^2 A_z}{\partial z^2} + \\ &\lambda_i^2 v_A^2 \frac{\partial^4 A_z}{\partial z^4} + \frac{\lambda_i^2 v_A^2 B_{0y}^2}{B_{0z}^2}\left(\frac{\partial^2}{\partial x^2} + \frac{\partial^2}{\partial y^2}\right)\frac{\partial^2 A_z}{\partial y^2} + \frac{\lambda_i^2 v_A^2 B_{0y}^2}{B_{0z}^2}\frac{\partial^4 A_z}{\partial y^2 \partial z^2} + \\ &\frac{2\lambda_i^2 v_A^2 B_{0y}}{B_{0z}}\left(\frac{\partial^2}{\partial x^2} + \frac{\partial^2}{\partial y^2}\right)\frac{\partial^2 A_z}{\partial y \partial z} + \frac{2\lambda_i^2 v_A^2 B_{0y}}{B_{0z}}\frac{\partial^4 A_z}{\partial y \partial z^3} = 0,\end{aligned} \tag{6.1}$$

where $\omega_{ce}\left(=\frac{eB_0}{m_e c}\right)$ is the electron gyrofrequency of the wave, $v_A\left(=\sqrt{\frac{B_0^2}{4\pi n_0 m_i}}\right)$ is Alfven wave's speed, n_0 denotes the background number density, c denotes the velocity of light, and $\lambda_i\left(=\sqrt{\frac{c^2 m_i}{4\pi n_0 e^2}}\right)$ is the collisionless ion skin depth, $\lambda_e\left(=\sqrt{\frac{c^2 m_e}{4\pi n_0 e^2}}\right)$ the collisionless electron skin depth. Additionally, it is reported that beam-driven growth rate is considered then, the aforementioned equation becomes $\frac{d}{dt} \to \left(\frac{d}{dt} + \gamma\right)$ (please see appendix),

$$\begin{aligned}&\left(\frac{\partial^2}{\partial t^2} + 2\gamma\frac{\partial}{\partial t}\right)A_z + \frac{\partial^6 A_z}{\partial t^2 \partial x^2}\lambda_e^4 + \frac{\partial^6 A_z}{\partial t^2 \partial y^2}\lambda_e^4 + \frac{\partial^6 A_z}{\partial t^2 \partial z^2}\lambda_e^4 + 2\lambda_e^4 \frac{\partial^4 A_z}{\partial t^2 \partial z^2}\left(\frac{\partial^2}{\partial x^2} + \frac{\partial^2}{\partial y^2}\right) - \\ &2\lambda_e^2\left(\frac{\partial^2}{\partial x^2} + \frac{\partial^2}{\partial y^2} + \frac{\partial^2}{\partial z^2}\right)\frac{\partial^2 A_z}{\partial t^2} + \lambda_i^2 v_A^2\left(\frac{\partial^2}{\partial x^2} + \frac{\partial^2}{\partial y^2}\right)\frac{\partial^2 A_z}{\partial z^2} + \lambda_i^2 v_A^2 \frac{\partial^4 A_z}{\partial z^4} + \\ &\frac{\lambda_i^2 v_A^2 B_{0y}^2}{B_{0z}^2}\left(\frac{\partial^2}{\partial x^2} + \frac{\partial^2}{\partial y^2}\right)\frac{\partial^2 A_z}{\partial y^2} + \frac{\lambda_i^2 v_A^2 B_{0y}^2}{B_{0z}^2}\frac{\partial^4 A_z}{\partial y^2 \partial z^2} + \\ &\frac{2\lambda_i^2 v_A^2 B_{0y}}{B_{0z}}\left(\frac{\partial^2}{\partial x^2} + \frac{\partial^2}{\partial y^2}\right)\frac{\partial^2 A_z}{\partial y \partial z} + \frac{2\lambda_i^2 v_A^2 B_{0y}}{B_{0z}}\frac{\partial^4 A_z}{\partial y \partial z^3} = 0.\end{aligned} \tag{6.2}$$

For this Eq. (6.2), the following envelope solution is assumed.

$$\tilde{A}_z = A_z(x,y,z,t)e^{i(k_{0x}\hat{x}+k_{0y}\hat{y}+k_{0z}\hat{z}-\omega_0 t)}. \tag{6.3}$$

The dynamical equation governing the nonlinear whistler wave traveling through plasma has been formulated by taking into consideration the influence of a whistler wave on the background density and substituting the solution into Eq. (6.2).

$$\begin{aligned}
&2i\omega_0(1+\lambda_e^4k_0^4+2\lambda_e^2k_0^2+2\lambda_e^4k_{0x}^2k_{0z}^2+2\lambda_e^4k_{0y}^2k_{0z}^2)\frac{\partial A_z}{\partial t}+(4\omega_0^2\lambda_e^4k_{0x}^2)\frac{\partial^2 A_z}{\partial x^2}+\\
&(4\omega_0^2\lambda_e^4k_{0y}^2)\frac{\partial^2 A_z}{\partial y^2}+(4\omega_0^2\lambda_e^4k_{0z}^2-4\lambda_i^2v_A^2k_{0z}^2)\frac{\partial^2 A_z}{\partial z^2}+\\
&2ik_{0x}(2\omega_0^2k_{0x}^2\lambda_e^4+2\omega_0^2k_{0z}^2\lambda_e^4+2\omega_0^2\lambda_e^2+k_{0z}^2\lambda_i^2v_A^2)\frac{\partial A_z}{\partial x}+\\
&2ik_{0y}(2\omega_0^2k_{0y}^2\lambda_e^4+2\omega_0^2k_{0z}^2\lambda_e^4+2\omega_0^2\lambda_e^2-k_{0z}^2\lambda_i^2v_A^2)\frac{\partial A_z}{\partial y}+\\
&2ik_{0z}(2\omega_0^2k_{0z}^2\lambda_e^4+2\omega_0^2k_{0x}^2\lambda_e^4+2\omega_0^2k_{0y}^2\lambda_e^4+2\omega_0^2\lambda_e^2-k_{0y}^2\lambda_i^2v_A^2-2k_{0z}^2\lambda_i^2v_A^2)\frac{\partial A_z}{\partial z}+\\
&(4\lambda_i^2v_A^2k_{0x}k_{0z}-8\omega_0^2\lambda_e^4k_{0z}k_{0x})\frac{\partial^2 A_z}{\partial x\partial z}+(4\lambda_i^2v_A^2-8\omega_0^2\lambda_e^4)k_{0y}k_{0z}\frac{\partial^2 A_z}{\partial y\partial z}+\\
&\frac{\lambda_i^2v_A^2B_{0y}^2}{B_{0z}^2}k^2k_{0y}^2A_z+\frac{2\lambda_i^2v_A^2B_{0y}}{B_{0z}}k^2k_{0y}k_{0z}A_z-(\lambda_i^2v_A^2k^2k_{0z}^2)\frac{\delta n}{n_0}A_z+2i\gamma' A_z=0,
\end{aligned} \tag{6.4}$$

where k_{0x}, k_{0y} and k_{0z} are wave vector components of whistler related to the background magnetic field are given as, $k_0^2=k_{0x}^2+k_{0y}^2+k_{0z}^2$. Here n' denotes the modified density, i.e., $n'=n_0+\delta n$, and $\frac{\delta n}{n_0}$ denotes the perturbation in plasma density due to non-linear whistler wave. We have used the relation of the magnetic field and vector potential $\left(\frac{B_{0y}}{B_{0z}}=\frac{\delta A_z}{A_0}\right)$.

Eq. (6.4) in normalized dimensionless form is given as

$$\begin{aligned}
&ic_1\frac{\partial A_z}{\partial t}+c_2\frac{\partial^2 A_z}{\partial x^2}+c_3\frac{\partial^2 A_z}{\partial y^2}+c_4\frac{\partial^2 A_z}{\partial z^2}+ic_5\frac{\partial A_z}{\partial x}+ic_6\frac{\partial A_z}{\partial y}+ic_7\frac{\partial A_z}{\partial z}+\\
&c_8\frac{\partial^2 A_z}{\partial x\partial z}+c_9\frac{\partial^2 A_z}{\partial y\partial z}+c_{10}\left(\frac{\delta A_z}{A_0}\right)^2A_z+c_{11}\left(\frac{\delta A_z}{A_0}\right)A_z-\frac{\delta n}{n_0}A_z+2i\gamma' A_z=0,
\end{aligned} \tag{6.5}$$

where Eq. (6.5) represents the whistler wave's normalized dynamical equation, which causes turbulence. In this section, the beam instability that generates the whistler wave will be described. The growth rate of whistler wave generated by an energetic electron beam, which is included phenomenologically, and its value corresponding with the data published by (Zhao et al., 2021 [41]) will be utilized in simulations here. To get the dynamical equation, we introduce

the field perturbation due to magnetic islands profile, since the magnetic reconnection is visualized within the framework of magnetic island as mentioned by Fitzpatrick & Waelbroeck, 2005 [42],

$$\frac{\delta A_z}{A_0}=\left(-\frac{x^2}{2}+\left|A_z\right|\cos(ky)\right). \tag{6.6}$$

So, using the profile of field perturbation Eq. (6.5) modifies as-

$$ic_1\frac{\partial A_z}{\partial t}+c_2\frac{\partial^2 A_z}{\partial x^2}+c_3\frac{\partial^2 A_z}{\partial y^2}+c_4\frac{\partial^2 A_z}{\partial z^2}+ic_5\frac{\partial A_z}{\partial x}+ic_6\frac{\partial A_z}{\partial y}+ic_7\frac{\partial A_z}{\partial z}+c_8\frac{\partial^2 A_z}{\partial x\partial z}+$$
$$c_9\frac{\partial^2 A_z}{\partial y\partial z}+c_{10}\left(-\frac{x^2}{2}+\left|A_z\right|\cos(ky)\right)^2 A_z+c_{11}\left(-\frac{x^2}{2}+\left|A_z\right|\cos(ky)\right)A_z-\frac{\delta n}{n_0}A_z+2i\gamma' A_z=0, \tag{6.7}$$

where $c_1=\dfrac{2\omega_0(1+\lambda_e^4k_0^4+2\lambda_e^2k_0^2+2\lambda_e^4k_{0x}^2k_{0z}^2+2\lambda_e^4k_{0y}^2k_{0z}^2)}{(\lambda_i^2v_A^2k^2k_{0z}^2)}.$

$$c_2=\frac{2k_{0x}(2\omega_0^2\lambda_e^4k_{0x}^2+2\omega_0^2\lambda_e^4k_{0z}^2+2\omega_0^2\lambda_e^2-\lambda_i^2k_{0z}^2v_A^2)}{(\lambda_i^2v_A^2k^2k_{0z}^2)}.$$

$$c_3=\frac{2k_{0y}(2\omega_0^2\lambda_e^4k_{0y}^2+2\omega_0^2\lambda_e^4k_{0z}^2+2\omega_0^2\lambda_e^2-\lambda_i^2k_{0z}^2v_A^2)}{(\lambda_i^2v_A^2k^2k_{0z}^2)}.$$

$$c_4=\frac{2k_{0z}(2\omega_0^2\lambda_e^2k_{0z}^2+2\omega_0^2\lambda_e^2k_{0x}^2+2\omega_0^2\lambda_e^2k_{0y}^2+2\omega_0^2\lambda_e^2-\lambda_i^2v_A^2k_{0y}^2-2\lambda_i^2v_A^2k_{0z}^2)}{\lambda_i^2v_A^2k^2k_{0z}^2}.$$

$$c_5=\frac{4\omega_0^2k_{0x}^2\lambda_e^4}{\lambda_i^2v_A^2k_0^2k_{0z}^2},\qquad c_6=\frac{4\omega_0^2k_{0y}^2\lambda_e^4}{\lambda_i^2v_A^2k_0^2k_{0z}^2},\qquad c_7=\frac{\left(4\omega_0^2k_{0z}^2\lambda_e^4-4\lambda_i^2v_A^2k_{0z}^2\right)}{\lambda_i^2v_A^2k_0^2k_{0z}^2}.\ b_0=0.5,$$

$$c_8=\frac{\left(8\omega_0^2\lambda_e^4-4\lambda_i^2v_A^2\right)k_{0z}k_{0x}}{\lambda_i^2v_A^2k_0^2k_{0z}^2},\quad c_9=\frac{\left(8\omega_0^2\lambda_e^4-4\lambda_i^2v_A^2\right)k_{0z}k_{0y}}{\lambda_i^2v_A^2k_0^2k_{0z}^2},\qquad c_{10}=\frac{k_{0y}^2}{k_{0z}^2}\ \text{and}\ c_{11}=\frac{2k_{0y}}{k_{0z}}.$$

and $\gamma'=\dfrac{\gamma}{\omega_0}$ is the normalized growth rate. $\gamma\left(=0.5083\omega_{ce}\right)$ is the growth rate of beam-driven whistler waves. The normalizing parameters are-

$t_n=1/\omega_0.$

$$x_n=\frac{k_{0x}(2\omega_0^2k_{0x}^2\lambda_e^4+2\omega_0^2k_{0z}^2\lambda_e^4+2\omega_0^2\lambda_e^2+k_{0z}^2\lambda_i^2v_A^2)}{\omega_0(1+\lambda_e^4k_0^4+2\lambda_e^2k_0^2+2\lambda_e^4k_{0x}^2k_{0z}^2+2\lambda_e^4k_{0y}^2k_{0z}^2)}.$$

$$z_n=\frac{2i(-2\omega_0^2k_{0x}^3\lambda_e^4+2\omega_0^2k_{0x}k_{0z}^2\lambda_e^4+2\omega_0^2\lambda_e^2k_{0x}+k_{0x}k_{0z}^2\lambda_i^2v_A^2+2k_{0z}^3\lambda_i^2v_A^2)}{2\omega_0(1+\lambda_e^4k_{0x}^4+\lambda_e^4k_{0z}^4+2\lambda_e^2k_{0x}^2+2\lambda_e^2k_{0z}^2)}.$$

6.2.2 Magnetosonic waves dynamics (MSWs)

Consider a magnetosonic wave propagating in the x-direction, i.e., $\vec{k} = k_{0x}\hat{x}$ along with the background magnetic field in the z-direction, i.e., $\vec{B} = B_0\hat{z}$. The electric field is polarized in y-direction i.e., $\vec{E} = E_y\hat{y}$. The dynamical equation for the magnetosonic wave is obtained from the basic equations such as the equation of motion, Faraday's law, continuity equation, and Ampere's -Maxwell's equation following the procedure used by [43] as

$$\left(\frac{\partial^2}{\partial t^2} - c_{12}\frac{\partial^2}{\partial x^2}\right)\frac{n}{n_0} = -c_{13}\frac{\partial^2}{\partial x^2}|A_z|^2, \tag{6.8}$$

where c_{12}, c_{13} is the constant, whose value is given below:

$$c_{12} = c^2\left(\frac{c_s^2 + v_A^2}{c^2 + v_A^2}\right)$$

and $c_{13} = \left[\frac{e^2}{m_e m_i \omega_{ce}^2} - \frac{e^2\omega_0}{m_e m_i \omega_{ce}\alpha_1}\left\{\left(1 + \frac{\omega_{ce}^2}{\alpha_1}\right) + \frac{\omega_0^3}{\alpha_1\omega_{ce}}\right\} + \frac{e^2}{m_i^2\omega_{ci}^2} - \frac{e^2\omega_0}{m_e m_i \omega_{ce}\alpha_1}\left\{\left(1 + \frac{\omega_{ci}^2}{\alpha_1}\right) + \frac{\omega_0^3}{\alpha_1\omega_{ci}}\right\}\right]$

$c_s\left(= \frac{v_{th_e}^2 + v_{th_i}^2}{m_i}\right)^{\frac{1}{2}}$ is the speed of the sound wave. And $\alpha_1 = -k^2\lambda_e^2(\omega_0^2 - \omega_{ce}^2) - \omega_0^2$.

Now, using the same normalizing parameter as in the whistler wave dynamics, i.e., x_n, z_n and t_n. After taking the adiabatic response of Eq. (6.8), we obtain

$$\frac{n}{n_0} = \frac{c_{13}}{c_{12}}|A_z|^2. \tag{6.9}$$

we obtain the following normalization equation,

$$A_n = \left[\frac{c_{12}}{c_{13}}n_0\right]^{\frac{1}{2}} \tag{6.10}$$

using this Eq. (6.9) in Eq. (6.7), we obtain

$$\begin{aligned} &ic_1\frac{\partial A_z}{\partial t} + c_2\frac{\partial^2 A_z}{\partial x^2} + c_3\frac{\partial^2 A_z}{\partial y^2} + c_4\frac{\partial^2 A_z}{\partial z^2} + ic_5\frac{\partial A_z}{\partial x} + ic_6\frac{\partial A_z}{\partial y} + ic_7\frac{\partial A_z}{\partial z} + c_8\frac{\partial^2 A_z}{\partial x\partial z} + c_9\frac{\partial^2 A_z}{\partial y\partial z} \\ &+c_{10}\left(-\frac{x^2}{2} + |A_z|\cos(ky)\right)^2 A_z + c_{11}\left(-\frac{x^2}{2} + |A_z|\cos(ky)\right)A_z - \frac{c_{13}}{c_{12}}|A_z|^2 A_z + 2i\gamma' A_z = 0, \end{aligned} \tag{6.11}$$

This is the model equation of dynamical system of 3D nonlinear whistler in the presence of magnetic islands.

Parameters used in numerical simulations are:

$n_0 = 21cm^{-3}$, $B_0 = 45nT$, $T_e = 42eV$, $T_I = 235eV$, $\omega_{pe} = 2.5\times10^5\, rad/\sec$, $\omega_{ce} = 7.9\times10^3\, rad/\sec$,

$\omega_{ci} = 4.31\, rad/\sec$, $v_A = 2.14\times10^7\, cm/\sec$, $c_s = 1.6\times10^7\, cm/\sec$, $\lambda_i = 4.9\times10^6\, cm$, $\lambda_e = 1.16\times10^5\, cm$,

$A_n = 5.03\times10^8\, G$ cm, $x_n = y_n = 1.02\times10^6\, cm$, $z_n = 1.5\times10^6\, cm$, $t_n = 0.015\sec$,

The values of numerical constants are given below-

$c_1 = 0.0155$, $c_2 = c_3 = 1.02\times10^6$, $c_4 = 1.5\times10^6$, $c_5 = c_6 = 2.5\times10^{10}$, $c_7 = -2.0\times10^{11}$, $c_8 = c_9 = -7.2\times10^{11}$,

$c_{10} = 12.41$, $c_{11} = 7.04$, $c_{12} = 1.6\times10^5$, $c_{12} = 7.2\times10^{14}$, $c_{13} = 3.43\times10^{14}$.

6.3 Numerical Simulation and Result Discussion

For solving the dynamics of Eq. (6.11), we have developed a modified nonlinear Schrödinger model (MNLS). To solve Eq. (6.11) numerically, we have used the 3D pseudospectral method. For space integration having periodic length $L_x = \frac{2\pi}{\alpha_x}$ and $L_y = \frac{2\pi}{\alpha_y}$, a pseudospectral approach and finite difference approach for time evolution utilizing a modified version of the predictor-corrector method have been used [44] For doing numerical simulation, periodic domain $(10\pi\times10\pi\times10\pi)$ and grid size $(128\times128\times128)$ of the system are used. The model equation has been transformed into the nonlinear Schrodinger (NLS) equation to evaluate its accuracy, by testing the consistency of the plasmon number up to order of 10^{-6}, and then we modify this code according to our problem and run this code. The initial condition for numerical simulation consists of a single O-point representing the magnetic reconnection (Fitzpatrick & Waelbroeck, 2005 [42]): -

$$\frac{\delta A_z}{A_0} = \left(-\frac{x^2}{2} + |A_z|\cos(ky)\right)$$ Here, $|A_z|$ is the initial amplitude of the wave.

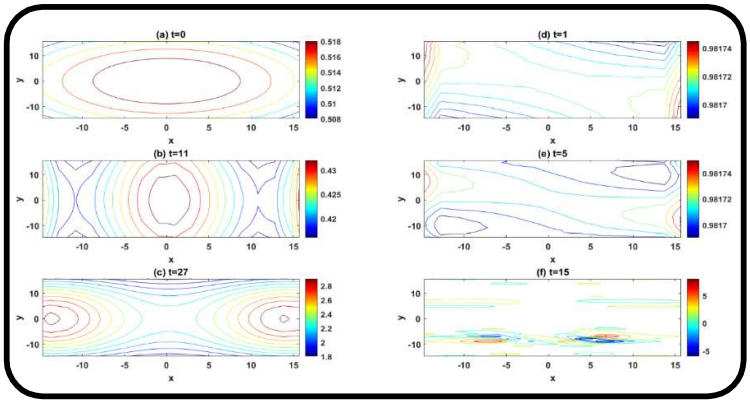

Figure 6.1 Contour plot (left panel) and current sheet (right panel) of nonlinear whistler wave at different times.

Figure 6.1 depicts the contour plot of vector potential (left panel) at different times. Magnetic field lines initially develop into a single O structure. Over the time, this single O-point reassembles into several O-points linked to X-points, forming X-O structures with increasing amplitude. In this figure, the formation of a separatix between the X and O locations is evident. In right panel, we have shown the temporal evolution of current sheets. By using the relation of $j = \nabla^2 A_z$, current density can be obtained.

Power spectrum

Since the beam-driven mode's continuous growth rate was taken into consideration, the quasi-steady state has not yet been reached and will not be for some time. Therefore, we switch off the growth rate part from our system's equation (6.11) to see the turbulent power spectrum.

$$ic_7\frac{\partial A_z}{\partial z}+c_2\frac{\partial^2 A_z}{\partial x^2}+c_3\frac{\partial^2 A_z}{\partial y^2}+ic_5\frac{\partial A_z}{\partial x}+ic_6\frac{\partial A_z}{\partial y}+c_8\frac{\partial^2 A_z}{\partial x\partial z}+c_9\frac{\partial^2 A_z}{\partial y\partial z}-\frac{c_{13}}{c_{12}}\left|A_z\right|^2 A_z=0. \qquad (6.12)$$

After that, Eq. (6.12) is solved numerically utilizing the pseudospectral approach for spatial integration (along the x- and y-direction) and the finite difference method for time evolution (along the z-direction). Then simulating this Equation (6.12) for a higher grid size (512×512). Figure 6.2 illustrates the power spectra. The top panel of Figure 6.2 shows the time evolution of electric energy spectrum. It approaches a power-law spectrum following the Kolmogorov scaling i.e., close to $k^{-5/3}$ in the inertial range after that we obtain a steeper spectrum. The bottom panel shows the magnetic (blue) and electric (red) at time range, 65-80. The energy spectra have been computed with the 2D Fourier decomposition of magnetic and electric fields. The observed power law behavior is in the range of $0.1<k\lambda_e<1$. These power spectra illustrate the signature of turbulence. The charged particles can be accelerated by this energy.

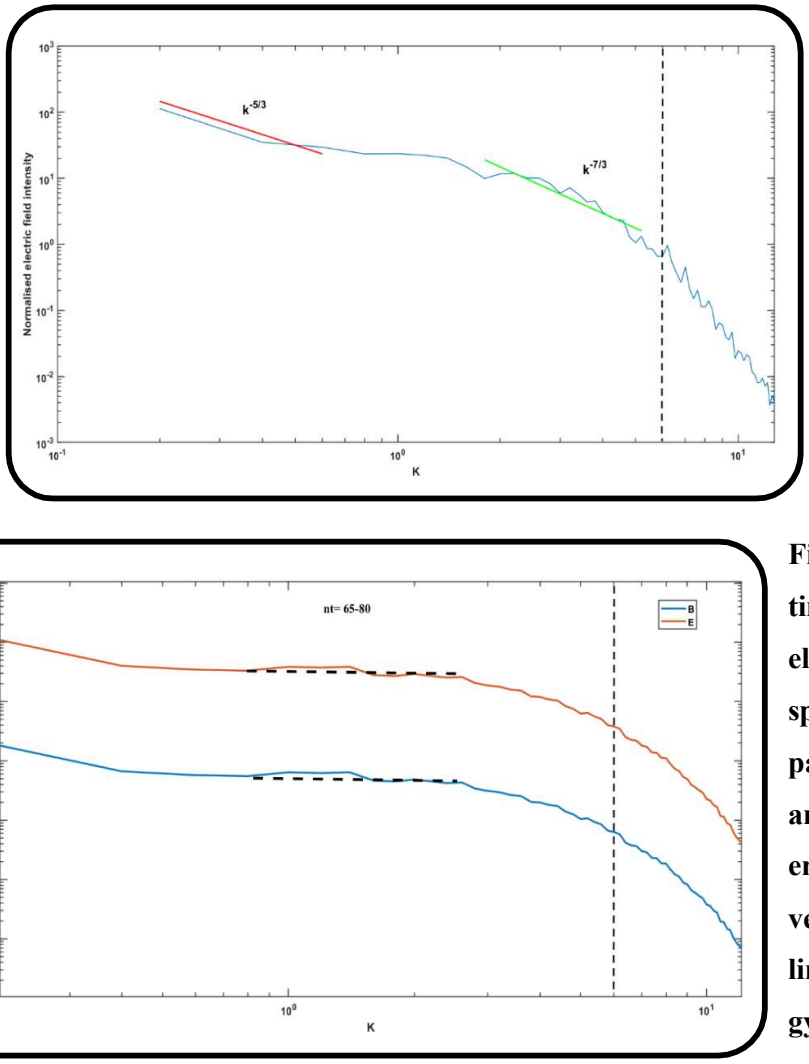

Figure 6.2 Top panel: time evolution of electric energy spectrum. The bottom panel: magnetic (blue) and electric (Red) energy spectra. The vertical dashed black line shows the electron gyroscale.

The acceleration of charged particles in plasmas has been studied using a variety of methods, including Fermi acceleration, resonant wave-particle acceleration, and acceleration through radiative-resonant interactions. In this study, we examine the development of the thermal tail of energetic electrons, which may be the root of the electron acceleration and heating, caused by the power-law scaling of turbulence generation. By using the Fokker-Plank equation, it is possible to comprehend how localized structures and plasma particles interact. Particle energization can result from these kinds of random and frequent interactions. This is accomplished using second-order Fermi acceleration [45], [46].

The quasi-linear diffusion equation may be used to examine the interactions between strongly localized fields (structures) and plasma particles. Here is an expression for the quasi-linear diffusion equation [46], [47].

$$\frac{\partial f}{\partial t} = \frac{\partial}{\partial v}\left\{ D(v)\frac{\partial f}{\partial v} \right\}. \tag{6.13}$$

Here, $f(t,v)$ denotes the velocity distribution function, and $D(v)$ denotes the velocity space diffusion coefficient. When the observation time is longer than the characteristic time of setting up of ponderomotive nonlinearity, the distribution function $f(t,v)$ can be assumed as time independent. In this context, the relation between spectral index η, and distribution function $f(v)$ [48] is given below-

$$f(v) \propto v^{2-\eta}. \tag{6.14}$$

In our current analysis $\eta \simeq 2.3$, therefore $f(v) \sim v^{-0.3}$ it leads to the formation of the thermal tail of energetic electrons. Therefore, this enhances the thermal tail segment of the distribution function and paves the way for the thermal heating of the particles.

6.4 Semianalytical model

It is critical to comprehend the creation and behaviour of current sheets in magnetic reconnection in a variety of astrophysical and lab plasma systems. So, to understand the formation of current sheet and their size, we have studied a simplified model named as semianalytical or steady-state model. For simplification, we have modified Eq. (4), and obtained the following Eq.,

$$\begin{aligned}
&i\frac{2}{k_{\|}}\frac{\partial A_z}{\partial z} + \frac{(4\omega_0^2\lambda_e^4 k_{\perp}^2)}{(2\omega_0^2k_{\|}^2\lambda_e^4 + 2\omega_0^2k_{\perp}^2\lambda_e^4 + 2\omega_0^2k_{\perp}^2\lambda_e^4 + 2\omega_0^2\lambda_e^2 - k_{\perp}^2\lambda_i^2v_A^2 - 2k_{\|}^2\lambda_i^2v_A^2)k_{\|}^2}\frac{\partial^2 A_z}{\partial x^2} + \\
&\frac{(4\omega_0^2\lambda_e^4 k_{\perp}^2)}{(2\omega_0^2k_{\|}^2\lambda_e^4 + 2\omega_0^2k_{\perp}^2\lambda_e^4 + 2\omega_0^2k_{\perp}^2\lambda_e^4 + 2\omega_0^2\lambda_e^2 - k_{\perp}^2\lambda_i^2v_A^2 - 2k_{\|}^2\lambda_i^2v_A^2)k_{\|}^2}\frac{\partial^2 A_z}{\partial y^2} + \\
&\frac{\lambda_i^2v_A^2k^2k_{\perp}^2}{(2\omega_0^2k_{\|}^2\lambda_e^4 + 2\omega_0^2k_{\perp}^2\lambda_e^4 + 2\omega_0^2k_{\perp}^2\lambda_e^4 + 2\omega_0^2\lambda_e^2 - k_{\perp}^2\lambda_i^2v_A^2 - 2k_{\|}^2\lambda_i^2v_A^2)k_{\|}^2}\left(\frac{\delta A_z}{A_0}\right)^2 A_z + \\
&\frac{2\lambda_i^2v_A^2k^2k_{0y}k_{\|}}{(2\omega_0^2k_{\|}^2\lambda_e^4 + 2\omega_0^2k_{\perp}^2\lambda_e^4 + 2\omega_0^2k_{\perp}^2\lambda_e^4 + 2\omega_0^2\lambda_e^2 - k_{\perp}^2\lambda_i^2v_A^2 - 2k_{\|}^2\lambda_i^2v_A^2)k_{\|}}\left(\frac{\delta A_z}{A_0}\right)A_z \\
&-\frac{(\lambda_i^2v_A^2k^2)}{(2\omega_0^2k_{\|}^2\lambda_e^4 + 2\omega_0^2k_{\perp}^2\lambda_e^4 + 2\omega_0^2k_{\perp}^2\lambda_e^4 + 2\omega_0^2\lambda_e^2 - k_{\perp}^2\lambda_i^2v_A^2 - 2k_{\|}^2\lambda_i^2v_A^2)}\frac{\delta n}{n_0}A_z + A_z\exp(k_i z) = 0.
\end{aligned} \tag{6.15}$$

Or we can rewrite the above equation in simplified equation as-

$$\begin{aligned}
&i\frac{2}{k_{\|}}\frac{\partial A_z}{\partial z} + \theta_1\lambda_e^2\left(\frac{\partial^2 A_z}{\partial x^2} + \frac{\partial^2 A_z}{\partial y^2}\right) + \theta_2\left(-\frac{x^2}{2} + A_z\cos(ky)\right)^2 A_z + \\
&\theta_3\left(-\frac{x^2}{2} + A_z\cos(ky)\right)A_z - \theta_4\frac{\delta n}{n_0}A_z + A_z\exp(k_i z) = 0,
\end{aligned} \tag{6.16}$$

where, $\theta_1 = \dfrac{(4\omega_0^2\lambda_e^2k_\perp^2)}{(2\omega_0^2k_\parallel^2\lambda_e^4+2\omega_0^2k_\perp^2\lambda_e^4+2\omega_0^2k_\perp^2\lambda_e^4+2\omega_0^2\lambda_e^2-k_\perp^2\lambda_i^2v_A^2-2k_\parallel^2\lambda_i^2v_A^2)k_\parallel^2}.$

$$\theta_2 = \frac{\lambda_i^2v_A^2k^2k_\perp^2}{(2\omega_0^2k_\parallel^2\lambda_e^4+2\omega_0^2k_\perp^2\lambda_e^4+2\omega_0^2k_\perp^2\lambda_e^4+2\omega_0^2\lambda_e^2-k_\perp^2\lambda_i^2v_A^2-2k_\parallel^2\lambda_i^2v_A^2)k_\parallel^2}.$$

$$\theta_3 = \frac{2\lambda_i^2v_A^2k^2k_\perp}{(2\omega_0^2k_\parallel^2\lambda_e^4+2\omega_0^2k_\perp^2\lambda_e^4+2\omega_0^2k_\perp^2\lambda_e^4+2\omega_0^2\lambda_e^2-k_\perp^2\lambda_i^2v_A^2-2k_\parallel^2\lambda_i^2v_A^2)k_\parallel}.$$

$$\theta_4 = \frac{(\lambda_i^2v_A^2k^2)}{(2\omega_0^2k_\parallel^2\lambda_e^4+2\omega_0^2k_\perp^2\lambda_e^4+2\omega_0^2k_\perp^2\lambda_e^4+2\omega_0^2\lambda_e^2-k_\perp^2\lambda_i^2v_A^2-2k_\parallel^2\lambda_i^2v_A^2)}.$$

Now we are assuming the envelope solution of the vector potential $\tilde{A}_z = A_{00}e^{ik_{0z}s(x,y,z)}$, and putting this envelope solution in Eq. (6.16) we obtained the following equation-

$$\begin{aligned}&i\frac{2}{k_{0z}}\frac{\partial A_{00}}{\partial z}-2A_{00}\frac{\partial s}{\partial z}+\theta_1\lambda_e^2\left(\frac{\partial^2A_{00}}{\partial x^2}+\frac{\partial^2A_{00}}{\partial y^2}\right)+2ik_\parallel\theta_1\lambda_e^2\left(\frac{\partial A_{00}}{\partial x}\frac{\partial s}{\partial x}+\frac{\partial A_{00}}{\partial y}\frac{\partial s}{\partial y}\right)-\\&k_\parallel^2\theta_1\lambda_e^2\left(\frac{\partial s}{\partial x}+\frac{\partial s}{\partial y}\right)^2A_{00}+ik_\parallel\theta_1\lambda_e^2\left(\frac{\partial^2s}{\partial x^2}+\frac{\partial^2s}{\partial y^2}\right)A_{00}+\theta_2\left[\left(-\frac{x^2}{2}+A_z\cos(ky)\right)\right]^2A_{00}+\\&\theta_3\left[\left(-\frac{x^2}{2}+A_z\cos(ky)\right)\right]A_{00}-\theta_4\frac{\delta n}{n_0}A_{00}+A_z\exp(k_iz)=0.\end{aligned} \tag{6.17}$$

Further separating the real and imaginary parts of Eq. (6.17)

$$\begin{aligned}&-2\frac{\partial s}{\partial z}A_{00}+\theta_1\lambda_e^2\left(\frac{\partial^2A_{00}}{\partial x^2}+\frac{\partial^2A_{00}}{\partial y^2}\right)-k_\parallel^2\theta_1\lambda_e^2\left(\frac{\partial s}{\partial x}+\frac{\partial s}{\partial y}\right)^2A_{00}+\theta_2\left[\left(-\frac{x^2}{2}+A_z\cos(ky)\right)\right]^2A_{00}\\&+\theta_3\left[\left(-\frac{x^2}{2}+A_z\cos(ky)\right)\right]A_{00}-\theta_4\left[\exp(\alpha|A_z|^2-1\right]A_{00}+A_{00}\exp(k_iz)=0.\end{aligned} \tag{6.18}$$

$$\frac{2}{k_\parallel}\frac{\partial A_{00}}{\partial z}+2k_\parallel\theta_1\lambda_e^2\left(\frac{\partial A_{00}}{\partial x}\frac{\partial s}{\partial x}+\frac{\partial A_{00}}{\partial y}\frac{\partial s}{\partial y}\right)+k_\parallel\lambda_e^2\theta_1\left(\frac{\partial^2s}{\partial x^2}+\frac{\partial^2s}{\partial y^2}\right)A_{00}=0. \tag{6.19}$$

Further assuming the Gaussian profile for the initial distribution of wave i.e.,

$$\begin{aligned}&A_{00}^2=\frac{A_{00}^2}{f_1(z)f_2(z)}\exp\left(\frac{-x^2}{r_{01}^2}-\frac{y^2}{r_{01}^2}+k_iz\right)\\&s=\beta_1(z)\frac{x^2}{2}+\beta_2(z)\frac{y^2}{2}+\phi(z)\end{aligned} \tag{6.20}$$

Using Eq. (6.20) in Eq. (6.19), and collecting the terms x^2 and y^2, we obtain the following Eqs.

$$\beta_1(z)=\frac{1}{k_\parallel^2\theta_1\lambda_e^2}\frac{1}{f_1}\frac{\partial f_1}{\partial z}. \tag{6.21}$$

$$\beta_2(z)=\frac{1}{k_{\|}^2\theta_1\lambda_e^2}\frac{1}{f_2}\frac{\partial f_2}{\partial z}.$$

Here r_{01} and r_{02} represents the length and width of current sheet, respectively; $\beta_1(z)$ and $\beta_2(z)$ represents the slowly varying function, and f_1, f_2 represents the beam width parameter of the whistler wave. Now, for obtaining the beam-width parameters, use Eq. (6.20) in Eq. (6.18) with paraxial approximation i.e., $x<<r_{01}^2 f_1,\ y<<r_{02}^2 f_2$ after that equating coefficient of x^2 and y^2, we obtained the following Eq.

$$\frac{\partial^2 f_1}{\partial\xi^2}=R_d^2k_{\|}^2\left(\frac{4\theta_1^2\lambda_e^4}{r_{01}^4f_1^4f_2}+\frac{\theta_1\theta_3f_1}{2}-\frac{2\theta_1\theta_4\lambda_e^2\left(\alpha A_{00}^{'2}\right)}{r_{01}^2f_1^3f_2}\right). \tag{6.22}$$

And, $$\frac{\partial^2 f_2}{\partial\xi^2}=R_d^2k_{\|}^2\left(\frac{4\theta_1^2\lambda_e^4}{r_{02}^4f_2^4f_1}+\frac{\theta_1\theta_3k^2\lambda_e^2f_2}{2}-\frac{\theta_1\theta_4\lambda_e^2\left(\alpha A_{00}^{'2}\right)}{r_{02}^2f_2^3f_1}\right), \tag{6.23}$$

where $\xi=z/R_d$ and $R_d=k_{0z}r_{01}^2$. Eqs. (6.22) & (6.23) are solved for the plain wavefront imposing the following initial conditions- $\frac{\partial^2 f_1}{\partial\xi^2}=\frac{\partial^2 f_2}{\partial\xi^2}=0, f_1=f_2=1$ at z=0. When the power of the whistler wave $\left(\alpha A_{00}^{'2}\right)$ is zero, then the length and width of the whistler's localized structures are obtained as $r_{01}=0.9\lambda_e$, $r_{02}=1.2\lambda_e$, respectively. Further, when we take the finite value of power $\left(\alpha A_{00}^{'2}=0.5\right)$, then the length and width of the whistler's localized structures are obtained as, $r_{01}=15\lambda_e$, $r_{02}=15.63\lambda_e$, respectively. Also, by using Ampere's law $\left(J=-\nabla^2A_{00}^{'}\right)$, we have studied the current sheet size. One can calculate the length and width of the whistler's localized structures of the current sheet comes out to be of the order of $r_{01}/\sqrt{3}$ and $r_{02}/\sqrt{3}$, respectively. Therefore, when power is finite then the length and width of whistler's localized structures of current sheet is $8.6\lambda_e$, and $9.03\lambda_e$, respectively. When power is zero then the length and width of whistler's localized structures of current sheet is $0.52\lambda_e$, and $0.69\lambda_e$, respectively. As a result, it shows how the whistler power also influences the scale size of current sheet. Recently, scale size of super thin current sheets in the Earth's magnetotail has been reported which is of the order of few (1–5) gyroradii of thermal electrons [49]. Also, the scale size of whistler wave's structures of the order of $(10-20)\lambda_e$ has been reported at the magnetic reconnection sites in the magnetopause [50]. Electron-scale

current sheets has been reported in the vicinity of Earth's magnetosheath, solar corona and other astrophysical system [51].

6.5 Summary and Conclusion

This study focuses on the effect of the perturbed background density and magnetic islands on the whistler wave at the site of magnetic reconnection. We proposed a model of beam-driven whistler wave originating from the noise caused by the energy of beam and rising to a large amplitude, where nonlinear effects from ponderomotive force drive the whistler wave. The model equation to represent the coupling of whistler wave and magnetosonic wave has been developed with the help of a two-fluid model. To address the model concern, the pseudo-spectral approach is employed for spatial integration, and the finite difference method is used for temporal integration. The outcomes of the numerical simulations are discussed below:

1) Separatrix plays a key role in magnetic reconnection by forming a line separating portions of magnetic field lines with varying connectivity. It acts as a site for the breaking and reconnecting of magnetic field lines, resulting in the release of accumulated magnetic energy. The features of the separatrix are a helpful source of information for the mechanism and energetics of the reconnection process.
2) Contour plots of vector potential or drawings of magnetic field lines may be used to locate magnetic islands caused by reconnection. A single O-point evolves into many O-points associated with X-points, forming X-O structures with increasing amplitude. It is possible to observe the emergence of a new field linked with these X-O structures. To understand the expansion of magnetic flux, which is associated with current density function by Ampere's law, the spatial development of current density function must also be considered. Over time, the essential X-O structures begin to distort, resulting in a chaotic pattern. Because of these chaotic structures, whistler turbulence will occur. In our simulation, we discovered that current sheets also get turbulent.
3) In this model, the beam-driven mode's continuous growth rate was taken into consideration; the quasi-steady state has not yet been reached and will not be for some time. So, to see the turbulent spectrum, quasi-steady state has been achieved by switching off the growth rate of beam. The estimated spectral power indices reveal a scaling of nearly -5/3 in the inertial range [which agrees with the observations of (Biskamp et al. [38]] and steeper spectra of nearly -7/3 at smaller scales. This power spectrum depicts the turbulence signature. This energy may be used to accelerate charged particles.

4) We observe that electron-scale current sheets contribute significantly to the particle energization [49] as determined by semianalytical model. Also, we observed that whistler wave influences the scale size of the current sheet. When the power of the whistler wave $\left(\alpha A_{00}^{2}\right)$ is zero, then the length and width of whistler wave's structures are obtained as $r_{01}=0.9\lambda_e$, $r_{02}=1.2\lambda_e$, respectively. Further, when we take the finite value of power $\left(\alpha A_{00}^{2}=0.5\right)$, then the length and width of whistler wave's structures are obtained as, $r_{01}=15\lambda_e$, $r_{02}=15.63\lambda_e$, respectively. In addition, by using Ampere's law $\left(J=-\nabla^2 A_{00}^{'}\right)$, we have studied the current sheet size. One can calculate the length and width of the current sheet comes out to be of the order of $r_{01}/\sqrt{3}$ and $r_{02}/\sqrt{3}$, respectively. Therefore, when power is finite then the length and width of current sheet is $8.6\lambda_e$, and $9.03\lambda_e$, respectively. When power is zero then the length and width of current sheet $0.52\lambda_e$, and $0.69\lambda_e$, respectively. As a result, it shows how the whistler power also influences the dimension of whistler wave's structure and its current sheet dimension.

Even though spectra in quasi-steady state are nearly around the order of -5/3 in the inertial range [which is consistent with (Biskamp et al., 1996 [38])], At shorter wavelengths, we obtain steeper spectra with scaling factors on the order of -7/3, but the development of turbulent state is the unique aspect of our work in which we explored the formation of current sheets and how they emerge into turbulent states. The current sheet deeds as a location for intense plasma heating, energy dissipation and particle acceleration. Further, a detailed analysis of all different possibilities that are encountered in the beam-driven turbulence generation, and heating and acceleration of plasma particles is beyond the scope of this paper and will be left to future work.

References

1. A. Retinò, D. Sundkvist, A. Vaivads, F. Mozer, M. André, and C. J. Owen, Nat Phys **3**, 235 (2007).

2. T. D. Phan, J. P. Eastwood, M. A. Shay, J. F. Drake, B. U. O. Sonnerup, M. Fujimoto, P. A. Cassak, M. Øieroset, J. L. Burch, R. B. Torbert, A. C. Rager, J. C. Dorelli, D. J. Gershman, C. Pollock, P. S. Pyakurel, C. C. Haggerty, Y. Khotyaintsev, B. Lavraud, Y. Saito, M. Oka, R. E. Ergun, A. Retino, O. Le Contel, M. R. Argall, B. L. Giles, T. E. Moore, F. D. Wilder, R. J. Strangeway, C. T. Russell, P. A. Lindqvist, and W. Magnes, Nature **557**, 202-206 (2018).

3. J. L. Burch, T. E. Moore, R. B. Torbert, and B. L. Giles, Space Sci Rev **199**, 5-21 (2016).

4. S. Haaland, G. Paschmann, M. Øieroset, T. Phan, H. Hasegawa, S. A. Fuselier, V. Constantinescu, S. Eriksson, K. J. Trattner, S. Fadanelli, P. Tenfjord, B. Lavraud, C. Norgren, J. P. Eastwood, H. Hietala, and J. Burch, J Geophys Res Space Phys **125(3)**, (2020).

5. G. Le and C. T. Russell, Geophys Res Lett **21**, 2451-2454 (1994).

6. L. J. Cahill and P. G. Amazeen, J Geophys Res **68**, 1835-43 (1963).

7. C. Norgren, D. B. Graham, Y. V. Khotyaintsev, M. André, A. Vaivads, M. Hesse, E. Eriksson, P. A. Lindqvist, B. Lavraud, J. Burch, S. Fuselier, W. Magnes, D. J. Gershman, and C. T. Russell, J Geophys Res Space Phys **123**, 9222-38 (2018).

8. M. André, A. Vaivads, S. C. Buchert, A. N. Fazakerley, and A. Lahiff, Geophys Res Lett **31**, 3 (2004).

9. C. P. Escoubet, M. Fehringer, and M. Goldstein, Ann Geophys **19**, 1197-1200 (2001).

10. E. V. Panov, J. Büchner, M. Fränz, A. Korth, Y. Khotyaintsev, B. Nikutowski, S. Savin, K. H. Fornaçon, I. Dandouras, and H. Rème, Advances in Space Research **37**, 1363-72 (2006).

11. J. T. Gosling and A. Szabo, J Geophys Res Space Phys **113**, A10 (2008).

12. W. J. Hughes, Introduction to Space Physics, 227-285 (2019).

13. X. H. Deng and H. Matsumoto, Nature **410**, 557-560 (2001).

14. G. Paschmann, M. Øieroset, and T. Phan, Space Sci Rev **178**, 385-417 (2013).

15. D. A. Gurnett, R. R. Anderson, B. T. Tsurutani, E. J. Smith, G. Paschmann, G. Haerendel, S. J. Bame, and C. T. Russell, J Geophys Res **84**, 7043-7058 (1979).

16. B. U. Ö. Sonnerup, G. Paschmann, I. Papamastorakis, N. Sckopke, G. Haerendel, S. J. Bame, J. R. Asbridge, J. T. Gosling, and C. T. Russell, J Geophys Res **86**, 10049-10067 (1981).

17. G. Paschmann, B. U. Ö. Sonnerup, I. Papamastorakis, N. Sckopke, G. Haerendel, S. J. Bame, J. R. Asbridge, J. T. Gosling, C. T. Russell, and R. C. Elphic, Nature **282**, 243 (1979).

18. G. B. Field, Science **207**, 753 (1980).

19. J. Birn and E. R. Priest, *Reconnection of Magnetic Fields: Magnetohydrodynamics and Collisionless Theory and Observations* (2007).

20. T. Li, E. Priest, and R. Guo, Proceedings of the Royal Society A: Mathematical, Physical and Engineering Sciences **477**, 2249 (2021).

21. W. Gonzalez and E. Parker, Astrophysics and space science library, Magnetic Reconnection Concepts and Applications (2016).

22. G. R. Werner and D. A. Uzdensky, Astrophys. J. **843**, L27 (2017).

23. G. R. Werner, D. A. Uzdensky, M. C. Begelman, B. Cerutti, and K. Nalewajko, Monthly Notice Royal Astronomical Society **473**, 4840-61 (2018).

24. M. Hoshino and Y. Lyubarsky, Space Sci Rev **173**, 521-533 (2012).

25. H. Karimabadi, V. Roytershteyn, H. X. Vu, Y. A. Omelchenko, J. Scudder, W. Daughton, A. Dimmock, K. Nykyri, M. Wan, D. Sibeck, M. Tatineni, A. Majumdar, B. Loring, and B. Geveci, Phys. Plasmas **21(6)**, (2014).

26. W. H. Matthaeus, Phys. Plasmas **28(3)**, (2021).

27. J. P. Eastwood, T. D. Phan, S. D. Bale, and A. Tjulin, Phys. Rev. Lett. **102(3)**, 035001 (2009).

28. C. Dong, L. Wang, Y. M. Huang, L. Comisso, T. A. Sandstrom, and A. Bhattacharjee, Sci. Adv. **8**, eabn7627 (2022).

29. H. Karimabadi and A. Lazarian, Phys. Plasmas **20**, 1 (2013).

30. P. Sharma Pyakurel, M. A. Shay, T. D. Phan, W. H. Matthaeus, J. F. Drake, J. M. TenBarge, C. C. Haggerty, K. G. Klein, P. A. Cassak, T. N. Parashar, M. Swisdak, and A. Chasapis, Phys. Plasmas **26(8)**, (2019).

31. C. Vega, V. Roytershteyn, G. L. Delzanno, and S. Boldyrev, Astrophys. J. **893**, L10 (2020).

32. P. S. Pyakurel, M. A. Shay, J. F. Drake, T. D. Phan, P. A. Cassak, and J. L. Verniero, Phys. Rev. Lett. **127**, 155101 (2021).

33. L. Franci, E. Papini, A. Micera, G. Lapenta, P. Hellinger, D. Del Sarto, D. Burgess, and S. Landi, Astrophys. J. **936(1)**, 27 (2022).

34. A. Lazarian, L. Vlahos, G. Kowal, H. Yan, A. Beresnyak, and E. M. De Gouveia Dal Pino, Space Sci. Rev. **173**, 557-622 (2012).

35. H. Karimabadi, V. Roytershteyn, W. Daughton, and Y. H. Liu, Space Sci. Rev. **178**, 307 (2013).

36. E. Papini, A. Cicone, L. Franci, M. Piersanti, S. Landi, P. Hellinger, and A. Verdini, Astrophys. J. Lett. **917**, (2021).

37. H. Karimabadi, V. Roytershteyn, M. Wan, W. H. Matthaeus, W. Daughton, P. Wu, M. Shay, B. Loring, J. Borovsky, E. Leonardis, S. C. Chapman, and T. K. M. Nakamura, Phys. Plasmas **20(1)**, (2013).

38. D. Biskamp, E. Schwarz, and J. F. Drake, Phys. Rev. Lett. **76(8)**, 1264 (1996).

39. D. Biskamp, E. Schwarz, A. Zeiler, A. Celani, and J. F. Drake, Phys. Plasmas **6**, 751-758 (1999).

40. S. Adhikari, T. N. Parashar, M. A. Shay, W. H. Matthaeus, P. S. Pyakurel, S. Fordin, J. E. Stawarz, and J. P. Eastwood, Phys. Rev. E **104(6)**, 065206 (2021).

41. S. Q. Zhao, C. J. Xiao, T. Z. Liu, H. Chen, H. Zhang, M. J. Shi, S. Teng, H. S. Zhang, X. G. Wang, Z. Y. Pu, and M. Z. Liu, J. Geophys. Res.: Space Phys. **126**, 1 (2021).

42. R. Fitzpatrick and F. L. Waelbroeck, Phys Plasmas **12(2)**, (2005).

43. Jyoti, S. C. Sharma, and R. P. Sharma, Phys Plasmas **30(2)**, (2023).

44. J. Gazdag, J Comput Phys **20**, 196-207 (1976).

45. M. Colunga, J. F. Luciani, and P. Mora, Physics of Fluids **29**, 3407-3414 (1986).

46. S. Ichimaru., J. Plasma Phys. **13**, 324 (1975).

47. V. Fuchs, V. Krapchev, A. Ram, and A. Bers, Physica D **14**, 141-160 (1985).

48. N. H. Bian and P. K. Browning, Astrophys. J. **687**, L111 (2008).

49. M. V. Leonenko, E. E. Grigorenko, and L. M. Zelenyi, Geomagnetism and Aeronomy **61**, 688-695 (2021).

50. J. L. Burch, R. E. Ergun, P. A. Cassak, J. M. Webster, R. B. Torbert, B. L. Giles, J. C. Dorelli, A. C. Rager, K. J. Hwang, T. D. Phan, K. J. Genestreti, R. C. Allen, L. J. Chen, S. Wang, D. Gershman, O. Le Contel, C. T. Russell, R. J. Strangeway, F. D. Wilder, D. B. Graham, M. Hesse, J. F. Drake, M. Swisdak, L. M. Price, M. A. Shay, P. A. Lindqvist, C. J. Pollock, R. E. Denton, and D. L. Newman, Geophys Res Lett **45**, 1237-1245 (2018).

51. Vega, C., Roytershteyn, V., Delzanno, G. L., & Boldyrev, S., Monthly Notice of Royal Astronomical Society **524**, 1343-51, (2023).

CHAPTER-7

Summary, Conclusion and Future Scope

This chapter provides a summary of the conclusions derived from the current research and sheds light on potential future directions.

Turbulence illustrates the inherent characteristics of space and astrophysical plasma. The phenomenon under consideration encompasses a diverse array of fluctuations, including those related to field, velocity, and density. These fluctuations occur across a broad spectrum of length scales and temporal scales. Within the context of space plasma, a multitude of processes have been proposed to facilitate the transfer of energy from larger scales to smaller scales. Magnetic reconnection and turbulence are considered to be the primary factors for elucidating particle heating and acceleration phenomena. The association between magnetic reconnection occurrences and diverse plasma waves and turbulence is widely acknowledged in the scientific community. Various wave modes, such as whistler wave, kinetic alfven wave, lower hybrid wave, upper hybrid wave, magnetosonic wave, ion acoustic wave, electron acoustic wave, and electrostatic solitary wave, have been often seen in the Earth's magnetosphere. Hence, the establishment of a nonlinear wave-based model is crucial for elucidating the physics underlying the formation of turbulence in the magnetosphere region and reconnection locations inside the magnetosphere. The study conducted in Chapter 2 and Chapter 3 focuses on the amplification of beam driven whistler waves from background noise levels, resulting from the energy of the beam. This amplification is expected to reach a significant amplitude, leading to the emergence of nonlinear effects caused by the ponderomotive force. Consequently, these nonlinear effects are anticipated to induce the localization of whistler waves, ultimately leading to the development of a turbulent state. Also, fluctuations in whistler's electric field shows that it is turbulent in nature.

Moreover, to enhance comprehension of the physics behind the localization of whistler waves, a semianalytical model has been created. Furthermore, extensive research has been conducted on the simplified model to examine its convergent and divergent behavior in relation to whistler wave. The study's numerical results demonstrate the presence of whistler turbulence within the

magnetic reconnection sites generated by the electron beam. These outcomes also reveal the existence of localized structures and fluctuations associated with the whistler phenomenon.

Also, we have examined the generation of whistler coherent structures formation and later whistler turbulence generation at magnetic reconnection site due to the energetic electron beam (as observed by Magnetospheric Multiscale Mission (MMS)) along with the influence of magnetic island in chapter-3,4 & 5. Additionally, it was noticed that the power of the whistler wave has an impact on the scale size of coherent structures and the dimension of the current sheet. The transverse scale size of whistler's localized structures and the current sheet size have also been determined using a semianalytical model. In the present study, constant growth rate of beam-driven mode has been considered and, the quasi-steady state has not been achieved at this time and will not be achieved for further time also. So, we have examined the power-spectrum for quasi-steady state follows the Kolmogorov scaling. As a consequence of the wave's dispersive features, this power spectrum's steepening at smaller scales signifies energy transfer from larger to smaller length scales. This specific spectral index will promote the emergence of thermal tails of energetic particles which causes the acceleration of the particles. The results gained from the study are relevant to the observations made in the vicinity of the reconnection location in the magnetopause. Therefore, the examined wave interactions generate minor-scale fluctuations that are anticipated to induce particle heating and/or acceleration. The physical process responsible for turbulence in reconnection sites may be of significant interest.

The injection of energetic particles is well recognized as a crucial mechanism for the transport and dissipation of energy in the upper atmosphere. The phenomenon of energy release and its correlation with magnetic substorms has been a persistent challenge in the study of the Magnetopause. Still, the underlying principles of physics governing particle acceleration remain a subject of concern. In the future, it would be beneficial to investigate the potential interaction between whistler waves and other modes such as the lower hybrid mode, upper hybrid mode, and slow magnetosonic wave. This research could provide valuable insights into the formation of turbulence, plasmoids and the mechanisms involved in the release of energy at reconnection locations in the Earth's magnetopause.

APPENDIX

Appendix 2A: Dispersion relation of 2D whistler waves

Two fluid models are used to obtain the dynamical equation for whistler wave (2D plane) propagating in the x-z plane with wave vector $\vec{k} = k_x\hat{x} + k_z\hat{z}$, in a magnetized plasma with an ambient magnetic field along the z-axis.

The basic equations that are used to obtain the whistler dynamics are

Wave equation

$$\nabla^2\vec{E} - \nabla(\nabla.\vec{E}) = \frac{4\pi}{c^2}\frac{\partial\vec{J}}{\partial t} + \frac{1}{c^2}\frac{\partial^2\vec{E}}{\partial t^2}. \tag{2.A1}$$

Equation of motion for electrons

$$m_e\left[\frac{\partial\vec{v}_e}{\partial t} + (\vec{v}_e.\nabla\vec{v}_e)\right] = -e\vec{E} - \frac{e}{c}(\vec{v}_e\times\vec{B}_0). \tag{2.A2}$$

Equation of motion for ions

$$m_i\left[\frac{\partial\vec{v}_i}{\partial t} + (\vec{v}_i.\nabla\vec{v}_i)\right] = e\vec{E} + \frac{e}{c}(\vec{v}_i\times\vec{B}_0), \tag{2.A3}$$

Using Eqs. (2.A2), we obtain the velocity components of electrons as follows,

$$\frac{d\vec{v}_e}{dt} = \frac{\partial\vec{v}_e}{\partial t} + \vec{v}_e.(\vec{\nabla}\vec{v}_e) = \frac{-e\vec{E}}{m_e} - \frac{e}{m_e c}\vec{v}_e\times\vec{B}_0, \tag{2.A4}$$

Where $\vec{v}_e = \vec{v}_{e0} + \vec{v}_{e1}$

$\vec{v}_{e0} = 0 =$ No drift in equilibrium

$\vec{E} =$ perturbed electric field

$\vec{B} =$ perturbed magnetic field,

From eq. (2.A4) we obtain- $-i\omega_0\ \vec{v}_{e1} = \frac{-e\vec{E}}{m_e} - \frac{e}{m_e c}\vec{v}_{e1}\times\vec{B}_0$

Since $\vec{\omega}_{ce} = \frac{e\vec{B}_0}{m_e c}$, above eq. becomes

$$i\omega_0\ \vec{v}_{e1} = \frac{e\vec{E}}{m_e} + \vec{v}_{e1} \times \omega_{ce}\hat{z} \qquad \text{(2.A5)}$$

x -component of eq. (2.A5), $\quad i\omega_0\ \vec{v}_{e1x} = \frac{e\vec{E}_x}{m_e} + \vec{v}_{e1y}\omega_{ce}$ (2.A6)

y-component of eq. (2.A5), $\quad i\omega_0 \vec{v}_{e1y} = \frac{e\vec{E}_y}{m_e} - \vec{v}_{e1x}\omega_{ce}$

Or $\quad \vec{v}_{e1y} = \frac{e\vec{E}_y}{m_e i\omega_0} - \frac{\vec{v}_{e1x}\omega_{ce}}{i\omega_0}$ (2.A7)

Substituting eq. (2.A7) into eq. (2.A6), we obtain

$$v_{e1x} = \frac{-ie\omega_0}{m_e(\omega_0^2 - \omega_{ce}^2)} E_x - \frac{e\omega_{ce}}{m_e(\omega_0^2 - \omega_{ce}^2)} E_y. \qquad \text{(2.A8)}$$

Now substituting eq. (2.A8) in eq. (2.A7), we obtain

$$v_{e1y} = \frac{e\omega_{ce}}{m_e(\omega_0^2 - \omega_{ce}^2)} E_x - \frac{ie\omega_0}{m_e(\omega_0^2 - \omega_{ce}^2)} E_y. \qquad \text{(2.A9)}$$

z -component of eq. (2.A5), $\quad v_{e1z} = \frac{eE_z}{im_e\omega_0}.$ (2.A10)

Similarly, the velocity component of the whistler wave due to ion can be written as

$$v_{ix} = \frac{ie\omega_0}{m_i(\omega_0^2 - \omega_{ci}^2)} E_x - \frac{e\omega_{ci}}{m_i(\omega_0^2 - \omega_{ci}^2)} E_y. \qquad \text{(2.A11)}$$

$$v_{iy} = \frac{e\omega_{ci}}{m_i(\omega_0^2 - \omega_{ci}^2)} E_x + \frac{ie\omega_0}{m_i(\omega_0^2 - \omega_{ci}^2)} E_y. \qquad \text{(2.A12)}$$

$$v_{iz} = \frac{-eE_z}{im_i\omega_0}. \qquad \text{(2.A13)}$$

Now electron current density, $\vec{J}_{e1} = -n_e e\vec{v}_{e1}$, and x, y and z-component of current density due to electrons are given as follows,

$$J_{e1x} = n_e \frac{e^2}{m_e}\left(\frac{i\omega_0 E_x + \omega_{ce}E_y}{\omega_0^2 - \omega_{ce}^2}\right) \qquad \text{(2.A14)}$$

$$J_{e1y} = -n_e \frac{e^2}{m_e}\left(\frac{\omega_{ce}E_x - i\omega_0 E_y}{\omega_0^2 - \omega_{ce}^2}\right) \qquad \text{(2.A15)}$$

$$J_{e1z} = -n_e \frac{e^2 E_z}{m_e i\omega_0} \tag{2.A16}$$

Similarly, x, y and z-component of current density due to ions are given as follows,

$$J_{i1x} = n_i \frac{e^2}{m_i}\left(\frac{i\omega_0 E_x - \omega_{ci} E_y}{\omega_0^2 - \omega_{ci}^2}\right) \tag{2.A17}$$

$$J_{i1y} = -n_i \frac{e^2}{m_i}\left(\frac{-\omega_{ci} E_x - i\omega_0 E_y}{\omega_0^2 - \omega_{ci}^2}\right) \tag{2.A18}$$

$$J_{i1z} = -n_i \frac{e^2 E_z}{m_i i\omega_0} \tag{2.A19}$$

Now, from eq. (2.A1) we obtain the x, y and z components of wave equation,

x -component of wave equation, $\nabla^2 \vec{E}_x - \frac{\partial}{\partial x}(\nabla.\vec{E}) = \frac{4\pi}{c^2}\frac{\partial \vec{J}_x}{\partial t} + \frac{1}{c^2}\frac{\partial^2 \vec{E}_x}{\partial t^2}$.

Using equation of current density, $J_x = n_i e v_{i1x} - n_e e v_{e1x}$ in above equation, we obtain

$$\frac{\partial^2 \vec{E}_x}{\partial x^2} - \frac{\partial^2 E_z}{\partial x \partial z} = \frac{4\pi}{c^2}\frac{\partial (n_i e v_{i1x} - n_e e v_{e1x})}{\partial t} + \frac{1}{c^2}\frac{\partial^2 \vec{E}_x}{\partial t^2}.$$

Substituting the values v_{i1x} and v_{e1x} from (2.A8) and (2.A11), we obtain

$$\frac{\partial^2 \vec{E}_x}{\partial x^2} - \frac{\partial^2 E_z}{\partial x \partial z} = \frac{4\pi}{c^2}\frac{\partial}{\partial t}\left[\begin{array}{l} \dfrac{1}{\left(\omega_{ci}^2 + \dfrac{\partial^2}{\partial t^2}\right)}\left(\dfrac{e}{m_i}\dfrac{\partial E_x}{\partial t} + \dfrac{e\omega_{ci}}{m_i}E_y\right) \\ + \dfrac{1}{\left(\omega_{ce}^2 + \dfrac{\partial^2}{\partial t^2}\right)}\left(\dfrac{e}{m_e}\dfrac{\partial E_x}{\partial t} + \dfrac{e\omega_{ce}}{m_e}E_y\right) \end{array}\right] + \frac{1}{c^2}\frac{\partial^2 \vec{E}_x}{\partial t^2}, \tag{A20}$$

$$\left(\begin{array}{l} \dfrac{\partial^2}{\partial z^2} - \dfrac{1}{\lambda_i^2\left(\omega_{ci}^2 + \dfrac{\partial^2}{\partial t^2}\right)}\dfrac{\partial^2}{\partial t^2} \\ - \dfrac{1}{\lambda_e^2\left(\omega_{ce}^2 + \dfrac{\partial^2}{\partial t^2}\right)}\dfrac{\partial^2}{\partial t^2} - \dfrac{1}{c^2}\dfrac{\partial^2}{\partial t^2} \end{array}\right) E_x - \frac{\partial^2 E_z}{\partial x \partial z} - \left(\begin{array}{l} \dfrac{\omega_{ci}}{\lambda_i^2\left(\omega_{ci}^2 + \dfrac{\partial^2}{\partial t^2}\right)}\dfrac{\partial}{\partial t} \\ + \dfrac{\omega_{ce}}{\lambda_e^2\left(\omega_{ce}^2 + \dfrac{\partial^2}{\partial t^2}\right)}\dfrac{\partial}{\partial t} \end{array}\right) E_y = 0 \tag{2.A21}$$

y-component of wave equation,

$$\left(\begin{array}{l} \dfrac{\omega_{ci}}{\lambda_i^2\left(\omega_{ci}^2 + \dfrac{\partial^2}{\partial t^2}\right)}\dfrac{\partial}{\partial t} - \\ \dfrac{\omega_{ce}}{\lambda_e^2\left(\omega_{ce}^2 + \dfrac{\partial^2}{\partial t^2}\right)}\dfrac{\partial}{\partial t} \end{array}\right) E_x + \left(\begin{array}{l} \dfrac{\partial^2}{\partial x^2} + \dfrac{\partial^2}{\partial z^2} - \dfrac{1}{\lambda_i^2\left(\omega_{ci}^2 + \dfrac{\partial^2}{\partial t^2}\right)}\dfrac{\partial^2}{\partial t^2} - \\ \dfrac{1}{\lambda_e^2\left(\omega_{ce}^2 + \dfrac{\partial^2}{\partial t^2}\right)}\dfrac{\partial^2}{\partial t^2} - \dfrac{1}{c^2}\dfrac{\partial^2}{\partial t^2} \end{array}\right) E_y = 0. \tag{2.A22}$$

z -component of wave equation,

$$\left(\frac{\partial^2}{\partial x^2}-\frac{1}{c^2}\frac{\partial^2}{\partial t^2}-\frac{1}{\lambda_e^2}\right)E_z-\frac{\partial^2}{\partial x\partial z}E_x=0. \tag{2.A23}$$

From these linear relationship we have,

$$E_y=-\begin{pmatrix}\dfrac{\omega_{ci}}{\lambda_i^2\left(\omega_{ci}^2+\dfrac{\partial^2}{\partial t^2}\right)}\dfrac{\partial}{\partial t}-\\ \dfrac{\omega_{ce}}{\lambda_e^2\left(\omega_{ce}^2+\dfrac{\partial^2}{\partial t^2}\right)}\dfrac{\partial}{\partial t}\end{pmatrix}\begin{pmatrix}\dfrac{\partial^2}{\partial x^2}+\dfrac{\partial^2}{\partial z^2}-\dfrac{1}{\lambda_i^2\left(\omega_{ci}^2+\dfrac{\partial^2}{\partial t^2}\right)}\dfrac{\partial^2}{\partial t^2}-\\ \dfrac{1}{\lambda_e^2\left(\omega_{ce}^2+\dfrac{\partial^2}{\partial t^2}\right)}\dfrac{\partial^2}{\partial t^2}-\dfrac{1}{c^2}\dfrac{\partial^2}{\partial t^2}\end{pmatrix}^{-1}E_x$$

$$E_z=\frac{\partial^2}{\partial x\partial z}\left(\frac{\partial^2}{\partial x^2}-\frac{1}{c^2}\frac{\partial^2}{\partial t^2}-\frac{1}{\lambda_e^2}\right)^{-1}E_x$$

Combining Eqs. (2.A21)-(2.A23), with assumptions $k\lambda_i >> 1$ and neglecting displacement current, we obtain

$$\left(\frac{\partial^2}{\partial z^2}-\frac{1}{\lambda_i^2}-\frac{1}{\lambda_e^2\left(\omega_{ce}^2+\dfrac{\partial^2}{\partial t^2}\right)}\frac{\partial^2}{\partial t^2}\right)\left(\frac{\partial^2}{\partial x^2}+\frac{\partial^2}{\partial z^2}-\frac{1}{\lambda_e^2\left(\omega_{ce}^2+\dfrac{\partial^2}{\partial t^2}\right)}\frac{\partial^2}{\partial t^2}\right)\left(\frac{\partial^2}{\partial x^2}-\frac{1}{\lambda_e^2}\right)E_x$$
$$-\left(\frac{-\omega_{ci}}{\lambda_i^2\dfrac{\partial}{\partial t}}+\frac{\omega_{ce}}{\lambda_e^2\left(\omega_{ce}^2+\dfrac{\partial^2}{\partial t^2}\right)}\frac{\partial}{\partial t}\right)\left(\frac{\omega_{ci}}{\lambda_i^2\dfrac{\partial}{\partial t}}-\frac{\omega_{ce}}{\lambda_e^2\left(\omega_{ce}^2+\dfrac{\partial^2}{\partial t^2}\right)}\frac{\partial}{\partial t}\right)\left(\frac{\partial^2}{\partial x^2}-\frac{1}{\lambda_e^2}\right)E_x$$
$$+\left(\frac{\partial^2}{\partial x^2}+\frac{\partial^2}{\partial z^2}-\frac{1}{\lambda_e^2\left(\omega_{ce}^2+\dfrac{\partial^2}{\partial t^2}\right)}\frac{\partial^2}{\partial t^2}\right)\frac{\partial^4 E_x}{\partial x^2\partial z^2}=0.$$

Or,

$$-\left(\frac{\partial^2}{\partial x^2}+\frac{\partial^2}{\partial z^2}-\frac{1}{\lambda_e^2\left(\omega_{ce}^2+\dfrac{\partial^2}{\partial t^2}\right)}\frac{\partial^2}{\partial t^2}\right)\begin{bmatrix}\dfrac{\partial^4}{\partial x^2\partial z^2}-\dfrac{\omega_{ce}^2\lambda_e^2\left(1-\lambda_i^2\dfrac{\partial^2}{\partial z^2}\right)\left(1-\lambda_e^2\dfrac{\partial^2}{\partial x^2}\right)}{\lambda_e^4\lambda_i^2\left(\omega_{ce}^2+\dfrac{\partial^2}{\partial t^2}\right)}-\\ \dfrac{\lambda_i^2\left(1-\lambda_i^2\dfrac{\partial^2}{\partial z^2}\right)\left(1-\lambda_e^2\dfrac{\partial^2}{\partial x^2}\right)}{\lambda_e^4\lambda_i^2\left(\omega_{ce}^2+\dfrac{\partial^2}{\partial t^2}\right)}\dfrac{\partial^2}{\partial t^2}\end{bmatrix}E_x$$
$$+\frac{\omega_{ce}^2\left(1-\lambda_e^2\dfrac{\partial^2}{\partial x^2}\right)}{\lambda_e^6\left(\omega_{ce}^2+\dfrac{\partial^2}{\partial t^2}\right)^2}\frac{\partial^2 E_x}{\partial z^2}=0.$$

On solving above equation, we obtain

$$\frac{-\lambda_e^2\lambda_i^2\omega_{ce}^2\left(\frac{\partial^2}{\partial x^2}+\frac{\partial^2}{\partial z^2}\right)\left(1-\lambda_e^2\left(\frac{\partial^2}{\partial x^2}+\frac{\partial^2}{\partial z^2}\right)\right)\frac{\partial^2 E_x}{\partial t^2}-\lambda_e^4\omega_{ce}^2\left(1-\lambda_e^2\frac{\partial^2}{\partial x^2}-\lambda_i^2\frac{\partial^2}{\partial z^2}\right)\left(\frac{\partial^2}{\partial x^2}+\frac{\partial^2}{\partial z^2}\right)}{\lambda_e^6\lambda_i^2\left(\omega_{ce}^2+\frac{\partial^2}{\partial t^2}\right)^2}$$

$$+\frac{\lambda_i^2\left(1-\lambda_e^2\left(\frac{\partial^2}{\partial x^2}+\frac{\partial^2}{\partial z^2}\right)\right)^2\frac{\partial^4 E_x}{\partial t^4}+\omega_{ce}^2\lambda_e^2\left(1-\lambda_e^2\left(\frac{\partial^2}{\partial x^2}+\frac{\partial^2}{\partial z^2}\right)\right)\left(1-\lambda_e^2\frac{\partial^2}{\partial x^2}-\lambda_i^2\frac{\partial^2}{\partial z^2}\right)\frac{\partial^2 E_x}{\partial t^2}+\omega_{ce}^2\lambda_i^2\left(1-\lambda_e^2\frac{\partial^2}{\partial x^2}\right)\frac{\partial^2 E_x}{\partial t^2}}{\lambda_e^6\lambda_i^2\left(\omega_{ce}^2+\frac{\partial^2}{\partial t^2}\right)^2}=0$$

or

$$-\lambda_e^2\omega_{ce}^2\left(\frac{\partial^2}{\partial x^2}+\frac{\partial^2}{\partial z^2}\right)\left(1-\lambda_e^2\left(\frac{\partial^2}{\partial x^2}+\frac{\partial^2}{\partial z^2}\right)\right)\frac{\partial^2 E_x}{\partial t^2}-\lambda_e^2\omega_{ce}^3\omega_{ci}\left(1-\lambda_e^2\frac{\partial^2}{\partial x^2}-\lambda_i^2\frac{\partial^2}{\partial z^2}\right)\left(\frac{\partial^2}{\partial x^2}+\frac{\partial^2}{\partial z^2}\right)$$
$$+\lambda_i^2\left(1-\lambda_e^2\left(\frac{\partial^2}{\partial x^2}+\frac{\partial^2}{\partial z^2}\right)\right)^2\frac{\partial^4 E_x}{\partial t^4}+\omega_{ce}\omega_{ci}\left(1-\lambda_e^2\left(\frac{\partial^2}{\partial x^2}+\frac{\partial^2}{\partial z^2}\right)\right)\left(1-\lambda_e^2\frac{\partial^2}{\partial x^2}-\lambda_i^2\frac{\partial^2}{\partial z^2}\right)\frac{\partial^2 E_x}{\partial t^2}$$
$$+\omega_{ce}^2\left(1-\lambda_e^2\frac{\partial^2}{\partial x^2}\right)\frac{\partial^2 E_x}{\partial t^2}=0$$

or

$$\left(-\frac{\partial^2}{\partial t^2}-\omega_{ce}^2\right)\left[-\left(1-\lambda_e^2\left(\frac{\partial^2}{\partial x^2}+\frac{\partial^2}{\partial z^2}\right)\right)^2\frac{\partial^2 E_x}{\partial t^2}-\lambda_i^2 v_A^2\left(\frac{\partial^2}{\partial x^2}+\frac{\partial^2}{\partial z^2}\right)\frac{\partial^2 E_x}{\partial z^2}\right.$$
$$\left.+\omega_{ce}\omega_{ci}\lambda_e^2\left(1-\lambda_e^2\frac{\partial^2}{\partial x^2}\right)\left(\frac{\partial^2 E_x}{\partial x^2}+\frac{\partial^2 E_x}{\partial z^2}\right)\right]=0. \qquad (2.A24)$$

Using the conditions $-\frac{\partial^2}{\partial t^2}>\omega_{ce}\omega_{ci}$, we obtain

$$\left(-\frac{\partial^2}{\partial t^2}-\omega_{ce}^2\right)\left[-\left(1-\lambda_e^2\left(\frac{\partial^2}{\partial x^2}+\frac{\partial^2}{\partial z^2}\right)\right)^2\frac{\partial^2 E_x}{\partial t^2}-\lambda_i^2 v_A^2\left(\frac{\partial^2}{\partial x^2}+\frac{\partial^2}{\partial z^2}\right)\frac{\partial^2 E_x}{\partial z^2}\right]=0. \qquad (2.A25)$$

From Eq. (2.A25), the dynamical equation of whistler wave can be written as

$$\frac{-\partial^2 E_x}{\partial t^2}-\lambda_e^4\frac{\partial^6 E_x}{\partial x^4\partial t^2}-\lambda_e^4\frac{\partial^6 E_x}{\partial z^4\partial t^2}-2\lambda_e^4\frac{\partial^6 E_x}{\partial x^2\partial z^2\partial t^2}$$
$$+2\lambda_e^2\frac{\partial^4 E_x}{\partial x^2\partial t^2}+2\lambda_e^2\frac{\partial^4 E_x}{\partial z^2\partial t^2}=\lambda_i^2 v_A^2\left(\frac{\partial^4 E_x}{\partial z^2\partial x^2}+\frac{\partial^4 E_x}{\partial z^4}\right). \qquad (2.A26)$$

Moreover, this is the same equation as given in eq. (2.9) in the manuscript. It is also mentioned here that beam driven growth is also considered then from equation of motion,

$$m\frac{dv}{dt}=-eE-mv\gamma \qquad \rightarrow\frac{dv}{dt}=-\frac{eE}{m}-v\gamma$$
$$(-i\omega+\gamma)=-\frac{eE}{mv} \qquad \rightarrow\frac{d}{dt}=\left(\frac{d}{dt}+\gamma\right)$$

$\frac{d^2}{dt^2}=\left(\frac{d^2}{dt^2}+2\gamma\frac{d}{dt}\right)$, neglecting higher order terms.

Appendix 3A: Dispersion relation of 2D whistler waves

The whistler wave dynamical equation is obtained using a two-fluid model. The whistler wave is propagating in a magnetized plasma with the magnetic field along the z-axis and wave vector, $\vec{k} = k_{0x}\hat{x} + k_{0z}\hat{z}$. Here, $B\,(=B_0+\delta B)$ is the magnetic field, B_0 the background magnetic field, and δB the perturbation in the magnetic field.

To determine the whistler dynamics, the following basic equations are used:

Wave equation

$$\nabla^2\vec{E} - \nabla(\nabla.\vec{E}) = \frac{4\pi}{c^2}\frac{\partial\vec{J}}{\partial t} + \frac{1}{c^2}\frac{\partial^2\vec{E}}{\partial t^2}. \tag{3.A1}$$

Equation of motion for electrons

$$m_e\left[\frac{\partial\vec{v}_e}{\partial t} + (\vec{v}_e.\nabla\vec{v}_e)\right] = -e\vec{E} - \frac{e}{c}\left[\vec{v}_e\times(\vec{B}_0+\delta B)\right]. \tag{3.A2}$$

Equation of motion for ions

$$m_i\left[\frac{\partial\vec{v}_i}{\partial t} + (\vec{v}_i.\nabla\vec{v}_i)\right] = e\vec{E} + \frac{e}{c}\left[\vec{v}_i\times(\vec{B}_0+\delta B)\right], \tag{3.A3}$$

Using Eqs. (3.A2), we obtain the velocity components of electrons as follows,

$$\frac{d\vec{v}_e}{dt} = \frac{\partial\vec{v}_e}{\partial t} + \vec{v}_e.(\vec{\nabla}\vec{v}_e) = \frac{-e\vec{E}}{m_e} - \frac{e}{m_e c}(\vec{v}_e\times\vec{B}_0) - \frac{e}{m_e c}(\vec{v}_e\times\vec{B}_0)\frac{\delta B}{B_0}, \tag{3.A4}$$

Where $\vec{v}_e = \vec{v}_{e0} + \vec{v}_{e1}$

$\vec{v}_{e0}$ =0=No drift in equilibrium

$\vec{B}$ and $\vec{E}$ represents the perturbed magnetic field and electric field respectively.

From eq. (3.A4) we obtain- $-i\omega_0\ \vec{v}_{e1} = \frac{-e\vec{E}}{m_e} - \frac{e}{m_e c}(\vec{v}_{e1}\times\vec{B}_0) - \frac{e}{m_e c}(\vec{v}_{e1}\times\vec{B}_0)\frac{\delta B}{B_0}$

Since $\vec{\omega}_{ce} = \frac{e\vec{B}_0}{m_e c}$, above eq. becomes

$$i\omega_0\ \vec{v}_{e1} = \frac{e\vec{E}}{m_e} + (\vec{v}_{e1}\times\omega_{ce}\hat{z}) + (\vec{v}_{e1}\times\omega_{ce}\hat{z})\frac{\delta B}{B_0} \tag{3.A5}$$

x -component of Eq. (3.A5), $$i\omega_0 \vec{v}_{e1x} = \frac{e\vec{E}_x}{m_e} + \vec{v}_{e1y}\omega_{ce}\left(1+\frac{\delta B}{B_0}\right) \tag{3.A6}$$

y -component of Eq. (3.A5), $$i\omega_0 \vec{v}_{e1y} = \frac{e\vec{E}_y}{m_e} - \vec{v}_{e1x}\omega_{ce}\left(1+\frac{\delta B}{B_0}\right)$$

Or $$\vec{v}_{e1y} = \frac{e\vec{E}_y}{m_e i\omega_0} - \frac{\vec{v}_{e1x}\omega_{ce}}{i\omega_0}\left(1+\frac{\delta B}{B_0}\right) \tag{3.A7}$$

We obtain Eq. (3.A8) by using Eq. (3.A7) into Eq. (3.A6),

$$v_{e1x} = \frac{-e(i\omega_0 E_x + \omega_{ce}E_y)}{m_e(\omega_0^2-\omega_{ce}^2)} - \frac{e\omega_0 E_y}{m_e(\omega_0^2-\omega_{ce}^2)}\frac{\delta B}{B_0} \tag{3.A8}$$

Now substituting Eq. (3.A8) in Eq. (3.A7), we obtain

$$v_{e1y} = \frac{e(\omega_{ce}E_x - i\omega_0 E_y)}{m_e(\omega_0^2-\omega_{ce}^2)} + \frac{e\omega_0 E_y}{m_e(\omega_0^2-\omega_{ce}^2)}\frac{\delta B}{B_0}. \tag{3.A9}$$

z -component of eq. (3.A5), $$v_{e1z} = \frac{eE_z}{im_e\omega_0}. \tag{3.A10}$$

Similarly, the velocity component of ions can be expressed as

$$v_{ix} = \frac{e(i\omega_0 E_x - \omega_{ci}E_y)}{m_i(\omega_0^2-\omega_{ci}^2)} - \frac{e\omega_0 E_y}{m_i(\omega_0^2-\omega_{ci}^2)}\frac{\delta B_0}{B_0}. \tag{3.A11}$$

$$v_{iy} = \frac{e(\omega_{ci}E_x + i\omega_0 E_y)}{m_i(\omega_0^2-\omega_{ci}^2)}E_x + \frac{e\omega_0 E_y}{m_i(\omega_0^2-\omega_{ci}^2)}\frac{\delta B_0}{B_0}. \tag{3.A12}$$

$$v_{iz} = \frac{-eE_z}{im_i\omega_0}. \tag{3.A13}$$

Now electron current density, $\vec{J}_{e1} = -n_e e\vec{v}_{e1}$, and x, y, and z-component of current density due to electrons are-

$$J_{e1x} = n_e\frac{e^2}{m_e}\left(\frac{i\omega_0 E_x + \omega_{ce}E_y}{\omega_0^2-\omega_{ce}^2}\right) + \frac{n_e e^2\omega_0 E_y}{m_e(\omega_0^2-\omega_{ce}^2)}\frac{\delta B}{B_0} \tag{3.A14}$$

$$J_{e1y} = -n_e\frac{e^2}{m_e}\left(\frac{\omega_{ce}E_x - i\omega_0 E_y}{\omega_0^2-\omega_{ce}^2}\right) - \frac{n_e e^2\omega_0 E_y}{m_e(\omega_0^2-\omega_{ce}^2)}\frac{\delta B}{B_0}. \tag{3.A15}$$

$$J_{e1z} = -n_e\frac{e^2 E_z}{m_e i\omega_0} \tag{3.A16}$$

Similarly, x, y, and z-component of current density due to ions are-

$$J_{i1x} = n_i \frac{e^2}{m_i}\left(\frac{i\omega_0 E_x - \omega_{ci} E_y}{\omega_0^2 - \omega_{ci}^2}\right) - \frac{n_i e^2 \omega_0 E_y}{m_i(\omega_0^2 - \omega_{ci}^2)}\frac{\delta B_0}{B_0}. \tag{3.A17}$$

$$J_{i1y} = -n_i \frac{e^2}{m_i}\left(\frac{-\omega_{ci} E_x - i\omega_0 E_y}{\omega_0^2 - \omega_{ci}^2}\right) - \frac{n_i e^2 \omega_0 E_y}{m_i(\omega_0^2 - \omega_{ci}^2)}\frac{\delta B_0}{B_0}. \tag{3.A18}$$

$$J_{i1z} = -n_i \frac{e^2 E_z}{m_i i\omega_0} \tag{3.A19}$$

Now, from eq. (3.A1) we obtain the x, y, and z components of wave equation,

x -component of wave equation, $\nabla^2 \vec{E}_x - \frac{\partial}{\partial x}(\nabla.\vec{E}) = \frac{4\pi}{c^2}\frac{\partial \vec{J}_x}{\partial t} + \frac{1}{c^2}\frac{\partial^2 \vec{E}_x}{\partial t^2}$.

Using equation of current density, $J_x = n_i e v_{i1x} - n_e e v_{e1x}$ in the above equation, we obtain

$$\frac{\partial^2 \vec{E}_x}{\partial x^2} - \frac{\partial^2 E_z}{\partial x \partial z} = \frac{4\pi}{c^2}\frac{\partial (n_i e v_{i1x} - n_e e v_{e1x})}{\partial t} + \frac{1}{c^2}\frac{\partial^2 \vec{E}_x}{\partial t^2}.$$

Substituting the values v_{i1x} and v_{e1x} from (3.A8) and (3.A11), we obtain

$$\frac{\partial^2 \vec{E}_x}{\partial x^2} - \frac{\partial^2 E_z}{\partial x \partial z} = \frac{4\pi}{c^2}\frac{\partial}{\partial t}\left[\begin{array}{l} \dfrac{1}{\left(\omega_{ci}^2 + \dfrac{\partial^2}{\partial t^2}\right)}\left(\dfrac{e}{m_i}\dfrac{\partial E_x}{\partial t} + \dfrac{e\omega_{ci}}{m_i}E_y\right) \\ + \dfrac{1}{\left(\omega_{ce}^2 + \dfrac{\partial^2}{\partial t^2}\right)}\left(\dfrac{e}{m_e}\dfrac{\partial E_x}{\partial t} + \dfrac{e\omega_{ce}}{m_e}E_y\right) \end{array}\right] + \frac{1}{c^2}\frac{\partial^2 \vec{E}_x}{\partial t^2}, \tag{3.A20}$$

Or,

$$\left(\begin{array}{l} \dfrac{\partial^2}{\partial z^2} - \dfrac{1}{\lambda_i^2\left(\omega_{ci}^2 + \dfrac{\partial^2}{\partial t^2}\right)}\dfrac{\partial^2}{\partial t^2} \\ - \dfrac{1}{\lambda_e^2\left(\omega_{ce}^2 + \dfrac{\partial^2}{\partial t^2}\right)}\dfrac{\partial^2}{\partial t^2} - \dfrac{1}{c^2}\dfrac{\partial^2}{\partial t^2} \end{array}\right) E_x - \left(\begin{array}{l} \dfrac{\omega_{ci}}{\lambda_i^2\left(\omega_{ci}^2 + \dfrac{\partial^2}{\partial t^2}\right)}\dfrac{\partial}{\partial t} + \dfrac{\omega_{ce}}{\lambda_e^2\left(\omega_{ce}^2 + \dfrac{\partial^2}{\partial t^2}\right)}\dfrac{\partial}{\partial t} \\ - \left(\dfrac{1}{\lambda_e^2\left(\omega_{ce}^2 + \dfrac{\partial^2}{\partial t^2}\right)}\dfrac{\partial}{\partial t} + \dfrac{1}{\lambda_i^2\left(\omega_{ci}^2 + \dfrac{\partial^2}{\partial t^2}\right)}\dfrac{\partial}{\partial t}\right)\dfrac{\delta B}{B_0} \end{array}\right) E_y \tag{3.A21}$$

$$-\frac{\partial^2 E_z}{\partial x \partial z} = 0$$

y -component of wave equation,

$$\left(\begin{array}{c}\dfrac{\omega_{ci}}{\lambda_i^2\left(\omega_{ci}^2+\dfrac{\partial^2}{\partial t^2}\right)}\dfrac{\partial}{\partial t}- \\ \dfrac{\omega_{ce}}{\lambda_e^2\left(\omega_{ce}^2+\dfrac{\partial^2}{\partial t^2}\right)}\dfrac{\partial}{\partial t}\end{array}\right)E_x+\left(\begin{array}{c}\dfrac{\partial^2}{\partial x^2}+\dfrac{\partial^2}{\partial z^2}-\dfrac{1}{\lambda_i^2\left(\omega_{ci}^2+\dfrac{\partial^2}{\partial t^2}\right)}\dfrac{\partial^2}{\partial t^2}-\dfrac{1}{\lambda_e^2\left(\omega_{ce}^2+\dfrac{\partial^2}{\partial t^2}\right)}\dfrac{\partial^2}{\partial t^2} \\ -\dfrac{1}{c^2}\dfrac{\partial^2}{\partial t^2}+\left(\dfrac{1}{\lambda_e^2\left(\omega_{ce}^2+\dfrac{\partial^2}{\partial t^2}\right)}\dfrac{\partial}{\partial t}+\dfrac{1}{\lambda_i^2\left(\omega_{ci}^2+\dfrac{\partial^2}{\partial t^2}\right)}\dfrac{\partial}{\partial t}\right)\dfrac{\delta B}{B_0}\end{array}\right)E_y=0. \tag{3.A22}$$

z -component of wave equation,

$$\left(\frac{\partial^2}{\partial x^2}-\frac{1}{c^2}\frac{\partial^2}{\partial t^2}-\frac{1}{\lambda_e^2}\right)E_z-\frac{\partial^2}{\partial x\partial z}E_x=0. \tag{3.A23}$$

From these linear relationships we have,

$$E_y=-\left(\begin{array}{c}\dfrac{\omega_{ci}}{\lambda_i^2\left(\omega_{ci}^2+\dfrac{\partial^2}{\partial t^2}\right)}\dfrac{\partial}{\partial t}- \\ \dfrac{\omega_{ce}}{\lambda_e^2\left(\omega_{ce}^2+\dfrac{\partial^2}{\partial t^2}\right)}\dfrac{\partial}{\partial t}\end{array}\right)\left(\begin{array}{c}\dfrac{\partial^2}{\partial x^2}+\dfrac{\partial^2}{\partial z^2}-\dfrac{1}{\lambda_i^2\left(\omega_{ci}^2+\dfrac{\partial^2}{\partial t^2}\right)}\dfrac{\partial^2}{\partial t^2}-\dfrac{1}{\lambda_e^2\left(\omega_{ce}^2+\dfrac{\partial^2}{\partial t^2}\right)}\dfrac{\partial^2}{\partial t^2}- \\ \dfrac{1}{c^2}\dfrac{\partial^2}{\partial t^2}+\left(\dfrac{1}{\lambda_e^2\left(\omega_{ce}^2+\dfrac{\partial^2}{\partial t^2}\right)}\dfrac{\partial}{\partial t}+\dfrac{1}{\lambda_i^2\left(\omega_{ci}^2+\dfrac{\partial^2}{\partial t^2}\right)}\dfrac{\partial}{\partial t}\right)\dfrac{\delta B}{B_0}\end{array}\right)^{-1}E_x$$

$$E_z=\frac{\partial^2}{\partial x\partial z}\left(\frac{\partial^2}{\partial x^2}-\frac{1}{c^2}\frac{\partial^2}{\partial t^2}-\frac{1}{\lambda_e^2}\right)^{-1}E_x$$

Combining Eqs. (A21)-(A23), by assumptions $k\lambda_i \gg 1$ and neglecting displacement current, we obtain

$$\left(\frac{\partial^2}{\partial z^2}-\frac{1}{\lambda_i^2}-\frac{1}{\lambda_e^2\left(\omega_{ce}^2+\dfrac{\partial^2}{\partial t^2}\right)}\frac{\partial^2}{\partial t^2}\right)\left(\frac{\partial^2}{\partial x^2}+\frac{\partial^2}{\partial z^2}-\frac{1}{\lambda_e^2\left(\omega_{ce}^2+\dfrac{\partial^2}{\partial t^2}\right)}\frac{\partial^2}{\partial t^2}+\frac{1}{\lambda_e^2\left(\omega_{ce}^2+\dfrac{\partial^2}{\partial t^2}\right)}\frac{\partial}{\partial t}\frac{\delta B}{B_0}\right)\left(\frac{\partial^2}{\partial x^2}-\frac{1}{\lambda_e^2}\right)E_x$$

$$-\left(\frac{-\omega_{ci}}{\lambda_i^2}\frac{\partial}{\partial t}+\frac{\omega_{ce}}{\lambda_e^2\left(\omega_{ce}^2+\dfrac{\partial^2}{\partial t^2}\right)}\frac{\partial}{\partial t}+\frac{1}{\lambda_e^2\left(\omega_{ce}^2+\dfrac{\partial^2}{\partial t^2}\right)}\frac{\partial}{\partial t}\frac{\delta B}{B_0}\right)\left(\frac{\omega_{ci}}{\lambda_i^2}\frac{\partial}{\partial t}-\frac{\omega_{ce}}{\lambda_e^2\left(\omega_{ce}^2+\dfrac{\partial^2}{\partial t^2}\right)}\frac{\partial}{\partial t}\right)\left(\frac{\partial^2}{\partial x^2}-\frac{1}{\lambda_e^2}\right)E_x$$

$$+\left(\frac{\partial^2}{\partial x^2}+\frac{\partial^2}{\partial z^2}-\frac{1}{\lambda_e^2\left(\omega_{ce}^2+\dfrac{\partial^2}{\partial t^2}\right)}\frac{\partial^2}{\partial t^2}+\frac{1}{\lambda_e^2\left(\omega_{ce}^2+\dfrac{\partial^2}{\partial t^2}\right)}\frac{\partial}{\partial t}\frac{\delta B}{B_0}\right)\frac{\partial^4 E_x}{\partial x^2\partial z^2}=0.$$

On solving above equation, we obtain

$$\frac{-\lambda_e^2\lambda_i^2\omega_{ce}^2\left(\frac{\partial^2}{\partial x^2}+\frac{\partial^2}{\partial z^2}\right)\left(1-\lambda_e^2\left(\frac{\partial^2}{\partial x^2}+\frac{\partial^2}{\partial z^2}\right)\left(1+\frac{\delta B}{B_0}\right)\right)\frac{\partial^2 E_x}{\partial t^2}-\lambda_e^4\omega_{ce}^2\left(1-\lambda_e^2\frac{\partial^2}{\partial x^2}-\lambda_i^2\frac{\partial^2}{\partial z^2}\right)\left(\frac{\partial^2}{\partial x^2}+\frac{\partial^2}{\partial z^2}\right)}{\lambda_e^6\lambda_i^2\left(\omega_{ce}^2+\frac{\partial^2}{\partial t^2}\right)^2}$$

$$+\frac{\lambda_i^2\left(1-\lambda_e^2\left(\frac{\partial^2}{\partial x^2}+\frac{\partial^2}{\partial z^2}\right)\right)^2\frac{\partial^4 E_x}{\partial t^4}+\omega_{ce}^2\lambda_e^2\left(1-\lambda_e^2\left(\frac{\partial^2}{\partial x^2}+\frac{\partial^2}{\partial z^2}\right)\right)\left(1-\lambda_e^2\frac{\partial^2}{\partial x^2}-\lambda_i^2\frac{\partial^2}{\partial z^2}\right)\frac{\partial^2 E_x}{\partial t^2}+\omega_{ce}^2\lambda_i^2\left(1-\lambda_e^2\frac{\partial^2}{\partial x^2}\right)\frac{\partial^2 E_x}{\partial t^2}}{\lambda_e^6\lambda_i^2\left(\omega_{ce}^2+\frac{\partial^2}{\partial t^2}\right)^2}=0$$

or

$$-\lambda_e^2\omega_{ce}^2\left(\frac{\partial^2}{\partial x^2}+\frac{\partial^2}{\partial z^2}\right)\left(1-\lambda_e^2\left(\frac{\partial^2}{\partial x^2}+\frac{\partial^2}{\partial z^2}\right)\left(1+\frac{\delta B}{B_0}\right)\right)\frac{\partial^2 E_x}{\partial t^2}-\lambda_e^2\omega_{ce}^3\omega_{ci}\left(1-\lambda_e^2\frac{\partial^2}{\partial x^2}-\lambda_i^2\frac{\partial^2}{\partial z^2}\right)\left(\frac{\partial^2}{\partial x^2}+\frac{\partial^2}{\partial z^2}\right)$$
$$+\lambda_i^2\left(1-\lambda_e^2\left(\frac{\partial^2}{\partial x^2}+\frac{\partial^2}{\partial z^2}\right)\right)^2\frac{\partial^4 E_x}{\partial t^4}+\omega_{ce}\omega_{ci}\left(1-\lambda_e^2\left(\frac{\partial^2}{\partial x^2}+\frac{\partial^2}{\partial z^2}\right)\right)\left(1-\lambda_e^2\frac{\partial^2}{\partial x^2}-\lambda_i^2\frac{\partial^2}{\partial z^2}\right)\frac{\partial^2 E_x}{\partial t^2}$$
$$+\omega_{ce}^2\left(1-\lambda_e^2\frac{\partial^2}{\partial x^2}\right)\frac{\partial^2 E_x}{\partial t^2}=0$$

or

$$\left(-\frac{\partial^2}{\partial t^2}-\omega_{ce}^2\right)\left[\begin{array}{l}-\left(1-\lambda_e^2\left(\frac{\partial^2}{\partial x^2}+\frac{\partial^2}{\partial z^2}\right)\right)^2\frac{\partial^2 E_x}{\partial t^2}-\lambda_i^2 v_A^2\left(\frac{\partial^2}{\partial x^2}+\frac{\partial^2}{\partial z^2}\right)\frac{\partial^2 E_x}{\partial z^2}\\ \left(1+\frac{\delta B}{B_0}\right)+\omega_{ce}\omega_{ci}\lambda_e^2\left(1-\lambda_e^2\frac{\partial^2}{\partial x^2}\right)\left(\frac{\partial^2 E_x}{\partial x^2}+\frac{\partial^2 E_x}{\partial z^2}\right)\end{array}\right]=0. \qquad (3.A24)$$

Using the conditions $-\frac{\partial^2}{\partial t^2}>\omega_{ce}\omega_{ci}$, we obtain

$$\left(-\frac{\partial^2}{\partial t^2}-\omega_{ce}^2\right)\left[-\left(1-\lambda_e^2\left(\frac{\partial^2}{\partial x^2}+\frac{\partial^2}{\partial z^2}\right)\right)^2\frac{\partial^2 E_x}{\partial t^2}-\lambda_i^2 v_A^2\left(\frac{\partial^2}{\partial x^2}+\frac{\partial^2}{\partial z^2}\right)\left(1+\frac{\delta B}{B_0}\right)\frac{\partial^2 E_x}{\partial z^2}\right]=0. \qquad (3.A25)$$

From Eq. (3.A25), The whistler wave's dynamical equation is expressed as

$$\begin{aligned}&\frac{-\partial^2 E_x}{\partial t^2}-\lambda_e^4\frac{\partial^6 E_x}{\partial x^4\partial t^2}-\lambda_e^4\frac{\partial^6 E_x}{\partial z^4\partial t^2}-2\lambda_e^4\frac{\partial^6 E_x}{\partial x^2\partial z^2\partial t^2}\\&\quad+2\lambda_e^2\frac{\partial^4 E_x}{\partial x^2\partial t^2}+2\lambda_e^2\frac{\partial^4 E_x}{\partial z^2\partial t^2}=\lambda_i^2 v_A^2\left(\frac{\partial^4 E_x}{\partial z^2\partial x^2}+\frac{\partial^4 E_x}{\partial z^4}\right)\left(1+\frac{\delta B}{B_0}\right).\end{aligned} \qquad (3.A26)$$

APPENDIX 4A: DISPERSION RELATION OF 3D WHISTLER WAVE

The dynamical equation for a 3D whistler wave with an ambient magnetic field along the z-axis in a magnetized plasma propagating in the x, y, and z planes with a wave vector $\vec{k} = k_x\hat{x} + k_y\hat{y} + k_z\hat{z}$, is derived utilizing two fluid models.

To establish the dynamics of whistler wave, the following key equations are used:

Wave equation

$$\nabla^2\vec{E} - \nabla(\nabla.\vec{E}) = \frac{4\pi}{c^2}\frac{\partial\vec{J}}{\partial t} + \frac{1}{c^2}\frac{\partial^2\vec{E}}{\partial t^2}. \tag{4.A1}$$

Equation of motion for electrons

$$m_e\left[\frac{\partial\vec{v}_e}{\partial t} + (\vec{v}_e.\nabla\vec{v}_e)\right] = -e\vec{E} - \frac{e}{c}(\vec{v}_e \times \vec{B}_0). \tag{4.A2}$$

Equation of motion for ions

$$m_i\left[\frac{\partial\vec{v}_i}{\partial t} + (\vec{v}_i.\nabla\vec{v}_i)\right] = e\vec{E} + \frac{e}{c}(\vec{v}_i \times \vec{B}_0), \tag{4.A3}$$

where m_e m_i denotes the mass of an electron and ion, v_i, v_e denotes the velocity of the ion and electron, B_0 denotes the background magnetic field, and e denotes the charge on the electron. Where $B_0(=B_{0z}\hat{z} + B_{0y}\hat{y})$, denotes the background magnetic field along z direction and also B_{0y} denotes the magnetic field owing to the presence of magnetic islands (at the reconnection sites).

Velocity components of whistler wave are derived using Eqs. (4.A2) and (4.A3),

$$\frac{d\vec{v}_e}{dt} = \frac{\partial\vec{v}_e}{\partial t} + \vec{v}_e.(\vec{\nabla}\vec{v}_e) = \frac{-e\vec{E}}{m_e} - \frac{e}{m_e c}\left[\vec{v}_e \times \left(\vec{B}_{0z}\hat{z} + \vec{B}_{0y}\hat{y}\right)\right]. \tag{4.A4}$$

Where $\vec{v}_e = \vec{v}_{e0} + \vec{v}_{e1}$, $\vec{v}_{e0}$ =0=No drift in equilibrium

$\vec{B}\left(= B_{0z}\hat{z} + B_{0y}\hat{y}\right)$, background magnetic field.

We can write the x-component of Eq. (4.A4) as:

$$-i\omega_0\ \vec{v}_{e1x} = -\frac{e\vec{E}_x}{m_e} - \vec{v}_{e1y}\omega_{ce} + \frac{e}{m_e c}v_{e1z}B_{0y}. \tag{4.A5}$$

Similarly, y-component of Eq. (4.A4) is:

$$-i\omega_0\ \vec{v}_{e1y} = -\frac{e\vec{E}_y}{m_e} + \vec{v}_{e1x}\omega_{ce}. \tag{4.A6}$$

z-component of Eq. (4.A4) is:

$$-i\omega_0\ \vec{v}_{e1z} = -\frac{e\vec{E}_z}{m_e} - \frac{e}{m_e c} v_{e1x} B_{0y}. \tag{4.A7}$$

From Eq. (4.A6)

$$\vec{v}_{e1y} = \frac{e\vec{E}_y}{i\omega_0 m_e} + \frac{\vec{v}_{e1x}\omega_{ce}}{i\omega_0}. \tag{4.A8}$$

Using Eqs. (4.A8) and (4.A7) in Eq. (4.A5), we can obtain the x-component of whistler wave's velocity due to electron.

$$v_{e1x} = -\frac{i\omega_0 e}{m_e\left(\omega_0^2 - \omega_{ce}^2\right)} E_x - \frac{e\omega_{ce}}{m_e\left(\omega_0^2 - \omega_{ce}^2\right)} E_y + \frac{e^2\omega_0 B_{0y}}{m_e^2 c\left(\omega_0^2 - \omega_{ce}^2\right)} E_z. \tag{4.A9}$$

y-component of whistler wave's velocity due to electron,

$$v_{e1y} = \frac{e\omega_{ce}}{m_e\left(\omega_0^2 - \omega_{ce}^2\right)} E_x - \frac{i\omega_0 e}{m_e\left(\omega_0^2 - \omega_{ce}^2\right)} E_y + \frac{ie^2\omega_{ce} B_{0y}}{m_e^2 c\omega_0\left(\omega_0^2 - \omega_{ce}^2\right)} E_z. \tag{4.A10}$$

z-component of whistler wave's velocity due to electron,

$$v_{e1z} = \frac{eE_z}{im_e\omega_0} + \left[\frac{-e^2 B_{0y}}{m_e^2 c(\omega_0^2 - \omega_{ce}^2)} E_x + \frac{ie^2\omega_{ce} B_{0y}}{m_e^2 c\omega_0(\omega_0^2 - \omega_{ce}^2)} E_y\right]. \tag{4.A11}$$

Similarly, we can obtain the components of whistler wave's velocity due to ions,

$$v_{i1x} = \frac{i\omega_0 e}{m_i\left(\omega_0^2 - \omega_{ci}^2\right)} E_x - \frac{e\omega_{ci}}{m_i\left(\omega_0^2 - \omega_{ci}^2\right)} E_y - \frac{e^2\omega_0 B_{0y}}{m_i^2 c\left(\omega_0^2 - \omega_{ci}^2\right)} E_z. \tag{4.A12}$$

$$v_{i1y} = \frac{e\omega_{ci}}{m_i\left(\omega_0^2 - \omega_{ci}^2\right)} E_x + \frac{i\omega_0 e}{m_i\left(\omega_0^2 - \omega_{ci}^2\right)} E_y + \frac{ie^2\omega_{ci} B_{0y}}{m_i^2 c\omega_0\left(\omega_0^2 - \omega_{ci}^2\right)} E_z. \tag{4.A13}$$

$$\text{And, } v_{i1z} = \frac{-eE_z}{im_i\omega_0} + \left[\frac{-e^2 B_{0y}}{m_i^2 c(\omega_0^2 - \omega_{ci}^2)} E_x + \frac{ie^2\omega_{ci} B_{0y}}{m_i^2 c\omega_0(\omega_0^2 - \omega_{ci}^2)} E_y\right]. \tag{4.A14}$$

Now, use these velocity components in driving the current density, by using relation, $\vec{J} = n_i e\vec{v}_i - n_e e v_e$, and then substitute in Eq. (4.A1),

x-component of Eq. (A1),

$$\left(\frac{\partial^2}{\partial y^2}+\frac{\partial^2}{\partial z^2}-\frac{1}{\left(\omega_0^2-\omega_{ci}^2\right)\lambda_i^2}\frac{\partial^2}{\partial t^2}+\frac{1}{\left(-\frac{\partial^2}{\partial t^2}-\omega_{ce}^2\right)\lambda_e^2}\frac{\partial^2}{\partial t^2}-\frac{1}{c^2}\frac{\partial^2}{\partial t^2}\right)E_x+$$
$$\left(-\frac{\partial}{\partial x}\frac{\partial}{\partial y}-\frac{\omega_{ci}}{\left(-\frac{\partial^2}{\partial t^2}-\omega_{ci}^2\right)\lambda_i^2}\frac{\partial}{\partial t}-\frac{\omega_{ce}}{\left(-\frac{\partial^2}{\partial t^2}-\omega_{ce}^2\right)\lambda_e^2}\frac{\partial}{\partial t}\right)E_y+ \tag{4.A15}$$
$$\left(-\frac{\partial}{\partial x}\frac{\partial}{\partial z}+\frac{ie\omega_0 B_{0y}}{m_i c\left(\omega_0^2-\omega_{ci}^2\right)\lambda_i^2}+\frac{ie\omega_0 B_{0y}}{m_e c\left(\omega_0^2-\omega_{ce}^2\right)\lambda_e^2}\right)E_z=0.$$

y-component Eq. (4.A1),

$$\left(-\frac{\partial}{\partial y}\frac{\partial}{\partial x}-\frac{\omega_{ci}}{\left(-\frac{\partial^2}{\partial t^2}-\omega_{ci}^2\right)\lambda_i^2}\frac{\partial}{\partial t}+\frac{\omega_{ce}}{\left(-\frac{\partial^2}{\partial t^2}-\omega_{ce}^2\right)\lambda_e^2}\frac{\partial}{\partial t}\right)E_x$$
$$+\left(\frac{\partial^2}{\partial x^2}+\frac{\partial^2}{\partial z^2}+\frac{1}{\left(-\frac{\partial^2}{\partial t^2}-\omega_{ci}^2\right)\lambda_i^2}\frac{\partial^2}{\partial t^2}+\frac{1}{\lambda_e^2\left(-\frac{\partial^2}{\partial t^2}-\omega_{ce}^2\right)}\frac{\partial^2}{\partial t^2}-\frac{1}{c^2}\frac{\partial^2}{\partial t^2}\right)E_y \tag{4.A16}$$
$$\left(-\frac{\partial}{\partial y}\frac{\partial}{\partial z}-\frac{e\omega_{ce}B_{oy}}{\lambda_e^2\left(-\frac{\partial^2}{\partial t^2}-\omega_{ce}^2\right)}+\frac{e\omega_{ci}B_{oy}}{\lambda_i^2\left(-\frac{\partial^2}{\partial t^2}-\omega_{ci}^2\right)}\right)E_z=0.$$

z-component Eq. (4.A1),

$$\left(-\frac{\partial}{\partial x}\frac{\partial}{\partial z}-\frac{ie\omega_0 B_{0y}}{m_e c\left(-\frac{\partial^2}{\partial t^2}-\omega_{ce}^2\right)}+\frac{ie\omega_0 B_{0y}}{m_i c\left(-\frac{\partial^2}{\partial t^2}-\omega_{ci}^2\right)}\right)E_x+$$
$$\left(-\frac{\partial}{\partial y}\frac{\partial}{\partial z}-\frac{e\omega_{ce} B_{0y}}{m_e c\left(-\frac{\partial^2}{\partial t^2}-\omega_{ce}^2\right)}+\frac{e\omega_{ci} B_{0y}}{m_i c\left(-\frac{\partial^2}{\partial t^2}-\omega_{ci}^2\right)}\right)E_y \qquad (4.A17)$$
$$\left(\frac{\partial^2}{\partial x^2}+\frac{\partial^2}{\partial y^2}-\frac{1}{\lambda_e^2}-\frac{1}{c^2}\frac{\partial^2}{\partial t^2}\right)E_z=0.$$

where $\omega_{ce}\left(=\frac{eB_0}{m_e c}\right)$ is the electron gyrofrequency of wave, n_0 denotes the background number density, c denotes the velocity of light and $\lambda_e\left(=\sqrt{\frac{c^2 m_e}{4\pi n_0 e^2}}\right)$ is the collisionless electron skin depth.

Now, Compounding Eqs. (4.A15), (4.A16), and (4.A17) and applying conditions $k\lambda_i \gg 1$, we get,

$$\left(\frac{\partial^2}{\partial y^2}+\frac{\partial^2}{\partial z^2}-\frac{1}{\lambda_e^2\left(-\frac{\partial^2}{\partial t^2}-\omega_{ce}^2\right)}\frac{\partial^2}{\partial t^2}\right)\left[\left(\frac{\partial^2}{\partial x^2}+\frac{\partial^2}{\partial z^2}+\frac{1}{\lambda_e^2\left(-\frac{\partial^2}{\partial t^2}-\omega_{ce}^2\right)}\frac{\partial^2}{\partial t^2}\right)\left(\frac{\partial^2}{\partial x^2}+\frac{\partial^2}{\partial y^2}-\frac{1}{\lambda_e^2}\right)\times\left(\frac{\partial}{\partial y}\frac{\partial}{\partial z}+\frac{e\omega_{ce}B_{0y}}{m_e c\lambda_e^2\left(-\frac{\partial^2}{\partial t^2}-\omega_{ce}^2\right)}\right)^2\right]-$$
$$\left(\frac{\partial}{\partial x}\frac{\partial}{\partial y}+\frac{\omega_{ce}}{\lambda_e^2\left(-\frac{\partial^2}{\partial t^2}-\omega_{ce}^2\right)}\frac{\partial}{\partial t}\right)\left[\left(\frac{\partial}{\partial y}\frac{\partial}{\partial z}+\frac{e\omega_{ce}B_{0y}}{m_e c\lambda_e^2\left(-\frac{\partial^2}{\partial t^2}-\omega_{ce}^2\right)}\right)\left(\frac{\partial}{\partial x}\frac{\partial}{\partial z}+\frac{eB_{0y}}{m_e c\lambda_e^2\left(-\frac{\partial^2}{\partial t^2}-\omega_{ce}^2\right)}\right)\times\left(\frac{\partial}{\partial x}\frac{\partial}{\partial y}+\frac{\omega_{ce}}{\lambda_e^2\left(-\frac{\partial^2}{\partial t^2}-\omega_{ce}^2\right)}\frac{\partial}{\partial t}\right)\left(\frac{\partial^2}{\partial x^2}+\frac{\partial^2}{\partial y^2}-\frac{1}{\lambda_e^2}\right)\right]$$
$$+\left(\frac{\partial}{\partial x}\frac{\partial}{\partial z}+\frac{eB_{0y}}{m_e c\lambda_e^2\left(-\frac{\partial^2}{\partial t^2}-\omega_{ce}^2\right)}\frac{\partial}{\partial t}\right)\left[\left(\frac{\partial}{\partial x}\frac{\partial}{\partial y}+\frac{\omega_{ce}}{\lambda_e^2\left(-\frac{\partial^2}{\partial t^2}-\omega_{ce}^2\right)}\frac{\partial}{\partial t}\right)\left(\frac{\partial}{\partial y}\frac{\partial}{\partial z}+\frac{e\omega_{ce}B_{0y}}{m_e c\lambda_e^2\left(-\frac{\partial^2}{\partial t^2}-\omega_{ce}^2\right)}\right)\times\left(\frac{\partial^2}{\partial x^2}+\frac{\partial^2}{\partial z^2}+\frac{1}{\lambda_e^2\left(-\frac{\partial^2}{\partial t^2}-\omega_{ce}^2\right)}\frac{\partial^2}{\partial t^2}\right)\left(\frac{\partial}{\partial x}\frac{\partial}{\partial z}+\frac{eB_{0y}}{m_e c\lambda_e^2\left(-\frac{\partial^2}{\partial t^2}-\omega_{ce}^2\right)}\frac{\partial}{\partial t}\right)\right]E_z=0. \tag{4.A18}$$

After solving eq. (4.A18), we obtain the dynamics of 3D whistler wave in the presence of magnetic island in terms of electric field under the condition $-\frac{\partial^2}{\partial t^2}>\omega_{ce}\omega_{ci}$. Now, we can write the dynamical equation of 3D whistler in terms of electric field.

$$\frac{\partial^2 E_z}{\partial t^2}+\frac{\partial^6 E_z}{\partial t^2\partial x^4}\lambda_e^4+\frac{\partial^6 E_z}{\partial t^2\partial y^4}\lambda_e^4+\frac{\partial^6 E_z}{\partial t^2\partial z^4}\lambda_e^4+2\lambda_e^4\frac{\partial^4 E_z}{\partial t^2\partial z^2}\left(\frac{\partial^2}{\partial x^2}+\frac{\partial^2}{\partial y^2}\right)-2\lambda_e^2\left(\frac{\partial^2}{\partial x^2}+\frac{\partial^2}{\partial y^2}+\frac{\partial^2}{\partial z^2}\right)\frac{\partial^2 E_z}{\partial t^2}+$$
$$\lambda_i^2 v_A^2\left(\frac{\partial^2}{\partial x^2}+\frac{\partial^2}{\partial y^2}\right)\frac{\partial^2 E_z}{\partial z^2}+\lambda_i^2 v_A^2\frac{\partial^4 E_z}{\partial z^4}+\frac{\lambda_i^2 v_A^2 B_{0y}^2}{B_{0z}^2}\left(\frac{\partial^2}{\partial x^2}+\frac{\partial^2}{\partial y^2}\right)\frac{\partial^2 E_z}{\partial y^2}+\frac{\lambda_i^2 v_A^2 B_{0y}^2}{B_{0z}^2}\frac{\partial^4 E_z}{\partial y^2\partial z^2}+$$
$$\frac{2\lambda_i^2 v_A^2 B_{0y}}{B_{0z}}\left(\frac{\partial^2}{\partial x^2}+\frac{\partial^2}{\partial y^2}\right)\frac{\partial^2 E_z}{\partial y\partial z}+\frac{2\lambda_i^2 v_A^2 B_{0y}}{B_{0z}}\frac{\partial^4 E_z}{\partial y\partial z^3}=0. \tag{4.A19}$$

Also, we can write above equation in following form which is the dispersion relation in the presence of magnetic islands,

$$\left(\omega_0^2(1+k^2\lambda_e^2)^2-\frac{k^2\lambda_i^2(k_zB_{0z}+k_yB_{0y})^2}{4\pi n_0 m_i}\right)E_z=0. \tag{4.A20}$$

Here, $B_0(=B_{0z}\hat{z}+B_{0y}\hat{y})$, denotes the background magnetic field along z direction and also B_{0y} denotes the magnetic field owing to the presence of magnetic islands (at the reconnection sites), and in the absence of magnetic islands, one can get the usual dispersion relation of whistler wave given below

$$\left[\omega_0^2(1+k^2\lambda_e^2)^2-k^2k_z^2\lambda_i^2v_A^2\right]E_z=0. \tag{4.A21}$$

Moreover, it is emphasized that the equation of motion is then used to examine beam-driven evolution.

$$m\frac{dv}{dt}=-eE-mv\gamma \qquad \rightarrow\frac{dv}{dt}=-\frac{eE}{m}-v\gamma$$

$$(-i\omega+\gamma)=-\frac{eE}{mv} \qquad \rightarrow\frac{d}{dt}=\left(\frac{d}{dt}+\gamma\right)$$

$\frac{d^2}{dt^2}=\left(\frac{d^2}{dt^2}+2\gamma\frac{d}{dt}\right)$, neglecting higher order terms.

The dispersion relation of the whistler wave under the conditions,

$k_{0x}=k_{0y}=0, k_0=k_{0z}$ and $k_0\lambda_e>>1$, $\omega_{ce}>\omega_0$

The eq. (4.A21) modifies to $\omega_0^2=k_{0z}^4\lambda_i^2v_A^2.$ (4.A22)

It should be noted that this formulation (equation (4.A22)) is identical to the dispersion relation of a circularly polarised wave[58]. (The widely recognised dispersion function of a circularly polarised whistler wave[58] is given as

$$k_0^2=\frac{\omega_0^2}{c^2}\left(1-\frac{\omega_{pe}^2}{\omega_0(\omega_0-\omega_{ce})}\right).$$

Now, after neglecting the displacement current and taking the conditions $k_{0x}=k_{0y}=0, k_0=k_{0z}$, $k_0\lambda_e>>1$ and $\omega_{ce}>\omega_0$ into account, it reduces $\omega_0=k_{0z}^2\lambda_e^2\omega_{ce}$. Further, using $\lambda_iv_A=\lambda_e^2\omega_{ce}$ and hence the similarity).

BIO-DATA

Ms. Jyoti is a research scholar at the Department of Applied Physics, Delhi Technological University, Delhi, India since December 2018. Prior to this, she received her master's degree in Physics from Hindu College Sonipat, Maharishi Dayanand University, Rohtak in the year 2013 and her bachelor's degree (B.Sc.) from Hindu Girls College Sonipat, Maharishi Dayanand University, Rohtak in the year 2011. She has been awarded the CSIR-JRF Fellowship from University Grant Commission, Govt. of India. She has also qualified the GATE in the year 2014. She has been awarded the Commendable Research Award for excellence in Research by DTU in the year 2023,2024.

Her present research interests include the the generation of turbulence at the vicinity of reconnection sites in magnetosphere by beam-generated whistler wave. Specifically, to explore the role that whistler waves play in the formation of coherent structures/current sheets in the presence of Harris field or Ponderomotive nonlinearity or both.